Mechanical Characterization and Finite Element Simulation of Carbon/PEEK Thermoplastic Composite Laminate Manufactured using Automated Fiber Placement (AFP) Process

Emad Pourahmadi

A Thesis

In the Department

of

Mechanical, Industrial and Aerospace Engineering

Presented in Partial Fulfillment of the Requirements

For the Degree of

Doctor of Philosophy (Mechanical Engineering) at

Concordia University

Montreal, Quebec, Canada

July 2025

CONCORDIA UNIVERSITY

SCHOOL OF GRADUATE STUDIES

This is to certify that the thesis prepared

By: Emad Pourahmadi

Entitled: Mechanical Characterization and Finite Element Simulation of Carbon/PEEK
            Thermoplastic Composite Laminate Manufactured using Automated Fiber
            Placement (AFP) Process

and submitted in partial fulfillment of the requirements for the degree of

DOCTOR OF PHILOSOPHY (Mechanical Engineering)

complies with the regulations of the University and meets the accepted standards with respect to
originality and quality.

Signed by the final examining committee:

_____ Chair
Dr. Christian Moreau

_____ External Examiner
Dr. John Montesano

_____ External to Program
Dr. Ahmed Soliman

_____ Examiner
Dr. Mehdi Hojjati

_____ Examiner
Dr. Suong Van Hoa

_____ Thesis Supervisor
Dr. Farjad Shadmehri

_____ Thesis Supervisor
Dr. Rajamohan Ganesan

Approved by   _____
                  Dr. Ramin Sedaghati, Graduate Program Director

July 3, 2025   _____
                  Dr. Mourad Debbabi, Dean
                  Gina Cody School of Engineering and Computer Science

ABSTRACT

Mechanical Characterization and Finite Element Simulation of Carbon/PEEK Thermoplastic Composite Laminate Manufactured using Automated Fiber Placement (AFP) Process

Emad Pourahmadi, Ph.D.

Concordia University, 2025

Despite fabrication difficulties, the utilization of thermoplastic composite laminates is expanding, especially in the aerospace industry, owing to their outstanding characteristics, such as high toughness and recyclability. Compared to established manufacturing procedures, such as hand layup autoclave process, automated manufacturing techniques, such as Automated Fiber Placement (AFP), offer the potential to economize time and costs. An advantage of manufacturing thermoplastic composite laminates using AFP lies in the possibility of in-situ consolidation, thereby eliminating the necessity of any secondary consolidation processes. However, short processing time during the AFP method leads to a significant contrast in the quality of in-situ-consolidated thermoplastic composite laminates in terms of interlaminar bond strength and other material properties when compared to that of their autoclave-reconsolidated counterparts. The present thesis focuses on this aspect and aims to develop an efficient micromechanical computational model based on the finite element method that can predict the interface strength and other material properties, including stiffness and strength, of in-situ-consolidated Carbon/PEEK thermoplastic composite laminate. Two batches of laminate samples are fabricated by AFP with in-situ consolidation. One of the batches is subsequently re-consolidated in an autoclave to serve as a reference for a comparative study (i.e., in-situ consolidated vs. autoclave re-consolidated). The Short-Beam Shear (SBS) test, due to delamination failure mode, is chosen to measure the Interlaminar Shear Strength (ILSS). The interface strength properties caused by AFP in-situ consolidation are computationally determined using the cohesive zone model and the SBS test results. The manufactured samples undergo micrographic study and thermoanalytical Differential Scanning Calorimetry (DSC) testing to gather the essential data for the computational model, including fiber volume fraction, interlaminar resin pocket, void content and degree of crystallinity. Then, realistic two-dimensional Representative Volume Elements (RVEs) are generated at a micro-scale based on the obtained information from micrographic examination and DSC analysis.

These 2D RVEs were first used in the finite element simulation to predict the transverse tensile strength, resulting from the AFP in-situ consolidation process, using the Drucker-Prager law along with ductile failure criterion to take into account the plastic deformation of the matrix, as well as crack onset and evolution in the neat PEEK resin. Furthermore, the effective stiffness properties, such as transverse elastic and out-of-plane shear moduli, influenced by AFP in-situ consolidation were predicted by applying periodic boundary conditions and using the homogenization theory. The obtained results reveal that while the AFP in-situ consolidation manufacturing process reduces the transverse stiffness properties of Carbon/PEEK thermoplastic composite laminate 10% to 20%, the transverse tensile strength value may even decrease up to 44%, in comparison with the autoclave treatment. The outcomes of this thesis demonstrate that the mechanical performance of Carbon/PEEK thermoplastic composite laminates is significantly affected by the AFP in-situ consolidation process. The predicted interfacial strength and effective material properties provide essential input parameters for subsequent finite element modeling, analysis, and structural design of thermoplastic composite components produced through the AFP in-situ consolidation process.

Acknowledgments

I am deeply thankful to my supervisors, Dr. Farjad Shadmehri and Dr. Rajamohan Ganesan at Concordia University, for their invaluable support, insightful guidance, and continuous encouragement throughout my Ph.D. journey. Their trust in my research ideas and their generous dedication of time were essential in helping me overcome the challenges of this program.

Dedication

I dedicate this dissertation work to my spouse, Mahshad Abbasirad, for her patience, support, and encouragement.

Contribution of Authors to Publications

Emad Pourahmadi: Conceptualization, Methodology, Software, Validation, Formal analysis, Investigation, Writing - Original Draft, Writing - Review & Editing, Visualization

Farjad Shadmehri: Conceptualization, Methodology, Resources, Writing - Review & Editing, Supervision, Funding acquisition

Rajamohan Ganesan: Conceptualization, Methodology, Resources, Writing - Review & Editing, Supervision, Funding acquisition

Journal Articles

1. E. Pourahmadi, F. Shadmehri, R. Ganesan, "Interlaminar shear strength of Carbon/PEEK thermoplastic composite laminate: effects of in-situ consolidation by automated fiber placement and autoclave re-consolidation", *Composites Part B: Engineering*, 269 (2024), 111104. https://doi.org/10.1016/j.compositesb.2023.111104. [presented in Chapter 2]

2. E. Pourahmadi, F. Shadmehri, R. Ganesan, "Prediction of transverse tensile strength of in-situ-consolidated Carbon/PEEK thermoplastic composite material based on micromechanical modeling and simulation", *Composites Part A: Applied Science and Manufacturing*, 197 (2025), 109062. https://doi.org/10.1016/j.compositesa.2025.109062. [presented in Chapter 3]

3. E. Pourahmadi, R. Ganesan, F. Shadmehri, "Micromechanical characterization of Carbon/PEEK thermoplastic composite material in-situ consolidated by automated fiber placement: Stiffness prediction", *Composites Science and Technology*, 246 (2024), 110390. https://doi.org/10.1016/j.compscitech.2023.110390. [presented in Chapter 4]

Conference Papers

1. E. Pourahmadi, F. Shadmehri, R. Ganesan, "Interlaminar shear strength of Carbon/PEEK thermoplastic composite laminate in-situ consolidated by automated fiber placement" in the *13th Canadian-International Conference on Composites (CANCOM2024)*, Waterloo, Ontario, Canada, Aug. 2024. [presented in Chapter 2]

2. E. Pourahmadi, F. Shadmehri, R. Ganesan, "Influence of void formation in AFP in-situ consolidation on the transverse tensile strength of Carbon/PEEK thermoplastic composite material" in the *24th International Conference on Composite Materials (ICCM24)*, Baltimore, Maryland, Aug. 2025, Accepted. [presented in Chapter 3]

3. E. Pourahmadi, R. Ganesan, F. Shadmehri, "Effect of in-situ consolidation on the in-plane elastic moduli of Carbon/PEEK thermoplastic composites made by Automated Fiber Placement (AFP) process" in the *21st European Conference on Composite Materials (ECCM21)*, Nantes, France, July 2024. [presented in Chapter 4]

Table of Contents

List of Figures

xii

List of Tables

CHAPTER 1

Introduction

1. Introduction

1.1. Background and motivation

Polymeric composites have found extensive applications in various fields owing to their remarkable specific stiffness, strength, corrosion resistance and lightweight characteristics, particularly in aerospace and automotive industries where weight reduction is crucial. Automated Fiber Placement (AFP) has emerged as an advanced automated manufacturing technique that offers benefits, such as reduced material waste, increased deposition rate and minimized production time and costs, when compared to conventional methods, such as the hand lay-up process. Robotic AFP machines utilize a fiber placement head (thermoset or thermoplastic) mounted on a robotic arm to precisely lay down narrow composite tows onto a tool surface, creating composite laminates, as shown in Figure 1.1. The fiber placement process involves applying a simultaneous compressive force and heat using a compaction roller and a heating system, such as a hot gas torch. Nowadays, the time-consuming and expensive curing process of thermoset-based composites has motivated the increasing adoption of thermoplastic counterparts as a viable alternative, offering more efficient and cost-effective solutions.
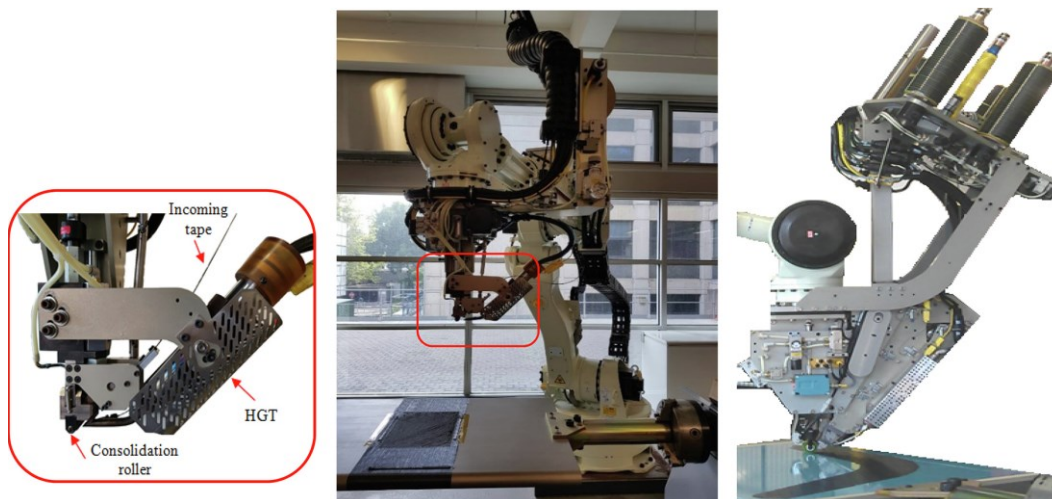
Figure 1.1. Components of an Automated Fiber Placement (AFP) machine: robotic arm and fiber placement head (either thermoplastic or thermoset) [1].

One of the major advantages of thermoplastic composites lies in the potential for in-situ consolidation during the Automated Fiber Placement (AFP) manufacturing process. This consolidation process is characterized by a higher cooling rate and limited duration in which the

tape is exposed to heat and compaction, leading to incomplete healing and a disparity in the quality of in-situ-consolidated thermoplastic composites compared to those treated inside an autoclave. These differences are attributed to critical factors, such as fiber volume fraction, void content, interlaminar resin pocket and degree of crystallinity. Thus, it is of great importance to thoroughly investigate the mechanical performance of thermoplastic composites manufactured by AFP in-situ consolidation and make a detailed comparison with those manufactured using the autoclave and hot press methods [2–5]

In-situ AFP manufacturing of thermoplastic composites involves three stages: heating, consolidation, and solidification. Consolidation and solidification are critical for reducing voids and ensuring strong interlayer bonding through heat and pressure, which improve mechanical properties [6]. Voids can be intralaminar (formed during tape fabrication) or interlaminar (arising between plies due to surface roughness) [7–9]. During consolidation, tape surfaces flatten to create "intimate contact" [10], followed by molecular chain motion that enables "healing" (autohesion) and bonding between layers [11]. Compared to autoclave or compression molding methods, although AFP in-situ consolidation offers an alternative manufacturing technique to save time and cost, it can significantly affect void content and bonding quality.

1.2. Literature review

1.2.1. Interface strength properties

Generally, limited research has focused on investigating the performance of thermoplastic composite laminates manufactured through the AFP in-situ consolidation method. Considering the bonding of layers as a primary concern during the in-situ consolidation manufacturing process, particularly due to its short processing time compared to autoclave treatment, the Short-Beam Shear (SBS) test, in which delamination is the dominant failure mode, is commonly used as a quality assessment technique to examine the impact of consolidation processes on the Interlaminar Shear Strength (ILSS). The sample shapes (i.e., flat or curved) and dimensions adhere to the guidelines specified in ASTM D2344 [12]. Following ASTM D2344 guidelines, the loading nose and supports of the fixture possess diameters of 6 mm and 3 mm, respectively. The ratio of span length to thickness is set at 4.0. Both the loading nose and the side supports extend beyond the specimen width by a minimum of 2 mm. The SBS test is usually carried out in a displacement

control mode with a crosshead movement rate of 1.0 mm/min using short-beam shear test fixtures, as shown in Figure 1.2. ILSS values for each sample are computed using the provided equation [12]:

$$F^{sbs} = 0.75 \times \frac{P_m}{b \times h} \qquad (1.1)$$

where F^{sbs} and P_m are the interlaminar shear strength and the maximum applied load. b and h denote the width and thickness of the specimen, respectively.

Some studies [13,14] attempted to optimize the in-situ AFP process parameters, namely torch temperature, torch location, deposition rate and compaction force, for increasing the quality of fabricated thermoplastic composite materials based on ILSS values, as shown in Figure 1.3. They reported that the layer morphology was significantly affected by the processing conditions. Moreover, severe fiber damage was observed in specimens fabricated under elevated temperature (950 °C) and high consolidation force (450 N). These findings underscore the critical influence of manufacturing parameters on both the mechanical performance and overall quality of the laminates, highlighting the necessity of their careful optimization to achieve desirable outcomes.
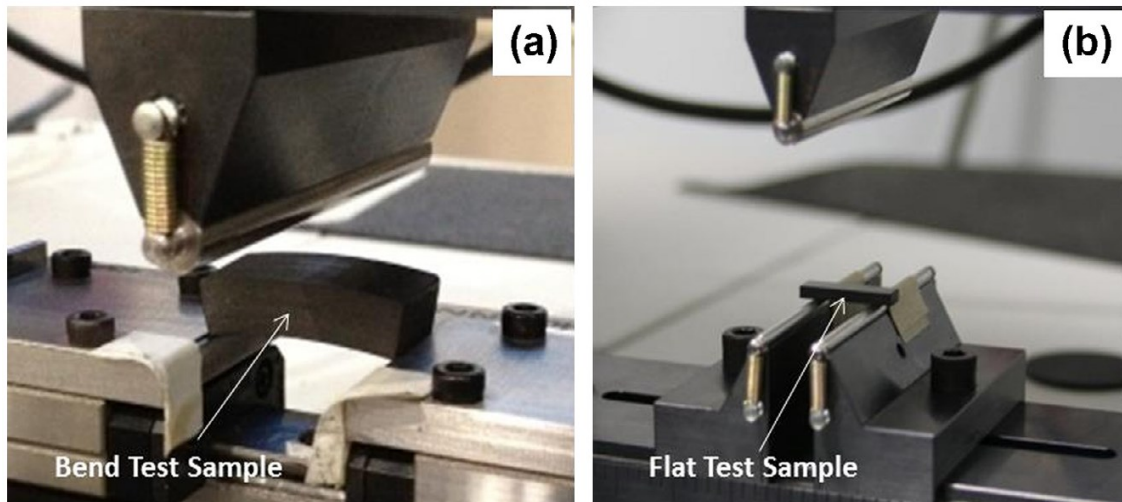
Figure 1.2. Sample shapes and test fixtures for short-beam shear test: (a) curved and (b) flat specimens [15].

Figure 1.3. AFP processing parameters used for the manufacturing of thermoplastic composite laminates for optimization purposes [14].

Few researchers explored the variations in ILSS values of Carbon/PEEK thermoplastic composite samples caused by AFP in-situ consolidation and autoclave re-consolidation methods, as listed in Table 1.1. Cai *et al*. [13] optimized AFP processing parameters using the Taguchi method and achieved an Interlaminar Shear Strength (ILSS) of 51 MPa for Carbon/PEEK composites with a hot gas torch heating system. Qureshi *et al.* [15] showed that the ILSS value can be increased to 78.9 MPa when laser heating is used. Khan *et al.* [16] demonstrated that deposition rate strongly influences interface strength properties by altering the cooling rate. Using a heated tool, they further increased the ILSS to 85.5 MPa by enhancing the degree of crystallinity. It should be noted that although Stokes-Griffin and Compston [17] reported even higher ILSS values for the in-situ-consolidated Carbon/PEEK thermoplastic composite sample compared to the autoclave-reconsolidated counterpart, no other studies have achieved the same results so far. The primary failure mode observed during the short-beam shear test is delamination (interlaminar damage), largely influenced by the matrix characteristics. To consider the layer separation phenomenon in finite element modeling, researchers commonly employ the Cohesive Zone Model (CZM), prevalent in the literature [18–23]. For this purpose, a linear elastic traction-separation response is considered within the cohesive zone, including three distinct delamination failure modes: mode I, mode II, and mode III. Because delamination typically arises under mixed-mode loading

5

conditions, the quadratic stress failure criterion is utilized to predict the initiation and propagation of delamination [18,19]. Moreover, regarding the composite damage modeling (intralaminar damage), El-Sisi *et al.* [24] examined three different material modeling approaches: The Ply Discount Model (PDM), the Simple Progressive Damage Model (SPDM), and the Continuum Damage Mechanics Model (CDMM). They recommended employing the Continuum Damage Mechanics Model (CDMM) combined with 3D Hashin failure criteria [22,25,26]. This combination has demonstrated the ability to closely align with experimental outcomes while minimizing sensitivity to mesh size variations, enabling accurate prediction of the onset and evolution of composite damage [24]. Liu *et al.* [27] conducted a computational simulation, by considering both models for intralaminar and interlaminar damage, to assess the response of Carbon/PEEK thermoplastic composite samples produced via out-of-autoclave methods, such as compression molding, under three-point bend flexural loading. The study illustrated a strong correspondence between simulation outcomes and experimental observations in terms of mechanical behavior and damage mechanism.

Table 1.1. ILSS values measured by the SBS test for Carbon/PEEK thermoplastic composite samples manufactured by autoclave re-consolidation and AFP in-situ consolidation with different deposition rates.

References	Autoclave re-consolidation	AFP In-situ consolidation	
	ILSS (MPa)	ILSS (MPa)	Rate (mm/s)
Cai *et al.* [13]	-	51	50.8
Tierney and Gillespie [28]	90	60	30
Qureshi *et al.* [15]	92.7	49.2	65
		78.9[1]	127
Khan *et al.* [16]	94.8	85.5[2]	50
Stokes-Griffin and Compston [17]	94.8	98[1]	100

[1]In-situ consolidation using a laser heating system
[2]In-situ consolidation using heated mandrel

While several studies have focused on optimizing the AFP processing parameters (i.e., temperature, compaction force and deposition rate) and evaluating the quality of Carbon/PEEK thermoplastic composite laminates by measuring the Interlaminar Shear Strength (ILSS) through the Short-Beam Shear (SBS) test, a significant gap remains in the availability of interface strength properties for in-situ-consolidated thermoplastic composite laminates, parameters essential for accurate finite element modeling and analyses.

1.2.2. Material properties

Fabricating thermoplastic composite laminates with absolute flatness proves to be challenging during the AFP in-situ consolidation process due to warpage and distortion of flat samples with open edges, as shown in Figure 1.4, whereby there is substantially limited literature on the material characterization of in-situ-consolidated thermoplastic composites. Warpage in AFP in-situ-consolidated thermoplastic laminates mainly results from nonuniform cooling, shrinkage, and thermal gradients through the thickness, which generate residual stresses and distortion. The main factors contributing to this effect are layup sequence, fiber orientation, and variations in applied heat and pressure during the consolidation process. Hoa *et al.* [29] proposed the utilization of a heated mandrel to address these difficulties in manufacturing undistorted thermoplastic composite laminates. They conducted various tests to compare the mechanical properties of these samples with those manufactured through conventional autoclave treatment. However, it is worth mentioning that the heated mandrel technique may lead to alterations in the mechanical properties of the final product compared to those resulting from the in-situ consolidation process.

Figure 1.4. Warpage and distortion introduced in the in-situ-consolidated thermoplastic composite laminate during the AFP process [29].

During the fabrication of thermoplastic composites, residual stresses may develop due to factors such as high processing temperatures, uneven cooling, and mismatched material properties between layers, often leading to warpage and dimensional instability. These process-induced stresses can compromise the load-bearing capacity of the composite by promoting fiber buckling or void formation during solidification, which may trigger microcracking and reduce strength properties [30]. To this end, several studies [30–33] have attempted to numerically and

experimentally investigate the effect of manufacturing-induced residual thermal stresses on the performance of thermoplastic composite materials.

Few researchers [5,34,35] conducted a microstructural comparison between in-situ-consolidated Carbon/PEEK thermoplastic composite samples and those re-consolidated in an autoclave. Fereidouni and Hoa [36] investigated various micro- and macro-scale defects in AFP-manufactured thermoplastic composites, with particular attention to Carbon/PEEK tapes consolidated using a Hot Gas Torch (HGT) heating system. Their study outlined defects arising from the supplied impregnated tape, performance limitations of the AFP system, and issues related to the in-situ consolidation process. Investigating the microstructure of thermoplastic samples manufactured by in-situ consolidation and autoclave re-consolidation offers a valuable understanding of the factors leading to mechanical performance differences.

Studies available in the literature [5,9,34,35,37–41] indicate that in-situ consolidation generally produces laminates with greater void content (up to 4%) and reduced degree of crystallinity (15-30%), depending on AFP parameters and the heating method. However, autoclave-reconsolidated laminates usually achieve lower void content (below 0.5%) and a higher degree of crystallinity (about 35%) as a result of slower cooling and extended heat and pressure application. Examination of the samples through microscopy imaging, as depicted in Figure 1.5, clearly highlights significant differences between thermoplastic composites fabricated by AFP in-situ consolidation and those re-consolidated through the autoclave process. The microstructure of the thermoplastic composites undergoes notable changes when it is treated with an autoclave, leading to improved fiber distribution and reduced visibility of layer boundaries. In contrast, samples manufactured through in-situ consolidation reveal resin-rich regions between layers (interlaminar resin pockets) and uneven fiber distribution, potentially giving rise to stress concentration zones [42]. The void content and fiber volume fraction can be assessed using the color thresholding technique by *ImageJ* software, which is capable of differentiating between voids, fibers, and resin [43,44]. Owing to the presence of resin pockets between layers, resulting from uneven fiber distribution, not only the total void percentage but also the void distribution (i.e., intralaminar and interlaminar voids) can negatively influence the mechanical performance of the composite material. It is worth mentioning that the damage mechanism of composite materials in the transverse direction highly depends on stress concentration areas emerging in the matrix phase. As a result, any factors causing

a discontinuity in stress distribution of the microstructure, such as the presence of interlaminar resin pockets and particularly voids, may affect the crack initiation and propagation substantially, leading to a significant reduction in the strength of composite materials [42,45].

| In-situ-consolidated sample | Autoclave-reconsolidated sample |
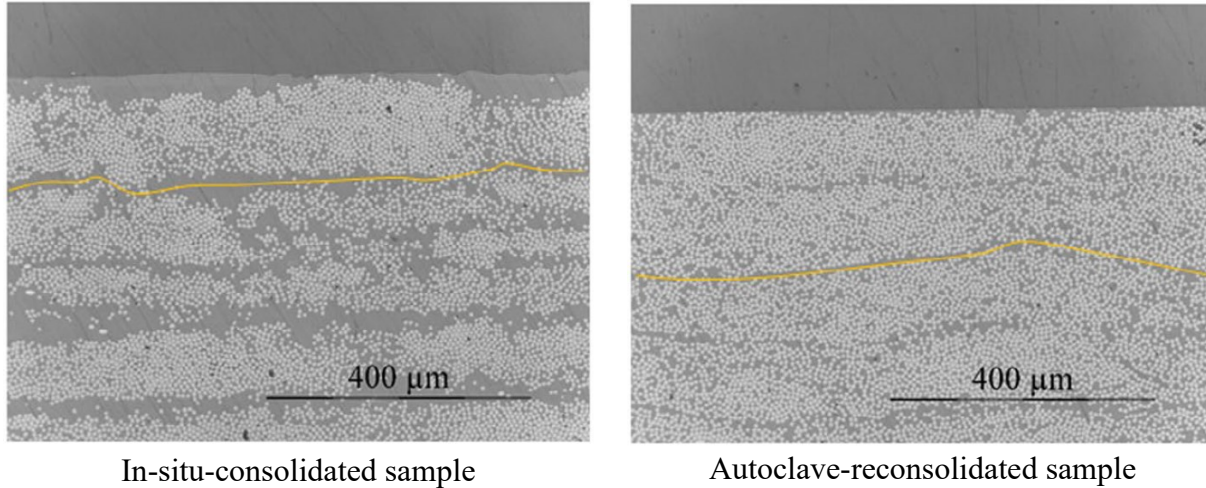
Figure 1.5. Typical 20X-magnified micrographs of Carbon/PEEK thermoplastic samples after in-situ consolidation and autoclave re-consolidation processes [5].

The degree of crystallinity of Carbon/PEEK thermoplastic composite laminate, manufactured by AFP in-situ consolidation, can be influenced by AFP processing parameters, such as deposition rate, temperature and compaction force, as well as the type of heating system used (e.g., hot gas torch, laser, etc.). As a result of these parameters, the degree of crystallinity may typically vary between 15 to 30 percent [5,38,40,41] and plays a crucial role in determining the elastic modulus and strength of neat PEEK resin, thereby exerting a substantial influence on the overall material properties of the composite material [30,46,47]. It should be also noted that especially in the transverse direction, where matrix behavior governs, any variations in the degree of crystallinity can lead to undesirable effects on the performance of the composite material.

Although experimental methods are essential for assessing material properties, conducting mechanical tests on unidirectional thermoplastic composite specimens poses challenges due to warpage and distortion induced during the AFP in-situ consolidation process. Micromechanical computational models offer a valuable tool for performing virtual experiments and analyzing various material systems during the design stage [48]. Two types of Representative Volume Elements (RVEs) are used in micromechanical analyses: periodic (i.e., hexagonal and square packing) and random distribution of fibers. It is essential to consider a realistic, non-uniform and random distribution of fibers in order to provide an accurate assessment of local stress

9

concentrations and precise prediction of mechanical properties, as well as the onset and propagation of local damage [42,49–51]. While employing the Representative Volume Element (RVE) technique enables researchers to simulate a wide range of microstructures, including their constituents, shapes, orientations, and distribution, generating an RVE capable of accurately representing the mechanical behavior and response of long-fiber-reinforced composites with a high fiber volume fraction (e.g., 60%) presents considerable modeling challenges. For this purpose, researchers have developed numerous algorithms, including Random Sequential Adsorption (RSA) [52], Random Sequential Expansion (RSE) [53], Event-Driven Molecular Dynamics (EDMD) [51] and Random Microstructure Generator (RAND_uSTRU_GEN) [54], with the aim of improving the genuineness and practicality of generated RVE models by incorporating non-uniform and random fiber distribution.

Numerous studies have explored the transverse mechanical behavior of composite materials using micromechanical analysis and generating different microstructures through either different algorithms or image processing methods [42,45,55–66]. Ghayoor et al. [42] studied the influence of intralaminar resin-rich regions, created by fiber removal and displacement, on the transverse modulus and damage initiation of Carbon/Epoxy composites through computational analysis. Their findings indicated that resin pockets could reduce the failure initiation strain by about 20%. Yang et al. [60] examined the transverse tensile and compressive behavior of unidirectional laminates using an RVE approach, incorporating matrix plasticity via the Drucker-Prager model and interfacial debonding with cohesive zone elements. Totry et al. [61] employed 3D RVEs to identify failure sites in Carbon/PEEK laminates under transverse compression and longitudinal shear. Fedulov et al. [63] introduced a material model combining plasticity with damage initiation and propagation for PEEK resin supplied by Cytec [67], which successfully predicted the transverse tensile strength of Carbon/PEEK laminates in agreement with experimental data.

In the present thesis, the RAND_uSTRU_GEN algorithm proposed by Melro et al. [54] was used. The initial stage in generating a Representative Volume Element (RVE) using this method involves creating a set of random center points for the fibers, while ensuring they do not overlap with previously generated fibers. Additionally, this step allows for defining a minimum distance between the fibers as needed. To attain high fiber volume fractions, the subsequent step involves identifying and repositioning the center points of the most isolated fibers within the RVE, thereby

facilitating the achievement of higher packing densities of fibers (fiber stirring method [54]). Ghayoor *et al.* [50] modified this algorithm by choosing the most isolated fibers to be stirred in order to increase the probability of creating empty areas, allowing for the incorporation of additional fibers. Fiber isolation is determined by calculating the average distances to their three or four closest neighbors, with the fibers having the largest average distance being classified as isolated. The number of fibers eligible for relocation can be tailored according to the iteration count and the target fiber volume fraction. During relocation, the isolated fibers move towards neighboring fibers at a random distance that falls between the specified minimum distance and the existing distance between two adjacent fibers (the complete RVE generation procedure is explained in detail in Chapters 3 and 4). Moreover, in addition to the random microstructure created inside the representative volume element, the RVE must be periodic on the opposite boundaries to enable precise prediction of the stress field, as shown in Figure 1.6.
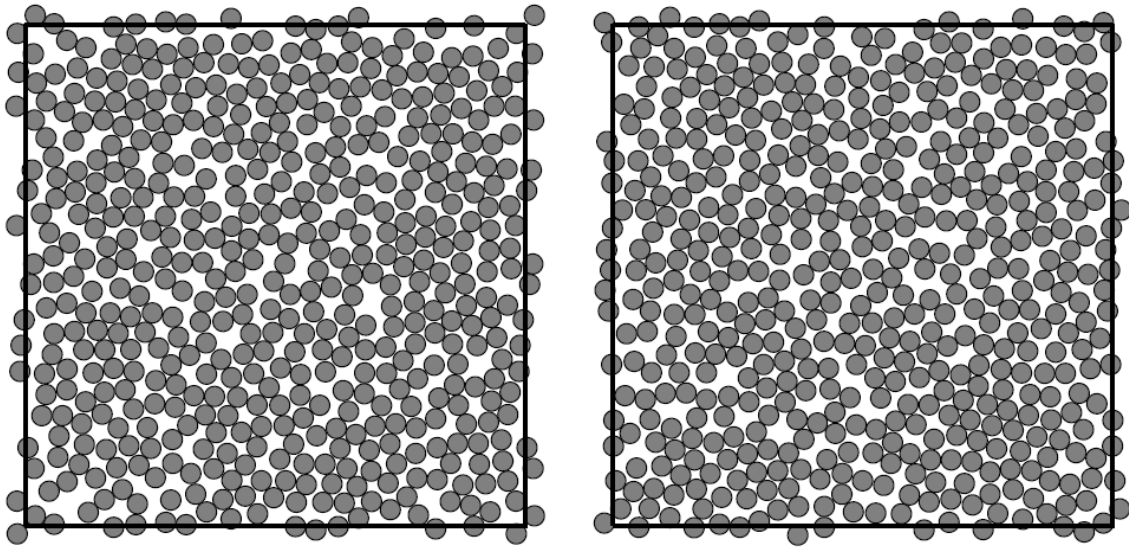
Figure 1.6 Examples of periodic RVEs with random fiber distribution and 60% fiber volume fraction [54].

Composite materials are often depicted in micromechanical models as an array of periodic RVEs, requiring the implementation of Periodic Boundary Conditions (PBCs). These boundary conditions ensure that the deformations of all RVEs are compatible, preventing any overlap or separation between adjacent RVEs. The periodic boundary conditions are generally formulated as follows [68,69]:

$$u_i = \bar{\varepsilon}_{ik} x_k + u_i^* \qquad (1.2)$$

where u_i denotes the displacement, $\bar{\varepsilon}_{ik}$ represents the average strain and x_k indicates the Cartesian coordinate of a point on the RVE boundary. u_i^* refers to the periodic part of the displacement field, which is an unknown function influenced by the applied loading conditions. The procedure for applying periodic boundary conditions is described in detail in Chapters 3 and 4.

The homogenization technique is also employed to analyze how the RVE responds to mechanical loads, allowing the prediction of its mechanical properties. This assumption suggests that the average mechanical properties of the RVE align with those observed in the unidirectional composite lamina at the macrostructural level. A wide range of material properties can be ascertained by applying distinct and independent displacement conditions, by calculation of volume average stress and strain components that are defined as follows [68,69]:

$$\bar{\sigma}_{ij} = \frac{1}{A_{RVE}} \int_A \sigma_{ij} dA = \frac{1}{A_{RVE}} \sum_{k=1}^{N} \sigma_{ij}^k A^k \tag{1.3}$$

$$\bar{\varepsilon}_{ij} = \frac{1}{A_{RVE}} \int_A \varepsilon_{ij} dA = \frac{1}{A_{RVE}} \sum_{k=1}^{N} \varepsilon_{ij}^k A^k \tag{1.4}$$

where A_{RVE} denotes the total area of the representative volume element. σ_{ij}^k and ε_{ij}^k represent the stress and strain components, respectively, calculated at the integration point of the kth element, which has an area of A^k. N refers to the total number of integration points within the RVE model.

Several research works have examined the influence of voids, resulting in the development of two distinct approaches for their modeling, as depicted in Figure 1.7. The first method involves explicit modeling of voids, usually assuming circular holes in the transverse direction [58,70–74]. Another method for void modeling entails attributing air properties to specific matrix elements [75–79]. The model that explicitly incorporates circular voids showed variations in predicted failure strengths which closely resemble the observed behavior in experiments, primarily influenced by void distribution and area. However, the model that introduces voids within elements yielded similar results. Therefore, the first method was used in the present thesis to model voids in RVEs.

| Voids explicitly established | Voids modeled within the element |
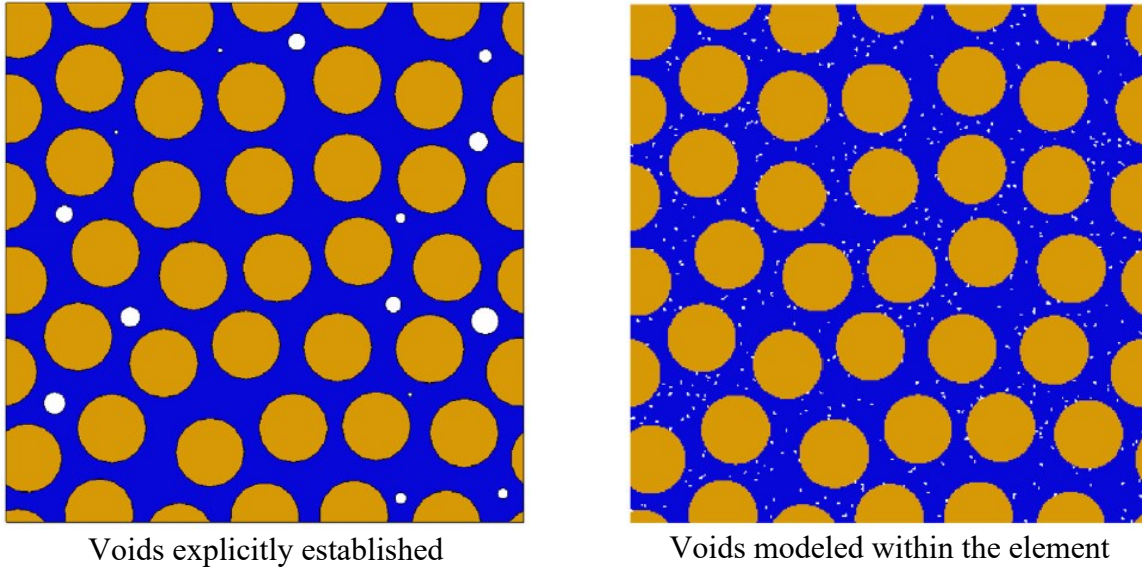
Figure 1.7. Example of RVEs containing voids with two different modeling approaches [45].

The reported material properties in the datasheet are attributed to either hot-pressed or autoclave-processed composite materials, which do not account for the distinct microstructural features introduced by the AFP process, such as increased void content, formation of resin-rich areas, and variations in the degree of crystallinity. These differences notably impact the material's behavior, particularly in the matrix-dominated transverse direction. Due to warpage introduced in AFP-fabricated thermoplastic composite laminates when a heated mandrel is not used, experimental characterization of the final composite part remains challenging. Thus, micromechanical modeling using the Representative Volume Elements (RVEs) approach emerges as a critical tool for predicting material properties and addressing the current gaps in mechanical property data for AFP-manufactured thermoplastic composite materials.

1.3. Scope and objectives of the thesis

In terms of the interlaminar bond strength resulting from the AFP in-situ consolidation versus that of the autoclave treatment, prior studies have only compared ILSS values measured by the SBS test for quality control purposes. None of them attempted to identify the interface strength properties that serve a vital contribution in finite element analyses of Carbon/PEEK thermoplastic composite laminates fabricated by in-situ consolidation, essential for advancing research on their mechanical behavior and response. Moreover, due to the difficulty in manufacturing flat thermoplastic composite laminate by the AFP technique in the absence of heated tool (warpage

phenomenon), the studies to date have been unable to investigate the stiffness and strength of in-situ-consolidated Carbon/PEEK thermoplastic composite laminate and draw a comparison with the material properties provided in technical datasheets for the autoclave-made counterpart. According to the identified knowledge gaps concerning Carbon/PEEK thermoplastic composite laminates in-situ consolidated by the Automated Fiber Placement (AFP) process, this thesis pursues three primary objectives related to the mechanical performance induced by the AFP in-situ consolidation technique: (1) to determine the interfacial strength properties governing delamination failure mode, (2) to predict the transverse tensile strength, and (3) to predict the effective stiffness properties, with particular emphasis on the transverse direction where the matrix phase predominantly influences the composite material response.

The present thesis will attempt to develop a methodology to predict the interface strength and material properties of Carbon/PEEK thermoplastic composite laminate manufactured by the AFP in-situ consolidation method. To achieve this, two sets of specimens will be produced by AFP in-situ consolidation and autoclave re-consolidation techniques to be evaluated by the Short-Beam Shear (SBS) test. Afterwards, Finite Element (FE) modeling will be implemented to computationally determine the proper interface strength properties, resulting from the AFP in-situ consolidation, using the cohesive element approach and ILSS values obtained through the SBS experiment. The outcome of this segment of the research work contributes directly to achieving the first objective outlined in the present thesis.

In composite structures, the initiation of transverse matrix microcracking typically marks the initial stage of failure and governs the development of fractures. Additionally, the existence of voids, interlaminar resin pockets, and a reduction in the degree of crystallinity substantially influence the material characteristics in the transverse direction. Thus, in the present thesis, the transverse cross-section of Carbon/PEEK thermoplastic composite material will also be investigated by computationally generating two-dimensional Representative Volume Elements (RVEs), featuring randomly distributed fibers, at a micro-scale. To ensure that comprehensive details are included in the micromechanical simulation, micrographic study and thermoanalytical Differential Scanning Calorimetry (DSC) analysis will be conducted on two distinct groups of Carbon/PEEK thermoplastic composite specimens fabricated through in-situ consolidation and autoclave re-consolidation processes. Finally, the effective transverse material properties (stiffness and

strength), caused by AFP in-situ consolidation, will be predicted by applying Periodic Boundary Conditions (PBCs) and using Asymptotic Homogenization Theory (AHT). The findings, meeting the second and third above-listed objectives of the present thesis, will prove highly beneficial in the finite element modeling, analysis, and design of Carbon/PEEK thermoplastic composite laminates in-situ consolidated by the AFP technique.

1.4. Thesis layout

This dissertation has been structured in accordance with the manuscript-based thesis format, as outlined in the "Thesis Preparation Guide" provided by the School of Graduate Studies at Concordia University. It comprises five chapters: an introductory chapter, three core chapters presenting the main research contributions aligned with the thesis objectives, and a concluding chapter summarizing the key findings and proposing directions for future research. Additionally, brief forewords are included to facilitate coherent transitions and interrelations between the individual journal papers.

Chapter 1 offers an overview of the Automated Fiber Placement (AFP) process, emphasizing its capabilities in fabricating both thermoset and thermoplastic composite components. Despite AFP's ability to in-situ consolidate the thermoplastic composite materials, thereby eliminating the need for post-processing steps like autoclave curing, achieving autoclave-level quality remains challenging due to the reduced processing time inherent in the AFP technique. This chapter identifies key knowledge gaps in the area of in-situ-consolidated thermoplastic composites, specifically concerning (a) interfacial strength characteristics and (b) mechanical properties (i.e., stiffness and strength). A concise literature review is provided on the Short-Beam Shear (SBS) test and associated failure mechanisms observed in experimental studies. Moreover, micromechanical modeling based on the Representative Volume Element (RVE) approach is introduced, with a focus on existing algorithms for generating realistic RVEs with high fiber volume fractions for accurate prediction of effective material properties. The chapter concludes with descriptions of the research scope, the thesis objectives, and the thesis outline.

Chapter 2 investigates the interlaminar shear performance of Carbon/PEEK thermoplastic composite laminates manufactured via Automated Fiber Placement (AFP) in-situ consolidation, in comparison to autoclave re-consolidation. Through Short-Beam Shear (SBS) testing, Interlaminar

Shear Strength (ILSS) values were measured for in-situ consolidated and autoclaved laminates. A finite element modeling approach employing cohesive elements was developed to simulate the experimentally observed shear behavior, considering both intralaminar and interlaminar damage types. By numerically determining the interface strength properties using the SBS test results, the model provides critical input parameters for future simulations of AFP-fabricated thermoplastic composite laminates and contributes to reaching the thesis's primary objective (i.e., AFP-influenced interfacial strength values) outlined before.

Chapter 3 presents a micromechanical investigation into the transverse tensile strength of in-situ consolidated Carbon/PEEK thermoplastic material produced by the AFP process. Accounting for manufacturing-induced variations, such as fiber volume fraction, void content, interlaminar resin pocket and degree of crystallinity, 2D Representative Volume Elements (RVEs) with randomly distributed fibers were developed to simulate the microstructure based on the data obtained by micrographic study and DSC analysis. The plastic deformation of the neat PEEK resin was modeled using the Drucker-Prager plasticity law, combined with the ductile failure criterion for matrix damage onset and evolution. A simulation methodology was proposed to address limitations in the experimental characterization of these materials due to induced warpage, highlighting the importance of accounting for reduced transverse properties in the design and analysis of AFP-manufactured thermoplastic composites. The findings from this portion of the research work support fulfilling the second aforementioned objective (i.e., prediction of transverse tensile strength resulting from the AFP process) of the present research.

Chapter 4 focuses on predicting the effective stiffness properties of in-situ consolidated Carbon/PEEK thermoplastic composite material, emphasizing the influence of microstructural variations introduced by the AFP manufacturing process. Utilizing 2D RVEs generated using the outcomes of micrographic and DSC analyses, the study quantifies the effects of fiber volume fraction, void content, degree of crystallinity, and resin-rich regions. The effective longitudinal elastic modulus, transverse modulus, out-of-plane shear modulus and out-of-plane Poisson's ratio, caused by the AFP in-situ consolidation process, were obtained through Periodic Boundary Conditions (PBCs) and Asymptotic Homogenization Theory (AHT). These findings underscore the necessity of incorporating transverse property degradation in the modeling and design of AFP-

made composite structures and allow for pursuing the third and final objective (i.e., prediction of effective stiffness properties caused by the AFP process) of the present thesis.

Chapter 5 provides overall conclusions and key contributions derived from the comprehensive investigation of Carbon/PEEK thermoplastic composite laminates manufactured by AFP in-situ consolidation. This chapter also offers some recommendations for potential future research work.

CHAPTER 2

Interlaminar shear strength of Carbon/PEEK thermoplastic composite laminate: Effects of in-situ consolidation by automated fiber placement and autoclave re-consolidation

This chapter contains the contents of the following journal and conference papers:

E. Pourahmadi, F. Shadmehri, R. Ganesan, "Interlaminar shear strength of Carbon/PEEK thermoplastic composite laminate: effects of in-situ consolidation by automated fiber placement and autoclave re-consolidation", *Composites Part B: Engineering*, 269 (2024), 111104. https://doi.org/10.1016/j.compositesb.2023.111104.

E. Pourahmadi, F. Shadmehri, R. Ganesan, "Interlaminar shear strength of Carbon/PEEK thermoplastic composite laminate in-situ consolidated by automated fiber placement" in the *13th Canadian-International Conference on Composites (CANCOM2024)*, Waterloo, Ontario, Canada, Aug. 2024

2. Interlaminar shear strength of Carbon/PEEK thermoplastic composite laminate: Effects of in-situ consolidation by automated fiber placement and autoclave re-consolidation

Foreword

Many researchers have worked on improving the processing conditions of Automated Fiber Placement (AFP), such as temperature, pressure and material feed rate. They evaluated the quality of Carbon/PEEK thermoplastic composite laminates by measuring their Interlaminar Shear Strength (ILSS) using the Short-Beam Shear (SBS) test. However, there is still a major gap in the available data on interface strength properties of in-situ-consolidated thermoplastic laminates. These properties are crucial for developing accurate finite element models and performing reliable structural analysis.

This chapter introduces a simulation methodology employing a three-dimensional model developed in ABAQUS/Explicit. This research work aims to numerically determine interface strength values based on Short-Beam Shear (SBS) test results, which was formerly identified as the first objective of the present thesis. Cohesive elements are placed between composite plies to accurately capture the delamination failure mode (interlaminar damage), observed during the SBS experiment. Furthermore, a user-defined VUMAT subroutine is implemented to incorporate Hashin failure criteria, enabling the prediction of intralaminar damage initiation and evolution, particularly in regions adjacent to the loading nose and supports, thereby enhancing simulation accuracy. Based on the findings, the interface strength values for AFP-fabricated Carbon/PEEK thermoplastic composite laminates were computationally determined to be 36 MPa and 45 MPa in the normal and shear directions, respectively. These properties are of great importance, as they are essential for future finite element analyses of in-situ-consolidated thermoplastic laminates, particularly when delamination is intended to be modeled as a potential failure mechanism.

Abstract

Automated manufacturing techniques, such as Automated Fiber Placement (AFP), offer an opportunity over conventional manufacturing methods, such as autoclave curing, to save time and expenses. The present research focuses on evaluating the Interlaminar Shear Strength (ILSS) of Carbon/PEEK thermoplastic composite laminates manufactured by AFP in-situ consolidation and autoclave re-consolidation using the Short-Beam Shear (SBS) test. Additionally, a methodology is proposed to capture the differences observed in ILSS using a finite element simulation. In this respect, a thermoplastic laminate was fabricated using AFP in-situ consolidation. Baseline laminate was also produced by re-consolidating another AFP-made laminate inside the autoclave. A micrographic study was conducted to investigate the void content and fiber distribution resulting from each manufacturing process. The test results showed that the AFP technique results in an ILSS of the laminate that is 37% lower than that of the autoclave-reconsolidated laminate. The distinct mechanical behavior in the SBS test arising from in-situ consolidation and autoclave re-consolidation was differentiated in the finite element modeling utilizing cohesive elements. This distinction was achieved by numerically finding the proper interface strength properties based on the SBS experimental results. These interface properties serve as valuable input parameters for conducting further finite element modeling and analyses of Carbon/PEEK thermoplastic composite laminates manufactured by AFP in-situ consolidation.

2.1. Introduction

Higher specific stiffness and strength, resistance to corrosion and lower weight compared to metals have resulted in the wide and constantly growing applications of polymeric composites in different structures such as aircraft and automotive structures. Automated manufacturing techniques, such as Automated Fiber Placement (AFP), offer an opportunity over conventional manufacturing techniques, such as hand lay-up, to reduce material waste, to increase the rate of deposition, to have greater design flexibility and to save manufacturing time and cost. These benefits make AFP a more cost-effective and efficient choice for fabricating composite components compared to the traditional autoclave treatment.

In-situ manufacturing of thermoplastic composites using the AFP process consists of three steps: 1- heating, 2- consolidation, and 3- solidification. The last two steps are of great importance in

terms of void content reduction and bonding between layers by applying heat and pressure in order to acquire optimum mechanical properties [6]. Void is one of the contributing factors which influences the mechanical performance of the final product. Generally, voids are divided into two categories: (a) Intralaminar voids, which are caused by the tape fabrication process, are those that are present within the tape. (b) Interlaminar voids are induced between plies during the tape placement which results from the surface roughness [7–9]. Because of the heat and pressure during the consolidation step, the tape surfaces, which have come into contact with each other, start flattening for the emergence of "intimate contact" [10]. Subsequently, due to the motion of molecular chains between the layers in intimate contact, which is known as "healing" (autohesion), bonding between layers occurs [11]. AFP in-situ consolidation is an attractive alternative technique to either the autoclave consolidation or compression press methods that can have a considerable influence on the consolidation step of the thermoplastic composite manufacturing process in terms of the void content and quality of the bonding between layers owing to the different approaches of applying heat and pressure.

Generally, the Short-Beam Shear (SBS) test is widely employed as a quality control method to investigate the effect of different parameters, such as defects and consolidation processes, on the Interlaminar Shear Strength (ILSS). Some studies [13,14] aimed to find the optimum in-situ AFP process parameters for the manufacturing of thermoplastic composites based on ILSS values. They focused on four processing parameters, namely process temperature, torch location, deposition rate and compaction force, and succeeded in determining the optimum conditions for carbon-fiber/PEEK composite with the help of the Taguchi method and a great number of experimental tests. Short-beam shear tests were used by Khan *et al.* [16] to assess the bonding degree of AFP-fabricated CF/PEEK laminates with various processing parameters, including heating, layup velocity, tool temperature and consolidation pressure. They found out that temperature and pressure should be kept under control in order to reduce the void content, improve the interface cohesion and prevent the thermal degradation of thermoplastic composites. Nevertheless, Qureshi *et al.* [15] reported that there is no correlation between interlaminar shear strength and compaction force for CF/PEEK composites. Changing the processing parameters can affect the cooling rate, which is responsible for the degree of crystallinity, and hence the material strength. Khan *et al.* [16] showed that layup velocity has a major impact on the quality and interface strength of CF/PEEK because of the change in the cooling rate. It should be noted that they succeeded in

obtaining the interlaminar shear strength of 85.5 MPa, which is close to the ILSS of autoclave-treated CF/PEEK, by lowering the deposition rate (50 mm/s) and the use of a heated mandrel which enhance the degree of crystallinity. Stokes-Griffin and Compston [17] also examined the relationship between the process temperature and Interlaminar shear strength of in-situ consolidated CF/PEEK samples using various deposition rates of Near Infra-Red (NIR) laser-assisted Automated Tape Placement (ATP). They reported that they even obtained higher ILSS values for the CF/PEEK thermoplastic samples manufactured by in-situ consolidation (using 100 mm/s deposition rate) compared to the autoclave-treated reference sample with 94.8 MPa ILSS. It is worth mentioning that no other studies repeated the above study so far. ILSS values that different researchers obtained for Carbon/PEEK thermoplastic composite using in-situ consolidation and autoclave re-consolidation manufacturing processes are listed in Table 2.1.

Table 2.1. Interlaminar shear strengths obtained by SBS test for CF/PEEK thermoplastic composite manufactured by autoclave reconsolidation and in-situ consolidation with various deposition rates.

References	Autoclave re-consolidation	AFP In-situ consolidation	
	ILSS (MPa)	ILSS (MPa)	Rate (mm/s)
Cai et al. [13]	-	51	50.8
Tierney and Gillespie [28]	90	60	30
Qureshi et al. [15]	92.7	49.2	65
		78.9[1]	127
Khan et al. [16]	94.8	85.5[2]	50
Stokes-Griffin and Compston [17]	94.8	98[1]	100

[1]In-situ consolidation using a laser heating system
[2]In-situ consolidation using heated mandrel

Nonetheless, according to the research performed by Chen et al. [80], void content and its distribution significantly influence the interlaminar shear and compressive strengths of CF/polyphenylene sulfide (PPS) composites. Furthermore, there are contradictions among researchers regarding the effect of roller passes during the AFP process. Khan et al. [16] concluded that interlaminar shear strength is increased by performing repasses whereas Chanteli et al. [41] only reported an improvement in the surface finish quality of CF/PEEK composites, similar to the results obtained by Shadmehri et al. [5]. Comer et al. [38] also presented the positive effect of repass on the degree of crystallinity while Shadmehri et al. [5] showed that repass treatment can lead to a decline of 6% (after two repasses) in the degree of crystallinity of carbon fiber/PEEK

composite. That's why it is challenging to manufacture a thermoplastic laminate using the AFP technique with the same quality as autoclave consolidation.

Delamination, which highly depends on the matrix behavior, is the dominant mode of failure during the short-beam shear test. In order to analyse the separation of the layers in the finite element modeling, the cohesive zone model (cohesive surface or element) is widely used in the literature [18–23]. Liu *et al.* [27] employed numerical analysis, integrating intralaminar and interlaminar damage models, to evaluate CF/PEEK, manufactured by out-of-autoclave methods such as hot press, performance in three-point bend flexural loading, demonstrating close alignment between simulation and experimental data in mechanical response and damage morphology.

There is a considerable difference in the interlaminar shear strengths of thermoplastic composite samples manufactured using AFP in-situ consolidation compared to those manufactured using autoclave re-consolidation (see Table 2.1). This disparity is due to variations in factors such as void content, degree of crystallinity and fiber distribution. These differences are caused by the AFP processing parameters and the limited period of time available for the healing process during in-situ consolidation. The objective of the present research is to propose a novel methodology to differentiate between the mechanical responses of in-situ-consolidated and autoclave-reconsolidated thermoplastic composite samples in the FE modeling by finding appropriate interface strength properties based on the SBS experimental results. In the present work, a thermoplastic (carbon fiber/PEEK) composite laminate was fabricated by in-situ consolidation using AFP. Afterward, half of the AFP-made laminate was reconsolidated inside the autoclave to be considered as the reference laminate. The manufacturing quality of both laminates was evaluated by performing a Short-Beam Shear (SBS) test according to ASTM D2344 [12]. Moreover, finite element analysis was carried out to predict the composite damage onset and propagation by combining a VUMAT subroutine along with cohesive elements in ABAQUS software to model the delamination, which is the dominant mode of failure during the SBS test. The interface properties that led to the correlation between finite element analysis and test results can be used for further FE modeling and analyses (e.g., for the investigation of the effect of defects) of Carbon/PEEK thermoplastic composite laminates manufactured by in-situ consolidation. The numerical and experimental results were compared with each other to find out the capability of the proposed FE model in predicting the interlaminar shear strength.

2.2. Experimentation

One of the great advantages of thermoplastic composites compared to thermoset counterparts during the AFP manufacturing process is the possibility of in-situ consolidation with the help of a heating source like a hot gas torch, laser, infrared or flashlamp/pulsed light heating systems, whereby any secondary process (e.g., autoclave and hot press) is avoided which is costly and time-consuming. The choice of a heating system depends on factors such as resin type, material, desired temperature profile and manufacturing flexibility. The traditional hot gas torch method suits both thermoset and thermoplastic composite applications and has been used since 1986 as the primary heat source for AFP due to its low cost and wide process window. Laser heating has high energy density, faster processing rates and a better surface finish compared to hot gas torch; it has gained more popularity among manufacturers recently. However, laser cannot be used in the manufacturing of glass fiber composites since glass fibers do not absorb the laser energy. Strict safety regulations regarding the use of the laser heating system must be considered during manufacturing. Additionally, challenges arise in precisely controlling the laser beam to focus on the nip point and heat the appropriate areas. On the other hand, a hot gas torch spreads out the heat which helps to preheat the tape and the substrate [81,82]. The infrared (IR) heating system has attracted less attention in comparison with its counterparts due to its inefficiency in transferring heat and its inability to provide uniform heating, which results from wide heat dispersal. Additionally, the heat produced by the IR is insufficient for the manufacturing of thermoplastic composite materials. The flashlamp/pulsed light systems offer precise heating control during the layup and are relatively new in the composite manufacturing sector [83,84].

Although in-situ consolidation provides engineers with a quick method of fabrication, some inherent defects may be introduced in the automated fiber placement technique which can affect the mechanical performance of the composite part adversely. One of the characteristics of AFP in-situ consolidation is the short period of time that the tape is under a compaction roller which leads to incomplete autohesion. Even though tape smoothness and high compaction force contribute to the reduction in the duration required for intimate contact generation, a certain amount of time is needed for perfect autohesion based on the type of thermoplastic resin, which is usually more than the period available during the in-situ consolidation. The number of passes can have a positive effect on this phenomenon whereas they cause other problems, e.g., a rise in manufacturing time.

Moreover, such a short processing time causes the laid-down tape to be exposed to ambient temperature quickly, leading to a significant cooling rate, whereby the degree of crystallinity is negatively affected. A heated mandrel is suggested to overcome this issue by lowering the cooling rate. However, such a solution is impractical for large samples and alters the mechanical properties to the point that it is not considered in-situ consolidation anymore. On the contrary, autoclave treatment involves subjecting the vacuum-bagged composite laminate to heat and pressure for an extended duration and allows for a well-controlled cooling process. Therefore, the autoclave manufacturing process contributes to considerably better bonding (i.e., intimate contact and autohesion) between thermoplastic composite layers and a higher degree of crystallinity compared to AFP in-situ consolidation.

In this regard, the Short-Beam Shear (SBS) test, which is considered a materials screening and quality control method, was employed to investigate the mechanical performance of thermoplastic composite laminates manufactured by in-situ consolidation. It should be noted that for comparison purposes, some reference samples were also reconsolidated using the autoclave as a secondary treatment after the Hot Gas Torch (HGT)-assisted AFP process to assess the impact of in-situ consolidation alone on the interlaminar shear strength. Moreover, a micrographic study was conducted for both types (in-situ-consolidated and autoclave-reconsolidated) of thermoplastic laminate samples to investigate the extent of void content and fiber distribution in serving as two contributing factors that result in a clear distinction between AFP in-situ consolidation and autoclave reconsolidation processes.

2.2.1. Materials and manufacturing

2.2.1.1. Automated fiber placement process

Concordia Centre for Composites (CONCOM) provides researchers with an AFP machine made of a 6-axis Kawasaki articulated robot arm with a 125 kg payload on which a thermoplastic head supplied by Trelleborg has been mounted. In the present research, HGT-assisted AFP was used along with a flat paddle tool (aluminum mandrel) to manufacture a carbon fiber/PEEK (AS4/APC-2) plate by in-situ consolidation. Unidirectional carbon fiber/PEEK tape from Solvay Group with a width and thickness of 6.35 mm (0.25 in) and 0.140 mm (0.0055 in), respectively, was used in this study. In order to apply pressure and heat to melt the incoming tape, a steel roller and a nitrogen hot gas torch were used. To this end, the hot gas torch temperature and flow were set to 875° C

and 80 SLPM, respectively. High-temperature resistant steel roller was employed to apply 60 lbf compaction force, and the deposition rate was adjusted to 50.8 mm/s (2 in/s).

In order to create a flat thermoplastic laminate, the paddle tool was first wrapped with a substrate layer. Afterward, tapes were laid down on top of the substrate layer to create a laminate with $[0]_{17}$ layup and dimensions of 40 cm × 12 cm as shown in Figure 2.1.
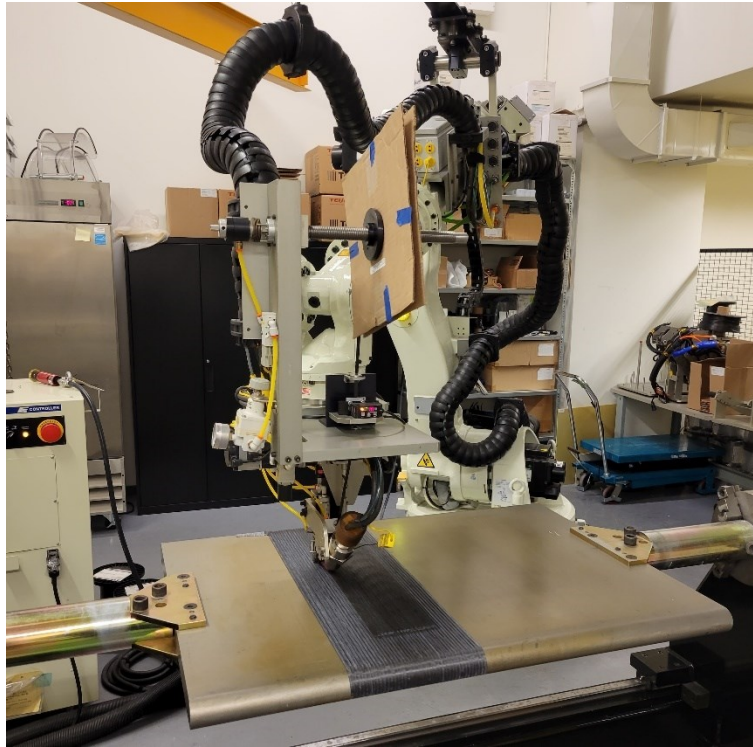
Figure 2.1. Automated fiber placement machine with a flat aluminum mandrel.

2.2.1.2. Autoclave curing and vacuum bagging processes

In order to compare the effect of the AFP in-situ consolidation manufacturing process on the interlaminar shear strength performance of thermoplastic composites, the in-situ-consolidated plate was cut in half, bagged and reconsolidated in the autoclave to be considered as a reference plate, as shown in Figure 2.2.
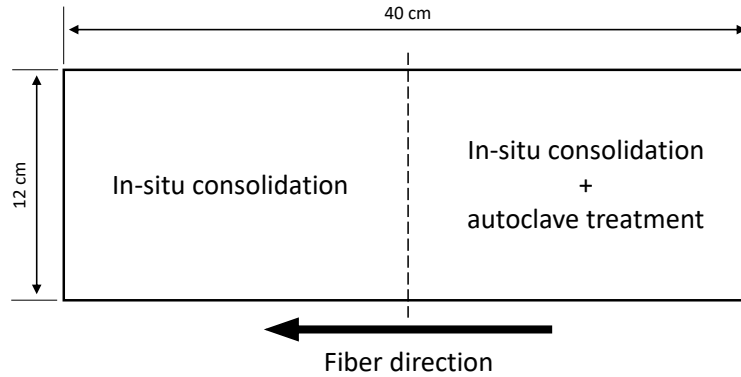
Figure 2.2. Thermoplastic plate which was fabricated by in-situ consolidation and cut in half to get treated inside the autoclave.

Because of the high temperature inside the autoclave, the vacuum bagging process for thermoplastic composites is different from that for thermoset composites. PEEK requires a temperature of 390° C (735° F), so all the materials used for the vacuum bagging process are able to withstand high temperature. In this regard, the autoclave-reserved plate was covered by Kapton® film and placed between two steel caul plates. It is worth mentioning that in order to make it easier for the Kapton® film to be peeled off from the laminate, it was coated with Frekote® 770-NC release agent. Thereafter, this structure was covered by glass fabric breather cloth. Kapton® film was again placed on top of it. In the end, the whole vacuum bag was sealed with the help of high-temperature sealant tape and clamped by a steel frame in order to prevent any possible leaks at the high temperature inside the autoclave, as shown in Figure 2.3. The aforementioned steps of the vacuum bagging process can be seen in Figure 2.4.
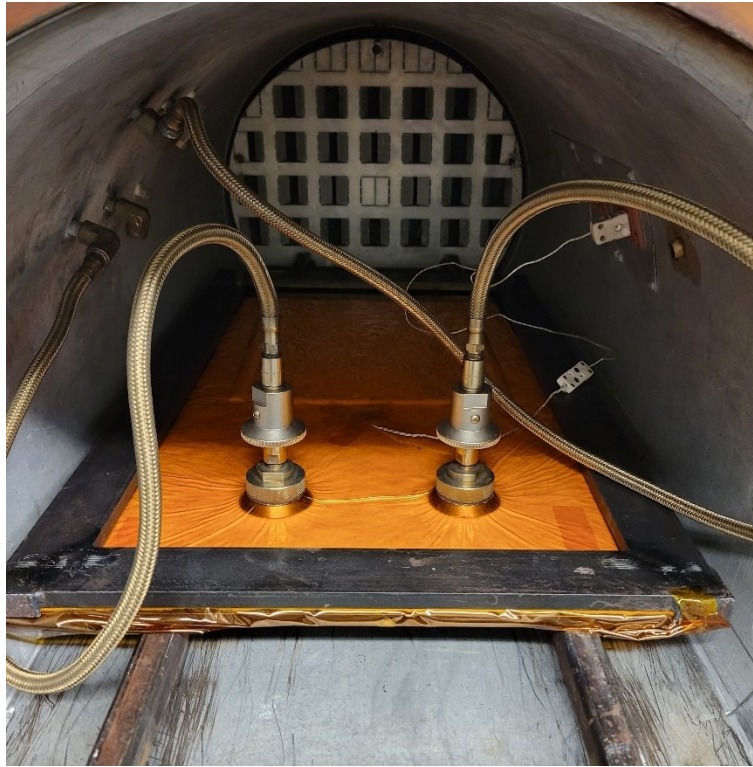
Figure 2.3. Vacuum-bagged thermoplastic laminate manufactured by in-situ consolidation.

1- Kapton film
2- Glass fabric breather cloth
3- Stainless steel plate
4- Woven fiberglass cloth

5- High-temperature sealant tape
6- AFP-manufactured CF/PEEK
7- Steel flat mold
8- Vacuum valve
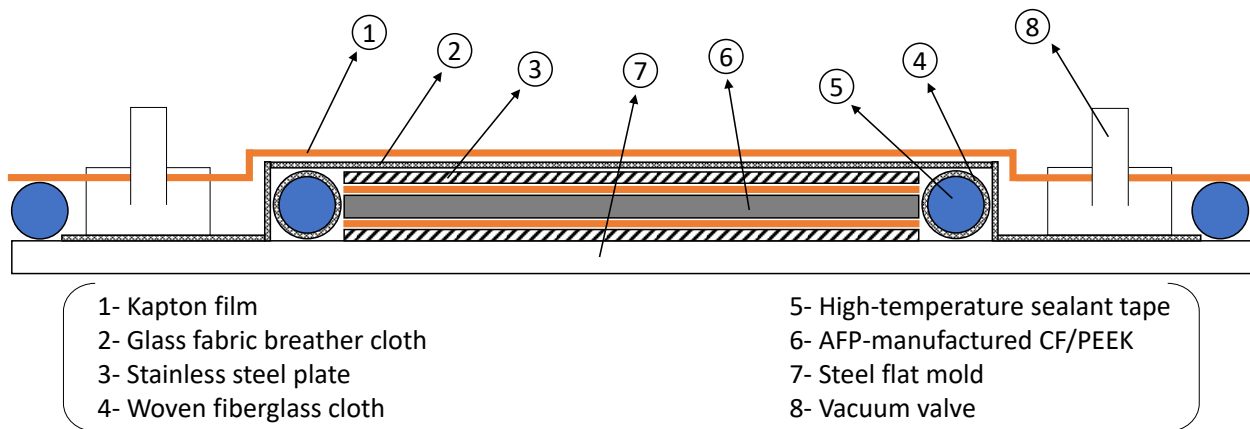
Figure 2.4. Schematic cross-section of the vacuum-bagged thermoplastic laminate.

Subsequently, the vacuum-bagged thermoplastic laminate was placed inside the autoclave. The temperature was increased to $390° \pm 10°$ C $(735° \pm 15°$ F) and was kept constant for 20 ± 5 minutes while the pressure of 100 ± 5 psi was applied to it [67]. The processing cycle of the autoclave can be seen in Figure 2.5

Hold at 735° ± 15° F, 100 ± 5 psi for 20 ± 5 minutes

Heat-up at any rate

Cool down at 1 - 1300° F/minute
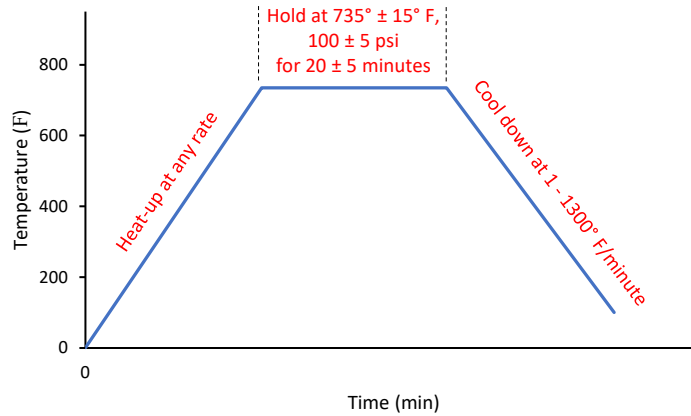
Figure 2.5. Cure cycle of CF/PEEK for autoclave consolidation.

2.2.2. Micrographic study

Investigating the microstructure of the thermoplastic composite samples manufactured by in-situ consolidation and autoclave treatment can provide researchers with valuable insights into the origins of variations in mechanical performance. In this regard, samples from both plates were cut, embedded in resin and cured for a day and polished (starting with 180, 326 and 600-grit sandpapers and proceeding to 9 and 3-micron diamond suspensions, respectively) to get ready for microscopy imaging. Micrographs of AFP and autoclave-made samples are depicted in Figure 2.6 with different magnifications. It is obvious from micrographs that autoclave treatment can have a significant influence on the microstructure (fiber distribution) of composites fabricated by AFP. Autoclave consolidation has allowed fibers to move along the thickness in a way that boundaries between adjacent layers are hardly discernible. On the contrary, resin-rich areas and nonuniform fiber distribution, which may be considered as stress concentration regions affecting the delamination failure mode, can be clearly noticed in the micrograph of the samples created by in-situ consolidation.

AFP – 5X magnification	Autoclave – 5X magnification
AFP – 20X magnification	Autoclave – 20X magnification
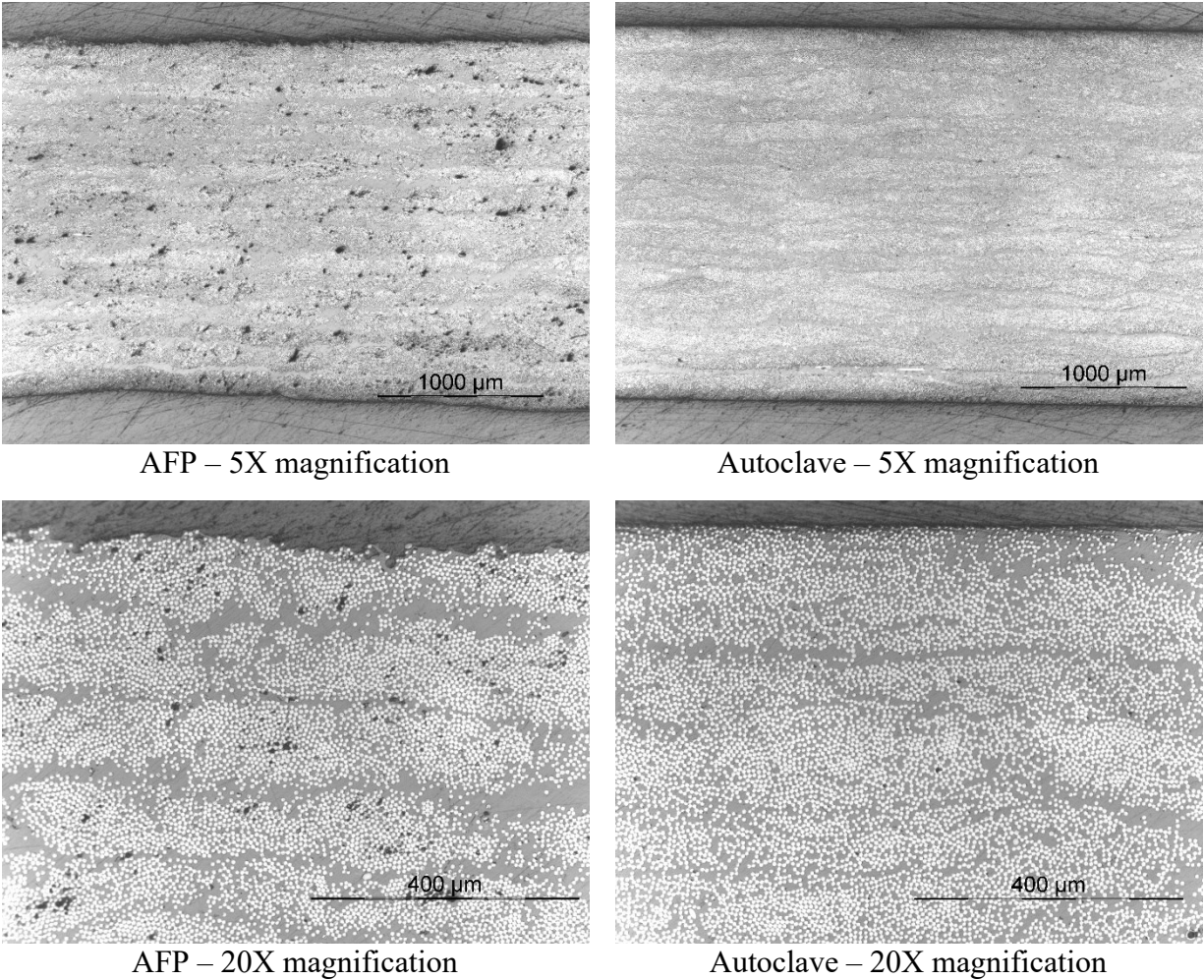
Figure 2.6. Micrographs of samples manufactured by AFP in-situ consolidation vs. autoclave reconsolidation.

Moreover, surface finish quality and void content are other features that should be regarded. According to the micrographs in Figure 2.6, it is evident that the surface roughness of the autoclave-manufactured samples has substantially improved. That's why an in-situ method called repass is used for the thermoplastic composites created by AFP to enhance surface smoothness, in particular for aerodynamic applications [5]. Concerning the void content, the influence of autoclave treatment was also investigated on the extent of voids with the help of micrograph analysis. In this regard, eight images with 20X magnification were obtained from each sample and placed next to each other by the stitching technique using the ImageJ software [43,44] in a way that covers the whole thickness. Afterward, void content was calculated with the help of the color thresholding technique which can differentiate between voids, fibers and resin. As presented in Figure 2.7, void content values are 1.57% and 0.09% in thermoplastic samples manufactured by

AFP in-situ consolidation and autoclave reconsolidation, respectively, which can be considered as one of the contributing factors having a negative impact on the mechanical performance of final products made by AFP.
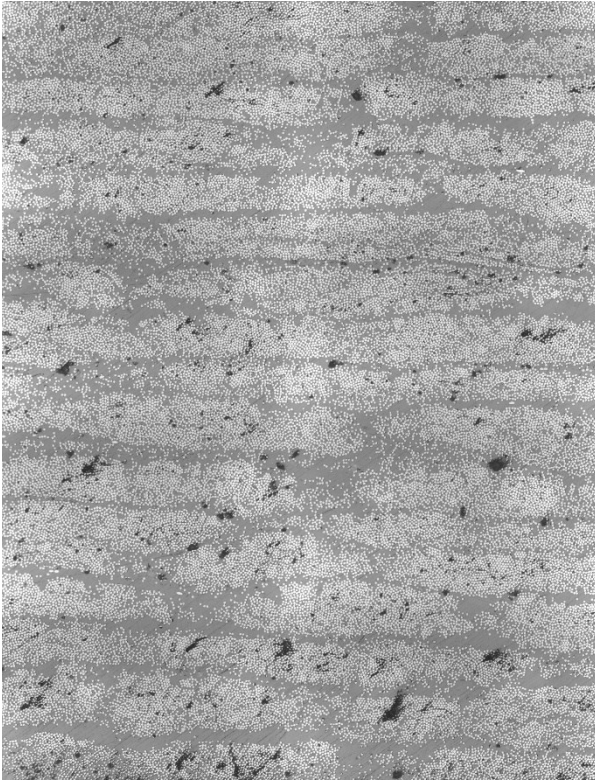
AFP – 20X magnification   Void content = 1.57%
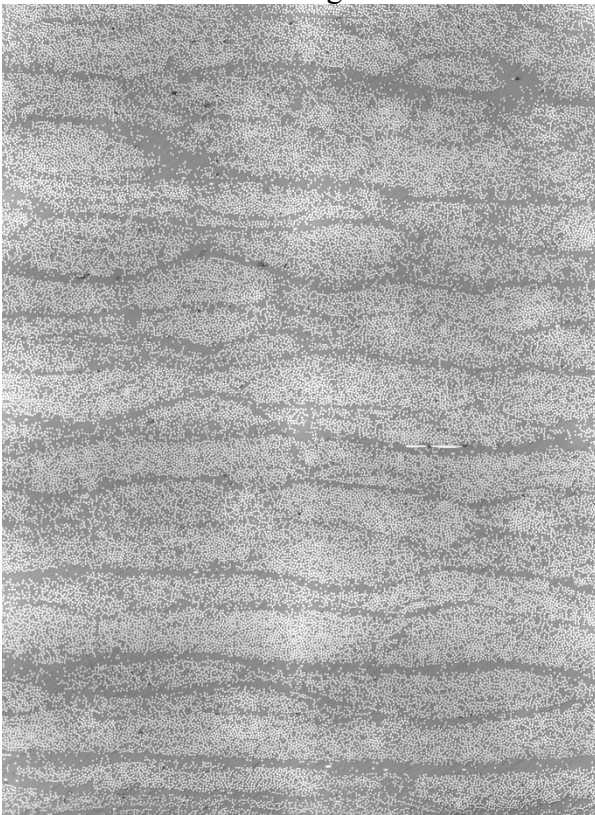
Autoclave – 20X magnification   Void content = 0.09%

Figure 2.7. Void content calculated with the help of image stitching and color thresholding techniques.

2.2.3. Short-beam shear test

Short-beam shear (SBS) test is a method to assess the interlaminar shear strength (ILSS) of high-modulus fiber-reinforced composite materials according to the ASTM standard D2344 [12]. It also allows researchers to use either flat coupon samples or curved ones for shear properties evaluation. In the present work, almost flat coupon samples were cut from the laminates manufactured by AFP and autoclave using the circular diamond saw. It should be noted that although the AFP-manufactured thermoplastic laminate exhibited warpage due to in-situ consolidation, the specimens were cut from the central region of the laminate in sufficiently small sizes, making the warpage negligible. Therefore, they can be regarded as flat, similar to autoclaved specimens. Dimensions of samples (19 mm × 6 mm × 2.4 mm) were followed according to the ASTM D2344 recommendation and presented in Figure 2.8. It should be noted that the thickness of the samples treated inside the autoclave decreased from 2.4 ± 0.037 mm to 2.3 ± 0.024 mm due to the elimination of voids and the release of the excessive amount of resin. Furthermore, a visual inspection was conducted in order to ensure that edge delamination has not happened during the cutting process.

(a)	(b)
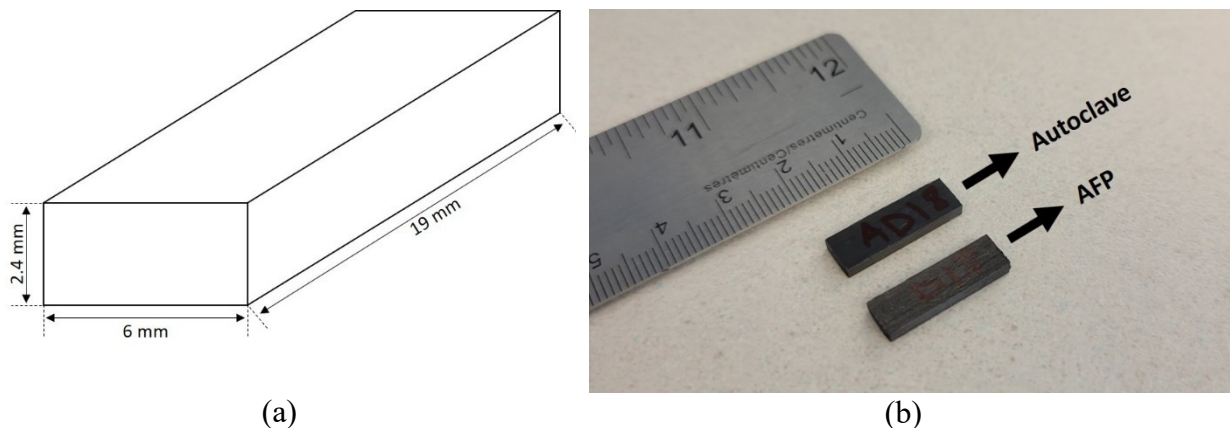
Figure 2.8. Dimensions of the flat coupon specimens manufactured using AFP in-situ consolidation and autoclave reconsolidation: (a) schematic view and (b) cut samples.

In order to perform the test, an SBS fixture, as shown in Figure 2.9, supplied by Wyoming Test Fixtures Inc. (WTF) was used. In accordance with ASTM D2344, the fixture's loading nose and supports have a diameter of 6 mm and 3 mm, respectively. The span length to thickness ratio was adjusted to 4.0. Both the loading nose and side supports overhung the specimen width by at least 2 mm. Five samples were tested from each plate to measure the interlaminar shear strength (ten samples in total). The test was run in displacement control mode at a rate of crosshead movement

of 1.0 mm/min using a universal hydraulic testing system. The ILSS values were calculated for each sample using the equation presented below:

$$F^{sbs} = 0.75 \times \frac{P_m}{b \times h}$$ (2.1)

where b and h are the specimen width and thickness. F^{sbs} and P_m represent short-beam strength and maximum applied load, respectively.
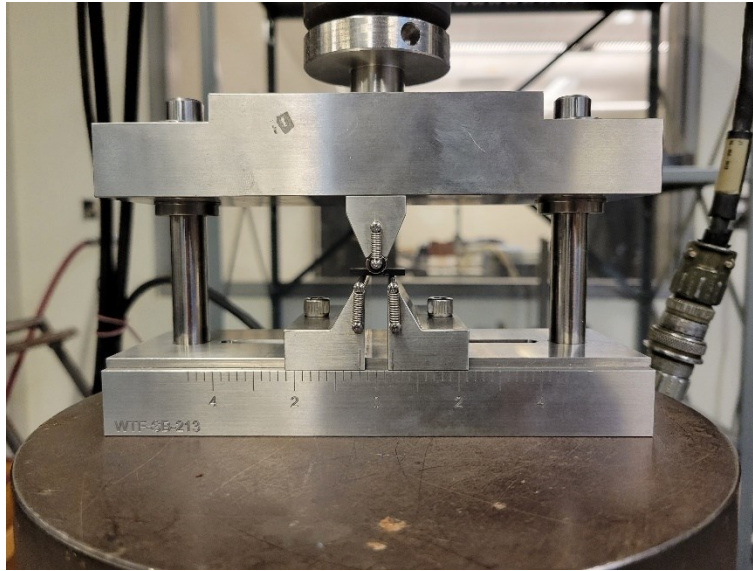
Figure 2.9. Experimental setup for the short-beam shear test using the WTF fixture.

2.3. Numerical simulation

Numerical simulation was conducted in the present work to predict the different mechanical response of CF/PEEK thermoplastic composites which is caused by in-situ consolidation and autoclave reconsolidation manufacturing processes. In this regard, a 3D model was created in ABAQUS/Explicit software to perform a finite element analysis for the short-beam shear test as shown in Figure 2.10. Because the dominant mode of failure in the SBS test is delamination, the cohesive element technique was employed to capture the layers separation phenomenon in conjunction with a VUMAT subroutine written in FORTRAN programing language (refer to "VUMAT subroutine" section in the Appendix for more details about the code) to do the composite damage modeling. Generally, cohesive elements are used to represent the cohesive forces (tractions) across a crack or interface between two adjacent material regions, where delamination

34

is expected to happen, during the computational modeling of material and structural behavior. These elements simulate cohesive behavior by defining a relationship between the normal and tangential tractions to outline how tractions vary with either sliding or separation of the crack surfaces. Specimens were modeled based on the aforementioned dimensions and layup using eight-node linear reduced integration solid elements C3D8R. Concerning the cohesive zone, the eight-node solid elements with cohesive characteristics COH3D8 and a thickness of 0.01 mm were placed between composite layers, which can be easily created by sectioning the model along the thickness. When cohesive elements are modeled using a traction-separation response, ABAQUS sets the constitutive thickness, which defines the relationship between stress and strain for the traction-separation law, to one by default. This assumption is based on the fact that, in most applications where traction–separation laws are suitable, the geometric thickness (physical thickness) of cohesive elements is either zero or negligible. By adopting this default value, the software ensures that the nominal strains directly correspond to the relative separation displacements [85]. Since maximum interlaminar shear stress occurs in the middle of the thickness, where it is more prone to delamination, cohesive elements were embedded in every other ply except in the middle, where they were placed successively, as depicted in Figure 2.11. The loading nose and supports were considered as discrete rigid shells. In order to prevent the penetration of rollers into the modeled composite beam, general contact interaction was defined between them. Hard contact mode was considered for normal behavior, and a friction coefficient of 0.3 was used for metal-laminate tangential behavior [22,86–88].
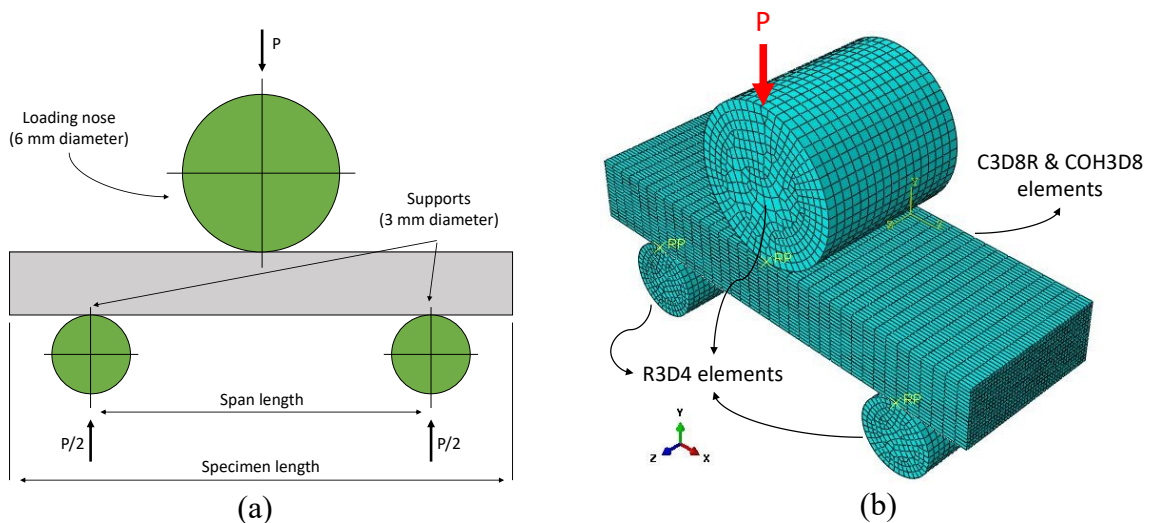
Figure 2.10. (a) Schematic of short-beam shear test and (b) Finite Element model created in ABAQUS software.
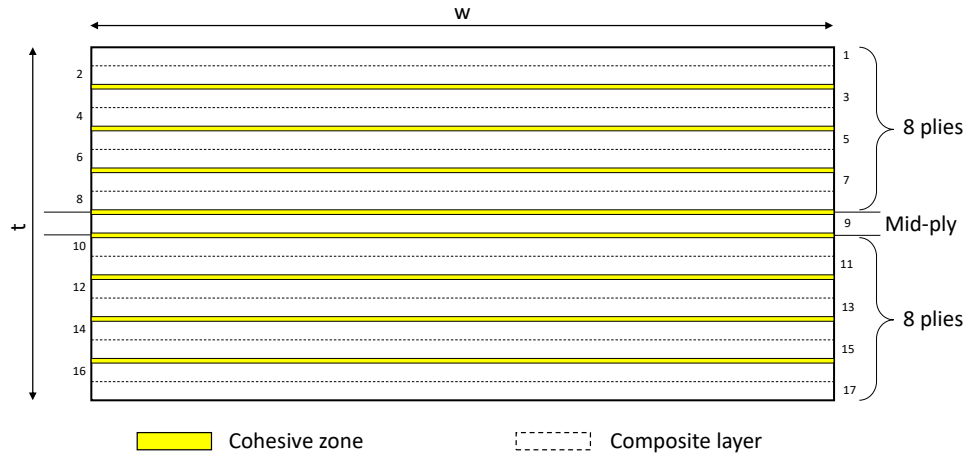
Figure 2.11. Cross-section view of the thermoplastic laminate model created in ABAQUS showing the locations of the cohesive zones.

2.3.1. Material damage model

Generally, two types of damage (intralaminar and interlaminar) can initiate and propagate in composite laminates. Intralaminar damage, which occurs inside a layer, can be captured by implementing different composite damage models whereas cohesive zone is required for the simulation of interlaminar damage (delamination). Furthermore, composite laminates are known for their nonlinear behavior in shear; therefore, this phenomenon must be considered in numerical analysis to achieve a good correlation with experimental results.

2.3.1.1. Composite damage model

El-Sisi *et al.* [24] investigated three distinct material models, namely the Ply Discount Model (PDM), Simple Progressive Damage Model (SPDM) and Continuum Damage Mechanics Model (CDMM). It was observed that CDMM can achieve a close correlation with experimental results with the least dependency on mesh size. Furthermore, the accuracy of three different damage evolution laws known as linear, quadratic and exponential was assessed. It was realized that all of them predict roughly the same outcome. In the present research, for damage initiation prediction in the composite specimen, the continuum damage mechanics model was used in conjunction with 3D Hashin failure criteria [26] which consider the fiber and matrix failure modes under both tensile and compressive loading conditions.

Regarding the damage propagation, the linear softening damage model [22,25] was employed for composite damage modeling based on the corresponding Hashin tensile and compressive modes

of failure. Once the damage initiates and propagates, the stiffness matrix of the failed element is degraded. During the damage evolution, components of the stiffness matrix need to be changed based on the type of failure mode in order to get the degraded stresses. In this regard, three damage parameters d_f, d_m and d_s representing fiber, matrix and shear damages, respectively, were defined during the finite element modeling (refer to "Composite damage model" section in the Appendix for more details about equations and formulae).

2.3.1.2. Nonlinearity

Generally, composite materials have nonlinear behavior, particularly in shear. Consequently, it is of vital importance to consider such a response in numerical analysis to establish a good correlation with experimental results. In the present research, one-parameter plasticity model proposed by Sun and Yoon [89] was employed. In order to form a relationship between the stress states in material and global directions, they introduced concepts of effective stress, σ_{eff}, and effective strain, ε_{eff}^p. A quadratic stress-based yield function for the general 3D fiber-reinforced composites is proposed as follows [90]:

$$
\begin{aligned}
2f(\sigma_{ij}) = {}& a_{11}\sigma_{11}^2 + a_{22}\sigma_{22}^2 + a_{33}\sigma_{33}^2 + 2a_{12}\sigma_{11}\sigma_{22} + 2a_{13}\sigma_{11}\sigma_{33} + 2a_{23}\sigma_{22}\sigma_{33} \\
& + 2a_{44}\tau_{23}^2 + 2a_{55}\tau_{13}^2 + 2a_{66}\tau_{12}^2
\end{aligned}
\tag{2.2}
$$

where f and a_{ij} denote the plastic potential function and amount of anisotropy in the plasticity, respectively.

The aforementioned yield function can be simplified by considering the fact that unidirectional composite laminates are transversely isotropic and behave in a linear elastic manner (linear stress-strain relation) in fiber direction [89] (refer to "Nonlinearity" section in the Appendix for more details).

2.3.1.3. Cohesive zone damage model

In addition to the intralaminar damage initiation and propagation modeling considered for the composite sample, cohesive elements were employed between layers to capture the delamination (interlaminar) initiation and evolution at the composite interface. This is exactly where the mechanical response of in-situ consolidated thermoplastic composite samples is differentiated from their autoclave-reconsolidated counterparts. To this end, traction-separation response with

linear elastic behavior, as shown in Figure 2.12, was taken into account in the cohesive zone for three different failure modes of delamination, namely mode I, mode II and mode III [18,19].
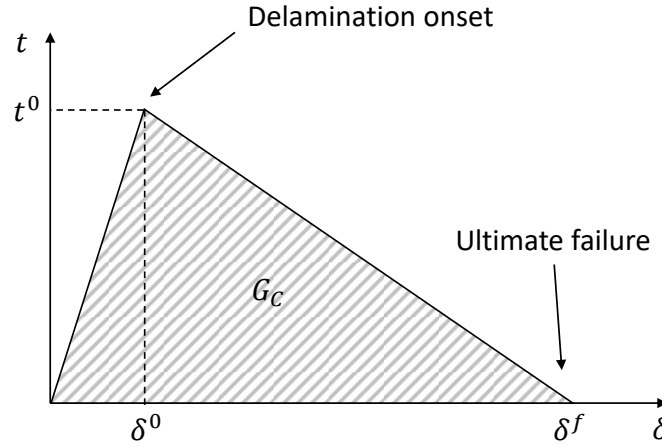
Figure 2.12. Bilinear traction-displacement diagram for a cohesive element under mixed-mode loading conditions.

Generally, delamination happens under mixed-mode loading conditions. Thus, the quadratic-stress failure criterion [18,19] was employed to predict the delamination onset, given by:

$$\left(\frac{t_n}{N}\right)^2 + \left(\frac{t_s}{S}\right)^2 + \left(\frac{t_t}{T}\right)^2 = 1 \tag{2.3}$$

where t_n, t_s and t_t are normal and shear tractions. N, S and T denote normal and shear cohesive strengths, respectively.

Once the delamination initiates, the linear softening law is used to predict the damage evolution. In the same way as that of aforementioned intralaminar damage modeling, cohesive stiffness should be degraded in order to obtain the effective tractions in the cohesive zone (refer to "Cohesive zone damage model" section in the Appendix for more details). The flow chart of the continuum damage mechanics model (CDMM) along with the interlaminar damage (delamination) initiation and evolution is presented in Figure 2.13.
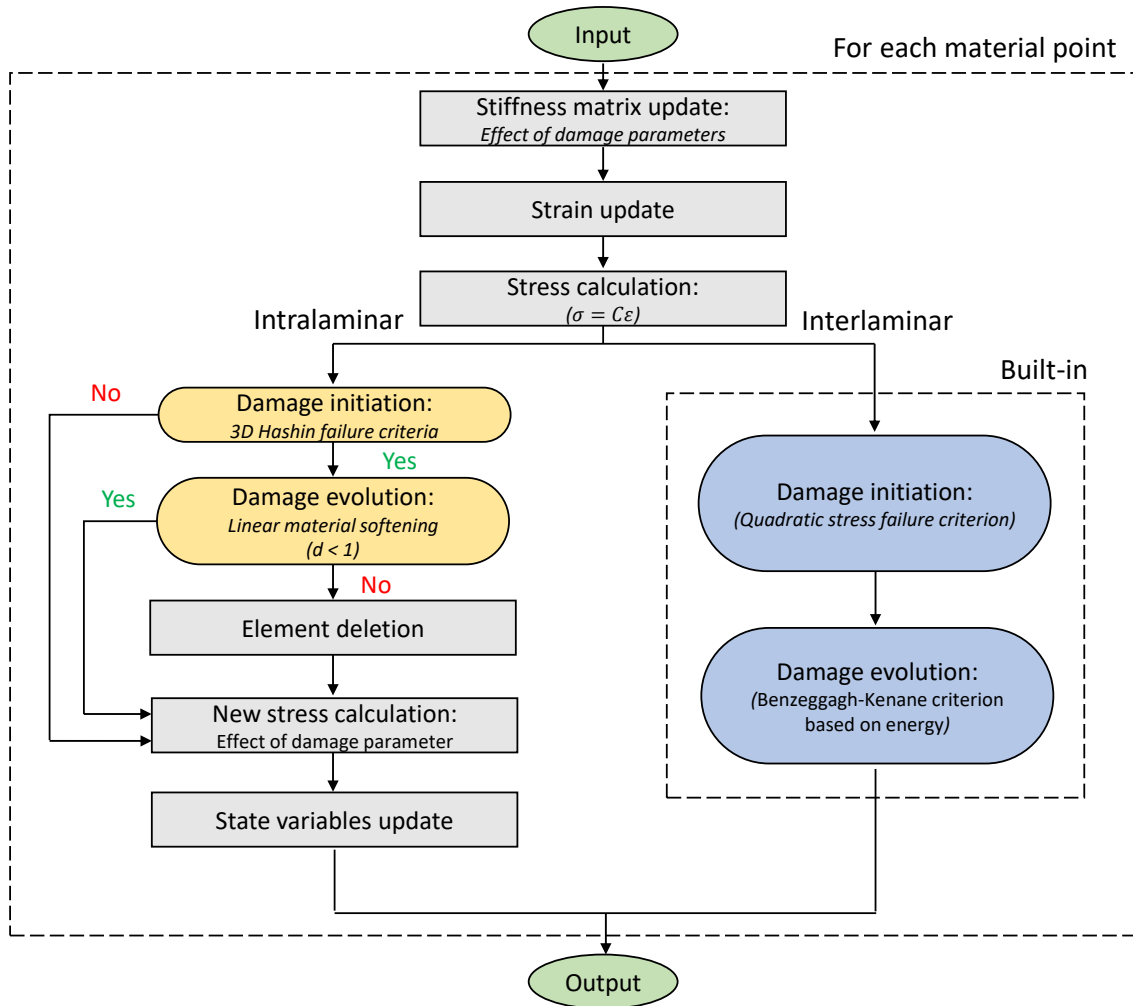
Figure 2.13. Flow chart of continuum damage mechanics and cohesive zone models implemented with the help of the VUMAT subroutine and built-in traction-separation response.

2.3.2. AFP in-situ consolidation vs. autoclave reconsolidation: Input parameters for the simulation

The major difference between the thermoplastic laminate samples manufactured by AFP in-situ consolidation and autoclave reconsolidation is related to the cohesion of layers. During the AFP in-situ consolidation, the top layer is subjected to heat and pressure just for few seconds whereas the thermoplastic composite layers reconsolidated inside the autoclave have an adequate amount of time to adhere to each other (discussed in detail in section 2.2). In order to reflect this distinction in simulation, different appropriate values of interfacial (interlaminar) properties, including strength and fracture toughness, should be used for in-situ-consolidated samples.

Unlike the interlaminar strengths for which there is no specific method to quantify them, intralaminar tensile and shear strengths can be measured by performing certain quite simple tests on unidirectional laminates [91,92]. Furthermore, the independent J integral path method is a technique to calculate the cohesive strengths based on the crack-tip opening displacement and linear elastic fracture mechanics (LEFM) [93,94]. Even though LEFM provides a way to compute the interface strength, since in practice delamination initiates and propagates in a split second, it is nearly impossible to measure the crack-tip opening precisely. In this respect, in-plane intralaminar strengths (transverse tensile and shear strengths) were employed for interfacial strengths in numerical simulations [95]. Few studies showed that such an assumption can cause a serious error in failure prediction in comparison with test results [96]. Thus, researchers attempted to find adjusted (reduced) values of interfacial strength by trial and error in order for simulation results to be in good agreement with experimental data [97–100]. As a result, in this study, appropriate interface strength properties for the AFP in-situ consolidation manufacturing process were found in such a way that the interlaminar shear strength measured by the SBS experiments matches the ILSS obtained in the numerical simulation, as listed in Table 2.2. It should be noted that although interface strengths were adjusted to predict the outcome of the experiment, there are other factors, such as composite damage modeling and nonlinear behavior, which prevent obtaining exactly the same experimental results in finite element modeling. A good literature review on interfacial strength values used by different researchers in numerical analyses under various loading conditions is presented by Lu *et al.* [95]. Moreover, regarding the mesh size in the cohesive zone which can have an effect on accuracy and computational effort, Turon *et al.* [20,21,101,102] recommended an engineering solution allowing for the use of coarser meshes, provided that material interfacial strengths are reduced. Consequently, with respect to the thickness of the cohesive zone considered in numerical analysis, suitable interfacial strengths were determined (by adjusting or by trials) during finite element modeling.

Concerning the fracture toughness, Ray *et al.* [40] conducted research to investigate the mode I fracture toughness of CF/PEEK composites manufactured by in-situ consolidation using laser-assisted tape placement (LATP) and by autoclave consolidation (hand layup) with the help of a double cantilever beam (DCB) test. They showed that due to the high cooling rate during the automated tape placement technique, ATP-made thermoplastic laminates have a lower degree of crystallinity compared to autoclave-treated ones which contributes to the decrease in fiber/matrix

adhesion and increase in ductility of the final product. They mentioned that the LATP manufacturing method can lead the fracture toughness of thermoplastic composite laminates to be raised by 60% compared to the autoclave consolidation. The required mechanical properties of the unidirectional carbon fiber/PEEK ply used in the present work for finite element modeling were derived from CYTEC technical datasheet [67] and literature, including Yoon and Sun [89,103], Turon *et al.* [104], Naderi and Khansari [105], Ray *et al.* [40] and Liu *et al.* [27,106]. In conclusion, the difference in the mechanical response of CF/PEEK thermoplastic composite fabricated by AFP in-situ consolidation and autoclave reconsolidation processes during the short-beam shear test was attempted to be captured using the distinct interface properties (i.e., lower interface strengths and higher interlaminar fracture toughness values), as presented in Table 2.2.

Table 2.2. Input parameters required for the simulation of unidirectional CF/PEEK ply [27,40,67,89,103–106].

	Elastic & shear moduli (MPa)	E_{11}	$E_{22}=E_{33}$	$G_{12}=G_{13}$	G_{23}		
		138,000	10,300	5700	3700		
Composite mechanical properties	Poisson's ratios	$\nu_{12}=\nu_{13}$	ν_{23}				
		0.3	0.45				
	Strengths (MPa)	X_T	X_C	Y_T	Y_C	$S_{12}=S_{13}$	S_{23}
		2070	1360	86	176	186	86
	Intralaminar fracture toughness (kJ/m^2)	G_1^t	G_1^c	G_2^t	G_2^c		
		201	128	1.7	2.0		
Interface properties	Penalty stiffness (MPa/mm)	K	B-K coefficient	η			
		10^6		1.89			
	Interlaminar fracture toughness (kJ/m^2)	Autoclave			AFP		
		G_I	G_{II}		G_I (+60%)	G_{II} (+60%)	
		1.7	2.0		2.72	3.2	
	Interface strengths (MPa)	N	S=T		N	S=T	
		56	70		36	45	

2.4. Results

In order to perform the short-beam shear test and assess the interlaminar shear strength of thermoplastic composites manufactured by AFP in-situ consolidation and autoclave reconsolidation, five samples were cut from each fabricated laminate. The test was run according to the ASTM D2344 standard in terms of the crosshead speed, sample size and dimensions of the

fixture with the help of a 5 kN load cell mounted on a universal hydraulic testing machine. The load-displacement diagram and calculated ILSS values are presented in Figure 2.14. The average ILSS for autoclave-consolidated samples is 86.16 MPa with a standard deviation (SD) and coefficient of variation (CV) of 1.12 MPa and 1.30%, respectively. Nonetheless, the in-situ consolidation technique led samples to have the ILSS of 54.52 MPa (with a standard deviation of 1.31 MPa and coefficient of variation of 2.41%) which is 37% lower than the ILSS of the thermoplastic samples treated inside the autoclave. Since during the AFP tape deposition, layers of thermoplastic composite laminate are subjected to heat and compaction force for a very short period of time (as compared to the autoclave in which elevated temperature and pressure are applied for a longer time frame), several sample characteristics such as degree of crystallinity, void content, fiber distribution, degree of intimate contact and degree of bonding are different between AFP and autoclave-made samples.

Generally, for computing effectiveness in quasi-static studies and some dynamic analyses possessing a few tiny elements that regulate the stable time increment, mass scaling is frequently used in ABAQUS/Explicit. As a result, mass scaling was selectively employed (cohesive zone) for computational efficiency of finite element modeling which was considered as a quasi-static analysis. It is worth mentioning that the energy-time diagram, including external work, internal energy, kinetic energy and total energy, was carefully monitored during the simulation in order to make sure that numerical analysis remains in quasi-static conditions. As a general rule, kinetic energy must not exceed 10% of the internal energy in quasi-static analysis. ILSS values were predicted with the help of the developed finite element model as 87.76 MPa and 56.51 MPa for autoclave and AFP-made samples, respectively, which were in good agreement, of less than 5% error, with experimental results.
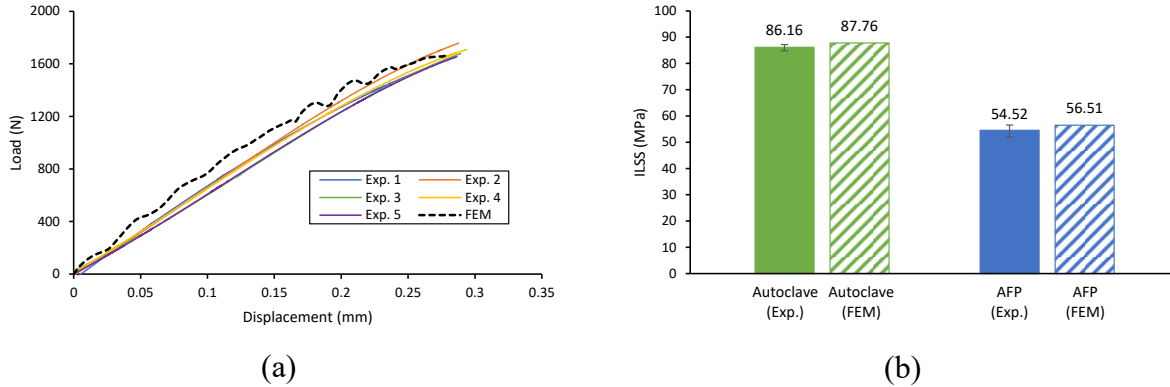
Figure 2.14. The response of CF/PEEK thermoplastic composite during the short-beam shear (SBS) test: (a) load-displacement diagram of reference samples and (b) interlaminar shear strength (ILSS) calculated experimentally and numerically.

Five different failure modes, interlaminar and intralaminar, were taken into account in the present research: (a) fiber tension, (b) fiber compression, (c) matrix tension, (d) matrix compression and (e) delamination as shown in Figure 2.15 and Figure 2.16. The major difference between the short-beam shear and flexural tests is that in addition to delamination, tension and compression failure modes occur on the bottom and top surfaces of the beam during the flexural test while delamination is the dominant mode of failure in the SBS test. In this regard, fiber tension, which is known as a catastrophic failure mode, did not occur (SDV5≠1; when the value of the state variables assigned to each failure mode equals 1, it means that those elements have failed) during the SBS test as shown in Figure 2.15 (a). However, other intralaminar-related failure modes were locally observed in the vicinity of the loading nose and supports as depicted in Figure 2.15 (b), (c) and (d). The deformed specimen after the SBS test can be also seen in Figure 2.15 (e). Concerning the interlaminar mode of failure, Figure 2.16 (a) shows the delamination initiation from the midway between the loading nose and supports in the middle of the thickness, where out-of-plane shear stress is maximized, as expected. The delamination introduced in the thermoplastic sample after the SBS test was captured with the help of a digital microscope (VHX 5000 Keyence) as shown in Figure 2.16 (b). As shown in Figure 2.15 and Figure 2.16, the failure modes replicated through finite element modeling corresponded to those observed in experimental tests. All this clear evidence confirms that the generated FE model is capable of accurately predicting the interlaminar shear strength. It should be noted that the manufacturing quality of AFP-fabricated thermoplastic composites is highly dependent on the specific AFP processing parameters. Therefore, the numerical and experimental results obtained for in-situ-consolidated Carbon/PEEK thermoplastic

43

composite are valid only for the processing parameters described in Section 2.2.1 ("Materials and manufacturing"). Nonetheless, the proposed simulation methodology remains applicable to other thermoplastic composites produced under different AFP conditions.
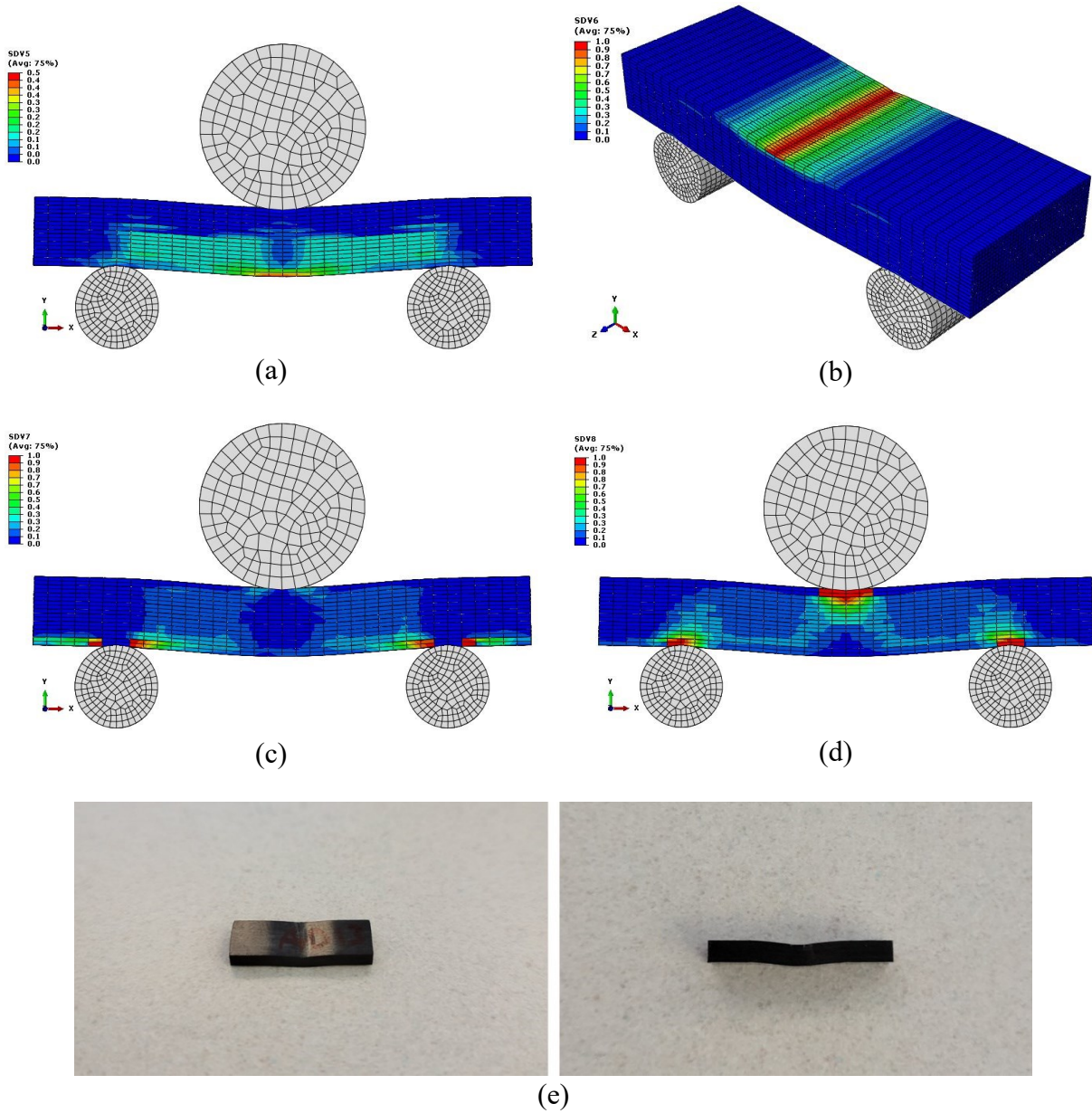
Figure 2.15. Different intralaminar failure modes happening during the short-beam shear test: (a) fiber tension (SDV5), (b) fiber compression (SDV6), (c) matrix tension (SDV7), (d) matrix compression (SDV8) and (e) deformed specimen.
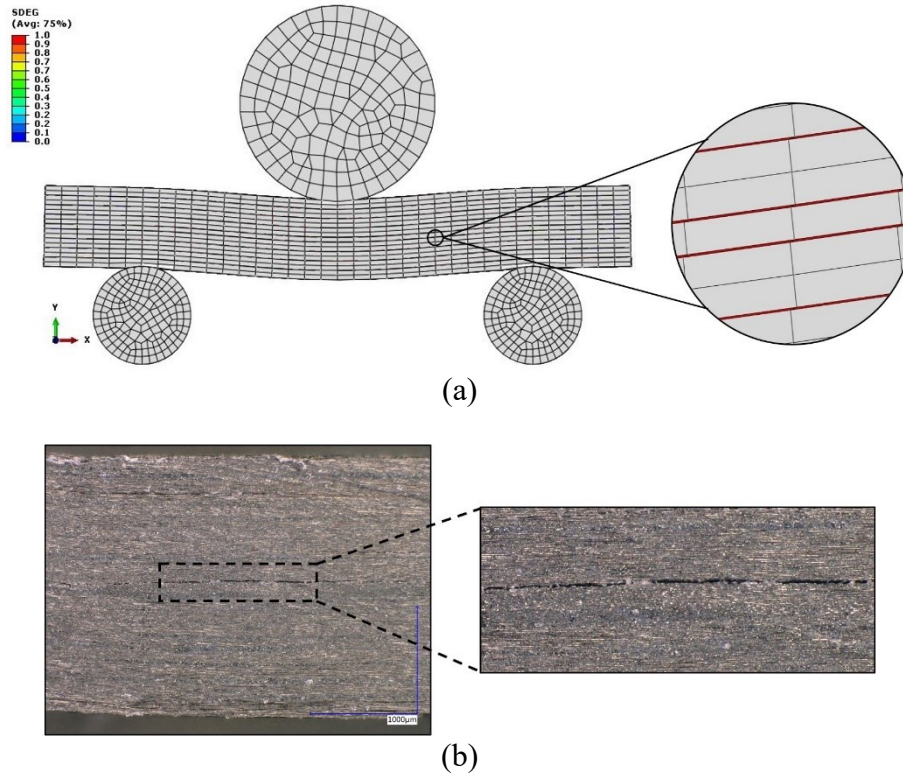
Figure 2.16. Delamination onset and propagation at the midway between the loading nose and supports: (a) simulation and (b) experiment.

In the SBS simulation, the same composite material properties (with different cohesive element strength properties) were applied to the Carbon/PEEK composites produced by AFP and autoclave processes, even though micromechanical analyses presented in Chapters 3 and 4 showed that in-situ consolidation leads to different stiffness and strength values. To address this, the SBS simulation was repeated for the in-situ-consolidated thermoplastic specimen using the predicted effective material properties, with the results provided in the Appendix of Chapter 4. The findings indicate that modifying the composite material properties has only a minor influence on the ILSS value, as delamination is primarily governed by the properties of the cohesive elements.

2.5.   Conclusion

In-situ consolidation using the automated fiber placement machine is a method which allows engineers to save time and money compared to the autoclave consolidation. The process of manufacturing thermoplastic composites is of great importance because it can affect the mechanical performance of the manufactured parts. Most of the problems arise out of the short period of time that thermoplastic composites are exposed to heat and pressure during the in-situ

consolidation in comparison with the autoclave treatment. This phenomenon adversely affects several factors (e.g., void content, fiber distribution, intimate contact, healing process and crystallization) which are responsible for the final quality of the manufactured laminate. Many researchers have been trying for many years to optimize the AFP processing parameters to fabricate thermoplastic composites with the same quality as conventional manufacturing processes (autoclave and compression press). However, there is still a considerable difference between the mechanical responses.

In the present study, an AS4/APC-2 thermoplastic plate was fabricated by AFP in-situ consolidation. Afterward, half of it was reconsolidated inside the autoclave in order to be considered as the reference plate. The micrographic study revealed that there are considerable differences between the samples fabricated by AFP and autoclave in terms of void content and fiber distribution. Short-Beam Shear (SBS) test was performed according to the ASTM D2344. The results showed that the Interlaminar Shear Strength (ILSS) of AFP-made samples experienced a 37% reduction in comparison with autoclave-treated samples. Furthermore, a finite element model was developed with the help of a VUMAT subroutine and cohesive elements in order to study the intralaminar and interlaminar (delamination) damage initiation and propagation, respectively. The discrepancy in mechanical performance was addressed by numerically finding proper interface strength properties based on the SBS experimental results for laminates manufactured using the AFP in-situ consolidation process. These interface strength properties can be employed in the future for further numerical analyses, such as the investigation of the effect of defects on the interlaminar shear strength of in-situ-consolidated Carbon/PEEK thermoplastic composites.

Appendix

❖ **Composite damage model**

3D Hashin failure criteria [26] considering the fiber and matrix failure modes are described as follows:

- Fiber tension ($\sigma_{11} \geq 0$):

$$F_{ft} = \left(\frac{\sigma_{11}}{X_T}\right)^2 + \frac{\sigma_{12}{}^2 + \sigma_{13}{}^2}{S_{12}{}^2} = 1 \tag{A.1}$$

- Fiber compression ($\sigma_{11} < 0$):

$$F_{fc} = \left(\frac{\sigma_{11}}{X_C}\right)^2 = 1 \tag{A.2}$$

- Matrix tension ($\sigma_{22} + \sigma_{33} \geq 0$):

$$F_{mt} = \frac{(\sigma_{22} + \sigma_{33})^2}{Y_T{}^2} + \frac{\sigma_{23}{}^2 - \sigma_{22}\sigma_{33}}{S_{23}{}^2} + \frac{\sigma_{12}{}^2 + \sigma_{13}{}^2}{S_{12}{}^2} = 1 \tag{A.3}$$

- Matrix compression ($\sigma_{22} + \sigma_{33} < 0$):

$$F_{mc} = \left[\left(\frac{Y_C}{2S_{23}}\right)^2 - 1\right]\left(\frac{\sigma_{22} + \sigma_{33}}{Y_C}\right) + \frac{(\sigma_{22} + \sigma_{33})^2}{4S_{23}{}^2} + \frac{\sigma_{23}{}^2 - \sigma_{22}\sigma_{33}}{S_{23}{}^2} + \frac{\sigma_{12}{}^2 + \sigma_{13}{}^2}{S_{12}{}^2} = 1 \tag{A.4}$$

where X_T and X_C are longitudinal tensile and compressive strengths. Y_T and Y_C represent transverse tensile and compressive strengths. S_{12}, S_{13} and S_{23} denote in-plane shear strength and out-of-plane shear strengths, respectively.

Damage parameter needed to calculate the effective stiffness matrix is defined as follows [22,25]:

$$d_i = \frac{\delta_{eq}^f\left(\delta_{eq} - \delta_{eq}^0\right)}{\delta_{eq}\left(\delta_{eq}^f - \delta_{eq}^0\right)} \; ; \; \delta_{eq}^0 \leq \delta_{eq} \leq \delta_{eq}^f \; ; \; i = ft, fc, mt, mc \tag{A.5}$$

where δ_{eq}^0 and δ_{eq}^f represent the equivalent displacements corresponding to initial (damage onset) and ultimate failure states. ft, fc, mt and mc denote fiber tension, fiber compression, matrix tension and matrix compression failure modes, respectively.

The formulas required for the calculation of the mentioned equivalent displacements based on fiber and matrix failure modes are as follows [22,25]:

- Fiber tension:

$$\delta_{eq} = L_C\sqrt{\varepsilon_{11}^2 + \varepsilon_{12}^2 + \varepsilon_{13}^2}$$

$$\delta_{eq}^0 = \frac{\delta_{eq}}{F_{ft}^{0.5}} \ , \qquad \delta_{eq}^f = \frac{2G_1^t}{\sigma_{eq}^0} \tag{A.6}$$

$$\sigma_{eq}^0 = \frac{L_C}{\delta_{eq}^0} (\sigma_{11}\varepsilon_{11} + \tau_{12}\varepsilon_{12} + \tau_{13}\varepsilon_{13})$$

- Fiber compression:

$$\delta_{eq} = L_C \sqrt{\varepsilon_{11}^2}$$

$$\delta_{eq}^0 = \frac{\delta_{eq}}{F_{fc}^{0.5}} \ , \qquad \delta_{eq}^f = \frac{2G_1^c}{\sigma_{eq}^0} \tag{A.7}$$

$$\sigma_{eq}^0 = \frac{L_C}{\delta_{eq}^0} (\sigma_{11}\varepsilon_{11})$$

- Matrix tension:

$$\delta_{eq} = L_C \sqrt{\varepsilon_{22}^2 + \varepsilon_{33}^2 + \varepsilon_{12}^2 + \varepsilon_{13}^2 + \varepsilon_{23}^2}$$

$$\delta_{eq}^0 = \frac{\delta_{eq}}{F_{mt}^{0.5}} \ , \qquad \delta_{eq}^f = \frac{2G_2^t}{\sigma_{eq}^0} \tag{A.8}$$

$$\sigma_{eq}^0 = \frac{L_C}{\delta_{eq}^0} (\sigma_{22}\varepsilon_{22} + \sigma_{33}\varepsilon_{33} + \tau_{12}\varepsilon_{12} + \tau_{13}\varepsilon_{13} + \tau_{23}\varepsilon_{23})$$

- Matrix compression:

$$\delta_{eq} = L_C \sqrt{\varepsilon_{22}^2 + \varepsilon_{33}^2 + \varepsilon_{12}^2 + \varepsilon_{13}^2 + \varepsilon_{23}^2}$$

$$\delta_{eq}^0 = \frac{\delta_{eq}}{F_{mc}^{0.5}} \ , \qquad \delta_{eq}^f = \frac{2G_2^c}{\sigma_{eq}^0} \tag{A.9}$$

$$\sigma_{eq}^0 = \frac{L_C}{\delta_{eq}^0} (\sigma_{22}\varepsilon_{22} + \sigma_{33}\varepsilon_{33} + \tau_{12}\varepsilon_{12} + \tau_{13}\varepsilon_{13} + \tau_{23}\varepsilon_{23})$$

where G_i^j ($i = 1, 2$; $j = t, c$) is intralaminar fracture toughness in fiber and matrix directions. σ_{eq}^0 and L_C represent the equivalent stress corresponding to damage onset and characteristic length of

an element which is determined based on the element geometry and formulation [85] (for solid elements, characteristic length is the cube root of the integration point volume), respectively.

Effective compliance matrix $[S_d]_{ijkl}$ considering the damage parameters d_f, d_m and d_s in principal material directions is as follows:

$[S_d]_{ijkl}$

$$
= \begin{bmatrix}
\dfrac{1}{(1-d_f)E_{11}} & \dfrac{-v_{12}}{E_{11}} & \dfrac{-v_{13}}{E_{11}} & 0 & 0 & 0 \\
 & \dfrac{1}{(1-d_m)E_{22}} & \dfrac{-v_{23}}{E_{22}} & 0 & 0 & 0 \\
 & & \dfrac{1}{(1-d_m)E_{33}} & 0 & 0 & 0 \\
 & & & \dfrac{1}{(1-d_s)G_{12}} & 0 & 0 \\
 & \text{Symmetric} & & & \dfrac{1}{(1-d_s)G_{23}} & 0 \\
 & & & & & \dfrac{1}{(1-d_s)G_{13}}
\end{bmatrix}
$$

$$d_s = 1 - (1-d_f)(1-d_m) \qquad\qquad (A.10)$$

where E_{ij}, G_{ij} and v_{ij} are elastic modulus, shear modulus and Poisson's ratio of the composite lamina, respectively.

In the end, degraded stress components can be computed by inverting the compliance matrix from $\{\sigma\}_{ij} = [C_d]_{ijkl}\{\varepsilon\}_{kl}$ in which $[C_d]_{ijkl}$ denotes the effective stiffness matrix.

❖ **Nonlinearity**

3D effective stress is defined as [107]:

$$\sigma_{eff} = \sqrt{\frac{3}{2}(\sigma_{22}^2 + \sigma_{33}^2) - 3\sigma_{22}\sigma_{33} + 3a_{66}(\tau_{12}^2 + \tau_{13}^2 + \tau_{23}^2)} \qquad\qquad (A.11)$$

where the value of a_{66} is experimentally determined with the help of performing uniaxial tensile off-axis tests, which are considered to be in a plane-stress state ($\sigma_{33} = \tau_{13} = \tau_{23} = 0$), at different angles (coupon specimens with 0°, 15°, 30°, 45° and 90° fiber orientations). More details can be found in the research done by Sun and Yoon [89].

Moreover, Effective strain, ε_{eff}^p, can provide information about the extent of nonlinearity caused by plastic strain. Basically, total strain consists of two components, namely elastic and plastic strains, as mentioned below:

$$\varepsilon_{ij} = \varepsilon_{ij}^e + \varepsilon_{ij}^p \qquad (A.12)$$

To make a relationship between the effective stress and strain, a power law function was used to fit experimental data obtained from the different-angle off-axis tensile tests [90]:

$$\varepsilon_{eff}^p = A\sigma_{eff}^n \qquad (A.13)$$

where A and n are coefficients of nonlinearity.

According to the research done by Liu et al [27] and Sun and Yoon [89], values of 2.05×10^{-17}, 7.0 and 1.5 were adopted for A, n and parameter a_{66}, respectively, in the present work. After determination of the unknown variables, the incremental strain tensor, $d\varepsilon_{ij}^p$, can be calculated by taking partial derivative of Eq. (A.15) with respect to each stress and strain components:

$$\begin{Bmatrix} d\varepsilon_{11}^p \\ d\varepsilon_{22}^p \\ d\varepsilon_{33}^p \\ d\gamma_{12}^p \\ d\gamma_{13}^p \\ d\gamma_{23}^p \end{Bmatrix} = An\sigma_{eff}^{(n-1)} \begin{Bmatrix} 0 \\ 3(\sigma_{22} - \sigma_{33})/2\sigma_{eff} \\ 3(\sigma_{33} - \sigma_{22})/2\sigma_{eff} \\ 3a_{66}\tau_{12}/\sigma_{eff} \\ 3a_{66}\tau_{13}/\sigma_{eff} \\ 3a_{66}\tau_{23}/\sigma_{eff} \end{Bmatrix} \begin{Bmatrix} d\sigma_{11} \\ d\sigma_{22} \\ d\sigma_{33} \\ d\tau_{12} \\ d\tau_{13} \\ d\tau_{23} \end{Bmatrix} \qquad (A.14)$$

Therefore, elastic-plastic constitutive relation can be defined using the above-mentioned plastic model and classic elastic constitutive equation to capture the nonlinear behavior of thermoplastic composites prior to the damage onset by [27]:

$$\{d\varepsilon\}_{ij} = [S]_{ijkl}\{d\sigma\}_{kl} + \{d\varepsilon^p\}_{ij} \qquad (A.15)$$

❖ **Cohesive zone damage model**

Damage parameter required to degrade the cohesive stiffness matrix is as follows [18,19]:

$$d = \frac{\delta^f(\delta - \delta^0)}{\delta(\delta^f - \delta^0)} \qquad (A.16)$$

where $\delta = \sqrt{\delta_n^2 + \delta_s^2 + \delta_t^2}$ represents the equivalent displacement in the cohesive zone. δ^0 and δ^f are corresponding displacements at delamination onset and ultimate failure states, respectively.

The most common criterion used to predict the delamination propagation is the power law. However, Camanho *et al.* [18,19] concluded that result obtained using the Benzeggagh-Kenane (B-K) [108] criterion for critical energy release rate in mixed-mode is more accurate for AS4/PEEK thermoplastic composite (manufactured by conventional methods: autoclave consolidation or compression molding). The B-K equation for critical energy release rate under mixed-mode loading conditions is as follows:

$$G_C = G_{IC} + (G_{IIC} - G_{IC})\left(\frac{G_{shear}}{G_T}\right)^{\eta}$$

$$G_{shear} = G_{II} + G_{III} \tag{A.17}$$

$$G_T = G_I + G_{shear}$$

where η represents the cohesive coefficient obtained from mixed-mode bending (MMB) test. G_I, G_{II} and G_{III} denote mode I, mode II and mode III energy release rates, respectively. G_{IC} and G_{IIC} are critical fracture toughness values in normal and shear modes. It is worth mentioning that delamination propagates when the total energy release rate is equal to or greater than G_C.

❖ VUMAT subroutine

```
    subroutine vumat(
C Read only (unmodifiable)variables -
   1 nblock, ndir, nshr, nstatev, nfieldv, nprops, lanneal,
   2 stepTime, totalTime, dt, cmname, coordMp, charLength,
   3 props, density, strainInc, relSpinInc,
   4 tempOld, stretchOld, defgradOld, fieldOld,
   5 stressOld, stateOld, enerInternOld, enerInelasOld,
   6 tempNew, stretchNew, defgradNew, fieldNew,
C Write only (modifiable) variables -
   7 stressNew, stateNew, enerInternNew, enerInelasNew )
C
    include 'vaba_param.inc'
C
    dimension props(nprops), density(nblock), coordMp(nblock,*),
   1 charLength(nblock), strainInc(nblock,ndir+nshr),
   2 relSpinInc(nblock,nshr), tempOld(nblock),
   3 stretchOld(nblock,ndir+nshr),
   4 defgradOld(nblock,ndir+nshr+nshr),
   5 fieldOld(nblock,nfieldv), stressOld(nblock,ndir+nshr),
   6 stateOld(nblock,nstatev), enerInternOld(nblock),
```

```
      7 enerInelasOld(nblock), tempNew(nblock),
      8 stretchNew(nblock,ndir+nshr),
      9 defgradNew(nblock,ndir+nshr+nshr),
      1 fieldNew(nblock,nfieldv),
      2 stressNew(nblock,ndir+nshr), stateNew(nblock,nstatev),
      3 enerInternNew(nblock), enerInelasNew(nblock)
C
      character*80 cmname

      real E11,E22,E33,NU12,NU13,NU23,G12,G13,G23,NU21,NU31,NU32,
      1    C11,C22,C33,C12,C13,C23,C44,C55,C66,C21,C31,C32,DELTA,BETA

      real F1t,F1c,F2t,F2c,F3t,F3c,F12,F13,F23,G1t,G1c,G2t,G2c

      integer nArray,nDmg

      parameter (ZERO=0.d0, ONE=1.d0, TWO=2.d0)
      parameter (n_svd_Required=28)

c    !State Variables

c statev(1) --> Fiber Damage in Tension
c statev(2) --> Fiber Damage in Compression
c statev(3) --> Matrix Damage in Tension
c statev(4) --> Matrix Damage in Compression

c statev(5) --> Fiber Damage Initiation in Tension
c statev(6) --> Fiber Damage Initiation in Compression
c statev(7) --> Matrix Damage Initiation in Tension
c statev(8) --> Matrix Damage Initiation in Compression

c statev(9) --> Strain(11)
c statev(10)--> Strain(22)
c statev(11)--> Strain(33)
c statev(12)--> Strain(12)
c statev(13)--> Strain(23)
c statev(14)--> Strain(13)

c statev(15)--> delta_eq_0_ft
c statev(16)--> delta_eq_0_fc
c statev(17)--> delta_eq_0_mt
c statev(18)--> delta_eq_0_mc

c statev(19)--> delta_eq_f_ft
c statev(20)--> delta_eq_f_fc
c statev(21)--> delta_eq_f_mt
c statev(22)--> delta_eq_f_mc

c statev(23)--> Damping Stress(11)
c statev(24)--> Damping Stress(22)
c statev(25)--> Damping Stress(33)
c statev(26)--> Damping Stress(12)
c statev(27)--> Damping Stress(23)
c statev(28)--> Damping Stress(13)

c    !Props
```

```
c props(1) --> Young modulus in direction 1, "E11"
c props(2) --> Young modulus in direction 2, "E22"
c props(3) --> Young modulus in direction 3, "E33"
c props(4) --> Poisson ratio, "NU12"
c props(5) --> Poisson ratio, "NU13"
c props(6) --> Poisson ratio, "NU23"
c props(7) --> Shear modulus, "G12"
c props(8) --> Shear modulus, "G13"
c props(9) --> Shear modulus, "G23"

c props(10) --> Ultimate tens strength in direction 1, "F1t"
c props(11) --> Ultimate comp strength in direction 1, "F1c"
c props(12) --> Ultimate tens strength in direction 2, "F2t"
c props(13) --> Ultimate comp strength in direction 2, "F2c"
c props(14) --> Ultimate tens strength in direction 3, "F3t"
c props(15) --> Ultimate comp strength in direction 3, "F3c"
c props(16) --> Ultimate shear strength in direction 12, "F12"
c props(17) --> Ultimate shear strength in direction 13, "F13"
c props(18) --> Ultimate shear strength in direction 23, "F23"

c props(19) --> Longitudinal Tensile Fracture Energy, "G1t"
c props(20) --> Longitudinal Compressive Fracture Energy, "G1c"
c props(21) --> Transverse Tensile Fracture Energy, "G2t"
c props(22) --> Transverse Compressive Fracture Energy, "G2c"

c props(23) --> beta damping coefficient, "BETA"

C     !Elastic properties

      E11=props(1)
      E22=props(2)
      E33=props(3)
      NU12=props(4)
      NU13=props(5)
      NU23=props(6)
      G12=props(7)
      G13=props(8)
      G23=props(9)

      NU21=(E22/E11)*NU12
      NU31=(E33/E11)*NU13
      NU32=(E33/E22)*NU23

      DELTA=ONE/(ONE-NU12*NU21-NU23*NU32-NU13*NU31-TWO*NU21*NU32*NU13)

C     !stiffness matrix

      C11=E11*(ONE-NU23*NU32)*DELTA
      C22=E22*(ONE-NU13*NU31)*DELTA
      C33=E33*(ONE-NU12*NU21)*DELTA
      C12=E11*(NU21+NU31*NU23)*DELTA
      C13=E11*(NU31+NU21*NU32)*DELTA
      C23=E22*(NU32+NU12*NU31)*DELTA
      C44=TWO*G12
      C55=TWO*G23
```

```fortran
      C66=TWO*G13
      C21=C12
      C31=C13
      C32=C23

C    !Strength properties

      F1t=props(10)
      F1c=props(11)
      F2t=props(12)
      F2c=props(13)
      F3t=props(14)
      F3c=props(15)
      F12=props(16)
      F13=props(17)
      F23=props(18)

      G1t=props(19)
      G1c=props(20)
      G2t=props(21)
      G2c=props(22)

      BETA=props(23)

      nArray=ndir+nshr
      nDmg=0

C    !Initial calculations and checks

      if ( totalTime .eq. ZERO ) then
        if (nstatev .lt. n_svd_Required) then
           call xplb_abqerr(-2,'Subroutine VUMAT requires the '//
     &      'specification of %I state variables. Check the '//
     &      'definition of *DEPVAR in the input file.',
     &      n_svd_Required,ZERO,' ')
           call xplb_exit
        end if

        call stressUpdate(nblock,nArray,
     &   stateOld(1,1),stateOld(1,2),stateOld(1,3),stateOld(1,4),
     &   C11,C22,C33,C12,C23,C13,C44,C55,C66,
     &   stressNew,strainInc,stressOld,strainInc)

      end if

C    !Strain update

      call strainUpdate(nblock,strainInc,stateOld(1,9),stateNew(1,9))

C    !Stress update with old state variables

      call stressUpdate(nblock,nArray,
     &  stateOld(1,1),stateOld(1,2),stateOld(1,3),stateOld(1,4),
     &  C11,C22,C33,C12,C23,C13,C44,C55,C66,
     &  stressNew,stateNew(1,9),stressOld,strainInc)
```

```fortran
C    !State variables update except for strains

     do k=1,nblock
       do i=1,8
         stateNew(k,i)=stateOld(k,i)
       end do
       do i=15,22
         stateNew(k,i)=stateOld(k,i)
       end do
     end do

C    !Hashin damage initiation

     call Hashin(nblock,nArray,nDmg,charLength,
    & F1t,F1c,F2t,F2c,F3t,F3c,F12,F13,F23,G1t,G1c,G2t,G2c,
    & stressNew,nstatev,stateNew)

C    !Damage evolution

     call Damage_Evolution(nblock,nArray,nDmg,charLength,
    & stressNew,nstatev,stateNew)

C    !Stress update with new state variables

     if (nDmg.GT.ZERO) then

       call stressUpdate(nblock,nArray,
    &   stateNew(1,1),stateNew(1,2),stateNew(1,3),stateNew(1,4),
    &   C11,C22,C33,C12,C23,C13,C44,C55,C66,
    &   stressNew,stateNew(1,9),stressOld,strainInc)

     end if

C    !Damping stress

     if (BETA.GT.ZERO) then

       call Damping(nblock,nArray,BETA,dt,
    &   stressOld,stressNew,stateOld(1,23),stateNew(1,23))

     end if

C    !Internal specific energy (per unit mass)

     call InternalEnergy(nblock,nArray,
    & density,strainInc,stressOld,stressNew,
    & enerInternOld,enerInternNew)

     return
     end


C-----------------------------------------------------------------------
C-----------------------------------------------------------------------
C-----------------------------------------------------------------------

     subroutine stressUpdate(nblock,nArray,
```

```fortran
     & dmgFiberT,dmgFiberC,dmgMatrixT,dmgMatrixC,
     & C11,C22,C33,C12,C23,C13,C44,C55,C66,
     & stress,strain,stressOld,strainInc)

      include 'vaba_param.inc'

      dimension dmgFiberT(nblock),dmgFiberC(nblock),dmgMatrixT(nblock),
     & dmgMatrixC(nblock),stress(nblock,nArray),strain(nblock,nArray)

      dimension stressOld(nblock,nArray),strainInc(nblock,nArray)

      real dft,dfc,dmt,dmc,df
      real dC11,dC22,dC33,dC12,dC13,dC23,dC44,dC55,dC66,dC21,dC31,dC32
      real s11,s22,s33,s12,s13,s23,sigEf,CP,dstress

      parameter(zero=0.d0, one=1.d0, two=2.d0, three=3.d0)
      parameter(smt=0.9d0, smc=0.5d0)
      parameter(A=2.05d-17, n=7.0d0, a66=1.5d0)

      do k=1,nblock

        dft=dmgFiberT(k)
        dfc=dmgFiberC(k)
        dmt=dmgMatrixT(k)
        dmc=dmgMatrixC(k)
        df=one-(one-dft)*(one-dfc)

        dC11=(one-df)*C11
        dC22=(one-dmt)*(one-dmc)*C22
        dC33=(one-dmt)*(one-dmc)*C33
        dC12=(one-df)*(one-dmt)*(one-dmc)*C12
        dC13=(one-df)*(one-dmt)*(one-dmc)*C13
        dC23=(one-df)*(one-dmt)*(one-dmc)*C23
        dC44=(one-smt*dmt)*(one-smc*dmc)*C44
        dC55=(one-smt*dmt)*(one-smc*dmc)*C55
        dC66=(one-smt*dmt)*(one-smc*dmc)*C66
        dC21=dC12
        dC31=dC13
        dC32=dC23

**********************************

        s11=stressOld(k,1)
        s22=stressOld(k,2)
        s33=stressOld(k,3)
        s12=stressOld(k,4)
        s23=stressOld(k,5)
        s13=stressOld(k,6)

        sigEf=sqrt(abs((three/two)*(s22**two+s33**two)-three*s22*s33+
     &          three*a66*(s13**two+s12**two+s23**two)))

        CP=A*n*sigEf**(n-one)

************************************
```

```fortran
      stress(k,1)=dC11*strain(k,1)+dC12*strain(k,2)+dC13*strain(k,3)
      stress(k,2)=dC21*strain(k,1)+dC22*strain(k,2)+dC23*strain(k,3)
      stress(k,3)=dC31*strain(k,1)+dC32*strain(k,2)+dC33*strain(k,3)
      stress(k,4)=dC44*strain(k,4) !sigma12
      stress(k,5)=dC55*strain(k,5) !sigma23

      dstress=(one/(one/C66+
     &      CP))*strainInc(k,6)

      stress(k,6)=stressOld(k,6)+dstress !sigma13

      end do

      return
      end

C////////////////////////////////////////////////////////////////////////

      subroutine strainUpdate(nblock,strainInc,strainOld,strainNew)

      include 'vaba_param.inc'

      dimension strainInc(nblock,6),strainOld(nblock,6),
     &      strainNew(nblock,6)

      do k=1,nblock
        do i=1,6
          strainNew(k,i)=strainOld(k,i)+strainInc(k,i)
        end do
      end do

      return
      end

C////////////////////////////////////////////////////////////////////////

      subroutine Hashin(nblock,nArray,nDmg,charLength,
     & F1t,F1c,F2t,F2c,F3t,F3c,F12,F13,F23,G1t,G1c,G2t,G2c,
     & stress,nstatev,stateNew)

      include 'vaba_param.inc'

      dimension charLength(nblock),stress(nblock,nArray),
     & stateNew(nblock,nstatev)

      real F1t,F1c,F2t,F2c,F3t,F3c,F12,F13,F23,G1t,G1c,G2t,G2c
      real s11,s22,s33,s12,s13,s23,e11,e22,e33,e12,e13,e23
      real Lc,delta_eq,delta_eq_0,delta_eq_f,s_eq_0
      real Rft,Rfc,Rmt,Rmc
      integer nDmg

      parameter(zero=0.d0, one=1.d0, two=2.d0, three=3.d0, half=0.5d0)

      do k=1,nblock

        Lc=charLength(nblock)
```

```fortran
      s11=stress(k,1)
      s22=stress(k,2)
      s33=stress(k,3)
      s12=stress(k,4)
      s23=stress(k,5)
      s13=stress(k,6)

      e11=stateNew(k,9)
      e22=stateNew(k,10)
      e33=stateNew(k,11)
      e12=stateNew(k,12)
      e23=stateNew(k,13)
      e13=stateNew(k,14)

C     !Fiber tension

      if ((s11.GT.zero).AND.(stateNew(k,5).LT.one)) then

         Rft=(s11/F1t)**two+(one/F12)**two*(s12**two+s13**two)
         stateNew(k,5)=max(Rft,stateNew(k,5))

         if (Rft.GE.one) then

            stateNew(k,5)=one

            delta_eq=Lc*sqrt(e11**two+e12**two+e13**two)
            delta_eq_0=delta_eq/sqrt(Rft)
            stateNew(k,15)=delta_eq_0
            s_eq_0=(Lc/delta_eq_0)*(s11*e11+s12*e12+s13*e13)
            delta_eq_f=two*G1t/s_eq_0
            stateNew(k,19)=delta_eq_f

            nDmg=1

         end if
      end if

C     !Fiber compression

      if ((s11.LT.zero).AND.(stateNew(k,6).LT.one)) then

         Rfc=(s11/F1c)**two
         stateNew(k,6)=max(Rfc,stateNew(k,6))

         if (Rfc.GE.one) then

            stateNew(k,6)=one

            delta_eq=Lc*sqrt(e11**two)
            delta_eq_0=delta_eq/sqrt(Rfc)
            stateNew(k,16)=delta_eq_0
            s_eq_0=(Lc/delta_eq_0)*(s11*e11)
            delta_eq_f=two*G1c/s_eq_0
            stateNew(k,20)=delta_eq_f
```

```fortran
            nDmg=1

         end if
       end if

C    !Matrix tension

      if (((s22+s33).GT.zero).AND.(stateNew(k,7).LT.one)) then

         Rmt=(one/F2t)**two*(s22+s33)**two+
     &        (one/F23)**two*(s23**two-s22*s33)+
     &        (one/F12)**two*(s12**two+s13**two)
         stateNew(k,7)=max(Rmt,stateNew(k,7))

         if (Rmt.GE.one) then

            stateNew(k,7)=one

            delta_eq=Lc*sqrt(e22**two+e33**two+e12**two+e13**two+
     &                 e23**two)
            delta_eq_0=delta_eq/sqrt(Rmt)
            stateNew(k,17)=delta_eq_0
            s_eq_0=(Lc/delta_eq_0)*(s22*e22+s33*e33+s12*e12+
     &                 s13*e13+s23*e23)
            delta_eq_f=two*G2t/s_eq_0
            stateNew(k,21)=delta_eq_f

            nDmg=1

         end if
       end if

C    !Matrix compression

      if (((s22+s33).LT.zero).AND.(stateNew(k,8).LT.one)) then

         Rmc=(one/F2c)*((F2c/(two*F23))**two-one)*(s22+s33)+
     &        (one/(two*F23))**two*(s22+s33)**two+
     &        (one/F23)**two*(s23**two-s22*s33)+
     &        (one/F12)**two*(s12**two+s13**two)
         stateNew(k,8)=max(Rmc,stateNew(k,8))

         if (Rmc.GE.one) then

            stateNew(k,8)=one

            delta_eq=Lc*sqrt(e22**two+e33**two+e12**two+e13**two+
     &                 e23**two)
            delta_eq_0=delta_eq/sqrt(Rmc)
            stateNew(k,18)=delta_eq_0
            s_eq_0=(Lc/delta_eq_0)*(s22*e22+s33*e33+s12*e12+
     &                 s13*e13+s23*e23)
            delta_eq_f=two*G2c/s_eq_0
            stateNew(k,22)=delta_eq_f

            nDmg=1
```

```fortran
        end if
       end if

      end do

      return
      end
```

C///

```fortran
      subroutine Damage_Evolution(nblock,nArray,nDmg,charLength,
     & stress,nstatev,stateNew)

      include 'vaba_param.inc'

      dimension charLength(nblock),stress(nblock,nArray),
     & stateNew(nblock,nstatev)

      real s11,s22,s33,s12,s13,s23,e11,e22,e33,e12,e13,e23
      real dft_f,dfc_f,dmt_f,dmc_f,dft,dfc,dmt,dmc
      real Lc,delta_eq,delta_eq_0,delta_eq_f,s_eq_0,P1,P2
      integer nDmg


      parameter(zero=0.d0, one=1.d0, two=2.d0, three=3.d0, half=0.5d0)

      dft_f = 0.99
      dfc_f = 0.90
      dmt_f = 0.99
      dmc_f = 0.90

      do k=1,nblock

       Lc=charLength(nblock)

       s11=stress(k,1)
       s22=stress(k,2)
       s33=stress(k,3)
       s12=stress(k,4)
       s23=stress(k,5)
       s13=stress(k,6)

       e11=stateNew(k,9)
       e22=stateNew(k,10)
       e33=stateNew(k,11)
       e12=stateNew(k,12)
       e23=stateNew(k,13)
       e13=stateNew(k,14)

C    !Fiber tension

       if ((s11.GT.zero).AND.(stateNew(k,5).EQ.one)) then

        delta_eq=Lc*sqrt(e11**two+e12**two+e13**two)
        delta_eq_0=stateNew(k,15)
```

60

```fortran
      delta_eq_f=stateNew(k,19)
      P1=delta_eq_f*(delta_eq-delta_eq_0)
      P2=delta_eq*(delta_eq_f-delta_eq_0)
      dft=P1/P2

      if (dft.GE.dft_f) then
         stateNew(k,1)=dft_f
      else
         stateNew(k,1)=max(dft,stateNew(k,1))
      end if

      nDmg=1

    end if

C    !Fiber compression

    if ((s11.LT.zero).AND.(stateNew(k,6).EQ.one)) then

      delta_eq=Lc*sqrt(e11**two)
      delta_eq_0=stateNew(k,16)
      delta_eq_f=stateNew(k,20)
      P1=delta_eq_f*(delta_eq-delta_eq_0)
      P2=delta_eq*(delta_eq_f-delta_eq_0)
      dfc=P1/P2

      if (dfc.GE.dfc_f) then
         stateNew(k,2)=dfc_f
      else
         stateNew(k,2)=max(dfc,stateNew(k,2))
      end if

      nDmg=1

    end if

C    !Matrix tension

    if (((s22+s33).GT.zero).AND.(stateNew(k,7).EQ.one)) then

      delta_eq=Lc*sqrt(e22**two+e33**two+e12**two+e13**two+
   &            e23**two)
      delta_eq_0=stateNew(k,17)
      delta_eq_f=stateNew(k,21)
      P1=delta_eq_f*(delta_eq-delta_eq_0)
      P2=delta_eq*(delta_eq_f-delta_eq_0)
      dmt=P1/P2

      if (dmt.GE.dmt_f) then
         stateNew(k,3)=dmt_f
      else
         stateNew(k,3)=max(dmt,stateNew(k,3))
      end if

      nDmg=1
```

```fortran
      end if

C     !Matrix compression

      if (((s22+s33).LT.zero).AND.(stateNew(k,8).EQ.one)) then

         delta_eq=Lc*sqrt(e22**two+e33**two+e12**two+e13**two+
     &              e23**two)
         delta_eq_0=stateNew(k,18)
         delta_eq_f=stateNew(k,22)
         P1=delta_eq_f*(delta_eq-delta_eq_0)
         P2=delta_eq*(delta_eq_f-delta_eq_0)
         dmc=P1/P2

         if (dmc.GE.dmc_f) then
            stateNew(k,4)=dmc_f
         else
            stateNew(k,4)=max(dmc,stateNew(k,4))
         end if

         nDmg=1

      end if

      end do

      return
      end

C////////////////////////////////////////////////////////////////////////////

      subroutine Damping(nblock,nArray,beta,dt,
     & sigOld,sigNew,sigDampOld,sigDampNew)

      include 'vaba_param.inc'

      dimension sigOld(nblock,nArray),sigNew(nblock,nArray),
     & sigDampOld(nblock,nArray),sigDampNew(nblock,nArray)

      real b

      b=beta/dt

      do k=1,nblock

         sigDampNew(k,1)=b*(sigNew(k,1)-(sigOld(k,1)-sigDampOld(k,1)))
         sigDampNew(k,2)=b*(sigNew(k,2)-(sigOld(k,2)-sigDampOld(k,2)))
         sigDampNew(k,3)=b*(sigNew(k,3)-(sigOld(k,3)-sigDampOld(k,3)))
         sigDampNew(k,4)=b*(sigNew(k,4)-(sigOld(k,4)-sigDampOld(k,4)))
         sigDampNew(k,5)=b*(sigNew(k,5)-(sigOld(k,5)-sigDampOld(k,5)))
         sigDampNew(k,6)=b*(sigNew(k,6)-(sigOld(k,6)-sigDampOld(k,6)))

         sigNew(k,1)=sigNew(k,1)+sigDampNew(k,1)
         sigNew(k,2)=sigNew(k,2)+sigDampNew(k,2)
         sigNew(k,3)=sigNew(k,3)+sigDampNew(k,3)
         sigNew(k,4)=sigNew(k,4)+sigDampNew(k,4)
```

```fortran
      sigNew(k,5)=sigNew(k,5)+sigDampNew(k,5)
      sigNew(k,6)=sigNew(k,6)+sigDampNew(k,6)

   end do

   return
   end

C///////////////////////////////////////////////////////////////////////////

   subroutine InternalEnergy(nblock,nArray,
   & density,strainInc,sigOld,sigNew,enerInternOld,enerInternNew)

   include 'vaba_param.inc'

   dimension density(nblock),strainInc(nblock,nArray),
   & sigOld(nblock,nArray),sigNew(nblock,nArray),
   & enerInternOld(nblock),enerInternNew(nblock)

   parameter(zero=0.d0, one=1.d0, two=2.d0, three=3.d0, half=0.5d0)

   real stressPower

   do k=1,nblock

      stressPower=half*((sigOld(k,1)+sigNew(k,1))*strainInc(k,1)+
   &            (sigOld(k,2)+sigNew(k,2))*strainInc(k,2)+
   &            (sigOld(k,3)+sigNew(k,3))*strainInc(k,3)+
   &        two*(sigOld(k,4)+sigNew(k,4))*strainInc(k,4)+
   &        two*(sigOld(k,5)+sigNew(k,5))*strainInc(k,5)+
   &        two*(sigOld(k,6)+sigNew(k,6))*strainInc(k,6))

      enerInternNew(k)=enerInternOld(k)+stressPower/density(k)

   end do

   return
   end
```

CHAPTER 3

Prediction of transverse tensile strength of in-situ-consolidated Carbon/PEEK thermoplastic composite material based on micromechanical modeling and simulation

3. Prediction of transverse tensile strength of in-situ-consolidated Carbon/PEEK thermoplastic composite material based on micromechanical modeling and simulation

Foreword

The material properties reported in the Cytec datasheet [67] are based on composites produced through compression molding or autoclave treatment, which do not fully reflect the microstructural characteristics introduced by the AFP process. These include increased void content, non-uniform fiber distribution, and variations in crystallinity, all of which can significantly influence the performance of composite materials, particularly in the transverse direction, where the matrix phase plays a dominant role. Additionally, the presence of warpage in AFP-manufactured thermoplastic composite laminates, especially when a heated mandrel is not used, makes experimental testing of the final part more difficult. As a result, a knowledge gap exists in mechanical property data for AFP-processed thermoplastic composite materials.

In composite laminates, transverse microcracking within the matrix often serves as the dominant failure mode, initiating and driving subsequent crack growth. However, the influence of aforementioned microstructural features introduced during the AFP in-situ consolidation process on the strength properties has not been fully investigated. This research work aims to predict the transverse tensile strength of Carbon/PEEK thermoplastic composites fabricated through AFP in-situ consolidation, as outlined in the second objective of the present thesis. To achieve this, 2D micro-scale Representative Volume Elements (RVEs) were generated based on the composite transverse cross-section, incorporating data from micrographic examination and DSC analysis. Finite element simulations employed the Drucker–Prager plasticity model along with a ductile damage criterion to capture the matrix's plastic behavior, as well as crack initiation and propagation in the neat PEEK resin. The results indicate that the AFP in-situ consolidation process may reduce the transverse tensile strength to about 46.9 MPa, a decrease of approximately 44% compared to the strength attainable through the autoclave method. This substantial reduction should be carefully considered in the design and simulation of AFP-fabricated thermoplastic composite laminates.

Abstract

Thermoplastic composite laminates have emerged as a compelling alternative to thermoset laminates for primary aerospace applications, following the industrial development of automated manufacturing technologies, such as the Automated Fiber Placement (AFP) process. The present research aims to predict the transverse tensile strength of in-situ-consolidated Carbon/PEEK thermoplastic composite material, considering inherent variations caused by the AFP process in fiber volume fraction, void content, interlaminar resin pocket and degree of crystallinity. To achieve this, two-dimensional Representative Volume Elements (RVEs) with randomly distributed fibers were developed at the micro-scale level. The Drucker-Prager model, combined with a ductile failure criterion, was used to capture the plastic behavior and damage accumulation in the PEEK resin during the numerical analysis. In order to acquire the necessary data for micromechanical modeling and analysis, two sets of specimens, manufactured using AFP in-situ consolidation and autoclave re-consolidation techniques, underwent micrographic examination and thermoanalytical Differential Scanning Calorimetry (DSC) analysis. The results reveal that AFP in-situ consolidation can reduce the transverse tensile strength of Carbon/PEEK thermoplastic composite material up to approximately 44%, compared to the autoclave re-consolidation technique. Due to the lack of experimental data caused by warpage occurring in the manufactured laminate in the absence of a heated mandrel, the present work proposes a simulation methodology to predict the transverse tensile strength resulting from the in-situ consolidation process. This crucial difference in strength values, most notably in the transverse direction, must be carefully considered in finite element analyses, analytical evaluations, and design procedures involving AFP-manufactured thermoplastic composite laminates and structures.

3.1. Introduction

Polymeric composites have found extensive applications in various fields owing to their remarkable specific stiffness, strength, corrosion resistance and lightweight characteristics, particularly in aerospace and automotive industries where weight reduction is crucial. Automated Fiber Placement (AFP) has emerged as an advanced automated manufacturing technique that offers benefits, such as reduced material waste, increased deposition rate and minimized production time and costs, compared to conventional methods, such as the hand lay-up process.

Robotic AFP machines employ a fiber placement head, compatible with either thermoset or thermoplastic materials, mounted on a robotic arm to precisely deposit narrow composite tows onto a tool surface for the fabrication of composite laminates. The time-consuming and expensive curing process of thermoset-based composites has caused the increasing applications of thermoplastic counterparts as a possible alternative, offering more efficient and cost-effective solutions.

A key advantage of manufacturing thermoplastic composite materials using AFP is the capability for in-situ consolidation, which eliminates the need for subsequent consolidation processes. In-situ consolidation during the AFP process applies localized heating (e.g., using a hot gas torch or laser) and compaction force, resulting in a rapid cooling rate and non-uniform thermal profiles that can induce defects such as voids and incomplete bonding. In contrast, autoclave re-consolidation involves post-processing the preformed laminate at elevated temperatures (~380–400 °C) under high pressure in a controlled environment, allowing a slower cooling rate and improved consolidation quality through enhanced bonding, removing voids and crystallinity control. Previous studies [5,9,34,35,37–41] have shown that in-situ consolidation typically results in higher void content (up to 4%) and lower crystallinity levels (i.e., 15-30%), depending on the AFP processing parameters and type of the heating system, compared to autoclave-reconsolidated laminates, which generally exhibit void content below 0.5% and higher degrees of crystallinity (i.e., 35%) due to slower cooling rates and longer exposure to heat and pressure. Furthermore, according to the literature [15,28,109], while the Interlaminar Shear Strength (ILSS) value of in-situ consolidated Carbon/PEEK thermoplastic composite samples ranges between 55 to 60 MPa, autoclave re-consolidation can increase it to almost 90 MPa.

The inherently short processing time and high cooling rate associated with the AFP process introduce significant variations in the microstructural features and the degree of crystallinity of in-situ-consolidated thermoplastic composite laminates. These variations can adversely influence their material properties when compared to their autoclave-reconsolidated counterparts. Thermoplastic composite samples produced through AFP in-situ consolidation display notable void content, interlaminar resin-rich regions and an uneven distribution of fibers. These characteristics result in the formation of stress concentration zones within the layers, primarily due

to the close proximity of fibers and the presence of voids, thereby affecting the damage initiation and propagation occurring in the composite material [5,37].

Voids are critical in that they substantially impact the mechanical performance of composite laminates. In the microstructure resulting from the AFP process, voids can generally be categorized into two types: (a) Intralaminar voids, which originate during the tape production phase and include entrapped air within individual plies; and (b) Interlaminar voids, which form between layers during the tape placement process and predominantly depend on the degree of intimate contact achieved between the plies. Due to the presence of resin pockets between layers caused by nonuniform fiber distribution, both the percentage and distribution of voids can adversely affect the mechanical performance of the composite material. This effect is particularly significant in the transverse direction, where the matrix behavior dominantly governs the mechanical response of the composite material. In composite laminates, the initiation of transverse matrix microcracking is generally regarded as the first indication of material failure. This phenomenon plays a pivotal role in governing the progression of fracture and significantly influences the overall structural integrity of the laminate [9,34,35,38,39].

Warpage in AFP in-situ-consolidated thermoplastic composite laminates primarily arises from uneven cooling and shrinkage, and asymmetric thermal gradients across the laminate thickness, leading to residual stresses and distortion. Key factors influencing warpage include the layup sequence, fiber orientation and the absence of uniform consolidation heat and pressure. Although experimental procedures remain crucial for accurately evaluating the material properties, the warpage induced during the AFP in-situ consolidation process poses significant challenges to the mechanical testing of unidirectional thermoplastic composite specimens according to the ASTM standards. While the application of a heated mandrel (tool) offers a potential solution to mitigate the distortion of open-edge thermoplastic samples [29], it is worth mentioning that the use of this method may lead to alterations in the mechanical properties of the final product compared to those resulting from the in-situ consolidation process. Nonetheless, micromechanical modeling techniques, such as the Representative Volume Element (RVE) approach, provide a powerful alternative by enabling the simulation of various microstructures, conducting virtual tests, and accurately predicting the effective material properties of composite materials [48]. There are considerable difficulties in obtaining a high fiber volume fraction in RVEs containing randomly

distributed fibers. To overcome this, researchers have developed various algorithms, such as Random Sequential Adsorption (RSA) [52], Random Sequential Expansion (RSE) [53], Event-Driven Molecular Dynamics (EDMD) [51], and the Random Microstructure Generator (RAND_uSTRU_GEN) [54]. Moreover, Elnekhaily and Talreja [110] developed an algorithm that transforms an initially uniform square fiber arrangement into a quantified nonuniform distribution through a shaking process, based on the degree of nonuniformity. In their subsequent studies [66,111], this approach was further refined by initiating the distribution from a hexagonal packing pattern. These algorithms enhance the realism and accuracy of the generated RVE models by ensuring efficient fiber packing while maintaining randomness in their distribution.

Many researchers attempted to investigate the mechanical response of composite materials in the transverse direction through micromechanical analysis [42,45,55–66]. Trias *et al.* [55] compared the stress and strain distributions obtained from both periodic (such as square and hexagonal packing) and random microstructure models that can be used for generating RVEs representing Carbon-reinforced polymers. They showed that although periodic models might be used to predict effective material properties due to their computational efficiency, random models have to be considered for the analysis of local phenomena, such as damage initiation and propagation. Proper representation of the real microstructure formed in a fiber-reinforced composite material is necessary for accurate damage modeling that originates from matrix cracks. To this end, Romanov *et al.* [56] generated two different fiber arrangements: one using the captured micrographs and the other based on a random microstructure generator algorithm. They drew a comparison between geometrical and mechanical parameters, including fiber distribution and stress states, in the transverse direction, and concluded that there is good agreement between the results of real and virtually generated microstructures. Ghayoor *et al.* [42] investigated the effect of intralaminar resin-rich areas, created by both removing and moving fibers methods, on the transverse modulus and damage onset of Carbon/epoxy composites using computational analysis. According to the results, the presence of resin pockets could lead to approximately 20% lower failure initiation strain in the composite laminates. Wang *et al.* [45] conducted the analyses about the influence of voids on the transverse tensile properties of composite laminates. They implemented two distinct methods for void modeling, namely explicit establishment of voids and voids modeled with the elements, and considered circular, elliptical and arbitrary shapes for the generated voids. The results showed more variations in tensile strength values for the microstructure simulated with

69

explicitly established voids, which is similar to the actual response of composite samples observed during the experiments. Mehdikhani *et al.* [57,58] investigated the effect of intralaminar voids, whose characteristics (such as size, shape, etc.) were obtained by micro-computed tomography, on the matrix cracking phenomenon in polymer-matrix composites. They developed a simulation approach consisting of micro- and meso-scales to capture the matrix cracks on the ply scale using the results of microstructural analysis. The outcome of the research indicated that although voids lead matrix cracks to initiate earlier, their propagation is marginally affected by the presence of voids. Elnekhaily and Talreja [66] showed through computational modeling that micro-void size and position in an epoxy matrix, relative to the crack initiation zone, significantly affect fiber-matrix debonding and kink-out phenomena during early stages of transverse crack development in unidirectional composite materials.

The mechanical behavior of Carbon and Glass fiber-reinforced polymer matrix composite under the transverse compressive loading condition was examined by González and LLorca [59]. They revealed that fiber-matrix interface strength and matrix yield stress have substantial effects on the outcome of the numerical analysis, such as compressive strength. Yang *et al.* [60] attempted to evaluate the mechanical response of unidirectional composite laminates subjected to tension and compression in a transverse direction using the RVE approach in which matrix plastic deformation and interfacial debonding were incorporated by Drucker-Prager and cohesive zone models, respectively. Their findings indicated that even though fiber-matrix interfacial bonding is mainly responsible for the failure mechanism in tension, transverse matrix cracking and its plastic deformation govern the fracture response of polymer-matrix composites during the compressive loading stage. Using the experimental data about damage mechanisms introduced during the multiaxial loading state, Totry *et al.* [61] simulated 3D representative volume elements to predict the failure locations of Carbon/PEEK thermoplastic composite laminate under transverse compression and longitudinal shear loads. Liu and Li [62] explored the failure behavior of Glass/PC thermoplastic composite material subjected to tensile and shear loadings by generating corresponding RVEs and applying periodic boundary conditions. Plastic deformation and damage evolution phenomena during the finite element analysis were captured using the implementation of a VUMAT subroutine. The results reveal that while tension/shear load ratio and interface strength values considerably affect the failure response of the material, fiber distribution has a minimal effect on the outcome. Fedulov *et al.* [63] proposed a material model that considers the

70

plasticity along with the damage initiation and propagation for PEEK thermoplastic resin supplied by Cytec [67]. According to the results, this model was successful in predicting the transverse tensile strength of Carbon/PEEK thermoplastic composite laminate, when it was compared to experimental data. They also performed analysis for fiber pull-out tests and showed that the PEEK material in the vicinity of the interface exhibits a strengthening effect, mainly due to the high plastic deformation and transition of shear stress state to compression-dominated counterpart.

In composite laminates, transverse matrix microcracking frequently acts as the primary failure mechanism, governing the subsequent crack initiation and propagation. Previous studies revealed microstructural features introduced by the AFP in-situ consolidation process, such as voids, interlaminar resin pockets, and variation in the degree of crystallinity, compared to autoclave treatment. While these features were shown to significantly influence the stiffness properties in the transverse direction [37], their effect on strength characteristics remains unanswered. Therefore, the present research work aims to predict the transverse tensile strength of Carbon/PEEK thermoplastic composite material fabricated using the AFP in-situ consolidation process. To accomplish this, 2D micro-scale Representative Volume Elements (RVEs) were developed based on random fiber distribution. In the numerical analysis, the Drucker-Prager model, coupled with a ductile failure criterion, is used to take into account the plastic behavior and damage progression within the PEEK resin. To obtain the essential inputs for micromechanical analysis, two groups of specimens, fabricated using the AFP in-situ consolidation and autoclave re-consolidation methods, were subjected to micrographic study and DSC analysis. Finite element modeling was thoroughly implemented using ABAQUS Scripting Interface (ASI), written in Python programming language, along with MATLAB code that aided in generating the RVE geometries (refer to "MATLAB code for transverse cross-section" section in the Appendix for more details). This approach ensured an accurate representation of the material's microstructure to predict the tensile strength in the transverse direction, addressing the gap in experimental data currently absent in the literature. The absence of such information is predominantly attributed to the warpage and distortion arising during the AFP process when a heated tool is not used. The results confirm that the AFP in-situ consolidation process negatively affects the material properties of Carbon/PEEK thermoplastic composite material, which must be paid attention to in the finite element analyses and design procedures of AFP-made thermoplastic composite laminates.

3.2. Experimentation

Although in-situ consolidation provides a fast and efficient fabrication approach, it is essential to consider the possible imperfections that can emerge during the automated fiber placement process, particularly because they can significantly compromise the mechanical performance of composite structures. The limited processing time associated with the in-situ consolidation method results in a very high cooling rate which adversely affects the crystallinity, the attainment of the desired fiber volume fraction, and the removal of void content compared to the autoclave manufacturing process. Additionally, due to the short time available for fiber redistribution, while the matrix remains molten, resin-rich regions are prone to form between the composite layers, causing a change in the stress distribution inside the plies.

Accurate input data is necessary for micromechanical analysis in order to distinguish between the RVEs representing Carbon/PEEK thermoplastic composite laminates made by different fabrication processes. In this regard, the upcoming sections provide the work plan to manufacture two Carbon/PEEK thermoplastic composite laminates by AFP in-situ consolidation and autoclave re-consolidation techniques. These laminates were subjected to micrographic study and thermoanalytical DSC analysis to gather the detailed information (i.e., fiber volume fraction, void content, interlaminar resin pocket and degree of crystallinity) required for a precise prediction of transverse tensile strength values resulting from each manufacturing method.

3.2.1. Manufacturing process

Researchers at the Concordia Centre for Composites (CONCOM) have access to an Automated Fiber Placement (AFP) machine that incorporates a thermoplastic head assisted by a Hot Gas Torch (HGT) heating system. This thermoplastic AFP head is mounted on a 6-axis Kawasaki articulated robotic arm, which has a payload capacity of 125 kg and is supplied by the Trelleborg Group, as shown in Figure 3.1 (a). The fabrication of composite laminates utilized unidirectional AS4/APC-2 prepreg tape, supplied by the Solvay Group (Cytec) [67], which comprises a fiber-to-resin weight ratio of 68:32, achieving a fiber volume fraction of 60%, with an individual ply thickness of 0.140 mm. During the AFP in-situ consolidation process, the applied parameters were meticulously adjusted to ensure obtaining a high-quality final product; the hot gas torch temperature was maintained at 875 °C, with a nitrogen flow rate of 80 SLPM, a compaction force

of 60 lbf, and a deposition rate of 2 in/s. These processing conditions closely correspond to the optimum values cited in the literature, thereby ensuring consistent material quality and performance [13,14].

Additionally, to establish a reference baseline, half of the in-situ-consolidated Carbon/PEEK thermoplastic composite laminate was sectioned, vacuum-bagged, and subsequently subjected to an autoclave re-consolidation process, as shown in Figure 3.1 (b). The autoclave treatment was carried out under controlled conditions, with a processing temperature of $390° \pm 10$ °C and a pressure of 100 ± 5 psi, sustained for a period of 20 ± 5 minutes [67]. A comparative analysis of these two laminate types allows for a comprehensive assessment of the influence of the AFP process on critical microstructural attributes, including fiber volume fraction, void content, interlaminar resin pockets, and degree of crystallinity.

<center>(a)   (b)</center>
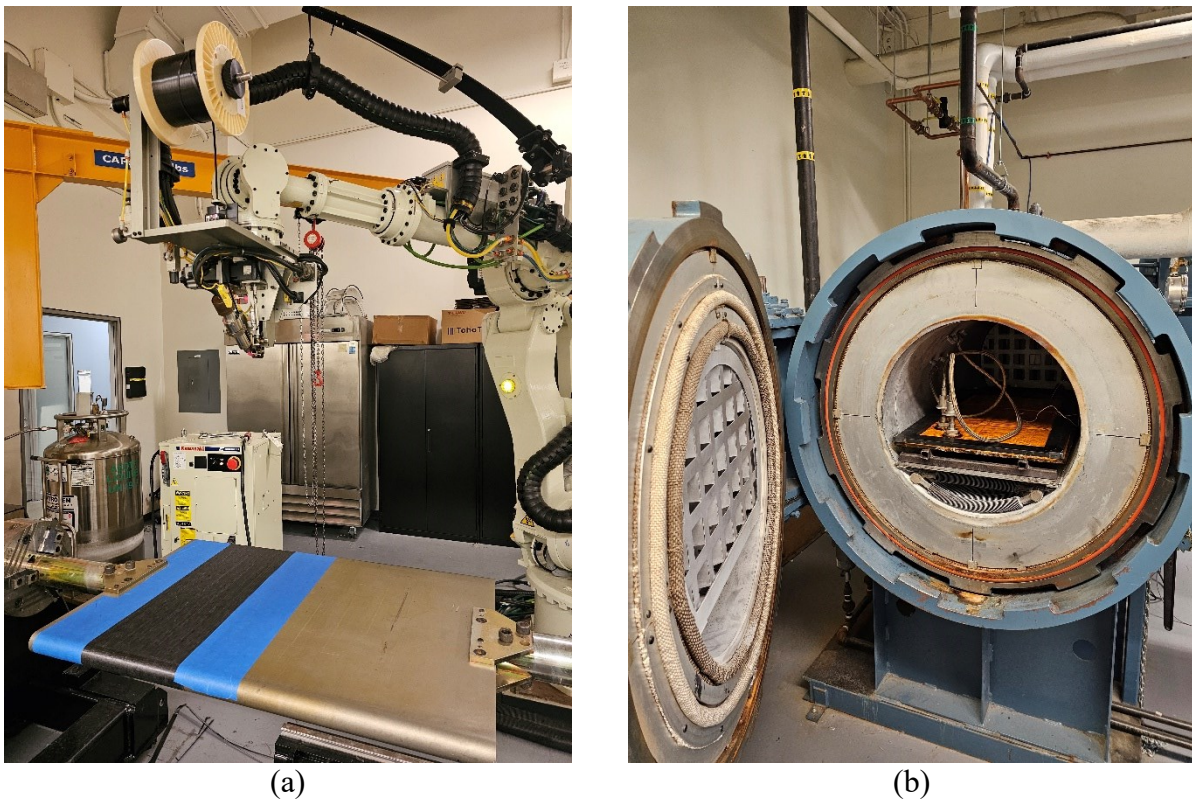
Figure 3.1. Manufacturing Carbon/PEEK thermoplastic composite laminates with two techniques: (a) HGT-assisted AFP machine available at CONCOM and (b) autoclave re-consolidation of AFP-made laminate.

3.2.2. Micrographic examination

A detailed microstructural analysis of Carbon/PEEK thermoplastic composite laminate samples manufactured using autoclave re-consolidation and AFP in-situ consolidation offers valuable insights into the fundamental causes of the observed differences in their mechanical performance. To achieve this, specimens from both fabrication methods were sectioned and polished to facilitate microscopic examination. The micrographic investigation unveiled significant differences between the two laminate types, particularly in terms of interlaminar resin-rich regions, void content, and void distribution, as shown in Figure 3.2. These microstructural discrepancies are identified as key contributors to the variations in the material properties of the resulting composite structures. The micrographic observations clearly indicate that the AFP in-situ consolidation process induces notable alterations in fiber distribution, leading to the formation of more distinguishable adjacent layers by introducing a separation between them. However, autoclave re-consolidation facilitates fiber mobility at the interfaces of the layers, yielding a more uniform laminate structure with indistinguishable layer boundaries. Unlike In-situ-consolidated thermoplastic laminates, those subjected to autoclave treatment exhibit no evident layer separation or resin-rich regions between adjacent plies, signifying a more homogeneous and well-consolidated microstructure.

The evaluation of fiber volume fraction, void content, and interlaminar resin pocket percentage was conducted using the color thresholding technique implemented in ImageJ software. This method enabled the distinction between voids, fibers, and resin within the composite microstructure. A series of randomly selected micrographs, representing different regions of the samples, were analyzed to obtain the average values for these factors. The findings reveal that autoclave re-consolidation substantially reduces the presence of voids and resin-rich areas, achieving a fiber volume fraction of approximately 60%. In contrast, the AFP in-situ consolidation process results in an average fiber volume fraction of 56%, accompanied by an average void content of 1.5% and an interlaminar resin pocket of 12%. Further details regarding the measurement methodology for each factor can be found in our previous research work [37].
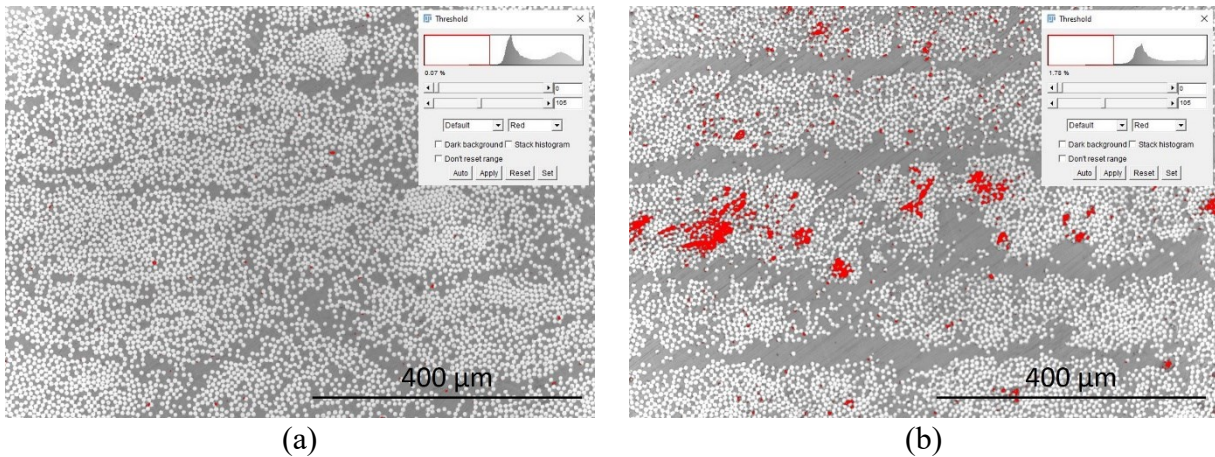
Figure 3.2. Typical micrographs of thermoplastic composite specimens manufactured by (a) autoclave re-consolidation and (b) AFP in-situ consolidation processes (20X magnification): threshold set to 0-105.

Voids play an essential role in influencing the mechanical properties of composite laminates. Within the microstructure resulting from the AFP process, voids can be broadly classified into two categories: (a) intralaminar voids and (b) interlaminar voids. Intralaminar voids are introduced during the tape manufacturing stage and typically comprise entrapped air, moisture, and other volatile substances that become dissolved or trapped within the individual ply. The formation of these voids can be mitigated during the AFP process using elevated compaction force and heat which facilitate the air evacuation. Nonetheless, interlaminar voids arise at the interfaces between adjacent layers during the tape placement stage. These voids are predominantly governed by the degree of intimate contact attained between plies, which is strongly influenced by the AFP processing parameters. According to the micrographic study of in-situ-consolidated thermoplastic composite specimens available in the literature, the elimination of interlaminar voids can be achieved by utilizing the optimum processing parameters during the in-situ consolidation process [9,34,38,39]. Therefore, the microstructure of AFP in-situ-consolidated thermoplastic laminates may exhibit either exclusively intralaminar voids or a combination of both intralaminar and interlaminar voids, depending on the applied processing parameters and their effectiveness in enhancing layer consolidation. It is important to highlight that, in the present research, the Carbon/PEEK thermoplastic composite specimens fabricated through AFP in-situ consolidation exhibit mostly intralaminar voids. This outcome can be attributed to the implementation of optimized AFP processing parameters, which effectively mitigated the formation of interlaminar voids by enhancing the degree of intimate contact between plies during the consolidation process, as shown in Figure 3.2.

When resin-rich areas are formed between the composite layers, fibers are forced to stay closer to one another at the center of each layer. This proximity of fibers causes stress concentration within the composite ply, adversely affecting the crack initiation and propagation in the transverse direction [37,50]. In these circumstances, the negative effect that intralaminar and interlaminar voids can produce on the transverse tensile strength of composite laminates is significantly different, as interlaminar voids, often found at ply interfaces, may promote delamination [14,34,38,39] rather than influencing the strength value in the transverse direction. Thus, it is of great importance to not only quantify the total void content but also accurately identify the specific type of voids present in the microstructure, as the intralaminar and interlaminar voids can exert significantly different influences on the transverse tensile strength of composite laminates.

3.2.3. DSC analysis

Another critical factor influencing the material properties is the degree of crystallinity, which can be quantitatively determined using a Differential Scanning Calorimetry (DSC) apparatus made by TA Instruments. For this purpose, 10 mg samples were extracted from both in-situ-consolidated and autoclave-reconsolidated Carbon/PEEK thermoplastic composite laminates and subjected to a heat-cool-heat cycle. The testing procedure involved heating at a controlled rate of 10 °C/min up to a peak temperature of 390 °C under a Nitrogen atmosphere, followed by cooling at a rate of 5 °C/min. The degree of crystallinity, X, was calculated using the following equation [5,112]:

$$X = \frac{\Delta H_m - \Delta H_c}{\Delta H_f(1 - \alpha)} \tag{3.1}$$

where α represents the weight fraction of Carbon fibers (i.e., 68%) within the Carbon/PEEK thermoplastic composite tape. The terms ΔH_m and ΔH_c correspond to the enthalpies of fusion at the endothermic melting point and exothermic crystallization peak. The enthalpy value for fully crystalline PEEK, ΔH_f, was taken as 130 J/g as reported in the literature [113]. Table 3.1 shows the outcome of the DSC analysis, with mean values of the degree of crystallinity and melting temperature measured from at least five Carbon/PEEK samples produced by each manufacturing method.

Table 3.1. Mean values of degree of crystallinity and melting temperature of Carbon/PEEK thermoplastic composite material manufactured by AFP in-situ consolidation and autoclave re-consolidation methods.

	Crystallinity (%)	SD[*]	Melting temperature (°C)	SD[*]
AFP In-situ consolidation	25.07	0.82	345.31	0.17
Autoclave re-consolidation	34.96	0.38	345.52	0.15

*SD = Standard Deviation

Depending on the AFP processing parameters (i.e., temperature, compaction force and deposition rate) and type of heating system, such as a hot gas torch, the in-situ consolidation process may result in a degree of crystallinity ranging from 15% to 30% [5,38,40,41]. For instance, higher deposition rate or insufficient compaction pressure can lead to rapid cooling and insufficient heat transfer, thereby reducing the degree of crystallinity. Several studies have investigated the influence of crystallinity on the material properties of neat PEEK resin, revealing that a reduction in crystallinity results in a decline in both elastic modulus [30,46,47] and tensile strength [46,112], with an approximately linear correlation within the AFP-related crystallinity range. As a result, in the present research, a reduction of 4% in elastic modulus and 7% in tensile strength of neat PEEK resin was assumed for every 5% decrease in the degree of crystallinity from the baseline value of 35%. This assumption is in good agreement with the findings reported in the literature and provides a reasonable and representative estimation [30,46,47,112].

3.3. Numerical analysis

After obtaining the results of the micrographic examination and DSC analysis for the Carbon/PEEK thermoplastic composite material, essential insights into the microstructure and the degree of crystallinity induced by the AFP process were obtained. Utilizing this information, RVEs representative of AFP in-situ consolidation could be developed to evaluate their mechanical performance. It is important to note that since, apart from the fiber volume fraction, all critical factors are associated with the resin phase, the transverse cross-section of the composite material, where matrix behavior plays a dominant role, was selected for numerical analysis to enhance computational efficiency. Afterwards, the modeled RVEs were subjected to Periodic Boundary Conditions (PBCs), and homogenization theory was applied to predict the transverse tensile strength values resulting from in-situ consolidation and autoclave re-consolidation processes.

3.3.1. RVE generation

Achieving a high fiber volume fraction in Representative Volume Elements (RVEs) with randomly distributed fibers presents a considerable challenge, as conventional random generators in programming languages such as MATLAB and Python struggle to determine suitable positions for new fiber center points. Thus, in the present research, an advanced algorithm originally proposed by Melro *et al.* [54] and subsequently refined by Ghayoor *et al.* [50] was employed. This method enhances the spatial distribution of fibers by strategically repositioning the most isolated fibers (called fiber stirring [54]) within the RVE, thereby enabling the attainment of a high fiber volume fraction, i.e., 60%.

To accurately simulate the influence of interlaminar resin pockets (i.e., resin-rich regions) observed in AFP in-situ-consolidated samples on the transverse tensile strength of composite laminates, a boundary constraint approach [37] was implemented in the RVE generation process. In fact, restrictions were imposed on the top and bottom boundaries to ensure that fibers would be positioned closer together in the central region of the RVE. This was achieved by limiting the random generation of fibers' center points within a predefined range along the y-direction of the RVE (e.g., from 6% to 94% of the RVE length results in the formation of a 12% interlaminar resin pocket). By maintaining the constant fiber volume fraction, this approach effectively relocated the fibers toward the core of the RVE to generate resin-rich regions at the top and bottom boundaries, closely replicating the microstructural characteristics observed in the micrographic study.

To consider voids within the matrix phase, the Random Sequential Adsorption (RSA) algorithm [52] was implemented to randomly generate void center points by eliminating the corresponding resin material (i.e., creating circular holes). If a newly generated point overlaps with an existing fiber-occupied region, the algorithm discards it and generates a new point. Once a proper position is identified, a void radius is randomly assigned within a range from zero to the shortest distance between the void center and the neighbouring fibers. This iterative process is repeated until the desired void percentage is successfully attained. The final geometries of RVEs representing AFP in-situ consolidation and autoclave re-consolidation processes are depicted in Figure 3.3 (for more information on void generation strategies and determining the RVE geometries, see our previous research work [37]).
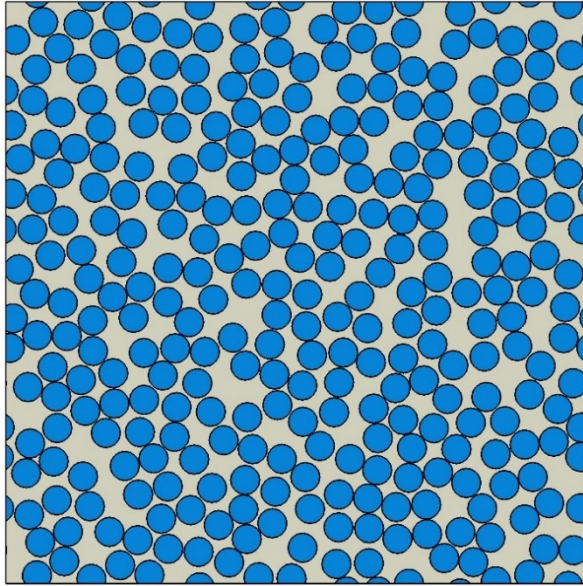
Fiber volume fraction = 60%
Void content = 0%
Interlaminar resin pocket = 0%
(a)
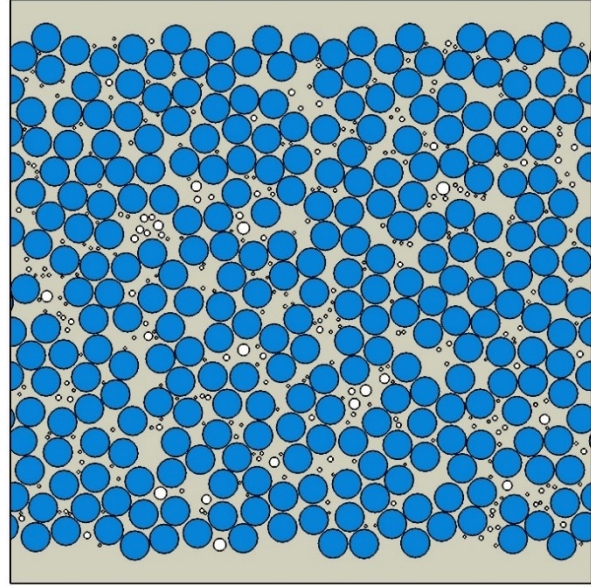
Fiber volume fraction = 56%
Void content (intralaminar) = 1.5%
Interlaminar resin pocket = 12%
(b)

Figure 3.3. Examples of RVE geometries generated to predict the transverse tensile strength of Carbon/PEEK thermoplastic composite material manufactured by (a) autoclave re-consolidation and (b) AFP in-situ consolidation.

It should be noted that the use of 2D RVEs limits the proposed simulation approach, as it cannot capture microstructural features that require three-dimensional representation, such as the volumetric morphology of voids or fiber waviness. In addition, only a limited set of material properties (stiffness and strength), which can be investigated through the transverse cross-section of the composite materials, can be assessed using 2D RVEs.

3.3.2. Finite element modeling

Following the completion of the RVE geometries based on the predefined fiber volume fraction, void content, and interlaminar resin pocket percentage, micro-scale finite element analysis was carried out on the transverse cross-section of the thermoplastic composite materials. These simulations were executed through the ABAQUS Scripting Interface (ASI), implemented in Python (refer to "Python script for strength prediction" section in the Appendix for more details), using an explicit solver with double-precision accuracy. The Representative Volume Elements (RVEs) were modeled with a length of 140 μm, which equals the thickness of a single Carbon/PEEK ply, along with 7-μm-diameter Carbon fibers that were randomly arranged within

79

the RVE, ensuring a minimum separation distance of 0.01 times the fiber radius. This RVE size allows for the accurate incorporation of interlaminar resin pockets on the top and bottom surfaces of the RVE. It is important to highlight that in fiber-reinforced composites, the size of the representative volume element (RVE) is generally determined by the ratio of the RVE length to the fiber radius, expressed as $\delta = l/r$. Selecting an appropriate RVE size is critical to ensure the material's morphology and mechanical behavior are accurately captured in a statistically representative way. According to the dimensions of the given RVE, the ratio δ equals 40, with l = 140 μm and r = 3.5 μm. This value is a good fit for the analysis because it has been shown to effectively characterize Carbon-reinforced polymers [50,114].

After conducting a mesh convergence analysis, quadrilateral 4-node bilinear plane strain elements with reduced integration (CPE4R) were selected, with an element size set to one-fourteenth (1/14) of the fiber radius, as shown in Figure 3.4. Due to the relatively small element size in comparison with the overall RVE dimensions, the model comprised more than 400,000 elements, whereby the computational effort required for the analysis exceeded the processing capacity of a standard desktop computer. To this end, all numerical simulations were carried out using the High-Performance Computing (HPC) facility, SPEED [115], which consists of twenty-four 32-core compute nodes. This HPC system is specifically designed to accommodate multi-core computations, memory-demanding operations, and iterative processing tasks. It also provides support for a wide range of open-source and commercial software, including ABAQUS, enabling efficient execution of computationally intensive analyses.
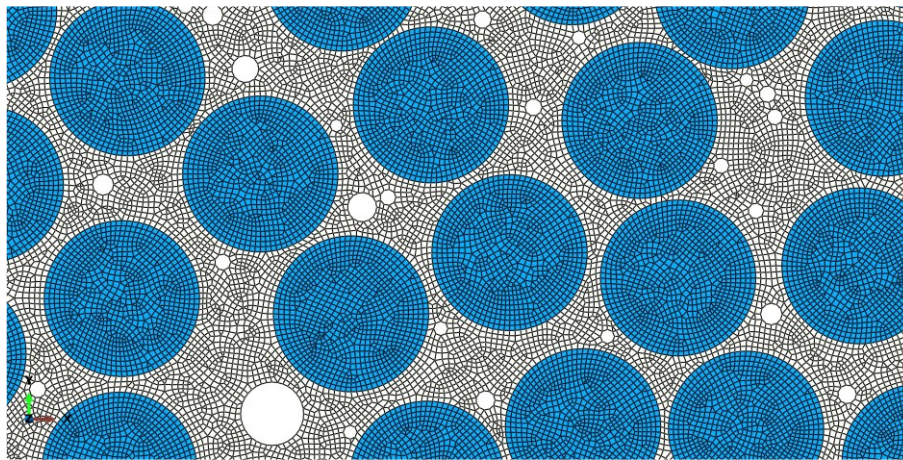
Figure 3.4. A portion of the RVE meshed using CPE4R elements with a size equal to 1/14 of the fiber radius.

Fedulov *et al.* [63] developed a material model, based on stress triaxiality, aimed at capturing the plastic deformation and damage evolution in thermoplastic PEEK resin supplied by Cytec, which considers the influence of the stress state imposed on the matrix during the loading step. The benefit of employing stress triaxiality, defined as the ratio of hydrostatic stress to the Mises equivalent stress, lies in its capacity to smoothly and continuously capture the dependence of material properties on variations in the stress state. For the PEEK material, the plasticity model with a linear dependence on the triaxiality parameter, η, was proposed as follows [63]:

$$f(\eta)q = k_0$$

$$f(\eta) = 1 + C\,\eta$$

$$\eta = -\frac{p}{q}$$

$$p = -\frac{1}{3}trace(\sigma) \tag{3.2}$$

$$q = \sqrt{\frac{3}{2}(S:S)}$$

where C and k_0 are two constants equal to 0.5 and 89.8 MPa, respectively. p represents the equivalent pressure stress (hydrostatic stress). q is the von Mises equivalent stress defined by the stress deviator tensor, S.

If certain conditions are met, this plasticity model becomes analogous to the extended linear Drucker-Prager criterion (F), accounting for the influence of hydrostatic stress on the yielding response of the material, which is expressed below [85]:

$$F = t - p\tan(\beta) - d = 0$$

$$t = \frac{1}{2}q\left[1 + \frac{1}{K} - \left(1 - \frac{1}{K}\right)\left(\frac{r}{q}\right)^3\right] \tag{3.3}$$

$$d = \left(\frac{1}{K} + \frac{1}{3}\tan(\beta)\right)\sigma_t$$

where β, d and σ_t denote the angle of friction (dilatation angle), cohesion of the material and yield stress of uniaxial tension, respectively. K is the ratio of the yield stress in triaxial tension to the yield stress in triaxial compression. r represents the third invariant of the deviatoric stress. t denotes the deviatoric stress factor determining the shape of the yield surface in the deviatoric plane.

The original Drucker-Prager model can be obtained by adjusting $K = 1$, which indicates that the yield stresses are identical in both triaxial tension and compression scenarios. Moreover, by considering the C and k_0 constants in the proposed plasticity model, as presented in Eq. (3.2), to be analogous with $\tan(\beta)$ and d parameters in the Drucker-Prager law, the extended linear Drucker-Prager criterion will be exactly transformed to the plasticity model formulated by Fedulov *et al.* [63].

Regarding the failure criterion, it would be appropriate to consider that under compressive stress conditions, the PEEK resin material exhibits a higher degree of plastic deformation prior to failure compared to tensile loading scenarios, mirroring the behavior commonly observed in thermoset polymers [116]. This implies that the failure model should consider the tendency for reduced damage progression under compressive plastic deformation while incorporating more damage accumulation under tensile loads. To accommodate these characteristics, the ductile failure criterion was introduced as follows [63]:

$$D = \int \frac{d\varepsilon_{eq}^{pl}}{\varepsilon_D^{pl}(\eta)} \tag{3.4}$$

where ε_{eq}^{pl} denotes the equivalent plastic strain corresponding to the tensile stress, σ_t^{pl}, which is determined from uniaxial tensile testing. ε_D^{pl} is failure strain that is experimentally characterized for the PEEK resin as a piecewise-defined linear function of stress triaxiality, η.

Therefore, the proposed model can be adjusted to take into account more accumulation of continuum damage under tensile loading relative to compressive loading. The damage variable, D, ranges from 0 to 1. While D remains below 1, it doesn't have an influence on the simulation. However, once it reaches a value of 1, the failure criterion is met, whereby the material stiffness is reduced to zero.

It should be noted that the aforementioned extended Drucker-Prager formulation and ductile failure criterion are readily implemented in the material model libraries of widely utilized finite element analysis software, including ABAQUS. The mechanical properties of the Carbon fibers along with the relevant mechanical constants of the PEEK resin, which together constitute the thermoplastic composite material, are summarized in Table 3.2.

Table 3.2. Mechanical constants and material properties used for the PEEK resin (APC-2) and Carbon fibers (AS4) in the transverse direction [63,67].

Properties of Carbon fiber		Tensile hardening of PEEK		Failure strain of PEEK	
$E_2\ (GPa)$	22	$\sigma_t^{pl}(MPa)$	ε_{eq}^{pl}	η	ε_D^{pl}
ν_{23}	0.25	77	0	-0.333	1.5
Properties of PEEK		81	0.1	0	1
$E\ (GPa)$	3.6	100	0.5	0.333	0.7
ν	0.38	101	2	0.495	0.55
$d\ (MPa)$	89.8			0.666	0.4
$\beta\ (°)$	27			1	0.2

The RVEs simulated in the transverse direction, employing the material model designated for the PEEK resin, assume perfect adhesion between the fiber and matrix phases. This assumption can be justified through three key points: (a) Thermoplastic resins, such as PEEK, typically exhibit an increased degree of crystallinity near the fibers due to the nucleation of crystals, which enhances the strength of the PEEK material in these regions. (b) As a result of the increased degree of crystallinity, Gao and Kim [112] revealed that the shear interface strength of Carbon/PEEK thermoplastic composite material during the fiber pull-out tests varies between 80 and 120 MPa, which is significantly greater than the shear strength of neat PEEK resin which is 55 MPa. (c) Fedulov *et al.* [63] conducted fiber pull-out analyses, demonstrating that the PEEK material near the interface exhibits a strengthening effect. This is primarily attributed to the transition of the shear to a compression-dominated stress state during which more plastic deformation can occur before failure. Therefore, matrix cracking precedes interfacial failure in the Carbon/PEEK thermoplastic composite laminates under transverse tensile loading conditions.

Since composite materials normally consist of an array of Representative Volume Elements (RVEs) that are arranged in close proximity to one another, applying Periodic Boundary Conditions (PBCs) is crucial to obtaining precise and trustworthy results. By ensuring that all

RVEs undergo uniform deformation, PBC execution helps to avoid gaps or overlaps at their interfaces. The RVE technique, combined with periodic boundary conditions, offers a strong foundation for carrying out micromechanical investigations. The formulation of periodic boundary conditions is expressed as follows [68,69]:

$$u_i^{j+} - u_i^{j-} = \bar{\varepsilon}_{ik}\left(x_k^{j+} - x_k^{j-}\right) = \bar{\varepsilon}_{ik}\Delta x_k^j \tag{3.5}$$

where u_i and $\bar{\varepsilon}_{ik}$ denote the displacement and the average strain, respectively, at a specific point along the boundary of the RVE. The variable x_k represents the Cartesian coordinate of the corresponding point. To distinguish between the opposing boundaries of the RVE, the superscripts $j+$ and $j-$ are introduced, which identify the jth pair of parallel and opposite edges within the representative volume element.

To ensure the continuity of both traction and displacement fields, periodic boundary conditions (PBCs) are imposed on the RVE using Eq. (3.5). The reduced form of the PBCs formulation for tensile loading conditions, as shown in Figure 3.5, is presented as follows:

$$\begin{cases} u_{DC} - u_{AB} = u_D - u_A \\ u_{BC} - u_{AD} = u_B - u_A \end{cases} \tag{3.6}$$

where a single-letter subscript designates a specific vertex, whereas a two-letter combination denotes an edge linking the corresponding vertices.
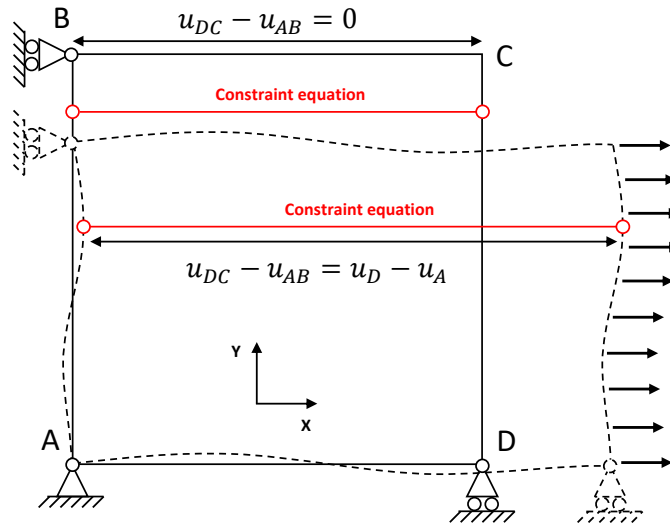
Figure 3.5. The schematic of periodic boundary conditions applied to the RVE that is subjected to tensile loading.

The mechanical behavior of the RVE is generally considered representative of the response observed in the unidirectional composite lamina at the macrostructural level. The effective material properties of the RVE are determined by employing homogenization theory [37,69], which evaluates the RVE's response under different loading scenarios. As a result, the volume average stress, $\bar{\sigma}$, was computed at each increment of the finite element simulation. The peak value of this stress, recorded immediately prior to the final failure in which load-carrying capacity decreases due to the crack propagation throughout the RVE, is identified as the transverse tensile strength of the composite material.

3.4. Results

In a previous study [37] of the present authors, the effects of microstructural features, including fiber volume fraction, void content, interlaminar resin pocket and degree of crystallinity, on the transverse stiffness properties of in-situ-consolidated Carbon/PEEK thermoplastic composite material, were investigated. The results revealed that the AFP process may on an average reduce the transverse elastic and out-of-plane shear moduli by almost 10% and 20%, respectively, while the out-of-plane Poisson's ratio doesn't undergo a change, in comparison with those of the autoclave-treated counterparts. It is worth mentioning that micromechanical approaches are used not only to explore the overall behavior of composite materials but also to analyze the crack onset and evolution, whereby strength properties could be estimated. To this end, in the present research, the transverse matrix cracking, incorporating both the plastic deformation and damage mechanism of the neat PEEK resin into the simulation, was studied to numerically predict the transverse tensile strength value, resulting from the AFP in-situ consolidation process, in which more deviation from autoclave method was expected to be observed.

Once the finite element model was generated, the initial step to ensure the accuracy of the numerical analysis involved selecting an appropriate mesh type and size. Generally, while 3-node triangular elements are often used for complex geometries due to their compatibility, 4-node quadrilateral elements provide more accurate results, particularly in damage modeling during which precision is of great importance. As a result, quadrilateral 4-node elements (CPE4R) were selected for the finite element analysis in the present research. Moreover, to determine the ideal element size to make a balance between accuracy and computational efficiency, a mesh

convergence study was performed, as shown in Figure 3.6. For this purpose, an RVE containing 60% fiber volume fraction, representing the autoclave manufacturing process, was generated with four different element sizes relative to the fiber radius (i.e., 1/4, 1/7, 1/10 and 1/14 of the fiber radius). According to the results indicated in Figure 3.6 (b), reducing the element size from 1/4 (0.875 micron) to 1/14 (0.250 micron) of the fiber radius for the same RVE significantly impacts the predicted transverse tensile strength, which decreases from approximately 90 MPa to 82 MPa. It should be noted that even though mesh ratios of 1/10 and 1/14 yield almost the same strength values, the latter element size was chosen for the analysis. This choice can be justified by the fact that using an element size of 1/14 of the fiber radius resulted in a considerably smaller failure strain, as illustrated in Figure 3.6 (a), which aligns with the failure strain of 0.0088 reported in the material datasheet [67].

(a)   (b)
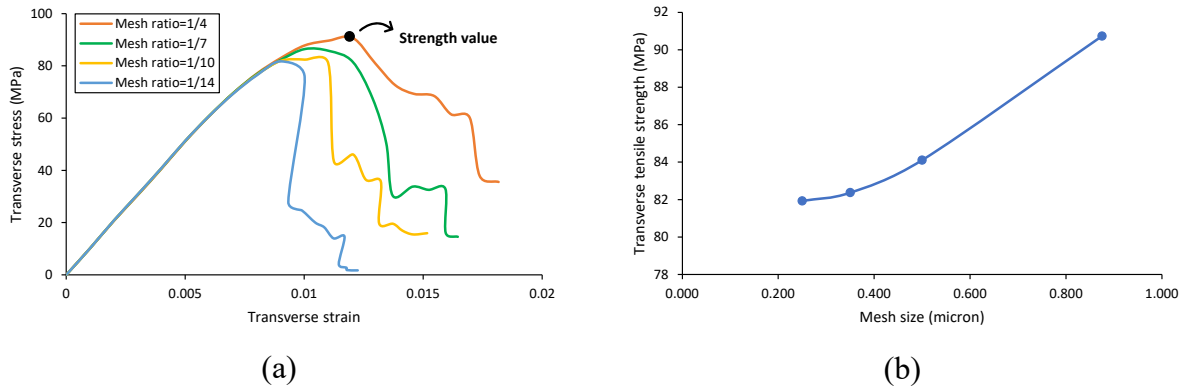
Figure 3.6. Mesh convergence study to determine the suitable element size in the finite element analysis.

3.4.1. Validation

Representative Volume Elements (RVEs) with a fiber volume fraction of 60% were generated to validate the outcomes obtained by finite element analysis, as shown in Figure 3.3 (a). This process ensured the absence of void content and interlaminar resin pockets to replicate the conditions of the autoclave manufacturing technique. Figure 3.7 shows the stress-strain curves obtained from the numerical analysis of five different RVEs for Carbon/PEEK thermoplastic composite material. While their elastic regions exactly coincide with each other and match the elastic modulus of 10.3 GPa provided by Cytec [67], their responses differ in terms of plastic deformation and failure behavior, resulting in achieving various strength values (peak points of stress-strain curves) in the transverse direction. This observation highlights the effect of stress concentration areas on the damage initiation and propagation, which, in this case, originate from fiber arrangement solely

(the closer the fibers are positioned next to each other, the higher stress concentration will be created in the matrix phase). Table 3.3 presents the robustness of the proposed simulation approach in estimating the transverse tensile strength of Carbon/PEEK thermoplastic composite material, with an error margin of less than 5%, based on a comparison between the numerical predictions and the data available in the Cytec technical datasheet [67].
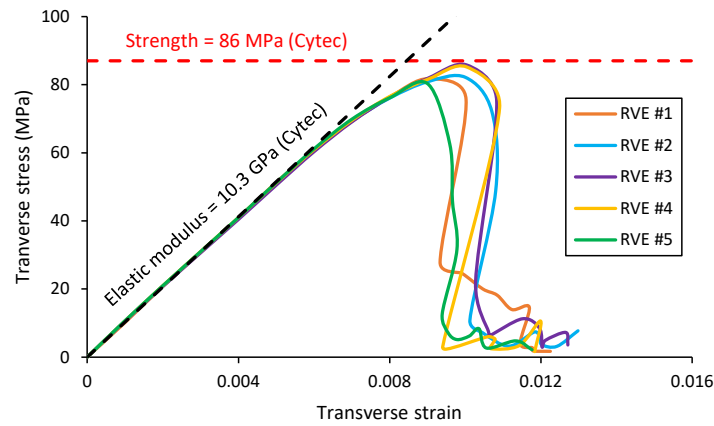
Figure 3.7. Stress-strain diagram of the RVEs representing autoclave manufacturing process that are subjected to transverse tensile loading.

Table 3.3. Predicted transverse tensile strength values for Carbon/PEEK thermoplastic composite material fabricated by autoclave process.

	RVE #1	RVE #2	RVE #3	RVE #4	RVE #5	Avg.	Cytec [67]	Error (%)
Transverse tensile strength (MPa)	82.2	82.6	85.8	85.2	81.3	83.4	86	3.0

Furthermore, to verify the transverse strength value reported in the Cytec datasheet [67], flat coupon specimens were extracted from the autoclave-reconsolidated Carbon/PEEK thermoplastic composite laminate using a circular diamond saw. The specimens, measuring 175 mm × 25 mm × 1.5 mm, featured fibers oriented at 90° to perform transverse tensile testing according to the ASTM D3039 standard [92]. The tests were run in displacement control mode, using a universal testing machine with a crosshead speed of 2.0 mm/min until complete failure of the specimens. Eventually, the strength values were calculated based on the maximum recorded load and the cross-sectional area of the samples. The mean transverse tensile strength obtained for autoclave-reconsolidated specimens was 81.0 MPa, with a standard deviation of 2.5 MPa (refer to "Tensile test" section in the Appendix for more details about specimen preparation and tensile testing of

AFP-made coupons). This further supports the notion that both experimental conditions and manufacturing variations (e.g., ply thickness, local crystallinity and voids not detectable in 2D micrographs) may contribute to lower-than-expected transverse tensile strength, independent of the modeling assumptions. This result is in good agreement with the average value predicted by numerical analysis and the value reported in the technical datasheet [67], as listed in Table 3.3.

3.4.2. Effect of each microstructural factor on the strength reduction

Upon validating the proposed Finite Element (FE) model, the effect of each factor, identified through micrographic examination and Differential Scanning Calorimetry (DSC) analysis as contributing to the differences between AFP in-situ consolidation and autoclave re-consolidation, can be evaluated. This investigation initially aims to quantify the significance of each factor in influencing the transverse tensile strength values. Afterwards, the objective is to develop Representative Volume Elements (RVEs) that closely replicate all the microstructural characteristics of the AFP in-situ-consolidated Carbon/PEEK thermoplastic composite material simultaneously, thereby enabling an accurate prediction of their tensile strength in the transverse direction.

To assess the significance of each factor, including fiber volume fraction, interlaminar resin pockets, void content and degree of crystallinity, in reducing the transverse tensile strength relative to that achieved through autoclave treatment, four distinct scenarios were analyzed. In each scenario, only one factor was changed from its autoclave-associated value to the corresponding mean value obtained from in-situ consolidation, while the remaining three factors remained unchanged. This approach facilitates the evaluation of the individual contribution of each factor to the overall reduction in the transverse tensile strength. The outcome of this investigation is presented in Table 3.4. The findings indicate that up to a 4% reduction in fiber volume fraction does not significantly affect the transverse tensile strength of the composite material, which is consistent with existing literature [117–120]. It is worth mentioning that reducing the fiber volume fraction from 60% to 56% results in minimal geometric changes, making the RVE visually similar to that shown in Figure 3.3 (a). This phenomenon can be attributed to the reduction in stress concentration regions within the matrix phase as the number of fibers decreases in the RVE, potentially even leading to a slight improvement in the strength. That is the reason why, despite the 100 MPa tensile strength of neat PEEK resin, the transverse tensile strength of Carbon/PEEK

thermoplastic composite material with a 60% fiber volume fraction is comparatively lower (i.e., 86 MPa) [67]. Introducing a 12% interlaminar resin pocket at the top and bottom of the RVE, as shown in Figure 3.3 (b), while maintaining the same number of fibers, forces the fibers to shift toward the center, resulting in a more compact fiber arrangement. The reduced spacing between fibers causes more stress concentration within the matrix phase, and subsequently earlier crack initiation and propagation, whereby the transverse tensile strength of the thermoplastic composite material is negatively affected, as listed in Table 3.4.

Voids, depending on their sizes, form areas inside the RVE through which the load cannot be properly transferred without causing stress concentration. The presence of these regions, therefore, creates localized stress concentration that may result in premature material failure. In other words, the empty spaces disrupt the continuous load path, adversely influencing the strength and integrity of the composite material. This explains why, incorporating 1.5% void content inside the RVE declined the transverse tensile strength of Carbon/PEEK thermoplastic composite material by almost 12%, as reported in Table 3.4. The final influencing factor is the degree of crystallinity which has a considerable effect on the stiffness and strength properties of the neat PEEK resin while it does not alter the geometry of the RVE. In the present research, 4% and 7% reductions were applied to the elastic modulus and tensile strength of the matrix phase, respectively, for every 5% decrease in the degree of crystallinity, in alignment with findings from previous research works [30,46,47,112].

To this end, the elastic modulus of PEEK was reduced to 3.312 GPa while its tensile strength was adjusted to 86 MPa, representing a 14% reduction from the initial value of 100 MPa. Similarly, all other hardening parameters, listed in Table 3.2, were proportionally scaled down by the same 14%. The results, as presented in Table 3.4, showed that the modification of neat PEEK material properties can negatively influence the tensile strength of the composite material by approximately 14%, highlighting the dominant matrix behavior in the transverse direction. In the end, this investigation revealed that the variation in the fiber volume fraction has a negligible effect on the transverse tensile strength. Although the presence of interlaminar resin pockets contributes to some reduction in the tensile strength, its effect remains relatively minor. In contrast, void content and degree of crystallinity prove to be the most influential factors, significantly degrading the transverse tensile strength of Carbon/PEEK thermoplastic composite material.

Table 3.4. The negative effect of each AFP-resulted factor on reducing the transverse tensile strength (MPa) of Carbon/PEEK thermoplastic composite material compared to the autoclave reference values (fiber volume fraction=60%, resin pocket=0%, void content=0% and degree of crystallinity=35%).

	RVE #1	RVE #2	RVE #3	RVE #4	RVE #5	Avg.	Difference* (%)
Scenario #1 (Fiber volume fraction=56%)	83.2	84.6	83.2	84.1	84.3	83.9	0.5
Scenario #2 (Interlaminar resin pocket=12%)	79.4	78.2	81.3	79.9	81.7	80.1	4.0
Scenario #3 (Void content=1.5%)	74.3	74.1	68.9	77.0	73.6	73.6	11.8
Scenario #4 (Degree of crystallinity=25%)	69.4	71.2	73.7	73.4	69.0	71.4	14.5

* With reference to the mean tensile strength that corresponds to the autoclave re-consolidation (i.e., 83.4 MPa).

3.4.2.1. Significance of void distribution

In order to show that not only the total void content but also void distribution (either intralaminar or interlaminar voids) plays a critical role in the reduction of transverse tensile strength caused by AFP in-situ consolidation, as compared to microstructure achieved through autoclave treatment, which features uniform fiber distribution and is largely void-free. To address this, two distinct scenarios were incorporated into the RVE generation process:

1) The first scenario focuses on simulating realistic microstructures that may be caused by the AFP process based on the processing parameters used. In this regard, two sets of RVEs were generated with respect to void content, containing either only intralaminar voids or a combination of interlaminar and intralaminar voids:

   - Total void content = 1.5% (intralaminar voids = 1.5%, interlaminar voids= 0.0%)
   - Total void content = 3.0% (intralaminar voids = 1.5%, interlaminar voids= 1.5%)

Due to the stress concentrations created within the RVE as a result of fibers' proximity, intralaminar voids are of particular importance. However, interlaminar voids are not expected to have a detrimental effect on the transverse tensile strength. The above-mentioned RVE sets were modeled to test this hypothesis.

2) The second scenario aims to demonstrate how void distribution, while maintaining a constant total void content, can impact the results by shifting voids from within the RVE (intralaminar)

90

to its top and bottom edges (interlaminar). To achieve this, three sets of RVEs were developed with the following void distributions:

- Total void content = 1.5% (intralaminar voids = 1.5%, interlaminar voids= 0.0%)
- Total void content = 1.5% (intralaminar voids = 0.75%, interlaminar voids= 0.75%)
- Total void content = 1.5% (intralaminar voids = 0.0%, interlaminar voids= 1.5%)

These analyses can help to clarify why the inclusion of interlaminar voids in the RVEs of the first scenario doesn't significantly affect the outcome. The final geometries of the above-mentioned RVE sets are illustrated in Figure 3.8.

Total void content = 1.5%
(Interlaminar voids = 0.0%)

Total void content = 3.0%
(Interlaminar voids = 1.5%)

(a) Scenario #1 – Intralaminar voids = 1.5%

Intralaminar voids = 1.5%
Interlaminar voids = 0.0%

Intralaminar voids = 0.75%
Interlaminar voids = 0.75%

Intralaminar voids = 0.0%
Interlaminar voids = 1.5%

(b) Scenario #2 – Total void content = 1.5%
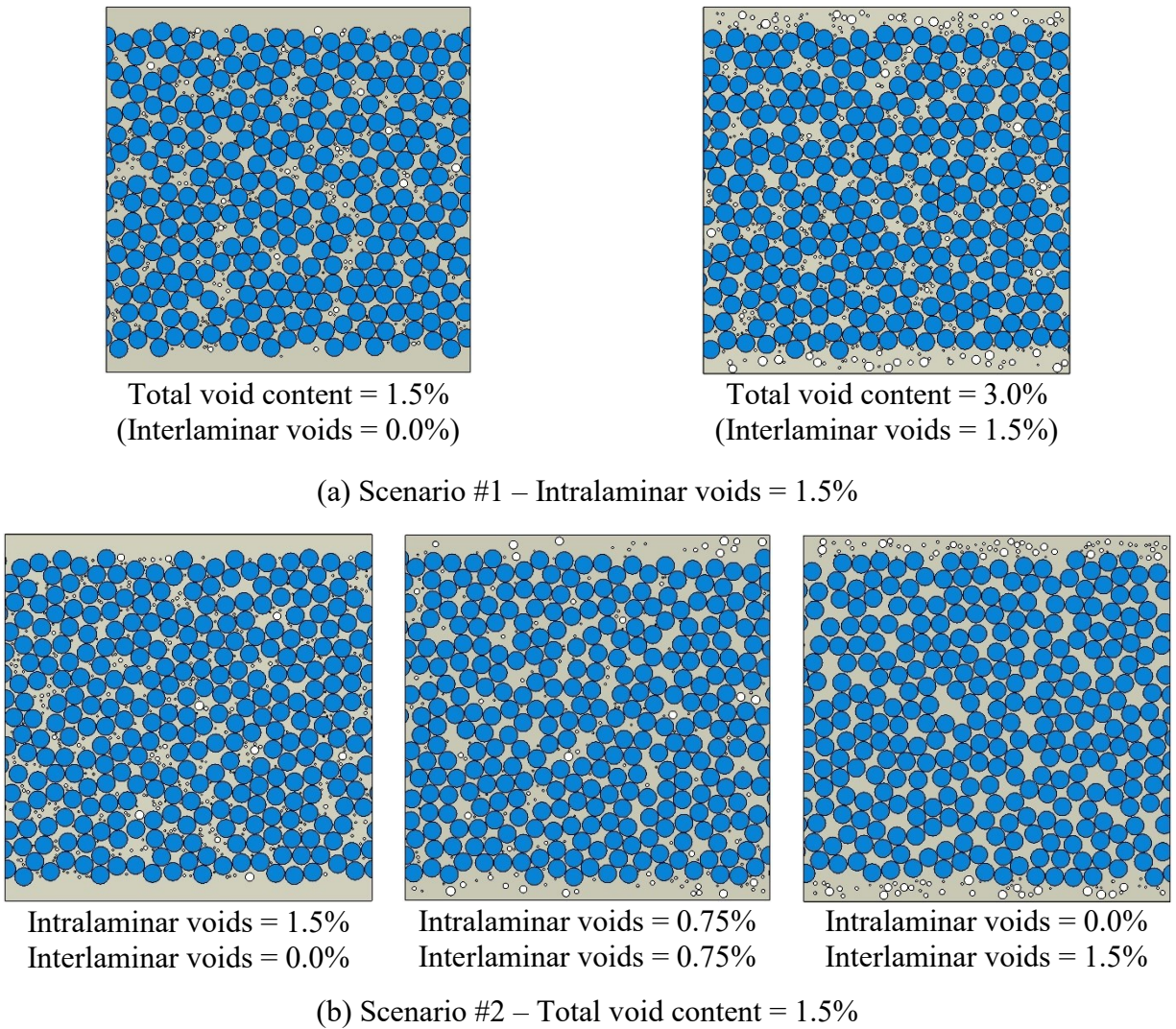
Figure 3.8. Examples of RVE geometries generated to investigate the effect of void content and void distribution with fiber volume fraction of 60% and interlaminar resin pocket of 12%: (a) first scenario and (b) second scenario.

91

The effects of voids introduced during the AFP in-situ consolidation process were investigated by changing the void content and distribution. These adjustments were intended to develop Representative Volume Elements (RVEs) that closely replicate the void formation characteristics of Carbon/PEEK thermoplastic composite laminates produced via in-situ consolidation. The average transverse tensile strength values derived from the corresponding RVE sets for each scenario are summarized in Table 3.5. It should be noted that five different RVEs were analyzed in each set. The results of Scenario #1 indicate that the presence of 1.5% intralaminar voids leads to a 17.64% reduction in transverse tensile strength compared to that of autoclave-reconsolidated laminates. Furthermore, increasing the total void content to 3% by introducing an additional 1.5% interlaminar voids into the microstructure does not significantly change the transverse tensile strength values of the RVEs. This observation can be attributed to the fact that, due to stress concentration inside the RVEs, the primary mechanisms of crack initiation and propagation are predominantly governed by intralaminar voids situated within the composite plies rather than those existing at the interface.

Table 3.5. Mean values (calculated from five different RVEs in each set) of predicted transverse tensile strength for Carbon/PEEK thermoplastic composite material with respect to void content and void distribution.

	RVE sets	Intralaminar voids (%)	Interlaminar voids (%)	Total void content (%)	Average transverse tensile strength (MPa)	Difference* (%)
Scenario #1	Set-1	1.5	0.0	1.5	68.72	17.64
	Set-2	1.5	1.5	3.0	67.01	19.68
Scenario #2	Set-1	1.5	0.0	1.5	68.72	17.64
	Set-2	0.75	0.75	1.5	75.83	9.11
	Set-3	0.0	1.5	1.5	80.47	3.55

* With reference to the mean tensile strength that corresponds to the autoclave re-consolidation (i.e., 83.43 MPa).

The findings from the RVE sets in Scenario #2 reveal the influence of void distribution within the RVEs while maintaining a constant total void content of 1.5%. The results show that relocating voids from the central regions of the RVEs to the upper and lower regions, where resin-rich areas are present, enhances the transverse tensile strength of the composite laminate. This improvement occurs because voids are shifted away from regions with stress concentration, caused by the proximity of fibers, to areas predominantly occupied by resin. Ultimately, transferring all voids to the resin-rich regions increases the transverse tensile strength to a level slightly below that of RVEs representing autoclave-reconsolidated laminates without void content. This phenomenon can be

explained by the fact that crack initiation mainly occurs at the center of the RVE due to stress concentration and subsequently propagates toward the resin pockets located in the top and bottom sections, perpendicular to the loading direction. As the crack progresses into the resin-rich regions, interlaminar voids begin to produce their effect; however, this typically occurs when the RVE approaches the final fracture. In other words, since interlaminar voids primarily affect the final stage of crack propagation, they have limited opportunity to significantly alter the overall results. Thus, it is crucial to perform a detailed micrographic study to identify the types of voids present in the microstructure (i.e., either intralaminar or interlaminar) in addition to quantifying the total void content resulting from the AFP in-situ consolidation process.

3.4.3. Prediction of AFP-influenced transverse tensile strength

Incorporating all these four factors simultaneously into the generated RVEs will allow for a reasonably precise prediction of the transverse tensile strength of the in-situ-consolidated Carbon/PEEK thermoplastic composite material. To this end, five distinct RVEs were created based on the mean values of the microstructural characteristics obtained by the micrographic study, including fiber volume fraction, interlaminar resin pocket percentage and void content, as depicted in Figure 3.3 (b). Additionally, the material properties (i.e., elastic modulus and tensile strength) of the PEEK resin were modified according to the mean degree of crystallinity measured by DSC analysis (i.e., 25%). It should be noted that the simultaneous occurrence of all these factors in the modeled RVEs can intensify the emergence of stress concentration regions, thereby influencing the crack onset and evolution, as depicted in Figure 3.9.
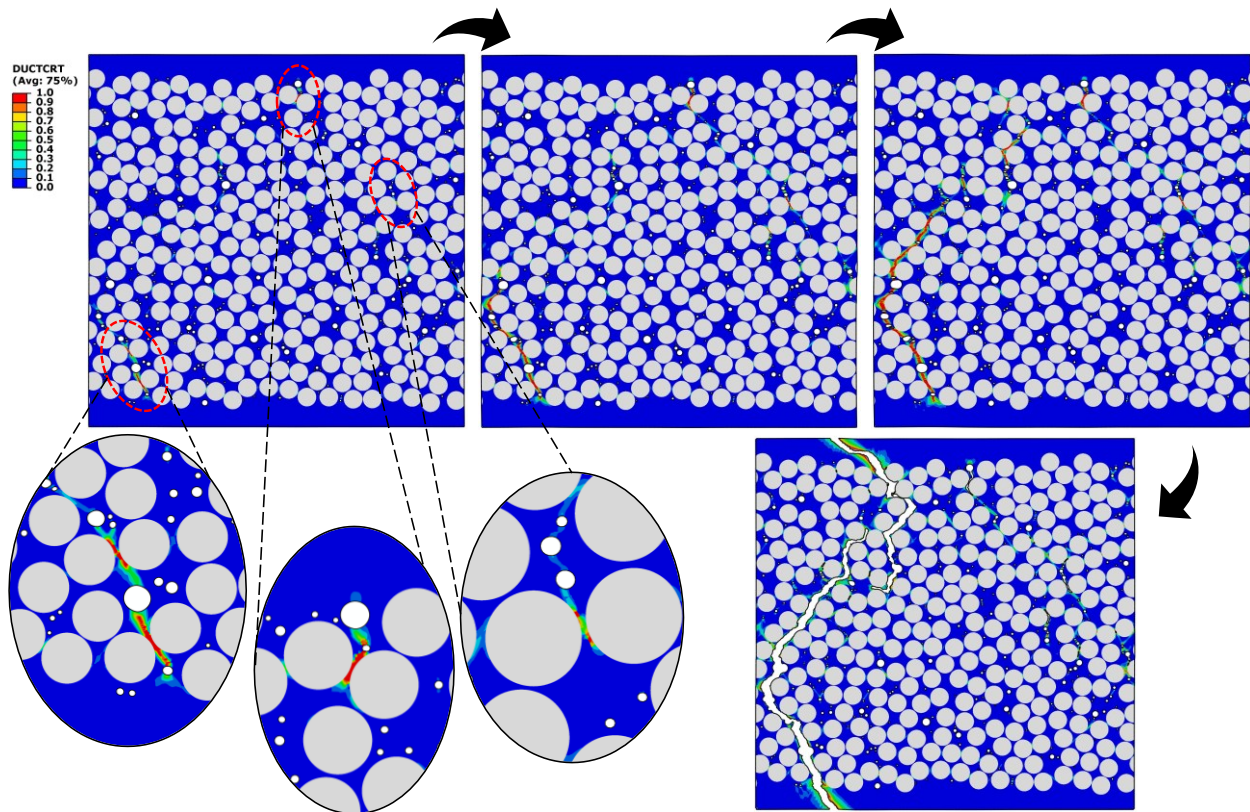
Figure 3.9. Example of crack onset and propagation inside an RVE generated based on the microstructural characteristics resulting from the AFP in-situ consolidation (i.e., with fiber volume fraction of 56 %, intralaminar void content of 1.5% and interlaminar resin pocket of 12%). Transverse displacement was applied to the RVE until final failure occurred.

To determine the mean values for intralaminar void content and the percentage of interlaminar resin pockets resulting from the in-situ consolidation, thirty micrographs were analyzed from various locations across the cross-section, all maintaining the same dimensions as the simulated RVEs [37]. The normal distribution plot of each factor, along with its mean value and standard deviation, is presented in Figure 3.10. Due to the relatively high standard deviation compared to the mean value for both factors, it cannot be claimed that the 1.5% intralaminar void content and 12% interlaminar resin pockets are uniformly distributed within the microstructure of the composite material. As a result, rather than relying solely on the mean values to predict the transverse tensile strength, it is more appropriate to consider a reasonable range for these two factors, thereby providing upper and lower bounds in addition to the average effective strength value. To account for these variations, a range spanning four standard deviations (from mean value - 2 times SD to mean value + 2 times SD) was considered for both factors, covering 95% of the

94

data points in the normal distribution diagrams. This range extends from 4% to 20% for the interlaminar resin pocket and from 0.5% to 2.5% for the intralaminar void content, as illustrated in Figure 3.10. Due to these inherent uncertainties in the AFP process, the mechanical behavior of different regions within the same composite laminate may vary, depending on the characteristics of the microstructure formed, even if the mean values of void content and interlaminar resin pockets remain consistent throughout the fabricated laminate.

Mean value = 12.13%
Standard deviation = 4.07%
(a)

Mean value = 1.49%
Standard deviation = 0.51%
(b)
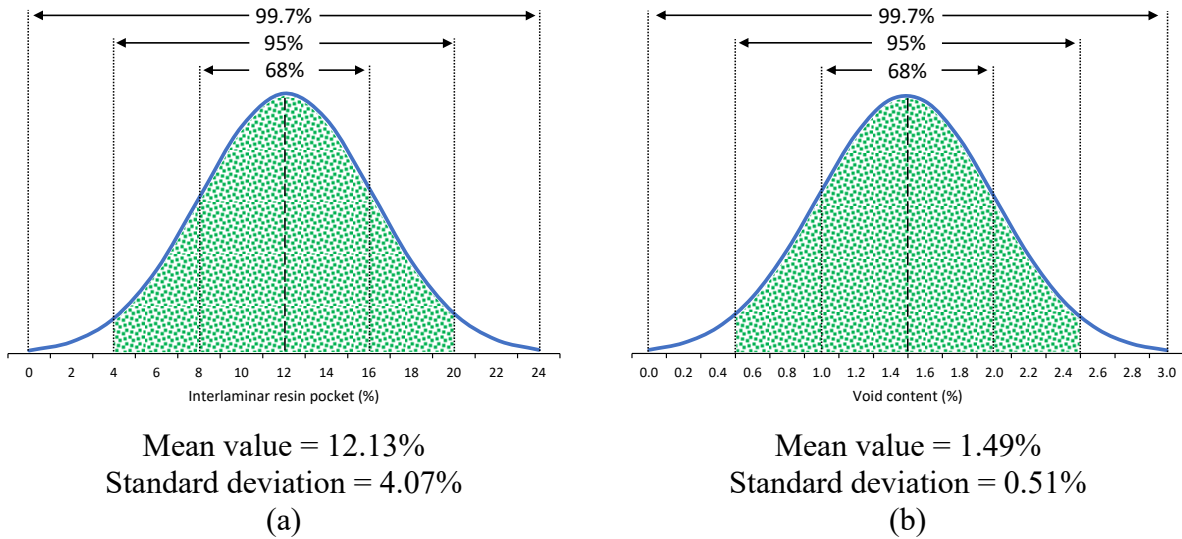
Figure 3.10. Normal distribution plots of (a) interlaminar resin pocket and (b) intralaminar void content which result from the AFP in-situ consolidation process based on micrographic examination.

This approach provides a broader insight into the possible variations in the transverse tensile strength induced by the AFP process, offering both minimum and maximum values. The effective transverse tensile strengths resulting from the in-situ consolidation manufacturing process are presented in Table 3.6. The results indicate that the in-situ consolidation of Carbon/PEEK thermoplastic composite material can on an average reduce its transverse tensile strength by 29.8% compared to the case of autoclave treatment. However, this reduction can reach as high as 43.8% depending on the microstructure, particularly in terms of intralaminar void content and interlaminar resin pocket, which exists in that specific part of the laminate.

Table 3.6. Predicted transverse tensile strength values of Carbon/PEEK thermoplastic composite material fabricated by AFP in-situ consolidation process (fiber volume fraction = 56% and degree of crystallinity = 25%).

	RVE #1	RVE #2	RVE #3	RVE #4	RVE #5	Avg.	Difference[*] (%)
Mean strength (MPa) Intralaminar void content=1.5% Interlaminar resin pocket=12%	61.5	56.6	56.4	59.7	58.8	58.6	29.8
Minimum strength (MPa) Intralaminar void content=2.5% Interlaminar resin pocket=20%	47.3	49.7	45.6	48.9	43.1	46.9	43.8
Maximum strength (MPa) Intralaminar void content=0.5% Interlaminar resin pocket=4%	67.4	66.7	70.7	69.9	70.6	69.1	17.2

* With reference to the mean tensile strength that corresponds to the autoclave re-consolidation (i.e., 83.4 MPa).

It is important to note that the RVE generation process and the proposed simulation methodology for virtual testing can also be utilized to predict compressive and shear strength properties. However, since the material model employed for neat PEEK resin in this study is specifically formulated for tensile loading conditions and has yet to be extended to other loading scenarios, the present research is limited to evaluating the transverse tensile strength of Carbon/PEEK thermoplastic composite material manufactured by the AFP in-situ consolidation process.

It is worth mentioning that the manufacturing quality of AFP-made thermoplastic composites, in terms of fiber volume fraction, void content, interlaminar resin pocket and degree of crystallinity, is highly dependent on the specific AFP processing parameters. Therefore, the numerical results obtained for in-situ-consolidated Carbon/PEEK thermoplastic composite based on the mean values of microstructural factors are valid only for the processing parameters described in Section 3.2.1 ("Manufacturing process"). Nonetheless, the proposed micromechanical simulation methodology remains applicable to other thermoplastic composites produced under different AFP conditions.

3.5. Conclusion

The in-situ consolidation by the Automated Fiber Placement (AFP) process presents significant advantages in terms of time and cost efficiency compared to the conventional autoclave method for producing thermoplastic composite materials. However, the AFP process introduces challenges

originating from the relatively short period of exposure to heat and pressure, in contrast to the extended curing cycles employed in autoclave manufacturing. The shorter processing time can adversely affect the fiber volume fraction, void content, interlaminar resin pocket and degree of crystallinity, as four key factors that have a profound influence on the mechanical properties of the resulting composite laminate.

Owing to the warpage induced during the AFP in-situ consolidation, researchers face challenges in manufacturing flat thermoplastic composite laminates, which are required for experimental characterization using standardized test methods. Therefore, a comprehensive simulation methodology based on micromechanical analysis can allow for virtual testing and precise prediction of material properties as an alternative approach.

In the present study, two sets of Carbon/PEEK thermoplastic composite laminates were fabricated using AFP in-situ consolidation and autoclave re-consolidation techniques. Specimens from both manufacturing processes underwent micrographic study and Differential Scanning Calorimetry (DSC) analysis to obtain the required data for micromechanical analysis, including fiber volume fraction, void content, interlaminar resin pocket, and degree of crystallinity. The results indicated that AFP in-situ consolidation led to reductions in the degree of crystallinity and fiber volume fraction, which were measured at 25% and 56%, respectively. Furthermore, the AFP process caused the formation of interlaminar resin pockets and intralaminar voids, with average values of 12% and 1.5%, respectively. As most of these factors are associated with the matrix phase, significantly influencing the stress distribution and concentration within the composite laminate, 2D micro-scale Representative Volume Elements (RVEs) were developed to investigate the transverse tensile strength of Carbon/PEEK thermoplastic composites produced via the AFP in-situ consolidation process. The findings revealed that this advanced manufacturing technique could lead up to a 44% reduction in the transverse tensile strength compared to the autoclave re-consolidation method. Further computational analyses of AFP in-situ-consolidated thermoplastic composite laminates should properly take into account this significant change in strength value from that of autoclave-reconsolidated laminates.

Appendix

❖ **Tensile test**

A series of Carbon/PEEK thermoplastic composite laminates with varying thicknesses were fabricated using the AFP in-situ consolidation process. Each laminate was then sectioned, vacuum-bagged, and subjected to autoclave re-consolidation to serve as baseline plates. As illustrated in Figure 3.11, the autoclave-reconsolidated laminates exhibited fully flat geometries, whereas the in-situ-consolidated counterparts showed noticeable warpage, the extent of which varied with the laminate dimensions.

Figure 3.11. Vacuum bagging process for re-consolidating the AFP-made Carbon/PEEK thermoplastic composite laminates inside the autoclave.

It is important to note that ASTM D3039 [92] recommends a thickness of 2 mm for tensile testing of unidirectional fiber-reinforced polymer matrix composites in the transverse direction. However, in this research work, laminates with a thickness of 1.5 mm were selected to evaluate the transverse tensile strength of Carbon/PEEK thermoplastic composites produced via AFP and autoclave processes. This adjustment was made due to the difficulty in controlling the warpage during the AFP fabrication of 2-mm-thick thermoplastic composite laminates.

In accordance with the ASTM D3039 standard [92], G10 fiberglass tabs were bonded to both ends of the thermoplastic composite laminates using 3M structural adhesive film. The bonding process involved vacuum bagging followed by curing in an oven at 110 °C for 90 minutes, as illustrated in Figure 3.12. Subsequently, both AFP-fabricated and autoclave-reconsolidated laminates were trimmed to standardized dimensions of 175 mm × 25 mm, with fibers aligned in the 90° orientation, as specified by the standard [92]. Tensile tests were conducted under displacement control mode using a universal testing machine at a crosshead speed of 2.0 mm/min, continuing until complete specimen failure. The transverse tensile strength was then measured based on the peak load and the specimen's cross-sectional area.

(a)

(b)
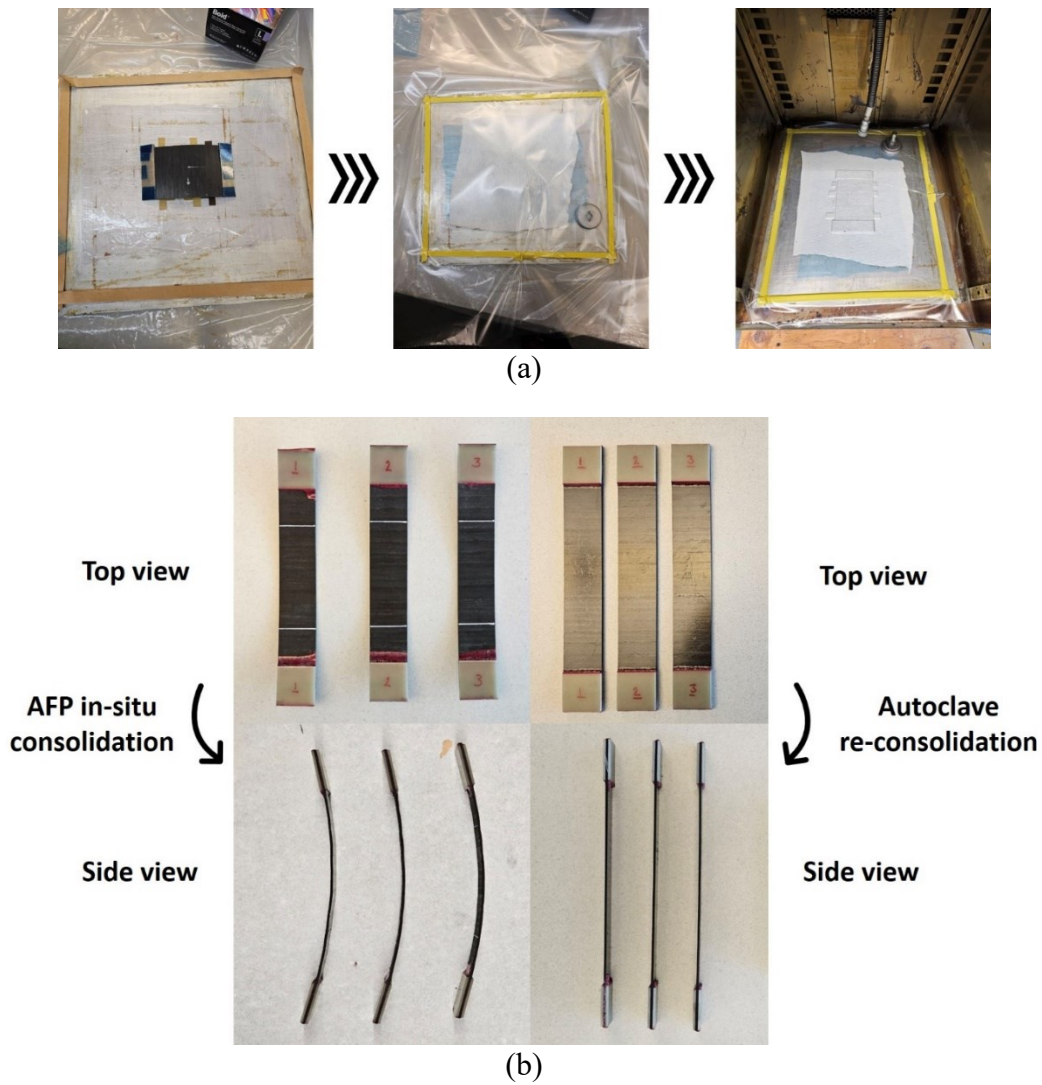
Figure 3.12. (a) Procedure used to attach G10 fiberglass tabs and (b) final shape of coupon specimens used to perform tensile test for measuring transverse tensile strength resulting from each manufacturing process.

All autoclave-reconsolidated Carbon/PEEK specimens exhibited failure at various locations within the gauge area, with an average transverse tensile strength of 81.0 MPa and a standard deviation of 2.5 MPa. In contrast, all in-situ-consolidated specimens failed at the same location and under nearly identical maximum tensile loads, as illustrated in Figure 3.13, resulting in a transverse tensile strength of less than 20.0 MPa. This consistent failure location suggests the presence of a localized defect introduced during the tape placement process, which may have weakened that specific region of the laminate. Despite efforts to minimize defects during AFP processing to achieve high-quality laminates, the occurrence of manufacturing-induced flaws in in-situ-consolidated thermoplastic composites is difficult to eliminate. For instance, the tape occasionally wrapped around the roller, requiring the machine to be stopped and the roller and laminate surface to be cleaned before continuing fabrication. Consequently, tensile testing of AFP-fabricated specimens often reflects the influence of process-induced defects rather than the intrinsic properties of the AFP-made Carbon/PEEK thermoplastic composite material itself, thereby complicating the experimental characterization.
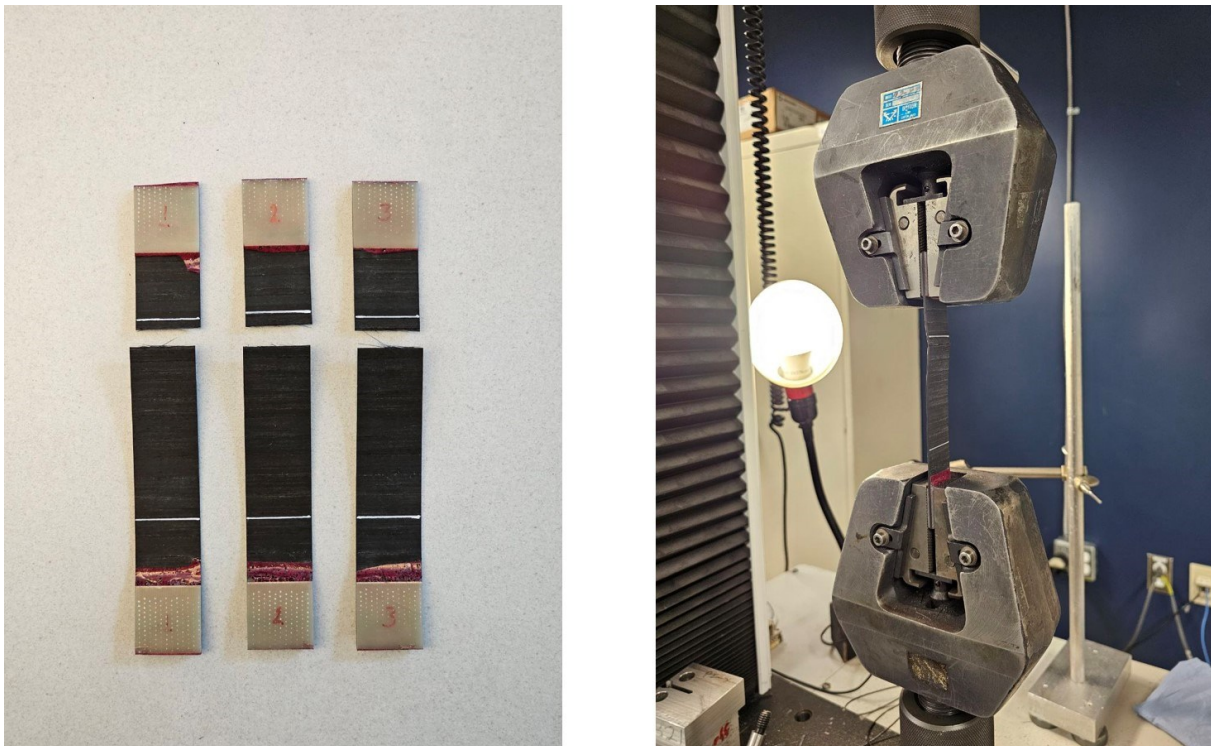
Figure 3.13. Failure of Carbon/PEEK thermoplastic composite specimens in-situ consolidated by the AFP process during the tensile test.

Moreover, shorter specimens fabricated by the AFP process were tested in an attempt to minimize the likelihood of manufacturing error-related defects within the test coupons. However, all of these specimens failed at the grip section, rendering the test results unreliable, even though the measured transverse tensile strength was approximately 25.0 MPa, which remains unexpectedly low. This outcome can be attributed to the presence of warpage in the specimens, which likely introduced a complex stress state and led to premature failure in the grip region.

❖ MATLAB code for transverse cross-section

```
clc
clear

disp ('Please input the diameter of fiber:')
Fd = input('D (micrometer) = '); %D=7 micrometer Fiber Diameter
Af = (pi*Fd^2)/4;

disp ('Please input the lenght of RVE:')
RVElength = input('L (micrometer) = '); %L=140 micrometer
Arve = RVElength*RVElength;

disp ('Please input fiber volume fraction:')
VF = input('Vf (%) = '); %Vf=56%, 60%
VF = VF/100;

disp ('number of fibers required:')
N = round((VF*Arve)/Af,0)

disp ('Please input the percentage of interlaminar resin pocket area:')
percentage = input('percentage(%) = ');
percentage = percentage/2;

disp ('Please input number of stirred fibers at each itteration:')
number = input('stirred fibers = ');

for i=1 : 1 : 2*N
    lx(i)=0;
    ly(i)=0;
end

mindist=0.15;
m=0;
mm=0;
mmm=0;
iter=0;
stir=0;
while 1

    a=(-Fd/2)+(Fd/8);
    b=RVElength+(Fd/2)-(Fd/8);

    aa=(percentage/100)*RVElength+(Fd/16);
```

```matlab
bb=(1-(percentage/100))*RVElength-(Fd/16);

%Finding a new location inside the RVE

rx=(b-a)*rand+(a);

if percentage==0
    ry=(b-a)*rand+(a);
else
    ry=(bb-aa)*rand+(aa);
end

%Intersection check (compatibility & periodicity)
n = compatibility(rx,ry,lx,ly,Fd,N,mm,mindist);
[nn,rx_new,ry_new,p] = periodicity (rx,ry,lx,ly,Fd,N,mm,mindist,RVElength);

%Adding the new location to the directory
if (n==0) && (nn==0)
    for k=1 : 1 : (N+mm)
        if lx(k) == 0
            lx(k) = rx;
            ly(k) = ry;

            if p==1
                lx(k+1) = rx_new;
                ly(k+1) = ry_new;
                mm=mm+1;
            end

            if p==2
                lx(k+1) = rx_new;
                ly(k+1) = ry;

                lx(k+2) = rx;
                ly(k+2) = ry_new;

                lx(k+3) = rx_new;
                ly(k+3) = ry_new;

                mm=mm+3;
                mmm=mmm+1;
            end

            m=m+1;
            break
        end
    end
end

if m == N
    disp('Done!');
    fprintf('Number of stirred fibers = %d \n',stir);
    break
end

%Isolated fiber
```

```
iter=iter+1;
if iter>50000
    for i=1 : 1 : (m+mm)
        for j=1 : 1: (m+mm)
            distance(i,j)=sqrt((lx(i)-lx(j))^2 + (ly(i)-ly(j))^2);
            if distance(i,j)==0
                distance(i,j)=NaN;
            end
        end
    end

    [min1,index1]=min(distance,[],2);
    for i=1 : 1 : (m+mm)
        distance(i,index1(i))=NaN;
    end

    [min2,index2]=min(distance,[],2);
    for i=1 : 1 : (m+mm)
        distance(i,index2(i))=NaN;
    end

    [min3,index3]=min(distance,[],2);

    for i=1 : 1 : (m+mm)
        avg(i)=(min1(i)+min2(i)+min3(i))/3;
    end

    for j=1 : 1 : number

        while 1
            [iso,index]=max(avg);
            if (lx(index)>(RVElength-Fd/2-mindist)) || (lx(index)<Fd/2+mindist) || (ly(index)>(RVElength-Fd/2-
mindist)) || (ly(index)<Fd/2+mindist)
                avg(index)=NaN;
            else
                break
            end
        end

        %%%%%%%%%%%%%%% FIRST MOVE

        fiber1=min1(index);
        fiber1_index=index1(index);
        [xnew,ynew]=move(fiber1,fiber1_index,index,lx,ly,Fd,mindist,RVElength);
        llxx=lx;
        llyy=ly;
        llxx(index)=NaN;
        llyy(index)=NaN;
        n = compatibility(xnew,ynew,llxx,llyy,Fd,N,mm,mindist);
        if n==0
            lx(index)=xnew;
            ly(index)=ynew;
        else
            %disp('not compatible for First move');
        end
```

```matlab
%%%%%%%%%%%%%%% SECOND MOVE

for i=1 : 1 : (m+mm)
    distance2(i)=sqrt((lx(i)-lx(index))^2 + (ly(i)-ly(index))^2);
end
distance2(index)=NaN;
distance2(fiber1_index)=NaN;
[fiber2,fiber2_index]=min(distance2);
[xnew,ynew]=move(fiber2,fiber2_index,index,lx,ly,Fd,mindist,RVElength);
llxx=lx;
llyy=ly;
llxx(index)=NaN;
llyy(index)=NaN;
n = compatibility(xnew,ynew,llxx,llyy,Fd,N,mm,mindist);
if n==0
    lx(index)=xnew;
    ly(index)=ynew;
else
    %disp('not compatible for Second move');
end

%%%%%%%%%%%%%%% THIRD MOVE

for i=1 : 1 : (m+mm)
    distance3(i)=sqrt((lx(i)-lx(index))^2 + (ly(i)-ly(index))^2);
end
distance3(index)=NaN;
distance3(fiber1_index)=NaN;
distance3(fiber2_index)=NaN;
[fiber3,fiber3_index]=min(distance3);
[xnew,ynew]=move(fiber3,fiber3_index,index,lx,ly,Fd,mindist,RVElength);
llxx=lx;
llyy=ly;
llxx(index)=NaN;
llyy(index)=NaN;
n = compatibility(xnew,ynew,llxx,llyy,Fd,N,mm,mindist);
if n==0
    lx(index)=xnew;
    ly(index)=ynew;
else
    %disp('not compatible for Third move');
end

%%%%%%%%%%%%%%% FOURTH MOVE

for i=1 : 1 : (m+mm)
    distance4(i)=sqrt((lx(i)-lx(index))^2 + (ly(i)-ly(index))^2);
end
distance4(index)=NaN;
distance4(fiber1_index)=NaN;
distance4(fiber2_index)=NaN;
distance4(fiber3_index)=NaN;
[fiber4,fiber4_index]=min(distance4);
[xnew,ynew]=move(fiber4,fiber4_index,index,lx,ly,Fd,mindist,RVElength);
llxx=lx;
llyy=ly;
```

```matlab
                llxx(index)=NaN;
                llyy(index)=NaN;
                n = compatibility(xnew,ynew,llxx,llyy,Fd,N,mm,mindist);
                if n==0
                    lx(index)=xnew;
                    ly(index)=ynew;
                else
                    %disp('not compatible for Fourth move');
                end


                %%%%%%%%%%%%%%

                stir=stir+1;
                avg(index)=NaN;
            end

        iter=0;

    end

end

%Creation of the text file
fileID = fopen('Locations.txt','w');
fprintf(fileID, 'X      Y\n');
for i=1 : 1 : (N+mm)
    fprintf(fileID,'%5.4f %5.4f\n',lx(i),ly(i));
end
fclose(fileID);

%%%%%%%%%%%%%%%%%%%% VOID CONTENT %%%%%%%%%%%%%%%%%%%%%%

disp ('Please input total void content:')
void = input('total void content(%) = '); %void content=1%, 2% or 3%

disp ('Please input the percentage of intralaminar void content:')
intra = input('percentage of intralaminar voids (0% to 100%) = '); %void content=0%, 100%
inter = 100-intra;

for i=1 : 1 : 10000
    vlx(i)=0;
    vly(i)=0;
    vld(i)=0;
end

MinVd=Fd/10;
MaxVd=Fd/2;

a=MaxVd/2+mindist;
b=RVElength-MaxVd/2-mindist;

aa=(percentage/100)*RVElength+(Fd/16);      % for intralaminar void content
bb=(1-(percentage/100))*RVElength-(Fd/16); % for intralaminar void content

Nv=1;
vn=0;
```

```matlab
varea=0;

%%%%%%%%%%%%%%%%%%%%%%% INTRALAMINAR VOIDS

while 1

    if void==0
        break
    end

    if intra==0
        break
    end

    vx=(b-a)*rand+(a);
    vy=(bb-aa)*rand+(aa); % Inside the layer

    %Intersection check (fiber with void)

    for i=1 : 1 : (N+mm)
        fvd(i)=NaN;
    end

    for i=1 : 1 : (N+mm)
        fvd(i) = sqrt((vx-lx(i))^2 + (vy-ly(i))^2);
        if fvd(i) <= (Fd/2+MinVd/2+mindist)
            n=1;
            break
        else
            n=0;
        end
    end

    %Intersection check (void with void)

    if n==0
        D=min(fvd);
        if (D-Fd/2) >= (MaxVd/2+mindist)
            Vd=(MaxVd-MinVd)*rand+(MinVd);
        else
            Vd=((D-Fd/2)-MinVd)*rand+(MinVd);
        end

        for i=1 : 1 : (Nv-1)
            d = sqrt((vx-vlx(i))^2 + (vy-vly(i))^2);
            if d <= (vld(i)/2+Vd/2+mindist)
                vn=1;
                break
            else
                vn=0;
            end
        end

    end

    if (n==0) && (vn==0)
```

```matlab
        vlx(Nv) = vx;
        vly(Nv) = vy;
        vld(Nv) = Vd;

        varea = varea + (pi*Vd^2)/4;

        if varea >= ((void*intra/100)/100)*Arve
            break
        else
            Nv=Nv+1;
        end

    end

end

    %%%%%%%%%%%%%%%%%%%%%%% INTERLAMINAR VOIDS (top)

MinVd=Fd/10;
MaxVd=Fd/2;

a=MaxVd/2+mindist;
b=RVElength-MaxVd/2-mindist;

aa=(percentage/100)*RVElength+(Fd/16);      % for intralaminar void content
bb=(1-(percentage/100))*RVElength-(Fd/16);  % for intralaminar void content

vn=0;
varea=0;

while 1

    if void==0
        break
    end

    if inter==0
        break
    end

    vx=(b-a)*rand+(a);
    vy=(b-bb)*rand+(bb);     % top section of the RVE

    %Intersection check (fiber with void)

    for i=1 : 1 : (N+mm)
        fvd(i)=NaN;
    end

    for i=1 : 1 : (N+mm)
        fvd(i) = sqrt((vx-lx(i))^2 + (vy-ly(i))^2);
        if fvd(i) <= (Fd/2+MinVd/2+mindist)
            n=1;
            break
        else
            n=0;
```

```matlab
        end
    end

    %Intersection check (void with void)

    if n==0
        D=min(fvd);
        if (D-Fd/2) >= (MaxVd/2+mindist)
            Vd=(MaxVd-MinVd)*rand+(MinVd);
        else
            Vd=((D-Fd/2)-MinVd)*rand+(MinVd);
        end

        for i=1 : 1 : (Nv-1)
            d = sqrt((vx-vlx(i))^2 + (vy-vly(i))^2);
            if d <= (vld(i)/2+Vd/2+mindist)
                vn=1;
                break
            else
                vn=0;
            end
        end

    end

    if (n==0) && (vn==0)
        vlx(Nv) = vx;
        vly(Nv) = vy;
        vld(Nv) = Vd;

        varea = varea + (pi*Vd^2)/4;

        if varea >= ((void*inter/2/100)/100)*Arve
            break
        else
            Nv=Nv+1;
        end

    end

end

    %%%%%%%%%%%%%%%%%%%%%% INTERLAMINAR VOIDS (bottom)

vn=0;
varea=0;

while 1

    if void==0
        break
    end

    if inter==0
        break
    end
```

```matlab
vx=(b-a)*rand+(a);
vy=(aa-a)*rand+(a);    % top section of the RVE

%Intersection check (fiber with void)

for i=1 : 1 : (N+mm)
    fvd(i)=NaN;
end

for i=1 : 1 : (N+mm)
    fvd(i) = sqrt((vx-lx(i))^2 + (vy-ly(i))^2);
    if fvd(i) <= (Fd/2+MinVd/2+mindist)
        n=1;
        break
    else
        n=0;
    end
end

%Intersection check (void with void)

if n==0
    D=min(fvd);
    if (D-Fd/2) >= (MaxVd/2+mindist)
        Vd=(MaxVd-MinVd)*rand+(MinVd);
    else
        Vd=((D-Fd/2)-MinVd)*rand+(MinVd);
    end

    for i=1 : 1 : (Nv-1)
        d = sqrt((vx-vlx(i))^2 + (vy-vly(i))^2);
        if d <= (vld(i)/2+Vd/2+mindist)
            vn=1;
            break
        else
            vn=0;
        end
    end

end

if (n==0) && (vn==0)
    vlx(Nv) = vx;
    vly(Nv) = vy;
    vld(Nv) = Vd;

    varea = varea + (pi*Vd^2)/4;

    if varea >= ((void*inter/2/100)/100)*Arve
        break
    else
        Nv=Nv+1;
    end

end
```

```matlab
end

%Creation of the text file
fileID = fopen('Voids.txt','w');
fprintf(fileID, 'X      Y      D\n');

if void==0
    fprintf(fileID, 'NO\n');
else
    fprintf(fileID, 'YES\n');
    for i=1 : 1 : Nv
        fprintf(fileID,'%5.4f %5.4f %5.4f\n',vlx(i),vly(i),vld(i));
    end
end

fclose(fileID);
disp('Finished!')

%%%%%%%%%%%%%%%%%%%%%%%%%%%%%%%%%%%%%%%%%%%%%%%%%%%%%%%%%%%%%%%%%%%%%%%%%%%
%%%%%%%%%%%%%%%%%%%%%%%%%%%%%%%%%%%%%%%%%%%%%%%%%%%%%%%%%%%%%%%%%%%%%%%%%%%
%%%%%%%%%%%%%%%%%%%%%%%%%%%%%%%%%%%%%%%%%%%%%%%%%%%%%%%%%%%%%%%%%%%%%%%%%%%

function n = compatibility(rx,ry,lx,ly,Fd,N,mm,mindist)
    for i=1 : 1 : (N+mm)
        d = sqrt((rx-lx(i))^2 + (ry-ly(i))^2);
        if d <= (Fd+mindist)
            n=1;
            break
        else
            n=0;
        end
    end
end

%%%%%%%%%%%%%%%%%%%%%%%%%%%%%%%%%%%%%%%%%%%%%%%%%%%%%%%%%%%%%%%%%%%%%%%%%%%

function [nn,rx_new,ry_new,p] = periodicity(rx,ry,lx,ly,Fd,N,mm,mindist,RVElength)
    p=0;
    rx_new=rx;
    ry_new=ry;

    if rx > (RVElength-Fd/2)
        rx_new = rx-RVElength;
        p=p+1;
    end
    if rx < (Fd/2)
        rx_new = rx+RVElength;
        p=p+1;
    end

    if ry > (RVElength-Fd/2)
        ry_new = ry-RVElength;
        p=p+1;
    end
    if ry < (Fd/2)
```

```matlab
            ry_new = ry+RVElength;
            p=p+1;
        end

        if p==0 % Not edge & Not cornet
            nn=0;
        end

        if p==1 % Edge
            for i=1 : 1 : (N+mm)
                d = sqrt((rx_new-lx(i))^2 + (ry_new-ly(i))^2);
                if d <= (Fd+mindist)
                    nn=1;
                    break
                else
                    nn=0;
                end
            end
        end

        if p==2 % Corner
            for i=1 : 1 : (N+mm)
                d1 = sqrt((rx_new-lx(i))^2 + (ry-ly(i))^2);
                d2 = sqrt((rx-lx(i))^2 + (ry_new-ly(i))^2);
                d3 = sqrt((rx_new-lx(i))^2 + (ry_new-ly(i))^2);
                if (d1<=(Fd+mindist)) || (d2<=(Fd+mindist)) || (d3<=(Fd+mindist))
                    nn=1;
                    break
                else
                    nn=0;
                end
            end
        end
end

%%%%%%%%%%%%%%%%%%%%%%%%%%%%%%%%%%%%%%%%%%%%%%%%%%%%%%%%%%%%%%%%%%%%%%%

function [xnew,ynew] = move(fiber1,fiber1_index,index,lx,ly,Fd,mindist,RVElength)
    while 1

        limit=fiber1-(Fd+mindist);
        dnew=limit*rand;
        slope=(ly(fiber1_index)-ly(index))/(lx(fiber1_index)-lx(index));

        if lx(fiber1_index)>lx(index)
            xnew=(dnew/sqrt(slope^2+1))+lx(index);
            ynew=slope*(xnew-lx(index))+ly(index);
        end

        if lx(fiber1_index)<lx(index)
            xnew=-(dnew/sqrt(slope^2+1))+lx(index);
            ynew=slope*(xnew-lx(index))+ly(index);
        end

        if (xnew<(RVElength-Fd/2-mindist)) && (xnew>Fd/2+mindist) && (ynew<(RVElength-Fd/2-mindist)) &&
(ynew>Fd/2+mindist)
```

```
            break
        end

    end
end
```

❖ Python script for strength prediction

```
# -*- coding: mbcs -*-
from part import *
from material import *
from section import *
from assembly import *
from step import *
from interaction import *
from load import *
from mesh import *
from optimization import *
from job import *
from sketch import *
from visualization import *
from connectorBehavior import *
from abaqus import *
from abaqusConstants import *

import __main__
import section
import regionToolset
import displayGroupMdbToolset as dgm
import part
import material
import assembly
import step
import interaction
import load
import mesh
import optimization
import job
import sketch
import visualization
import xyPlot
import displayGroupOdbToolset as dgo
import connectorBehavior

from caeModules import *
from odbAccess import *
from numpy import *
import math

averagestrain=zeros([100,1])
averagestress=zeros([100,1])
averagevolume=zeros([100,1])

stif=zeros([3,3])
RVEstrain=0.02    # 2%
RVEpredisp=[0.0000,0.0000,0.0000]

RVElength=140.0 # micrometer
Fd=7.0        # micrometer
meshsize=(Fd/2)/14
```

```
###########Part###########

mdb.models['Model-1'].ConstrainedSketch(name='__profile__', sheetSize=400.0)
mdb.models['Model-1'].sketches['__profile__'].rectangle(point1=(-Fd, -Fd),
    point2=(RVElength+Fd, RVElength+Fd))
mdb.models['Model-1'].Part(dimensionality=TWO_D_PLANAR, name='Part-1', type=
    DEFORMABLE_BODY)
mdb.models['Model-1'].parts['Part-1'].BaseShell(sketch=
    mdb.models['Model-1'].sketches['__profile__'])
del mdb.models['Model-1'].sketches['__profile__']

mdb.models['Model-1'].ConstrainedSketch(gridSpacing=10.0, name='__profile__',
    sheetSize=400.0, transform=
    mdb.models['Model-1'].parts['Part-1'].MakeSketchTransform(
    sketchPlane=mdb.models['Model-1'].parts['Part-1'].faces[0],
    sketchPlaneSide=SIDE1, sketchOrientation=RIGHT, origin=(0.0, 0.0, 0.0)))
mdb.models['Model-1'].parts['Part-1'].projectReferencesOntoSketch(filter=
    COPLANAR_EDGES, sketch=mdb.models['Model-1'].sketches['__profile__'])

f=open('Locations.txt','r')
line=f.readlines()
for i in range(1,len(line)):
    a=line[i].split()
    lx=float(a[0])
    ly=float(a[1])
    mdb.models['Model-1'].sketches['__profile__'].CircleByCenterPerimeter(center=(
        lx, ly), point1=(lx+Fd/2, ly))
f.close()

mdb.models['Model-1'].parts['Part-1'].PartitionFaceBySketch(faces=
    mdb.models['Model-1'].parts['Part-1'].faces[0]
    , sketch=mdb.models['Model-1'].sketches['__profile__'])
del mdb.models['Model-1'].sketches['__profile__']

f=open('Voids.txt','r')
line=f.readlines()
b=line[1].split()
if b[0]=='YES':
    mdb.models['Model-1'].ConstrainedSketch(gridSpacing=10.0, name='__profile__',
        sheetSize=400.0)
    for i in range(2,len(line)):
        a=line[i].split()
        lx=float(a[0])
        ly=float(a[1])
        ld=float(a[2])
        mdb.models['Model-1'].sketches['__profile__'].CircleByCenterPerimeter(center=(
            lx, ly), point1=(lx+ld/2, ly))
    mdb.models['Model-1'].parts['Part-1'].Cut(sketch=
        mdb.models['Model-1'].sketches['__profile__'])
    del mdb.models['Model-1'].sketches['__profile__']
f.close()

            #Cutting left and right
mdb.models['Model-1'].ConstrainedSketch(gridSpacing=10.0, name='__profile__',
    sheetSize=400.0)
mdb.models['Model-1'].sketches['__profile__'].rectangle(point1=(RVElength, -Fd),
```

```
            point2=(RVElength+Fd, RVElength+Fd))
mdb.models['Model-1'].sketches['__profile__'].rectangle(point1=(0.0, -Fd),
    point2=(-Fd, RVElength+Fd))
mdb.models['Model-1'].parts['Part-1'].Cut(sketch=
    mdb.models['Model-1'].sketches['__profile__'])
del mdb.models['Model-1'].sketches['__profile__']


                #Cutting top and bottom
mdb.models['Model-1'].ConstrainedSketch(gridSpacing=10.0, name='__profile__',
    sheetSize=400.0)
mdb.models['Model-1'].sketches['__profile__'].rectangle(point1=(-Fd, -Fd),
    point2=(RVElength+Fd, 0.0))
mdb.models['Model-1'].sketches['__profile__'].rectangle(point1=(-Fd, RVElength),
    point2=(RVElength+Fd, RVElength+Fd))
mdb.models['Model-1'].parts['Part-1'].Cut(sketch=
    mdb.models['Model-1'].sketches['__profile__'])
del mdb.models['Model-1'].sketches['__profile__']

############Property############

                #Fiber
mdb.models['Model-1'].Material(name='fiber')
mdb.models['Model-1'].materials['fiber'].Elastic(table=((22000.0, 0.25),
    ))
mdb.models['Model-1'].materials['fiber'].Density(table=((1.78e-15, ), ))


                #Matrix
mdb.models['Model-1'].Material(name='matrix')
mdb.models['Model-1'].materials['matrix'].Elastic(table=((3312.0, 0.38),
    ))
mdb.models['Model-1'].materials['matrix'].Density(table=((1.32e-15, ), ))


                #yielding and damage criteria of matrix
mdb.models['Model-1'].materials['matrix'].DruckerPrager(table=((27.0, 1.0,
    27.0), ))
mdb.models['Model-1'].materials['matrix'].druckerPrager.DruckerPragerHardening(
    table=((66.0, 0.0), (69.0, 0.1), (86.0, 0.5), (87.0, 2.0)), type=TENSION)
mdb.models['Model-1'].materials['matrix'].DuctileDamageInitiation(table=((1.5,
    -0.3333, 0.0), (1.0, 0.0, 0.0), (0.7, 0.3333, 0.0), (0.55, 0.495, 0.0), (
    0.4, 0.666, 0.0), (0.2, 1.0, 0.0)))
mdb.models['Model-1'].materials['matrix'].ductileDamageInitiation.DamageEvolution(
    table=((0.5, ), ), type=ENERGY)



mdb.models['Model-1'].HomogeneousSolidSection(material='fiber', name=
    'Section-fiber', thickness=1.0)
mdb.models['Model-1'].HomogeneousSolidSection(material='matrix', name=
    'Section-matrix', thickness=1.0)

face=mdb.models['Model-1'].parts['Part-1'].faces.getByBoundingBox(
    0.0,0.0,0.0,RVElength,RVElength,0.0)
for i in range(len(face)):
    area=face[i].getSize()
    area=area/RVElength**2
    if area>0.3:
        target1=face[i]
```

```python
        print('Matrix volume fraction is:')
        print(area)
        break
p=target1.pointOn
mdb.models['Model-1'].parts['Part-1'].Set(faces=
    mdb.models['Model-1'].parts['Part-1'].faces.findAt(
    ((p[0][0],p[0][1],p[0][2]),),), name='Set-matrix')
mdb.models['Model-1'].parts['Part-1'].SectionAssignment(offset=0.0,
    offsetField='', offsetType=MIDDLE_SURFACE, region=
    mdb.models['Model-1'].parts['Part-1'].sets['Set-matrix'], sectionName=
    'Section-matrix', thicknessAssignment=FROM_SECTION)

f=open('Locations.txt','r')
line=f.readlines()
for i in range(1,len(line)):
    a=line[i].split()
    lx=float(a[0])
    ly=float(a[1])
    mdb.models['Model-1'].parts['Part-1'].Set(faces=
        mdb.models['Model-1'].parts['Part-1'].faces.getByBoundingBox
        (lx-Fd/2,ly-Fd/2,0.0,lx+Fd/2,ly+Fd/2,1.0), name='Set-fiber-%d'%i)
    mdb.models['Model-1'].parts['Part-1'].SectionAssignment(offset=0.0,
        offsetField='', offsetType=MIDDLE_SURFACE, region=
        mdb.models['Model-1'].parts['Part-1'].sets['Set-fiber-%d'%i], sectionName=
        'Section-fiber', thicknessAssignment=FROM_SECTION)
f.close()

###########Assembly###########

mdb.models['Model-1'].rootAssembly.DatumCsysByDefault(CARTESIAN)
mdb.models['Model-1'].rootAssembly.Instance(dependent=OFF, name='Part-1-1',
    part=mdb.models['Model-1'].parts['Part-1'])

###########Step###########

mdb.models['Model-1'].ExplicitDynamicsStep(improvedDtMethod=ON, massScaling=((
    SEMI_AUTOMATIC, MODEL, AT_BEGINNING, 200000000000.0, 0.0, None, 0, 0, 0.0,
    0.0, 0, None), ), name='Step-1', previous='Initial')

mdb.models['Model-1'].fieldOutputRequests['F-Output-1'].setValues(variables=(
    'S', 'E', 'PE', 'LE', 'U', 'SDEG', 'DMICRT', 'EVOL'), numIntervals=20)

###########Mesh###########

                #for Quad element CPE4R

mdb.models['Model-1'].rootAssembly.setElementType(elemTypes=(ElemType(
    elemCode=CPE4R, elemLibrary=EXPLICIT, secondOrderAccuracy=OFF,
    hourglassControl=DEFAULT, distortionControl=DEFAULT, elemDeletion=ON),
    ElemType(elemCode=CPE3, elemLibrary=EXPLICIT, secondOrderAccuracy=OFF,
    distortionControl=DEFAULT, elemDeletion=ON)), regions=(
    mdb.models['Model-1'].rootAssembly.instances['Part-1-1'].faces.getByBoundingBox(
    0.0,0.0,0.0,RVElength,RVElength,0.0), ))


mdb.models['Model-1'].rootAssembly.seedPartInstance(deviationFactor=0.1,
```

```
    minSizeFactor=0.1, regions=(
    mdb.models['Model-1'].rootAssembly.instances['Part-1-1'], ), size=meshsize)

mdb.models['Model-1'].rootAssembly.generateMesh(regions=(
    mdb.models['Model-1'].rootAssembly.instances['Part-1-1'], ))

###########Set###########

edgeR=mdb.models['Model-1'].rootAssembly.instances['Part-1-1'].nodes.getByBoundingBox(
    RVElength,0.01,0.0,RVElength,RVElength-0.01,0.0)
for i in range(1,len(edgeR)+1):
    mdb.models['Model-1'].rootAssembly.Set(name='edgeR-%d'%i, nodes=edgeR[i-1:i])
    coord=edgeR[i-1].coordinates
    edgeL=mdb.models['Model-1'].rootAssembly.instances['Part-1-1'].nodes.getByBoundingBox(
        0.0,coord[1],0.0,0.0,coord[1],0.0)
    mdb.models['Model-1'].rootAssembly.Set(name='edgeL-%d'%i, nodes=edgeL[0:1])

edgeT=mdb.models['Model-1'].rootAssembly.instances['Part-1-1'].nodes.getByBoundingBox(
    0.01,RVElength,0.0,RVElength-0.01,RVElength,0.0)
for i in range(1,len(edgeT)+1):
    mdb.models['Model-1'].rootAssembly.Set(name='edgeT-%d'%i, nodes=edgeT[i-1:i])
    coord=edgeT[i-1].coordinates
    edgeB=mdb.models['Model-1'].rootAssembly.instances['Part-1-1'].nodes.getByBoundingBox(
        coord[0],0.0,0.0,0.0,coord[0],0.0,0.0)
    mdb.models['Model-1'].rootAssembly.Set(name='edgeB-%d'%i, nodes=edgeB[0:1])

#/////////////////////////////////////////////////////////////////////////

vertex=mdb.models['Model-1'].rootAssembly.instances['Part-1-1'].nodes.getByBoundingBox(
    0.0,0.0,0.0,0.0,0.0,0.0,0.0)
mdb.models['Model-1'].rootAssembly.Set(name='vertexC-1', nodes=vertex[0:1])

vertex=mdb.models['Model-1'].rootAssembly.instances['Part-1-1'].nodes.getByBoundingBox(
    RVElength,0.0,0.0,RVElength,0.0,0.0)
mdb.models['Model-1'].rootAssembly.Set(name='vertexB-1', nodes=vertex[0:1])

vertex=mdb.models['Model-1'].rootAssembly.instances['Part-1-1'].nodes.getByBoundingBox(
    0.0,RVElength,0.0,0.0,RVElength,0.0)
mdb.models['Model-1'].rootAssembly.Set(name='vertexD-1', nodes=vertex[0:1])

vertex=mdb.models['Model-1'].rootAssembly.instances['Part-1-1'].nodes.getByBoundingBox(
    RVElength,RVElength,0.0,RVElength,RVElength,0.0)
mdb.models['Model-1'].rootAssembly.Set(name='vertexA-1', nodes=vertex[0:1])

###########Equations###########

for i in range(1,len(edgeR)+1):
    mdb.models['Model-1'].Equation(name='edgeRL-1-%d'%i, terms=((1.0, 'edgeR-%d'%i, 1), (
        -1.0, 'edgeL-%d'%i, 1), (-1.0, 'vertexB-1', 1), (1.0, 'vertexC-1', 1)))
for i in range(1,len(edgeR)+1):
    mdb.models['Model-1'].Equation(name='edgeRL-2-%d'%i, terms=((1.0, 'edgeR-%d'%i, 2), (
        -1.0, 'edgeL-%d'%i, 2), (-1.0, 'vertexB-1', 2), (1.0, 'vertexC-1', 2)))

for i in range(1,len(edgeT)+1):
    mdb.models['Model-1'].Equation(name='edgeTB-1-%d'%i, terms=((1.0, 'edgeT-%d'%i, 1), (
        -1.0, 'edgeB-%d'%i, 1), (-1.0, 'vertexD-1', 1), (1.0, 'vertexC-1', 1)))
```

```python
for i in range(1,len(edgeT)+1):
    mdb.models['Model-1'].Equation(name='edgeTB-2-%d'%i, terms=((1.0, 'edgeT-%d'%i, 2), (
        -1.0, 'edgeB-%d'%i, 2), (-1.0, 'vertexD-1', 2), (1.0, 'vertexC-1', 2)))
```

###########Load###########

```python
mdb.models['Model-1'].TabularAmplitude(data=((0.0, 1.0), (1.0, 1.0)), name=
    'Amp-pin', smooth=SOLVER_DEFAULT, timeSpan=STEP)
mdb.models['Model-1'].TabularAmplitude(data=((0.0, 0.0), (1.0, 1.0)), name=
    'Amp-load', smooth=SOLVER_DEFAULT, timeSpan=STEP)

mdb.models['Model-1'].DisplacementBC(amplitude='Amp-pin', createStepName='Step-1',
    distributionType=UNIFORM, fieldName='', fixed=OFF, localCsys=None, name=
    'BC-rigid body', region=mdb.models['Model-1'].rootAssembly.sets['vertexC-1'],
    u1=0.0, u2=0.0, ur3=UNSET)

mdb.models['Model-1'].DisplacementBC(amplitude='Amp-pin', createStepName='Step-1',
    distributionType=UNIFORM, fieldName='', fixed=OFF, localCsys=None, name=
    'Roller-B', region=mdb.models['Model-1'].rootAssembly.sets['vertexB-1'],
    u1=UNSET, u2=0.0, ur3=UNSET)

mdb.models['Model-1'].DisplacementBC(amplitude='Amp-pin', createStepName='Step-1',
    distributionType=UNIFORM, fieldName='', fixed=OFF, localCsys=None, name=
    'Roller-D', region=mdb.models['Model-1'].rootAssembly.sets['vertexD-1'],
    u1=0.0, u2=UNSET, ur3=UNSET)

RVEpredisp=[0.0000,0.0000,0.0000]
RVEpredisp[0]=RVEstrain*RVElength

mdb.models['Model-1'].DisplacementBC(amplitude='Amp-load', createStepName='Step-1',
    distributionType=UNIFORM, fieldName='', fixed=OFF, localCsys=None, name=
    'BC-1', region=mdb.models['Model-1'].rootAssembly.sets['vertexB-1'],
    u1=RVEpredisp[0], u2=UNSET, ur3=UNSET)
```

###########Element###########

```python
elements=0
element=mdb.models['Model-1'].rootAssembly.instances['Part-1-1'].elements
elements=len(element)
```

###########Job###########

```python
job=mdb.Job(name='Job-1', model='Model-1', description='', type=ANALYSIS,
    atTime=None, waitMinutes=0, waitHours=0, queue=None, memory=90,
    memoryUnits=PERCENTAGE, getMemoryFromAnalysis=True,
    explicitPrecision=SINGLE, nodalOutputPrecision=SINGLE, echoPrint=OFF,
    modelPrint=OFF, contactPrint=OFF, historyPrint=OFF, userSubroutine='',
    scratch='', multiprocessingMode=THREADS, numCpus=16, numDomains=16,
    numGPUs=0)

mdb.jobs['Job-1'].submit(consistencyChecking=OFF)
```

###########Odb###########

```python
session.mdbData.summary()
o3 = session.openOdb(name='C:/Temp/Job-1.odb')
```

```python
session.viewports['Viewport: 1'].setValues(displayedObject=o3)
odb = session.odbs['C:/Temp/Job-1.odb']

numframe=session.viewports['Viewport: 1'].odbDisplay.fieldFrame[1]

for m in range(1,numframe+1):
    RVEvolume=0
    volume=[]

    s11=[]
    s22=[]                #stresses
    s12=[]

    ss11=0
    ss22=0                 #volume average stresses
    ss12=0


    e11=[]
    e22=[]                #strains
    e12=[]

    ee11=0
    ee22=0                  #volume average strains
    ee12=0

    session.writeFieldReport(fileName='volume.txt', append=OFF,
        sortItem='Element Label', odb=odb, step=0, frame=m,
        outputPosition=WHOLE_ELEMENT, variable=(('EVOL', WHOLE_ELEMENT), ))

    f=open('volume.txt','r')
    line=f.readlines()
    j=19
    for i in range(elements):
        if line[j]=='\n':
            a=line[j+8].split()
            RVEvolume=RVEvolume+float(a[1])
            j=j+16
        a=line[j].split()
        b=float(a[1])
        volume.append(b)
        j=j+1
    a=line[-3].split()
    RVEvolume=RVEvolume+float(a[1])
    f.close()

    for k in range(1,4):
        if k==3:           #shear stresses
            session.writeFieldReport(fileName='stress12.txt', append=OFF,
                sortItem='Element Label', odb=odb, step=0, frame=m,
                outputPosition=INTEGRATION_POINT, variable=(('S', INTEGRATION_POINT, ((
                COMPONENT, 'S12'), )), ))
            f=open('stress12.txt','r')
            line=f.readlines()
            j=19
            for i in range(elements):
```

```
        if line[j]=='\n':
            j=j+18
        a=line[j].split()
        b=float(a[2])
        s12.append(b)
        j=j+1
    f.close()

    if k<3:          #normal stresses
        session.writeFieldReport(fileName='stress%d%d.txt'%(k,k), append=OFF,
            sortItem='Element Label', odb=odb, step=0, frame=m,
            outputPosition=INTEGRATION_POINT, variable=(('S', INTEGRATION_POINT, ((
            COMPONENT, 'S%d%d'%(k,k)), )), ))
        f=open('stress%d%d.txt'%(k,k),'r')
        line=f.readlines()
        j=19
        for i in range(elements):
            if line[j]=='\n':
                j=j+18
            a=line[j].split()
            b=float(a[2])
            if k==1:
                s11.append(b)
            if k==2:
                s22.append(b)
            j=j+1
        f.close()

for i in range(elements):
    ss11=ss11+s11[i]*volume[i]
    ss22=ss22+s22[i]*volume[i]
    ss12=ss12+s12[i]*volume[i]
ss11=ss11/(RVElength**2)
ss22=ss22/(RVElength**2)
ss12=ss12/(RVElength**2)

#//////////////////////////////////////////////////////////////////////////////

for k in range(1,4):
    if k==3:          #shear strains
        session.writeFieldReport(fileName='strain12.txt', append=OFF,
            sortItem='Element Label', odb=odb, step=0, frame=m,
            outputPosition=INTEGRATION_POINT, variable=(('LE', INTEGRATION_POINT, ((
            COMPONENT, 'LE12'), )), ))
        f=open('strain12.txt','r')
        line=f.readlines()
        j=19
        for i in range(elements):
            if line[j]=='\n':
                j=j+18
            a=line[j].split()
            b=float(a[2])
            e12.append(b)
            j=j+1
        f.close()
```

```python
    if k<3:              #normal strains
        session.writeFieldReport(fileName='strain%d%d.txt'%(k,k), append=OFF,
            sortItem='Element Label', odb=odb, step=0, frame=m,
            outputPosition=INTEGRATION_POINT, variable=(('LE', INTEGRATION_POINT, ((
            COMPONENT, 'LE%d%d'%(k,k)), )), ))
        f=open('strain%d%d.txt'%(k,k),'r')
        line=f.readlines()
        j=19
        for i in range(elements):
            if line[j]=='\n':
                j=j+18
            a=line[j].split()
            b=float(a[2])
            if k==1:
                e11.append(b)
            if k==2:
                e22.append(b)
            j=j+1
        f.close()

    for i in range(elements):
        ee11=ee11+e11[i]*volume[i]
        ee22=ee22+e22[i]*volume[i]
        ee12=ee12+e12[i]*volume[i]
    ee11=ee11/(RVElength**2)
    ee22=ee22/(RVElength**2)
    ee12=ee12/(RVElength**2)

    averagestrain[m-1][0]=ee11
    averagestress[m-1][0]=ss11
    averagevolume[m-1][0]=RVEvolume

f=open('avgstress11.txt','w')
for i in range (numframe):        #number of increments
    f.write('%f\n'%averagestress[i][0])
f.close()

f=open('avgstrain11.txt','w')
for i in range (numframe):        #number of increments
    f.write('%f\n'%averagestrain[i][0])
f.close()

f=open('avgvolume.txt','w')
for i in range (numframe):        #number of increments
    f.write('%f\n'%averagevolume[i][0])
f.close()
```

CHAPTER 4

Micromechanical characterization of Carbon/PEEK thermoplastic composite material in-situ consolidated by automated fiber placement: Stiffness prediction

This chapter contains the contents of the following journal and conference papers:

E. Pourahmadi, R. Ganesan, F. Shadmehri, "Micromechanical characterization of Carbon/PEEK thermoplastic composite material in-situ consolidated by automated fiber placement: Stiffness prediction", *Composites Science and Technology*, 246 (2024), 110390. https://doi.org/10.1016/j.compscitech.2023.110390.

E. Pourahmadi, R. Ganesan, F. Shadmehri, "Effect of in-situ consolidation on the in-plane elastic moduli of Carbon/PEEK thermoplastic composites made by Automated Fiber Placement (AFP) process" in the *21st European Conference on Composite Materials (ECCM21)*, Nantes, France, July 2024.

4. Micromechanical characterization of Carbon/PEEK thermoplastic composite material in-situ consolidated by automated fiber placement: Stiffness prediction

Foreword

Owing to the challenges associated with producing flat thermoplastic composite laminates using the AFP process without a heated tooling system, primarily due to warpage, previous studies have not been able to examine the stiffness of in-situ-consolidated Carbon/PEEK thermoplastic composite laminates, especially in the transverse direction where matrix behavior is dominant. As a result, a direct comparison with the stiffness values reported in technical datasheets for autoclave- or hot-press-manufactured composite laminates remains largely unexplored.

While the composite material response in the fiber direction is mainly controlled by the fiber's characteristics, such as fiber volume fraction, microstructural features introduced during AFP in-situ consolidation, such as voids, interlaminar resin-rich zones, and variations in crystallinity, significantly influence the material behavior in the transverse direction. Addressing the third objective of the present thesis, this research work aims to predict the effective stiffness properties of in-situ-consolidated Carbon/PEEK thermoplastic composite material by accounting for these microstructural factors. To achieve this, 2D Representative Volume Elements (RVEs) were developed based on both longitudinal and transverse microstructural cross-sections. The input data for micromechanical modeling were derived from micrographic examination and DSC analysis. Simulations were carried out using the ABAQUS Scripting Interface (ASI), supplemented with a MATLAB code to determine RVE geometries. Effective stiffness properties were then predicted by applying Periodic Boundary Conditions (PBCs) and employing homogenization theory. The results indicated that AFP in-situ consolidation can reduce the longitudinal elastic modulus, transverse elastic modulus, and out-of-plane shear modulus by approximately 7%, 10%, and 20%, respectively, compared to autoclave-processed composites, while the out-of-plane Poisson's ratio remains unaffected. Given the challenges posed by warpage in fabricating flat thermoplastic composite laminates suitable for conventional mechanical testing by the AFP technique, this research proposes a virtual testing methodology as a viable alternative for characterizing the mechanical properties of such materials.

Abstract

Despite manufacturing challenges, Automated Fiber Placement (AFP) offers a viable alternative to conventional manufacturing methods, allowing for time and cost savings. Creating a Representative Volume Element (RVE) that realistically represents long-fiber-reinforced composites with high fiber volume fraction is a challenging task in modeling their response. The present research aims to predict effective stiffness properties of in-situ-consolidated Carbon/PEEK thermoplastic composite material by considering the effect of fiber volume fraction, void content, degree of crystallinity, and interlaminar resin pocket resulting from the AFP in-situ consolidation manufacturing process. In this regard, two sets of samples were manufactured by AFP in-situ consolidation and autoclave re-consolidation methods. Both of them were evaluated by micrographic study and thermoanalytical Differential Scanning Calorimetry (DSC) technique to obtain inputs required for micromechanical analysis. The 2D RVEs on a micro-scale are developed to predict the longitudinal elastic modulus (E_1), transverse elastic modulus (E_2), out-of-plane Poisson's ratio (v_{23}) and out-of-plane shear modulus (G_{23}) of the composite material by applying Periodic Boundary Conditions (PBCs) and using Asymptotic Homogenization Theory (AHT). Results show that AFP in-situ consolidation may lead the longitudinal elastic, transverse elastic and out-of-plane shear moduli of Carbon/PEEK thermoplastic composite material to be reduced by about 7%, 10% and 20%, respectively, compared to autoclave re-consolidation whereas the out-of-plane Poisson's ratio remains unchanged. The findings of the present work confirm that the mechanical performance of Carbon/PEEK thermoplastic composite material could be remarkably influenced by the AFP in-situ consolidation manufacturing process, particularly in the transverse direction, which must be taken into account in finite element modeling, analyses, and design of AFP-manufactured composite laminates and structures.

4.1. Introduction

Polymeric composites have been used in a wide range of applications due to their high specific stiffness and strength, corrosion resistance, and lightweight properties, particularly in structures such as aircraft and automotive components. Compared to traditional manufacturing methods, such as the hand lay-up process, automated manufacturing techniques, such as Automated Fiber Placement (AFP), provide the potential to decrease material waste, boost deposition rate, and

minimize manufacturing time and expenses. Robotic AFP machines use a robotic arm and a fiber placement head (thermoset or thermoplastic) to lay narrow composite tows onto a tool surface to manufacture a composite laminate. During the fiber placement process, compressive force and heat are simultaneously applied using a compaction roller and heating system, such as a hot gas torch. The aerospace industry has used thermoset-based composites for many years due to their ease of processing, high mechanical properties, and low viscosity. However, their time-consuming and costly curing process has led thermoplastic composites to be used more often as replacements for their thermoset counterparts. One of the biggest advantages of thermoplastic composites is the possibility of in-situ consolidation during the AFP manufacturing process. In spite of the aforementioned AFP-related benefits, there is a considerable difference between the quality of the in-situ-consolidated thermoplastic composite and autoclave-treated counterpart due to crucial factors, such as fiber volume fraction, void content, interlaminar resin pocket and degree of crystallinity.

Certain researchers [13,14] attempted to identify the optimum AFP processing parameters for manufacturing thermoplastic composite materials, with a focus on Interlaminar Shear Strength (ILSS) values. These studies concentrated on three key processing parameters: process temperature, deposition rate, and compaction force. Through the application of the Taguchi method and an extensive series of experimental tests, they successfully identified the optimal conditions for Carbon/PEEK thermoplastic composite laminates. Shadmehri *et al.* [5] compared the quality of in-situ-consolidated Carbon/PEEK thermoplastic composite samples with their counterparts re-consolidated inside the autoclave and proposed a method called "repass treatment" to improve surface finish quality during the AFP process, particularly for aerodynamic applications. They reported that the AFP in-situ consolidation technique can result in non-uniform fiber distribution, high void content and low degree of crystallinity for thermoplastic composite materials in comparison with the autoclave manufacturing method. Oromiehie *et al.* [34,35] also investigated the void content and degree of crystallinity of Carbon/PEEK thermoplastic composite samples. They revealed that the AFP in-situ consolidation process can introduce a void content ranging from 1.5% to 3.5% and increase the fracture toughness, which is attributed to the reduction in the degree of crystallinity. The short processing time of AFP in-situ consolidation results in a rapid exposure of the laid-down tape to ambient temperature, inducing a substantial cooling rate that adversely affects the degree of crystallinity. Based on the AFP processing parameters and type

of the heating system, such as a hot gas torch, laser, etc., the degree of crystallinity of the in-situ-consolidated Carbon/PEEK thermoplastic composite specimens can vary in a range of 15 to 30 percent [5,38,40,41]. As a result, it is of great importance to investigate the mechanical performance of the thermoplastic composites manufactured by AFP in-situ consolidation and draw a comparison between the effects of this technique and the autoclave method that is considered here as a reference method.

The determination of mechanical properties of composite materials relies on three primary methods: experimental measurements, analytical solutions and micromechanical computational models. Experimental approaches, although necessary for assessing final material properties, are often expensive for preliminary design purposes. Moreover, Manufacturing-related issues, such as residual deformation caused by AFP in-situ consolidation process, can pose challenges in conducting even relatively simple mechanical tests on unidirectional thermoplastic composite specimens [29]. It should be noted that the use of either a heated mandrel or an oven to avoid the warpage phenomenon affects the mechanical properties of the final product. Analytical models are suitable for evaluating the elastic properties of Fiber-Reinforced Polymers (FRPs), but they have limitations when either out-of-plane properties, such as out-of-plane shear modulus, are studied or local damage progression is investigated [121,122]. Furthermore, certain analytical models are intricate to implement, struggle to accurately capture the correct microstructure of the composite material, and fail to regard nonlinear material behavior. Micromechanical computational models, which employ the Finite Element Method (FEM), offer an effective approach to perform virtual experiments and assess various material systems during the design process. This method provides flexibility in evaluating material nonlinearities and tracking local damage progression in FRPs. By employing a Representative Volume Element (RVE), it becomes possible to simulate complex microstructures present in composite materials along with their spatial distribution, thereby enhancing the practicality of the approach. Micromechanical analysis is a useful tool for studying the local and global properties of composite materials. Although many studies in composite structural design and analysis utilize homogenized material properties at the macrostructural level, several macrostructural behaviors are controlled by fiber/matrix interactions and characteristics at the microstructural level. Therefore, accurate prediction and comprehension of the macrostructural behavior of composite materials depend on having an in-depth knowledge of these interactions and mechanisms, which are offered by the RVE approach [48]. This method is versatile and

applicable to a wide range of composite materials, such as particulate and fiber-reinforced composites. Its size-independence feature also allows for the use of smaller RVEs without compromising accuracy, leading to computational efficiency. As a result, the RVE technique enables researchers to model various microstructural features, including types of constituents, their shape, orientations and distributions, and to predict effective material properties of composites.

The RVEs with a periodic distribution of fibers (i.e., hexagonal and square packing) have been used in several research works to simplify the complex microstructure of FRPs [69,123–128]. The adoption of a periodic microstructure assumption limits researchers to the investigation of global phenomena, primarily focusing on overall effective properties. This approach often poses challenges in accurately predicting material properties and associated behavior under various loading conditions. Due to the non-uniform distribution of fibers within the composite cross-section, the accurate study of localized phenomena such as failure, which strongly rely on local morphology, is not feasible based on the assumption of periodic microstructure. To ensure precise calculation of mechanical properties, for accurate assessment of local stress concentrations, and for reliable prediction of the initiation and progression of local damage, it is imperative to incorporate a realistic non-uniform and random distribution of fibers [42,49–51,129–132].

Generating a Representative Volume Element (RVE) that accurately represents the real microstructure poses notable challenges, particularly for Fiber-Reinforced Polymers (FRPs) with high fiber volume fractions when dealing with the analysis of random microstructures. To this end, several algorithms have been developed by different researchers. The technique of Random Sequential Adsorption (RSA), which has been demonstrated to be statistically representative, is one of the methods used to produce random locations for either fibers or particles [52,114,133]. Gusev *et al.* [49,134] adopted an alternative approach utilizing Monte Carlo techniques to generate random microstructures by perturbing a regularly packed microstructure. Similarly, Wang *et al.* [135] employed a comparable method based on perturbations of a regular microstructure to generate meso-scale random Representative Volume Elements (RVEs). To generate microstructures that faithfully represent real composite materials, Vaughan *et al.* [136] utilized statistical data obtained through image processing of cross-sections. From the overlapping fibers phenomenon, a technique is also devised by Pathan *et al.* [137] in which fibers are moved in a series of steps to create a realistic RVE. Random Sequential Expansion (RSE) is another approach

that is capable of creating RVEs with high fiber volume fraction [53]. For the creation of random microstructures, Melro *et al.* [54] suggested a three-step, computationally effective approach called Random Microstructure Generator (RAND_uSTRU_GEN) that has been demonstrated to be capable of achieving high fiber volume fractions and being statistically representative. Bahmani *et al.* [51] developed an RVE with a fiber volume fraction of up to 80% using the theory of Event-Driven Molecular Dynamics (EDMD) to improve the realism of the generated RVE model with non-uniform fiber distribution. Ghayoor *et al.* [50] employed almost the same algorithm introduced by Melro *et al.* [54] with an innovative improvement whereby the algorithm moves the most isolated fibers to leave empty spaces in between (modified fibers stirring step [54]). In fact, the likelihood of a vacant space being created by finding the most isolated fibers raises the possibility of adding a new fiber.

Within composite structures, the occurrence of transverse matrix microcracking often serves as the initial failure mechanism and controls the progression of fractures [138,139]. Moreover, while fiber volume fraction is the determining factor for material response in fiber direction, the presence of voids, interlaminar resin pockets and the change in the degree of crystallinity, which are caused by the AFP in-situ consolidation process, affect the material properties in the transverse direction considerably. Therefore, in the present work, both longitudinal and transverse cross-sections in which fiber and matrix properties primarily govern the response of the composite material, respectively, were investigated. The arrangement of fibers and void content plays a crucial role in determining stress concentration and stress distribution throughout the matrix phase. In this regard, two sets of Carbon/PEEK thermoplastic composite samples were manufactured by AFP in-situ consolidation and autoclave re-consolidation techniques. These samples underwent micrographic study and thermoanalytical Differential Scanning Calorimetry (DSC) to gather the necessary data for micromechanical analysis. Various two-dimensional representative volume elements with randomly distributed fibers were modeled on a micro-scale to assess the influences of the fiber volume fraction, void content, interlaminar resin pocket and degree of crystallinity, that result from AFP in-situ consolidation and autoclave re-consolidation, on the stiffness properties of the material. Asymptotic Homogenization Theory (AHT) is used to examine the mechanical response of the RVEs subjected to Periodic Boundary Conditions (PBCs). All modeling steps are carried out by an ABAQUS Scripting Interface (ASI) written in the Python programming language, in conjunction with MATLAB, that determines the RVE Geometry. Considering the inherent

limitations of the in-situ consolidation process (i.e., warpage phenomenon) in manufacturing flat thermoplastic composite laminates for even certain simple mechanical tests, the present research introduces a virtual testing approach as an alternative method to characterize material properties. The obtained results substantiate that the AFP in-situ consolidation manufacturing process significantly affects the material properties of Carbon/PEEK thermoplastic composites in the transverse direction compared to the autoclave treatment.

4.2. Experimentation

Thermoplastic composites offer a notable advantage over thermoset counterparts in the AFP manufacturing process due to their ability to undergo in-situ consolidation. This eliminates the need for secondary processes, such as autoclave and hot press, which are both expensive and time-consuming. Nevertheless, the manufacturing process must also consider the quality of the final product. While in-situ consolidation offers a rapid fabrication method, it is important to address potential defects that may arise during the automated fiber placement method, as these can have a detrimental effect on the mechanical performance of composite components. AFP in-situ consolidation is characterized by a short duration in which the tape is heated by a heat source (e.g., hot gas torch, laser, etc.) and compacted under a roller, resulting in incomplete healing. Although the smoothness of the tape and the application of high compaction force can help shorten the time required for achieving intimate contact, perfect autohesion in thermoplastic resin typically requires more time than is available during in-situ consolidation [10]. Increasing the number of passes can improve this aspect, but it may lead to other issues such as increased manufacturing time. It is worth mentioning that the short processing time of the in-situ consolidation process negatively influences the degree of crystallinity, achievement of the nominal fiber volume fraction and elimination of void content as compared to the autoclave treatment. Furthermore, because fibers do not have enough time to be evenly distributed through the thickness of the composite laminate when the matrix is melted for a short period of time, resin-rich areas (resin pockets) are introduced between composite layers [5].

To differentiate between the RVEs representing Carbon/PEEK thermoplastic composite laminates manufactured by AFP in-situ consolidation and autoclave re-consolidation for the prediction of effective material properties, accurate input data is essential for micromechanical analysis. This

information can be obtained through micrographic study and the DSC thermoanalytical technique. To this end, two Carbon/PEEK laminates were manufactured by AFP in-situ consolidation. One of them was re-consolidated inside the autoclave to be considered as a baseline laminate. A micrographic examination was performed on thermoplastic laminate samples of both in-situ-consolidated and autoclave-reconsolidated types. This investigation aimed to analyze the presence of voids, distribution of fibers and the percentage of the fiber volume fraction, which serve as three decisive factors that contribute to the distinction between AFP in-situ consolidation and autoclave re-consolidation processes. Afterward, the degrees of crystallinity of both types of samples were measured using the thermoanalytical Differential Scanning Calorimetry (DSC) technique.

4.2.1. AFP manufacturing process

At Concordia Centre for Composites (CONCOM), researchers have access to an AFP machine consisting of a 6-axis Kawasaki articulated robot arm with a 125 kg payload, equipped with a thermoplastic head supplied by Trelleborg Group, as shown in Figure 4.1. In the present work, two Carbon/PEEK (AS4/APC-2) plates were manufactured using HGT-assisted AFP and a flat paddle tool (Aluminum mandrel) by in-situ consolidation. The study utilized Solvay Group's unidirectional tape consisting of Carbon fiber (AS4) and PEEK resin (APC-2) with a weight ratio of 68:32 and a nominal fiber volume fraction of 60%. The tape had a width and thickness of 6.35 mm (0.25 in) and 0.140 mm (0.0055 in), respectively [67]. A steel roller was used to apply pressure, while a Nitrogen hot gas torch with a temperature of 875° C (for more information on how to measure the nip point temperature, see reference [140]) and a flow rate of 80 SLPM was used to melt the tape during deposition. The high-temperature-resistant steel roller applied a compaction force of 60 lbf, and the deposition rate was set to 50.8 mm/s (2 in/s). It should be noted that these AFP processing parameters closely correspond to the optimum values recommended in the literature [13,14].

Figure 4.1. Automated fiber placement machine with a flat mandrel available at CONCOM.

4.2.2. Autoclave curing

To evaluate the influence of the AFP in-situ consolidation manufacturing process on void content, fiber volume fraction, and fiber distribution, the other in-situ-consolidated thermoplastic laminate was vacuum-bagged and subsequently placed in an autoclave, as shown in Figure 4.2. The temperature was raised to $390° \pm 10°$ C ($735° \pm 15°$ F) and maintained at a constant level for a duration of 20 ± 5 minutes, with an applied pressure of 100 ± 5 psi [67]. This re-consolidated plate served as a reference for comparison with a non-autoclave-treated Carbon/PEEK thermoplastic composite laminate.

Figure 4.2. In-situ-consolidated thermoplastic composite laminate to be re-consolidated inside the autoclave.

4.2.3. Micrographic study

Analyzing the microstructure of thermoplastic samples manufactured by in-situ consolidation and autoclave re-consolidation provides valuable insights into the sources of mechanical performance variations. For this purpose, samples from both plates (one AFP in-situ consolidated and one autoclave re-consolidated) were sectioned, embedded in resin, cured, and polished using different grit sandpapers and diamond suspensions [109]. Microscopy imaging of the samples, as shown typically in Figure 4.3 at 20X magnification, reveals notable distinctions between AFP and autoclave-made thermoplastic composites. Autoclave treatment exhibits a significant influence on the microstructure, resulting in improved fiber distribution and minimal discernibility of layer boundaries. Conversely, micrographs of samples fabricated by in-situ consolidation highlight the presence of resin-rich areas between layers and nonuniform fiber distribution (interlaminar resin pockets), which can lead to the emergence of regions with stress concentrations. It is worth mentioning that the compaction force (60 lbf) used in the present research contributes to reducing the size of the interlaminar resin pockets to a certain extent and guarantees that fibers will not be damaged after the AFP process [14].

| Autoclave-reconsolidated sample | In-situ-consolidated sample |
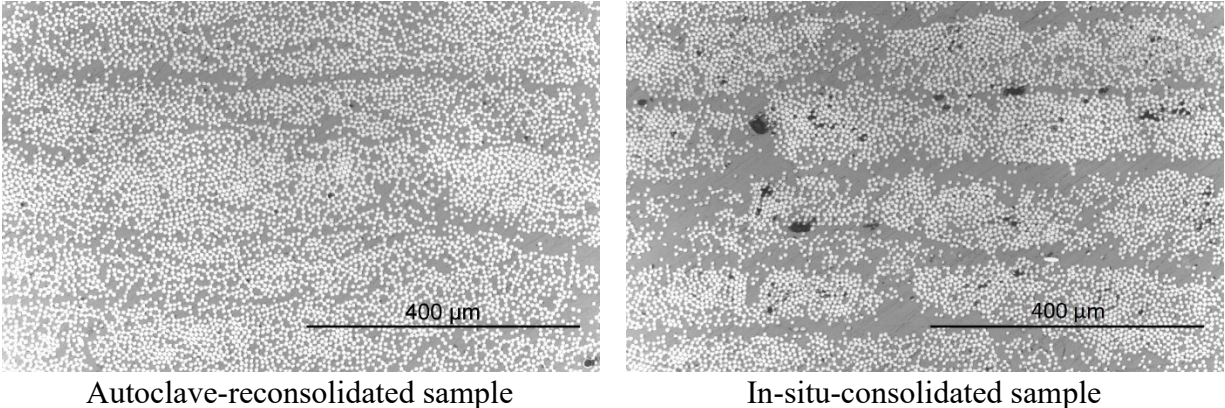
Figure 4.3. Micrographs of samples fabricated by AFP in-situ consolidation and autoclave re-consolidation at 20X magnification.

To assess the influence of the in-situ consolidation process on void content, a micrograph analysis was conducted. Void content and fiber volume fraction were determined using the color thresholding technique (using *ImageJ* software) that distinguishes between voids, fibers, and resin [43,44], as shown in Figure 4.4. The void contents of Carbon/PEEK thermoplastic samples manufactured by AFP in-situ consolidation and autoclave re-consolidation were determined to be averagely 1.5% and 0.09%, respectively. These values indicate a significant difference and

highlight the contribution of voids as a factor negatively affecting the mechanical performance of AFP-manufactured composite products. It is important to mention that initial uncertainty existed regarding the nature of the black spots, especially the larger ones, thought to be scratches. However, this procedure was also repeated for autoclave-reconsolidated Carbon/PEEK thermoplastic composite samples, in which scratch-like black spots didn't appear. Therefore, those large black spots are highly likely to be real voids rather than scratches.
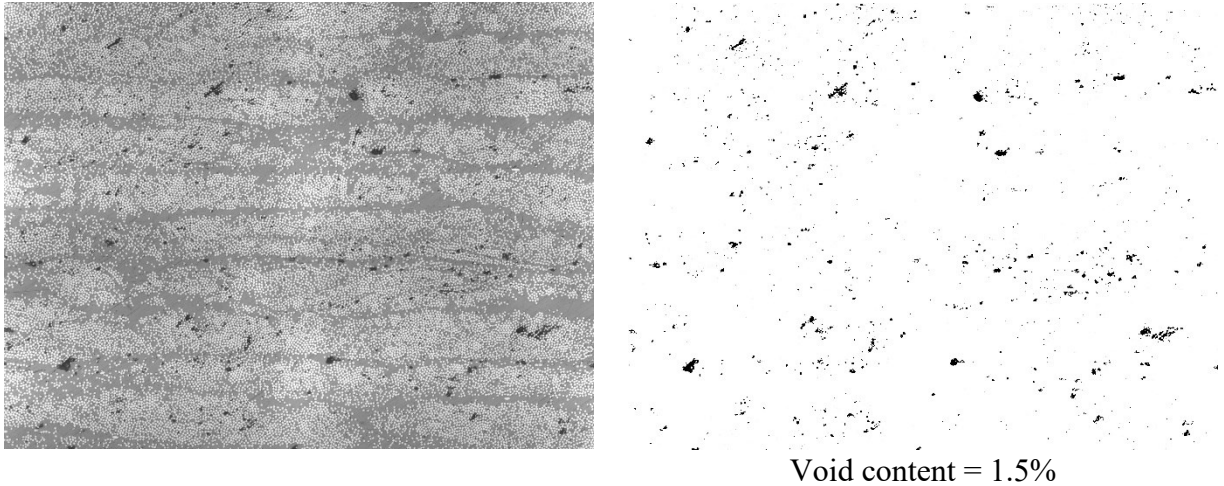
Void content = 1.5%

Figure 4.4. Example of the void content calculation for in-situ-consolidated Carbon/PEEK thermoplastic sample utilizing the color thresholding technique.

4.2.4. Measurement of crystallinity

The degree of crystallinity of manufactured Carbon/PEEK laminate samples was determined using a Differential Scanning Calorimetry (DSC) machine (product of *TA Instruments*). Specimens weighing approximately 10 mg were prepared and subjected to a heat-cool-heat cycle with a heating rate of 10 °C/min and a maximum temperature of 390° C in a Nitrogen atmosphere, followed by a cooling rate of 5 °C/min. The degree of crystallinity, X, is calculated using the equation presented below [5,112]:

$$X = \frac{\Delta H_m - \Delta H_c}{\Delta H_f (1 - \alpha)} \tag{4.1}$$

where ΔH_m and ΔH_c represent the enthalpies of fusion measured by the area under the endothermic peak (the area enclosed between the heat flow-temperature curve and the baseline) at the melting point and the exothermic crystallization peak, respectively. ΔH_f denotes the enthalpy of fusion for fully crystalline PEEK which was considered as 130 J/g [113]. α is the weight ratio

of Carbon fibers in the Carbon/PEEK thermoplastic composite. Table 4.1 presents the results of the DSC test, which includes average values of the degree of crystallinity and melting temperature obtained from a minimum of five specimens fabricated using each manufacturing technique: in-situ consolidation and autoclave re-consolidation.

Table 4.1. Degrees of crystallinity and melting temperatures of Carbon/PEEK samples.

	Crystallinity (%)	SD[*]	Melting temperature (°C)	SD[*]
AFP In-situ consolidation	25.07	0.82	345.31	0.17
Autoclave re-consolidation	34.96	0.38	345.52	0.15

[*]SD = Standard Deviation

As it can be observed from Table 4.1, there is a 9.89% difference between the crystallinity of Carbon/PEEK samples manufactured by in-situ consolidation and autoclave re-consolidation. It should be noted that AFP processing parameters, namely deposition rate, temperature and compaction force, type of the heating system (e.g., hot gas torch, laser, etc.) and repass treatment may affect the degree of crystallinity of Carbon/PEEK thermoplastic composite laminate manufactured by AFP in-situ consolidation, resulting in a range typically spanning 15 to 30 percent [5,38,40,41]. The degree of crystallinity holds significant importance as it strongly impacts the elastic modulus and strength of neat PEEK resin [30,46,47]. Consequently, it can have adverse effects on the overall material properties of the composite material, particularly in the transverse direction where matrix behavior is dominant.

4.3. Generation of Representative Volume Element (RVE)

Generating randomly distributed fibers in a Representative Volume Element (RVE) with a fiber volume fraction exceeding 50% presents a serious challenge due to the limitations of programming languages, such as MATLAB and Python, in finding suitable locations for adding new fiber center points using random generators alone. The approach employed in the present research follows the algorithm proposed by Melro *et al.* [54] and enhanced by Ghayoor *et al.* [50]. It involves relocating the most isolated fibers within the RVE to achieve a higher fiber volume fraction (e.g., 60%).

The process of creating a Representative Volume Element (RVE) begins by generating a set of random center points for the fibers, ensuring that there is no overlap with previously generated fibers. This step incorporates the option to specify a minimum distance between fibers. To achieve

higher fiber volume fractions, the next stage involves identifying and relocating the center points of the most isolated fibers within the RVE, creating space for additional fibers (referred to as fiber stirring [54]). Selecting the most isolated fibers enhances the likelihood of creating empty regions, thus increasing the opportunity to introduce new fibers. The isolation of fibers is determined by calculating the average distances to their three or four closest neighbors, and those with the largest average distance are considered isolated [50]. The number of fibers considered for relocation can be adjusted based on the iteration number and the desired fiber volume fraction. The relocation direction is towards neighboring fibers, and the distance of movement is randomly determined within the range between the minimum specified distance and the existing distance between two fibers.

While the microstructure within the Representative Volume Element (RVE) is inherently random, the RVE itself needs to exhibit periodicity. In other words, in cases where a fiber center point is located close to the border of the RVE, with a distance from the border less than the fiber radius, the remaining portion of the fiber is replicated on the opposite side of the RVE to maintain the periodicity of the microstructure. The requirement for a periodic RVE is essential to enable accurate estimation of the stress field within the RVE. It is worth mentioning that the aforementioned algorithm used to generate high-fiber-volume-fraction RVEs with randomly distributed fibers was implemented using the MATLAB programming language (refer to the Appendix of Chapter 3 for more details).

The micrographic comparison between in-situ consolidation and autoclave re-consolidation manufacturing processes of Carbon/PEEK thermoplastic composite samples revealed a clear distinction in fiber distribution across the thickness. To consider the influence of interlaminar resin pockets on the prediction of the composite material's effective material properties during the simulation, fibers were forced to stay in closer proximity by applying constraints on the top and bottom boundaries of the RVE based on the percentage of the desired interlaminar resin pocket. For instance, in order to create a 12% interlaminar resin pocket inside the RVE, center points of fibers were limited to be randomly generated between 6% and 94% of the RVE length in the y-direction. It is worth mentioning that these constraints were also in effect during the use of the fiber stirring algorithm in order to have control over the percentage of interlaminar resin pocket. This process generally involved moving the fibers towards the center while the fiber volume

fraction was maintained constant. Consequently, resin-rich regions, that are similar to those observed in the micrographic study, were formed at the top and bottom edges of the RVE, as shown in Figure 4.5.

<center>(a)</center> <center>(b)</center>
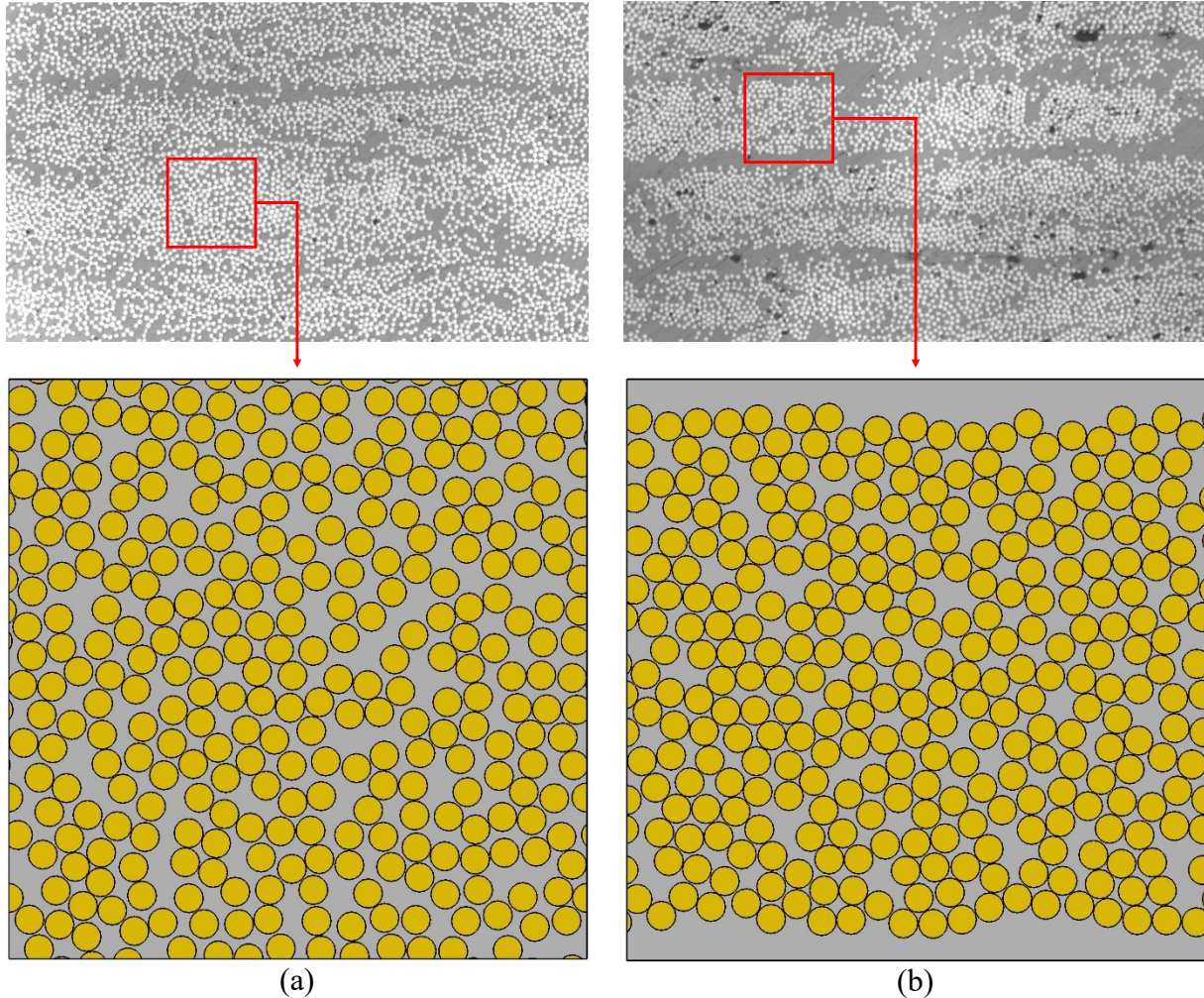
Figure 4.5. Examples of generated Representative Volume Element (RVE) with random fiber distribution (FVF = 60%): (a) without and (b) with 12% interlaminar resin pockets.

To predict the elastic moduli of Carbon/PEEK thermoplastic composite material in the fiber (E_1) and transverse (E_2) directions through two-dimensional micromechanical analysis, distinct Representative Volume Elements (RVEs) are required, generated based on the longitudinal and transverse cross-sections. The finite element analysis conducted for both types of RVEs in ABAQUS is identical, except for the method employed to generate the geometry using MATLAB programming code. For the longitudinal cross-section, fibers may exhibit full radii or be partially visible on the surface of the composite material, depending on their actual position within the

<center>136</center>

structure. To this end, the simulation approach for the longitudinal-cross-section RVE must involve generating random radii for fibers in addition to their random locations, whereas fibers' radii remain constant in the RVE depicting the transverse cross-section of the composite material. Thus, MATLAB code (refer to "MATLAB code for longitudinal cross-section" section in the Appendix for more details) already written for RVE generation based on the transverse cross-section in Chapter 3 was developed, particularly in terms of the compatibility conditions to prevent any intersections between either fibers or fibers and voids, to create those inspired by longitudinal cross-section from the ground up.

4.4.   Finite element modeling

Once the locations of the fibers within the Representative Volume Element (RVE) were identified to achieve the desired fiber volume fraction, a micro-scale numerical analysis of random and periodic microstructures, assuming ideal bonding between fibers and matrix, was performed using the ABAQUS Scripting Interface (ASI) in the Python programming language (refer to "Python script for stiffness prediction" section in the Appendix for more details). It has been established that the properties of the interface significantly influence the damage onset and evolution [45,59–62,141]. However, for the purpose of the present work, focusing on the elastic region of the material, the bond between fibers and matrix is assumed to be perfect. This simplification reduces the number of elements and computational time required for analyzing numerous RVEs.

To take into account the influence of interlaminar resin pockets in the simulation, the length of the Representative Volume Element (RVE) was selected as 140 μm, matching the thickness of each Carbon/PEEK layer [67]. The Carbon fibers have a diameter of 7 μm, with a minimum distance between them equal to 0.01 times the fiber radius. Triangular 3-node linear plane strain elements (CPE3), as shown in Figure 4.6, were utilized for the analysis. The mesh size was determined through sensitivity analysis for various element sizes, and a mesh size equivalent to one-fourth of the fiber radius was selected for the present work [42,50]. It should be noted that the size of the RVE in fiber-reinforced composites is typically defined as the ratio of the RVE length to the fiber radius ($\delta = l/r$). Choosing the appropriate RVE size is essential to accurately represent the material's morphology and behavior in a statistically meaningful manner. In the present work, the ratio of the δ is set to be equal to 40 ($l = 140 \ \mu m, r = 3.5 \ \mu m$) which has been demonstrated to

be a representative value for Carbon-reinforced polymers [50,114]. The material properties of the thermoplastic composite constituents, Carbon fiber and PEEK resin, are listed in Table 4.2.

Table 4.2. Stiffness properties of PEEK resin and Carbon fiber in principal directions [67].

	E_1 (GPa)	$E_2 = E_3$ (GPa)	$\nu_{12} = \nu_{13}$	ν_{23}
Carbon fiber (AS4)	228	22	0.20	0.25
PEEK resin (APC-2)	3.6	3.6	0.38	0.38
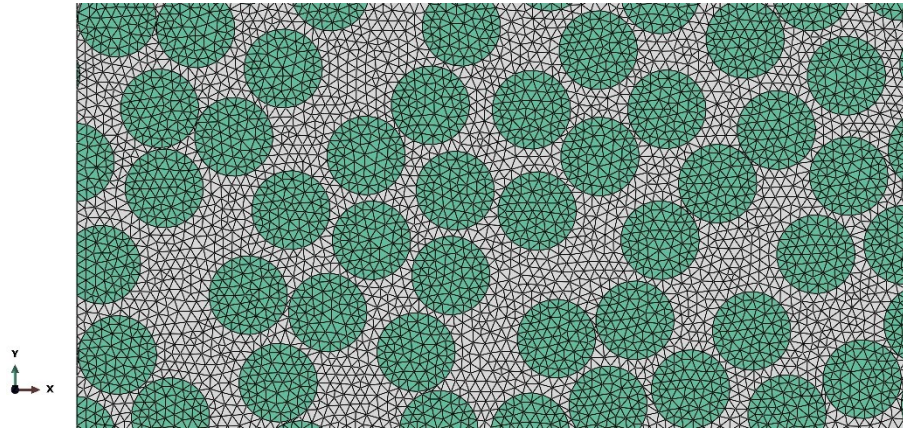
Figure 4.6. A section from the RVE meshed using triangular 3-node linear plane strain elements with the size of one-fourth of the fiber radius.

4.4.1. Generation of voids

The existence of voids originating from the manufacturing process is another important aspect that significantly affects the transverse properties of composites. Generally, voids in composite materials can exist in various sizes, and their formation can be attributed to two main sources during the manufacturing process. The first source is the air that gets trapped between composite plies when they are being laid up. Moreover, when impurities or volatile materials vaporize during the composite's high-temperature curing process, voids may be introduced, which is considered as the second source for voids [70].

Numerous studies have investigated the influence of voids, leading to the development of two distinct methods for modeling them. In the first method, voids are explicitly modeled, typically assuming circular holes in the transverse direction [58,70–74]. It has been observed that the presence of voids can lead to early damage initiation and a reduction in the failure strength of the composites. Another approach for void modeling involves assigning air properties to selected

138

matrix elements [75–79]. This method is also commonly employed to investigate the influence of voids on the stiffness and strength properties of composite materials. Wang *et al.* [45] conducted a comparison between the two void modeling techniques. In the model in which voids are explicitly incorporated, although variations in predicted failure strengths were observed due to differences in void distribution and void area, shapes of voids (i.e., circular, elliptical and arbitrary shapes) didn't have a substantial effect on the outcome. Nevertheless, the model with voids simulated within elements showed roughly similar results due to considering almost the same size for all of the voids. It should also be noted that the method with explicitly established voids predicted slightly lower failure strength when considering the same fiber distribution pattern. Therefore, the first method (explicit establishment of voids) with circular voids, because of geometrical simplicity and computational efficiency, was employed in the present work as it closely resembled the actual behavior observed in experiments.

The Random Sequential Adsorption (RSA) method [55] is utilized to determine the locations of voids in the RVE models randomly. If the chosen position falls within the area occupied by fibers, an alternate point is generated. On the other hand, if the selected position lies outside the fiber area, the void radius is randomly determined within the range of 0 to $D - r$, where D represents the distance between the void center and its nearest fiber center, and r denotes the fiber radius. The void volume fraction is computed and compared to a threshold (e.g., 2%). If the calculated void volume fraction is below this threshold, more void centers and radii are iteratively generated until the void volume fraction reaches or exceeds the desired value. An RVE with and without void content can be seen in Figure 4.7.
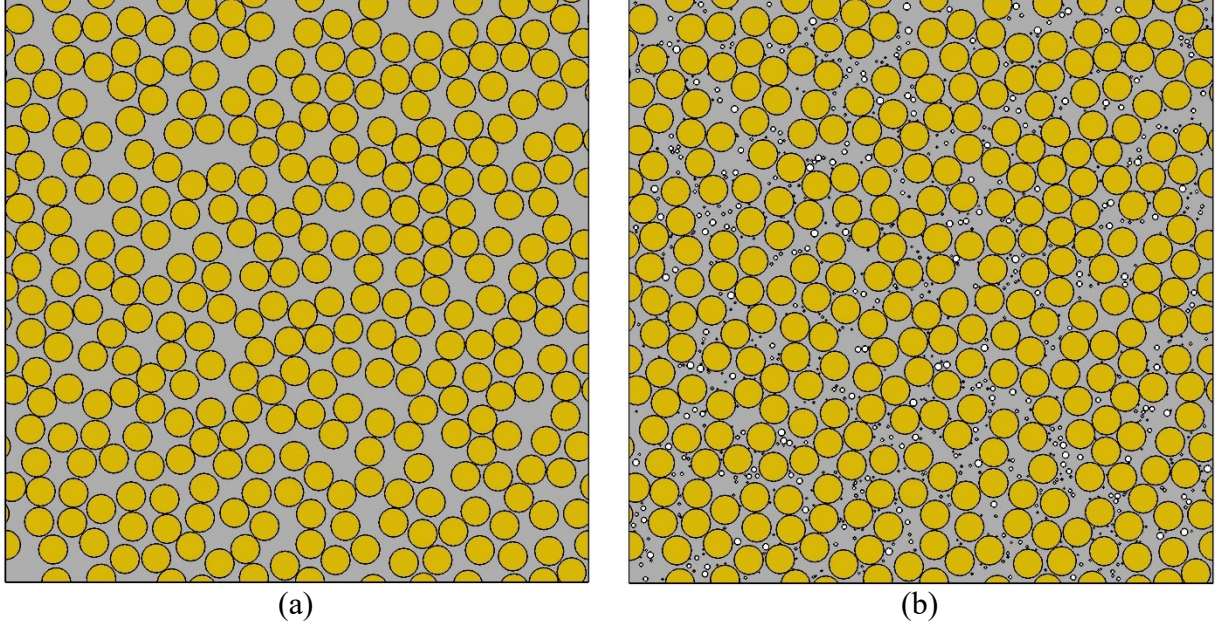
Figure 4.7. Examples of generated Representative Volume Element (RVE) with random fiber distribution (FVF = 60%): (a) without and (b) with 2% void content.

4.4.2. Periodic boundary conditions

Composite materials are typically represented as an array of periodic RVEs, necessitating the application of periodic boundary conditions. These kinds of boundary conditions ensure that the deformation of all RVEs is identical, with neither overlapping nor separation between adjacent RVEs. The periodic boundary conditions can be defined as follows [68,69]:

$$u_i = \bar{\varepsilon}_{ik} x_k + u_i^* \tag{4.2}$$

where u_i, $\bar{\varepsilon}_{ik}$ and x_k represent the displacement, the average strain and the Cartesian coordinate of a point on the RVE boundary, respectively. u_i^* is the periodic function of the displacement which is basically unknown and dependent on general loading conditions.

In order to ensure the periodic arrangement of RVEs within a structure, it is necessary to satisfy two types of continuity across opposite boundaries: displacement continuity and traction continuity. By assuming a displacement field in the form of Eq. (4.2), both types of continuity can be fulfilled. Within an RVE, the boundary surfaces are treated as parallel pairs, and the displacement on opposite boundary surfaces can be expressed as follows:

$$u_i^{j+} = \bar{\varepsilon}_{ik} x_k^{j+} + u_i^* \tag{4.3}$$

$$u_i^{j-} = \bar{\varepsilon}_{ik} x_k^{j-} + u_i^* \tag{4.4}$$

where $j+$ and $j-$ indices indicate jth pair of parallel opposite surfaces in an RVE.

As mentioned earlier, the periodic component of Eq. (4.2), represented by u_i^*, is unknown, but it has the same value for a pair of parallel surfaces. As a result, the difference between their displacements can be expressed as follows:

$$u_i^{j+} - u_i^{j-} = \bar{\varepsilon}_{ik}\left(x_k^{j+} - x_k^{j-}\right) = \bar{\varepsilon}_{ik}\Delta x_k^j \tag{4.5}$$

Such an approach removes the unknown periodic function of the displacement field. Because Δx_k^j remains constant in each RVE (length of the RVE), the right-hand side of Eq. (4.5) would also become a constant value with knowing the $\bar{\varepsilon}_{ik}$.

To achieve a uniformly distributed stress and displacement field at the macroscopic level, the RVE is subjected to periodic boundary conditions using Eq. (4.5) for tension and shear loading cases, as depicted in Figure 4.8. In order to satisfy the compatibility of boundary displacements, certain constraints need to be incorporated into the model [53,54]:

$$u_{DC} - u_{AB} = u_D - u_A \tag{4.6}$$

$$u_{BC} - u_{AD} = u_B - u_A \tag{4.7}$$

where u represents the displacement of a node located on the boundary. The subscript notation with a single letter indicates a vertex, while a combination of two letters represents an edge connecting the two respective vertices. The *Equation keyword can now be used in Python scripting to establish a constraint equation between nodes located on opposite surfaces. This allows for the creation of a mathematical relationship, Eq. (4.5), that enforces the necessary conditions between the selected node pair.
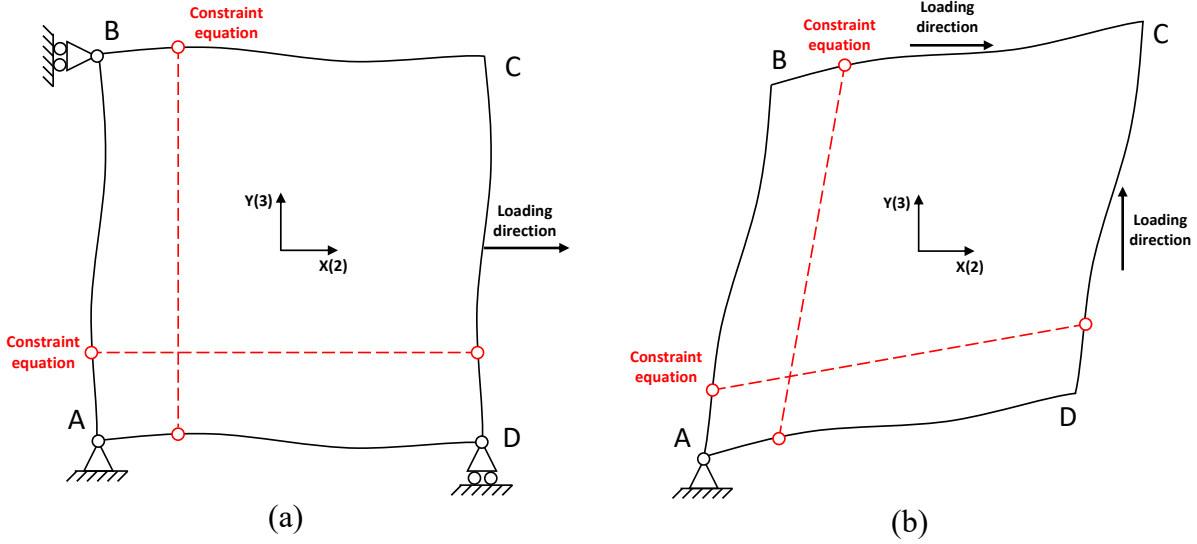
Figure 4.8. Schematic of periodic boundary conditions corresponding to (a) tension and (b) shear loading cases.

4.4.3. Homogenization

The homogenization technique is used to analyze the response of the Representative Volume Element (RVE) when it is subjected to mechanical loads, thereby facilitating the estimation of its effective mechanical properties. It is assumed that the average mechanical properties of the RVE correspond to those exhibited by the unidirectional composite lamina at the macrostructural level. The average stresses and strains within the RVE are defined as follows [68,69]:

$$\overline{\sigma}_{ij} = \frac{1}{A_{RVE}} \int_A \sigma_{ij} dA = \frac{1}{A_{RVE}} \sum_{k=1}^{N} \sigma_{ij}^k A^k \tag{4.8}$$

$$\overline{\varepsilon}_{ij} = \frac{1}{A_{RVE}} \int_A \varepsilon_{ij} dA = \frac{1}{A_{RVE}} \sum_{k=1}^{N} \varepsilon_{ij}^k A^k \tag{4.9}$$

where A_{RVE} represents the total area of the RVE. σ_{ij}^k and ε_{ij}^k are stress and strain components calculated at the integration point of the kth element with an area of A^k. N denotes the total number of integration points in the modeled RVE.

Various material properties can be determined by imposing different and independent displacement conditions. The determination of E_1, E_2 and ν_{23} involves applying a horizontal movement to the right side of the corresponding RVEs. G_{23} is obtained by applying horizontal displacement on the top side and vertical displacement to the right side of the RVE. Eventually,

142

the effective material properties of the composite material can be calculated using the following equations, depending on the chosen cross-section type in the simulation [54]:

$$E_1 = \frac{\bar{\sigma}_{11}}{\bar{\varepsilon}_{11}}, \qquad E_2 = \frac{\bar{\sigma}_{22}}{\bar{\varepsilon}_{22}}, \qquad \nu_{23} = -\frac{\bar{\varepsilon}_{33}}{\bar{\varepsilon}_{22}}, \qquad G_{23} = \frac{\bar{\sigma}_{23}}{\bar{\gamma}_{23}} \qquad (4.10)$$

4.5. Results

As previously stated, the micrographic study and characteristics of the AFP manufacturing method revealed four key factors as an origin of clear distinction between in-situ consolidation and autoclave re-consolidation processes: fiber volume fraction, void content, interlaminar resin pocket, and degree of crystallinity. Consequently, it is crucial to investigate the influence of each factor on the stiffness properties of in-situ-consolidated Carbon/PEEK composite parts, particularly in the transverse direction where the behavior of the matrix dominates. The present investigation aims to determine the extent to which these properties deviate from those indicated in the material datasheet provided by manufacturer [67], which is based on autoclave treatment.

The crystallinity results obtained from the DSC test have been documented in Table 4.1. Due to the nature of the AFP process (i.e., rapid heating and cooling), achieving a high level of crystallinity (similar to autoclave process) was not possible in this study. Considering the AFP processing parameters and the hot gas torch heating system utilized in the present work, degrees of crystallinity of 25.07% and 34.96% were measured using Differential Scanning Calorimetry (DSC) for in-situ consolidation and autoclave re-consolidation manufacturing processes, respectively. Several studies investigated the influence of crystallinity on the elastic modulus of neat PEEK resin. These studies have revealed an approximately linear relationship between the elastic modulus of PEEK resin and the degree of crystallinity within the range of 15% to 30% [30,46,47]. In the present research, a 4% reduction in the elastic modulus of neat PEEK resin was considered for every 5% decrease in the degree of crystallinity from the baseline value (i.e., 35%), which aligns with the existing literature [30,46,47] and represents a reasonable and average estimation.

Concerning the remaining three parameters, valuable insights can be obtained from micrographs. Following the autoclave re-consolidation process, because heat and pressure are uniformly applied for an extended duration compared to the AFP in-situ consolidation technique, some resin is

squeezed out and accumulated on the surface of the laminate. As a result, autoclave-reconsolidated Carbon/PEEK composite laminate experienced a reduction in thickness, and a noticeable release of excess resin was observed at the edges, indicating void elimination and a change in the final fiber volume fraction. To quantify the void content and fiber volume fraction, ImageJ software was employed, utilizing a color thresholding technique. Additionally, in order to accurately measure the thickness of interlaminar resin pockets, a scale was set within the ImageJ software, calibrated based on the magnification used during the micrographic study, allowing for precise distance measurements.

In this regard, thirty different Representative Volume Elements (RVEs) were carefully selected from various locations within the micrographs, all with the same size as that of the simulated RVEs. These RVEs were utilized to measure important factors such as fiber volume fraction, void content, and interlaminar resin pocket percentage. It should be noted that, in order to accurately measure the thickness of the interlaminar resin layer, micrographic RVEs were selected in such a way that cover half of the upper layer, the entire resin layer, and half of the lower layer, as illustrated in Figure 4.9. The frequency of results corresponding to each parameter for in-situ-consolidated Carbon/PEEK samples is presented in Figure 4.10. According to histograms, values of 56%, 1.5% and 12% were considered as average values for fiber volume fraction, void content and interlaminar resin pocket percentage, respectively, resulting from the AFP in-situ consolidation process.
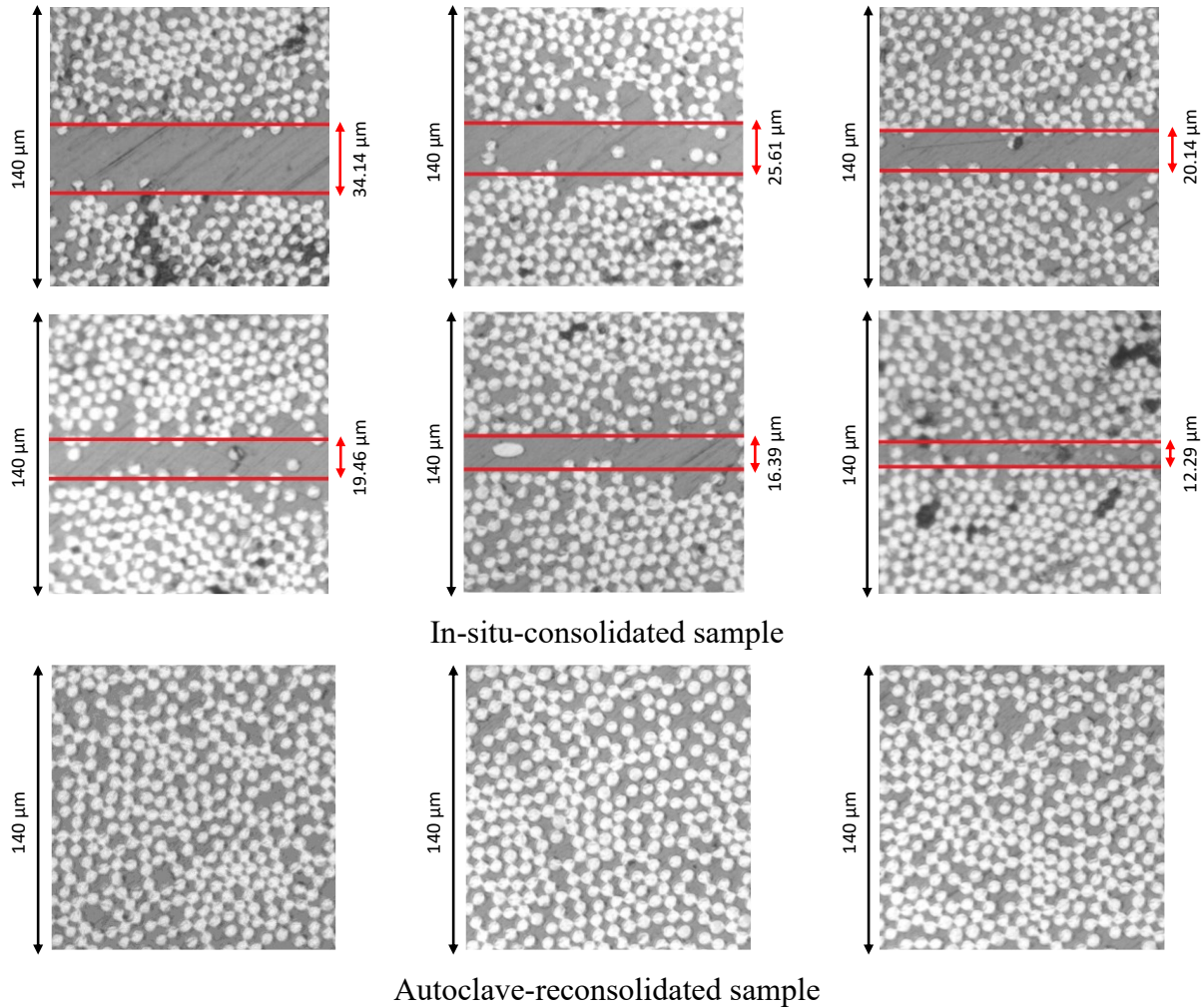
Figure 4.9. Examples of real RVEs extracted from micrographs Carbon/PEEK samples manufactured by in-situ consolidation and autoclave re-consolidation in order to measure the fiber volume fraction, void content and interlaminar resin pocket percentage.
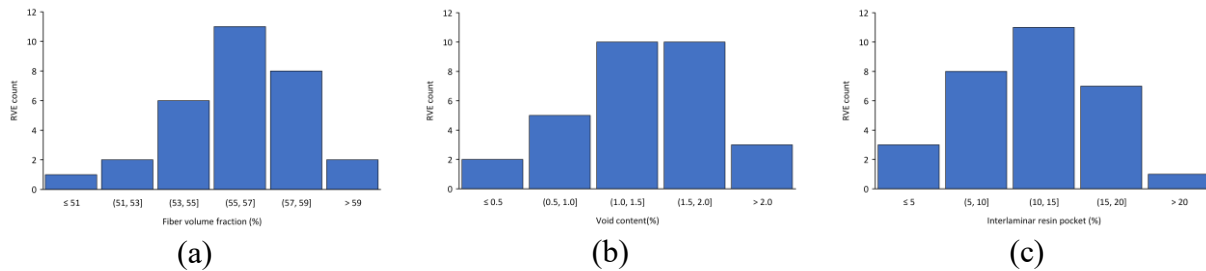
Figure 4.10. Distribution of (a) fiber volume fraction, (b) void content and (c) interlaminar resin pocket percentage based on the micrographic study of Carbon/PEEK thermoplastic composite manufactured by in-situ consolidation.

4.5.1. Validation

To ensure the validity of the finite element analysis results, autoclave consolidation conditions were considered by creating RVEs with a fiber volume fraction of 60%, no interlaminar resin pocket, no void content (void content of 0.09% is negligible) and a degree of crystallinity of 35%. It should be noted that these input data were obtained by micrographic study and DSC test for the purpose of micromechanical analysis. The final geometries of RVEs, representing the autoclave re-consolidation process, are illustrated in Figure 4.11 (a) based on their respective cross-sections. It should be noted that in the case of the longitudinal cross-section, the percentage of the fiber volume fraction might be either higher or lower than that calculated in the transverse cross-section, depending on the location of the cut. Therefore, the average fiber volume fraction was considered for the generation of longitudinal-cross-section RVEs representing each manufacturing process. Comparison of numerical results with the CYTEC technical datasheet [67] and reference studies [104,109] revealed that the developed finite element model is capable of predicting effective stiffness properties of Carbon/PEEK thermoplastic composite material, with less than 5% error, using the material properties of its constituents, as presented in Table 4.3.

Table 4.3. Predicted stiffness properties of Carbon/PEEK thermoplastic composite manufactured by autoclave treatment.

	E_1 (GPa)	E_2 (GPa)	ν_{23}	G_{23} (GPa)
Mean value	139.44	10.45	0.467	3.56
From Refs. [67,104,109]	138	10.30	0.450	3.70
Error (%)	1.04	1.46	3.78	3.78

4.5.2. Prediction of effective material properties

Once the proposed Finite Element (FE) model has been validated, the effect of the in-situ consolidation manufacturing process can be examined by changing the values of the four major factors mentioned earlier in order to generate Representative Volume Elements (RVEs) that accurately represent in-situ-consolidated Carbon/PEEK thermoplastic composites, as shown in Figure 4.11 (b).

146
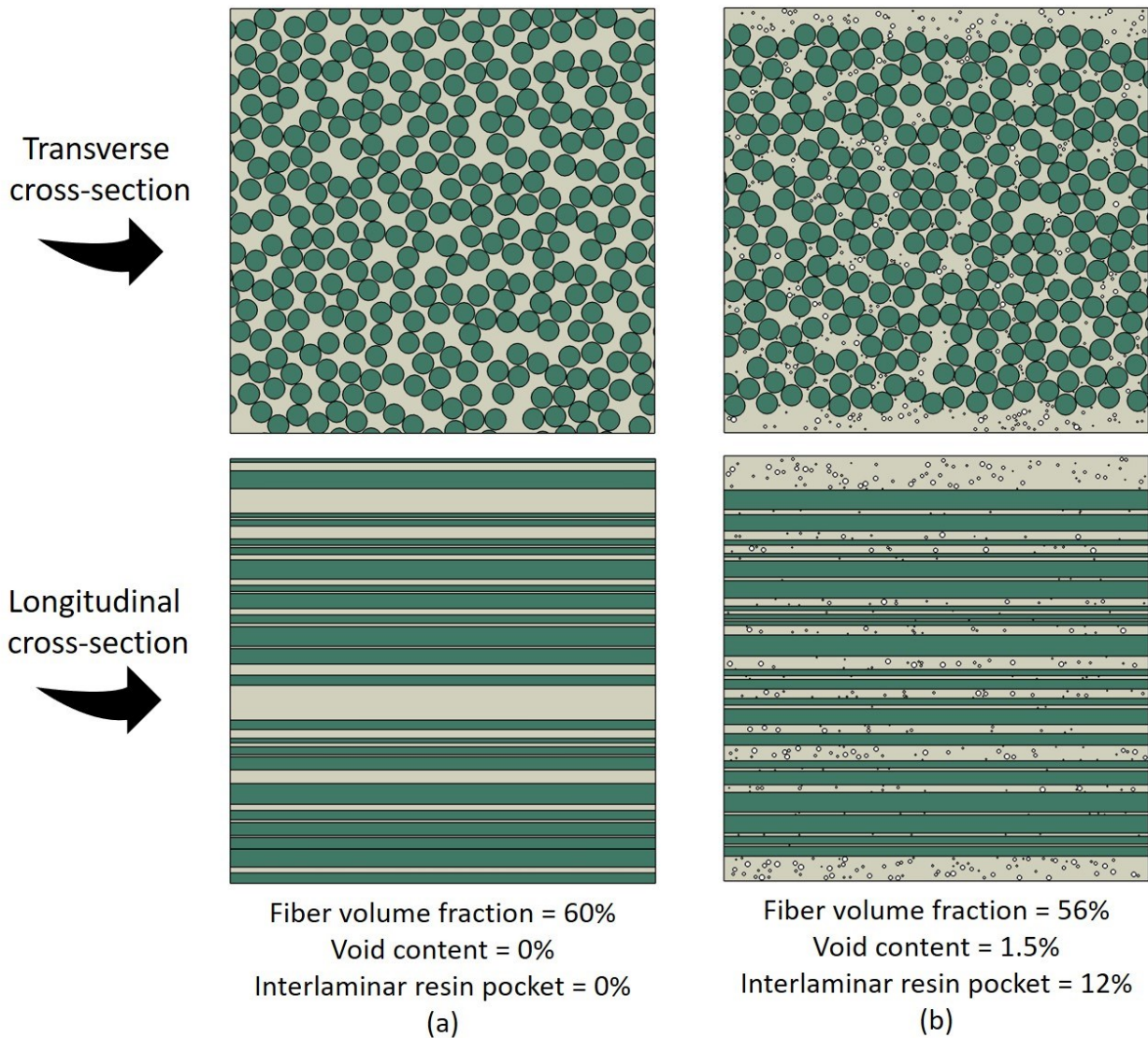
Figure 4.11. Example of RVEs created in numerical simulation to represent the (a) autoclave re-consolidation and (b) AFP in-situ consolidation manufacturing processes.

In order to draw a comparison between autoclave re-consolidation and AFP in-situ consolidation manufacturing processes, the predicted effective stiffness properties are listed in Table 4.4. It should be noted that the provided comparison is based on the average values measured for fiber volume fraction, void content, interlaminar resin pocket and degree of crystallinity by micrographic study and DSC test. According to the results, AFP in-situ consolidation caused the longitudinal elastic modulus, transverse elastic modulus and out-of-plane shear modulus to decrease by 6.83%, 10.43% and 20.22%, respectively, compared to autoclave re-consolidation while the out-of-plane Poisson's ratio remained unchanged.

Table 4.4. Comparison of the stiffness properties predicted by numerical analysis between in-situ consolidation and autoclave re-consolidation manufacturing processes.

	E_1 (GPa)	E_2 (GPa)	ν_{23}	G_{23} (GPa)
Autoclave re-consolidation	139.44	10.45	0.467	3.56
AFP In-situ consolidation	129.92	9.36	0.468	2.84
Difference[*] (%)	6.83	10.43	0.21	20.22

[*]With reference to the values that correspond to the autoclave process

It should be noted that although the effects of four factors were attempted to be considered during the simulation of RVEs representing the in-situ consolidation process, their relative significance is not the same in the prediction of E_1 and E_2 using the longitudinal and transverse cross-sections. Since void content, interlaminar resin pockets, and degree of crystallinity are associated with the matrix phase in composite materials, they significantly influence the prediction of the transverse elastic modulus (E_2). However, the primary factor impacting the behavior of composite material in the fiber direction (E_1) is the fiber volume fraction. To demonstrate this, the fiber volume fraction was reduced to 56% while the remaining three factors were maintained unchanged (i.e., the values resulting from autoclave treatment conditions).

Table 4.5. Influence of fiber volume fraction on the elastic moduli in fiber and transverse directions.

	60% fiber volume fraction	56% fiber volume fraction	Difference (%)
E_1 (GPa)	139.44	131.36	5.79
E_2 (GPa)	10.45	9.72	6.98

According to the results shown in Table 4.5, the decrease of (only) fiber volume fraction to 56% caused the elastic modulus in the fiber direction to be reduced by 5.79%, which is the majority part of the reduction presented in Table 4.4. In other words, the presence of voids and interlaminar resin pockets and the change in the degree of crystallinity have minimal effects on the elastic modulus in the fiber direction. Nonetheless, these matrix phase-related factors exert a significant influence on the transverse elastic modulus and take up a good portion of the decline listed in Table 4.4.

The fiber volume fraction, void content, interlaminar resin pocket, and degree of crystallinity of in-situ-consolidated thermoplastic composites are strongly influenced by the AFP processing parameters and the heating system. To ensure the applicability of the results to research works using different AFP conditions, and to find out the effect of each factor alone on the outcome, a

wider and reasonable range was considered for each key factor while the other three were kept constant (average values specific to in-situ consolidation process). This allows for the examination of variations in stiffness properties and facilitates the utilization of the findings in diverse research scenarios.
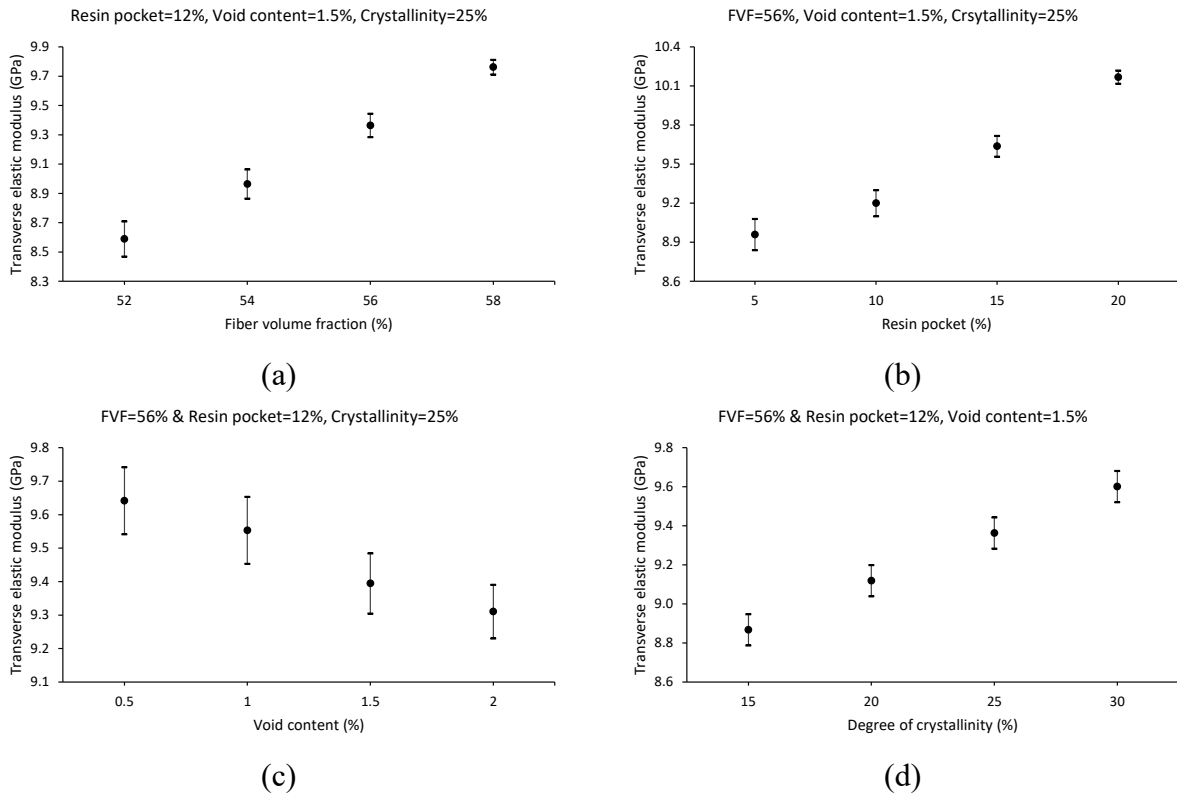
Figure 4.12. Variations of effective transverse elastic modulus (E_2) of in-situ-consolidated Carbon/PEEK thermoplastic composite due to the effects of change in (a) fiber volume fraction, (b) interlaminar resin pocket, (c) void content and (d) degree of crystallinity.

Figure 4.12 illustrates the influence of individual factors on the effective transverse elastic modulus of Carbon/PEEK thermoplastic composite manufacture by in-situ consolidation. A linear correlation is observed between the predicted transverse elastic modulus and fiber volume fraction within the range of 52 to 58 percent, as shown in Figure 4.12 (a). Moreover, as the fiber volume fraction increases, the scatter of results decreases due to limited space for the variation in the fiber arrangement within generated RVEs. The effect of the interlaminar resin pocket on the effective transverse elastic modulus is indicated in Figure 4.12 (b). Surprisingly, the presence of interlaminar resin pockets has a positive effect on the modulus. It can be explained by the fact that the creation of resin pockets forces the fibers to remain in closer proximity. The reduced distance between fibers induces stress concentration [42], leading to higher average stress throughout the

RVE and subsequently an increase in the transverse elastic modulus. Figure 4.13 shows the effect of interlaminar resin pockets on the creation of stress concentration between the fibers located close to each other inside an RVE under transverse tensile loading. By considering the same scale for von Mises stress values, as depicted in the legends of Figure 4.13 (a) and (b), It is evident that the RVE containing interlaminar resin pockets possesses more stress concentration regions. It is worth mentioning that although the presence of interlaminar resin pockets positively influences the modulus, it probably has a considerable adverse effect on the strength properties due to the premature crack initiation and propagation caused by stress concentrations [42,59–62,141]. The influence of void content on the transverse elastic modulus can be seen in Figure 4.12 (c). Among the four factors, void content has the least influence on the modulus of the composite. Even though increasing the void content from 0.5% to 2.0% only results in only a marginal reduction of 3.5% in E_2, it affects the strength properties profoundly owing to the creation of stress concentration [45,142]. Figure 4.12 (d) demonstrates the effect of degree of crystallinity on the transverse elastic modulus. As previously mentioned, a decrease in the degree of crystallinity leads to a decline in the elastic modulus of neat PEEK resin and subsequently affects the effective transverse elastic modulus of Carbon/PEEK thermoplastic composite.

(a)   (b)
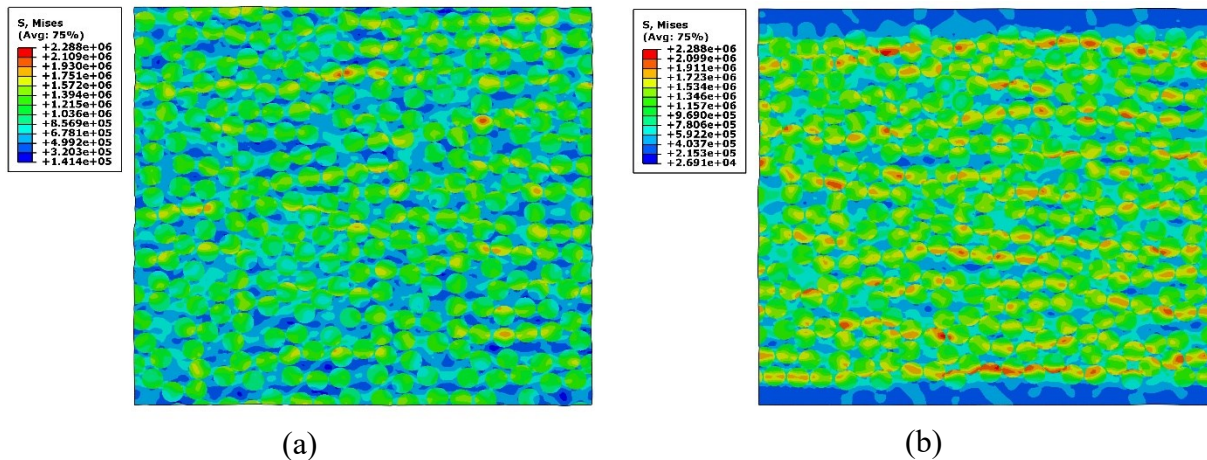
Figure 4.13. Distribution of regions with stress concentration caused by the proximity of fibers to each other in a Representative Volume Element (RVE) with 60% fiber volume fraction under transverse tensile loading conditions: (a) without and (b) with 12% interlaminar resin pocket.

To summarize, after examining the effects of the four factors, it can be concluded that although the presence of interlaminar resin pockets has an unexpected influence on the E_2, the negative effects of the other three factors outweigh this benefit. Consequently, the transverse elastic

modulus of in-situ-consolidated Carbon/PEEK thermoplastic composites is lower compared to its counterpart that was re-consolidated inside the autoclave, as presented in Table 4.4.

(a)

(b)

(c)

(d)
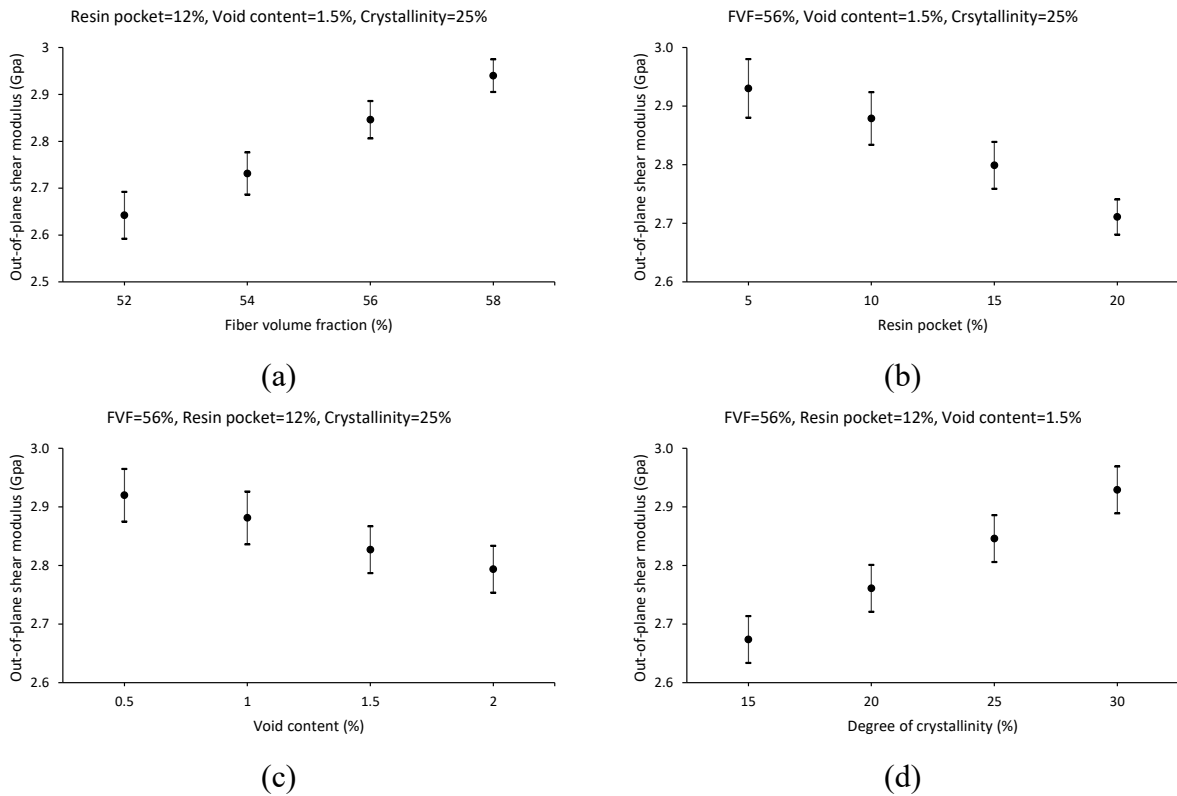
Figure 4.14. Variations of effective out-of-plane shear modulus (G_{23}) of in-situ-consolidated Carbon/PEEK thermoplastic composite by considering the effect of change in (a) fiber volume fraction, (b) interlaminar resin pocket, (c) void content and (d) degree of crystallinity.

Figure 4.14 presents the variations in the out-of-plane shear modulus caused by changes in each factor. The trends observed in all the diagrams are similar to those of the transverse elastic modulus. However, the effect of the interlaminar resin pocket on the shear modulus differs from that on E_2. Unlike the transverse elastic modulus, the presence of interlaminar resin pockets adversely affects the G_{23}. This can be attributed to the absence of fibers on the surface where a horizontal displacement is applied to the top of the RVE representing in-situ consolidation to create shear loading conditions (see Figure 4.8 (b)). Consequently, the matrix assumes the role of transferring the stress to the fibers. Since the matrix has a lower elastic modulus compared to the fibers, lower stresses are transferred to the fibers for the same amount of applied displacement. This phenomenon results in a lower calculated average stress throughout the RVE compared to the RVE representing autoclave treatment (without interlaminar resin pocket). As a result, the presence of interlaminar resin pockets has a negative effect on the out-of-plane shear modulus, as

shown in Figure 4.14 (b), in contrast to the transverse elastic modulus. This is the reason why the reduction observed in G_{23} of in-situ-consolidated Carbon/PEEK thermoplastic composite was greater than that in E_2, as presented in Table 4.4.
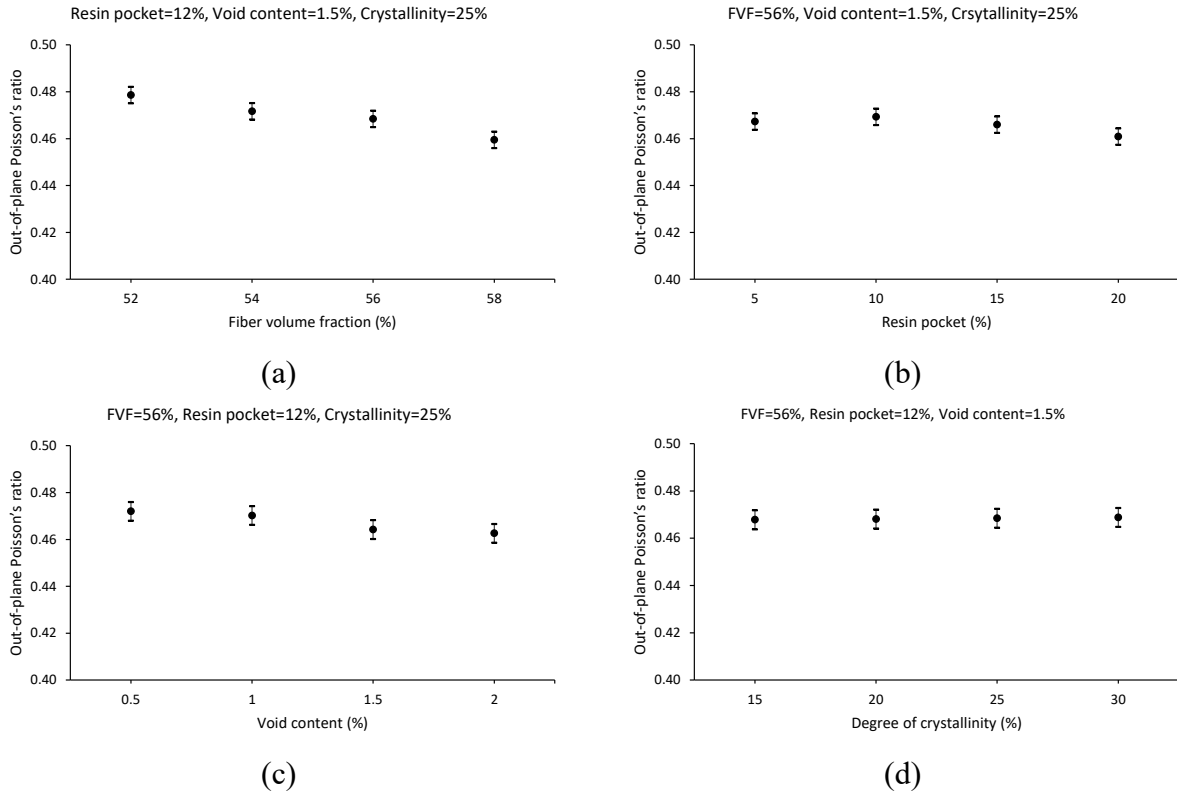
Figure 4.15. Variations of effective out-of-plane Poisson's ratio (v_{23}) of in-situ-consolidated Carbon/PEEK thermoplastic composite by considering the effect of change in (a) fiber volume fraction, (b) interlaminar resin pocket, (c) void content and (d) degree of crystallinity.

Variations of effective out-of-plane Poisson's ratio resulting from changes in the aforementioned factors can be seen in Figure 4.15. The diagrams indicate that none of the parameters within the considered range significantly influence the v_{23} of Carbon/PEEK thermoplastic composite. Thus, it can be assumed that in-situ consolidation and autoclave treatment result in the same value for the out-of-plane Poisson's ratio of 0.45.

It is important to note that the manufacturing quality of AFP-fabricated thermoplastic composites, specifically factors such as fiber volume fraction, void content, interlaminar resin pockets, and degree of crystallinity, is strongly influenced by the chosen AFP processing parameters. Consequently, the numerical results obtained for in-situ-consolidated Carbon/PEEK thermoplastic composites, which are based on the mean values of these microstructural characteristics, are valid

only for the processing conditions outlined in Section 4.2.1 ("AFP Manufacturing process"). However, the proposed micromechanical simulation methodology can be extended to other thermoplastic composites manufactured under different AFP conditions.

4.6.   Conclusion

The use of automated fiber placement (AFP) in-situ consolidation offers time and cost savings compared to the autoclave treatment in the manufacturing of thermoplastic composites. The manufacturing process plays a crucial role as it directly influences the mechanical performance of the produced parts. Challenges arise owing to the shorter duration of heat and pressure exposure as well as the higher cooling rate during the in-situ consolidation, unlike the autoclave curing. This limited exposure negatively affects various factors, such as void content, fiber distribution and crystallization, which are responsible for the final quality of the composite laminate. Numerous researchers have dedicated significant efforts to optimize AFP processing parameters, including compaction force, deposition rate and temperature, aiming to achieve thermoplastic composites with comparable quality to conventional manufacturing processes (e.g., autoclave and compression press). Nevertheless, there still exists a notable difference in the mechanical responses between these methods.

While experimental approaches are indispensable for evaluating the material properties, their utilization in preliminary design stages can prove to be cost-prohibitive. Furthermore, unlike the favorable aspects offered by the AFP in-situ consolidation manufacturing process, researchers encounter difficulties (i.e., residual deformation) in fabricating flat thermoplastic composite laminates for experimental characterization through either tensile or shear tests. As a result, a detailed simulation using micromechanical analysis can provide an alternative method, allowing for performing virtual experiments to predict effective material properties.

In the present research, two thermoplastic plates of Carbon/PEEK were manufactured using AFP in-situ consolidation. Subsequently, one of the plates was re-consolidated in an autoclave to serve as the reference sample. Through micrographic study, significant distinctions were observed between the AFP-fabricated and autoclave-reconsolidated samples in terms of fiber volume fraction, void content and interlaminar resin pocket. Furthermore, DSC test was performed on the both types of samples to measure the degree of crystallinity. Autoclave-reconsolidated

153

Carbon/PEEK samples exhibited a degree of crystallinity of 35%, a fiber volume fraction of 60% with evenly distributed fibers, and negligible void content. On the other hand, AFP in-situ consolidation resulted in a decrease in the degree of crystallinity and fiber volume fraction to 25% and 56%, respectively, and formation of 12% interlaminar resin pocket and void content of 1.5%.

Since the aforementioned differences are mostly related to matrix phase, and the performance of composites in the transverse direction is also dominated by matrix behavior, an investigation was mainly conducted on a transverse cross-section of the composite laminate where the behavior of the material is primarily influenced by the characteristics of the matrix. The arrangement of fibers and the presence of voids in this region have a significant influence on the stress distribution and concentration within the matrix phase. To evaluate the effect of changes in fiber volume fraction, void content, interlaminar resin pocket, and degree of crystallinity caused by in-situ consolidation, two-dimensional representative volume elements (RVEs) with randomly distributed fibers were modeled on a micro-scale in accordance with the longitudinal and transverse cross-sections. This modeling was based on a micrographic study performed on Carbon/PEEK thermoplastic samples. The stiffness properties of the RVEs were analyzed using the Asymptotic Homogenization Theory (AHT) and applying Periodic Boundary Conditions (PBCs) to the models by a Python script implemented in the ABAQUS software. The findings of the numerical analysis revealed that AFP in-situ consolidation of Carbon/PEEK thermoplastic composite can decrease the longitudinal elastic, transverse elastic and out-of-plane shear moduli by 6.83%, 10.43% and 20.22%, respectively. Such a deviation from the material properties of an autoclave-reconsolidated thermoplastic composite laminate is noticeable and must be paid attention to for further numerical analysis of thermoplastic composites manufactured by AFP in-situ consolidation, particularly in the transverse direction.

Appendix

❖ **Effect of void distribution on the prediction of stiffness properties**

In the present thesis, stiffness properties were predicted based on the average total void content obtained from the micrographic study, under the assumption that voids were uniformly distributed throughout the RVEs, as shown in Figure 4.16 (a). However, during the prediction of the transverse tensile strength resulting from the AFP in-situ consolidation process, it became evident that stress

154

concentration areas play a critical role and can affect the simulation outcome considerably. As discussed in Chapter 3, the formation of interlaminar resin pockets on the top and bottom of the RVEs forces the fibers to stay closer to each other in the central region, thereby creating stress concentration inside the composite layer. In these circumstances, the position of voids becomes crucial, as it can significantly influence the crack initiation and propagation, and subsequently reduce the strength value of the RVE. To this end, a detailed micrographic study was conducted again with a focus on void distribution, by extracting samples from various locations of the AFP-made Carbon/PEEK thermoplastic composite laminate.

The micrographic examination revealed that the majority of voids are located inside the composite layer, rather than at the interface where resin-rich regions are typically found. As a result, the RVEs representing the in-situ consolidation process were modified, reflecting the more accurate void placement characteristic of the AFP method, in order to predict the transverse tensile strength value, as shown in Figure 4.16 (b).

(a)   (b)
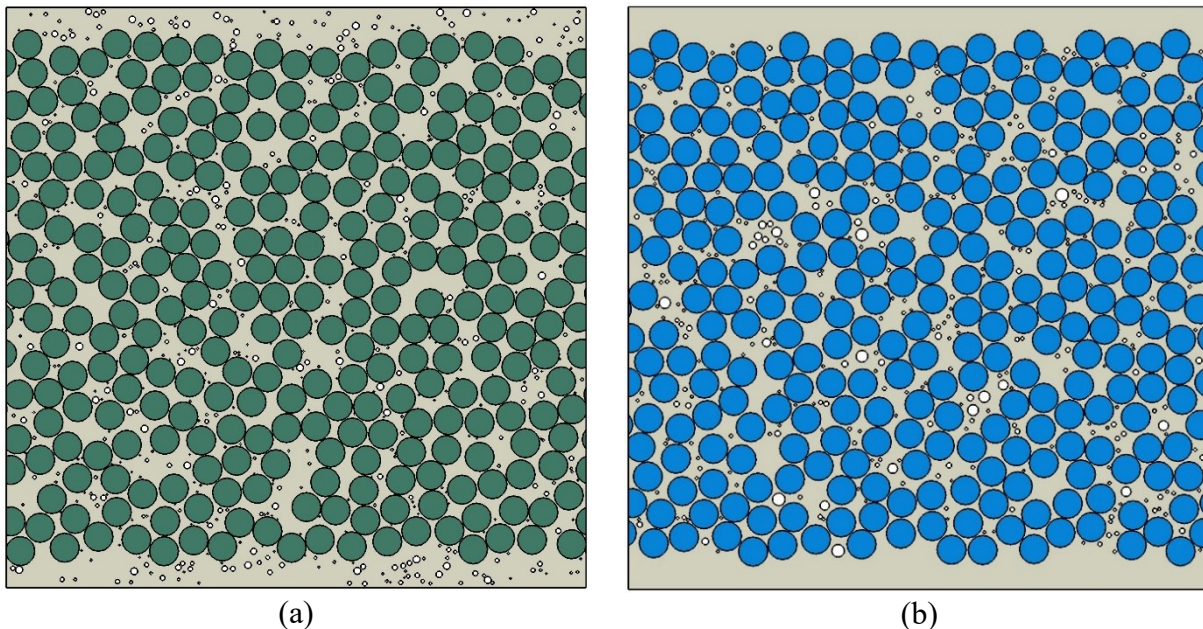
Figure 4.16. Example of RVEs generated to represent the AFP in-situ consolidation process with fiber volume fraction of 56%, void content of 1.5% and interlaminar resin pocket of 12%: (a) uniformly distributed voids and (b) intralaminar voids.

Although AFP-influenced stiffness properties were initially predicted using the RVEs with uniformly and randomly distributed voids, as illustrated in Figure 4.16 (a), the findings presented in Chapter 4 remain valid. This can be explained by the fact that because a relatively small amount

of displacement was applied to the RVEs, without reaching the threshold for crack onset and evolution inside them, the created stress concentration was negligible, leading the void distribution not to be a determining factor for predicting the stiffness properties. To support this hypothesis, additional micromechanical simulation was performed, using the modified RVEs shown in Figure 4.16 (b), to re-evaluate the transverse elastic modulus, out-of-plane Poisson's ratio and out-of-plane shear modulus values. According to the results presented in Table 4.6, the variation in void distribution does not have a considerable effect on the prediction of stiffness properties, confirming the reliability of the conclusions drawn in Chapter 4.

Table 4.6. Investigating the effect of void distribution on the predicted stiffness properties of RVEs representing the AFP in-situ consolidation process (fiber volume fraction=56%, void content=1.5%, interlaminar resin pocket=12% and degree of crystallinity=25%).

	E_2 (GPa)	v_{23}	G_{23} (GPa)
RVEs with uniformly distributed voids	9.36	0.468	2.84
RVEs with intralaminar voids	9.27	0.464	2.88
Difference (%)	0.96	0.85	1.41

❖ **Short-Beam Shear (SBS) test simulation**

SBS finite element analysis was conducted as the first research work of the present thesis, during which the differences between the material properties that could arise from AFP in-situ consolidation and autoclave treatment had not been quantified yet. Thus, the same material properties were used to model the AFP-manufactured and autoclaved Carbon/PEEK thermoplastic composite specimens in ABAQUS software. Since delamination was observed as the primary failure mechanism during the short-beam shear test, the cohesive element approach was used to effectively simulate and differentiate between the mechanical performance of thermoplastic composite specimens fabricated by each manufacturing method. Eventually, the interface strength properties, specific to AFP in-situ-consolidated Carbon/PEEK thermoplastic composite laminates, were determined through numerical calibration based on the SBS test results.

A potential concern may arise about whether the interface strength properties would have differed if the AFP-resulted composite material properties had been initially applied in the SBS simulation to model the in-situ-consolidated composite specimen. It is worth mentioning that modifying the composite material properties will not significantly change the outcome of this finite element

analysis. As mentioned earlier, delamination (interlaminar damage) is the dominant mode of failure during the SBS test and is predominantly governed by the characteristics of the cohesive elements, particularly the strength values. That's why intralaminar damage, captured by Hashin failure criteria, was limited to the vicinity of the loading nose and supports, as shown in Figure 2.15. To prove this hypothesis, the predicted material properties were assigned to the thermoplastic composite specimen representing the AFP manufacturing process in the SBS simulation. Using the same interface strength properties previously determined for the AFP method (i.e., N=36 MPa and S=45 MPa), the new Interlaminar Shear Strength (ILSS) value was obtained and compared with its counterpart from Chapter 2. According to the results listed in Table 4.7, modifying the composite material properties does not have a considerable effect on the ILSS values obtained by SBS simulation, confirming the robustness and validity of the simulation outcomes reported in Chapter 2.

Table 4.7. ILLS value obtained through SBS finite element simulation using effective material properties of AFP-manufactured Carbon/PEEK thermoplastic composite laminate, with normal and shear interface strengths of 36 MPa and 45 MPa, respectively.

	E_1 (GPa)	E_2(GPa)	G_{23}(GPa)	Y_T(MPa)	ILSS (MPa)
Cytec datasheet [67] material properties	138	10.3	3.7	86	56.51
AFP-influenced material properties	129.92	9.36	2.84	58.6	55.22
Difference (%)					2.28

❖ **MATLAB code for longitudinal cross-section**

```
clc
clear

disp ('Please input the maximum diameter of fiber:')
Fd = input('D (micrometer) = '); %D=7 micrometer Fiber Diameter

disp ('Please input the lenght of RVE:')
RVElength = input('L (micrometer) = '); %L=140 micrometer

Arve = RVElength*RVElength;

disp ('Please input fiber volume fraction:')
VF = input('Vf (%) = '); %Vf=0.6 or 0.56
VF = VF/100;

disp ('Please input the percentage of interlaminar resin pocket area:')
percentage = input('percentage(%) = ');
percentage = percentage/2;
```

```
for i=1 : 1 : 100
    ly(i)=1000;           % for random Y coordinate
    ld(i)=1000;           % for random diameter
end

mindist=0.06;
m=0;
mm=0;
nn=0;
Af=0;

while 1

    ay = (-Fd/2)+(Fd/8);
    by = RVElength+(Fd/2)-(Fd/8);

    aay=(percentage/100)*RVElength+(Fd/16);
    bby=(1-(percentage/100))*RVElength-(Fd/16);

    if percentage==0
        ry = (by-ay)*rand+(ay);          %Random Y without resin pocket
    else
        ry = (bby-aay)*rand+(aay);       %Random Y with resin pocket
    end

    ad = Fd/8;
    bd = Fd;
    rd = (bd-ad)*rand+(ad);          %Random diameter

    %Intersection check (compatibility & periodicity)
    n = compatibility(rd,ry,ld,ly,m,mm,mindist);
    [nn,rd_new,ry_new,p] = periodicity (rd,ry,ld,ly,m,mm,mindist,RVElength);

    %Adding the new location to the directory
    if (n==0) && (nn==0)
        for k=1 : 1 : (m+mm+1)
            if ly(k) == 1000
                ly(k) = ry;
                ld(k) = rd;
                Af = Af + rd;

                if p==1
                    ly(k+1) = ry_new;
                    ld(k+1) = rd_new;
                    mm=mm+1;
                end

                m=m+1;
                break
            end
        end
    end

    if Af > ((VF-0.007)*RVElength)
        disp('Done!');
```

```matlab
            break
        end
    end

%Creation of the text file
fileID = fopen('Locations.txt','w');
fprintf(fileID, 'Y          D\n');
for i=1 : 1 : (m+mm)
    fprintf(fileID,'%5.4f %5.4f\n',ly(i),ld(i));
end
fclose(fileID);

%%%%%%%%%%%%%%%%% VOID CONTENT %%%%%%%%%%%%%%%%%%%%

disp ('Please input void content:')
void = input('void content(%) = '); %void content=1%, 2% or 3%

for i=1 : 1 : 10000
    vlx(i)=0;
    vly(i)=0;
    vld(i)=0;
end

MinVd=Fd/20;        % minimum void diameter is one-twentieth of fiber diameter
MaxVd=Fd/4;         % maximum void diameter is one-fourth of fiber diameter
a=MaxVd/2+mindist;
b=RVElength-MaxVd/2-mindist;
Nv=1;
vn=0;
varea=0;

while 1

    if void==0
        break
    end

    %Finding a new location inside the RVE
    vx=(b-a)*rand+(a);
    vy=(b-a)*rand+(a);

    %Intersection check (fiber with void)

    for i=1 : 1 : (m+mm)
        fvd(i)=NaN;
        distance(i)=NaN;
    end

    for i=1 : 1 : (m+mm)
        fvd(i) = sqrt((vy-ly(i))^2);
        distance(i) = fvd(i)-ld(i)/2;
        if fvd(i) <= (ld(i)/2+MinVd/2+mindist)
            n=1;
            break
        else
            n=0;
```

159

```matlab
        end
    end

    %Intersection check (void with void)

    if n==0
        [D,index]=min(distance);
        if (D) >= (MaxVd/2+mindist)
            Vd=(MaxVd-MinVd)*rand+(MinVd);
        else
            Vd=((D)-MinVd)*rand+(MinVd);
        end

        for i=1 : 1 : (Nv-1)
            d = sqrt((vx-vlx(i))^2 + (vy-vly(i))^2);
            if d <= (vld(i)/2+Vd/2+mindist)
                vn=1;
                break
            else
                vn=0;
            end
        end

    end

    if (n==0) && (vn==0)
        vlx(Nv) = vx;
        vly(Nv) = vy;
        vld(Nv) = Vd;

        varea = varea + (pi*Vd^2)/4;

        if varea >= (void/100)*Arve
            break
        else
            Nv=Nv+1;
        end

    end

end

%Creation of the text file
fileID = fopen('Voids.txt','w');
fprintf(fileID, 'X      Y      D\n');

if void==0
    fprintf(fileID, 'NO\n');
else
    fprintf(fileID, 'YES\n');
    for i=1 : 1 : Nv
        fprintf(fileID,'%5.4f %5.4f %5.4f\n',vlx(i),vly(i),vld(i));
    end
end

fclose(fileID);
```

160

```matlab
disp('Finished!')

%%%%%%%%%%%%%%%%%%%%%%%%%%%%%%%%%%%%%%%%%%%%%%%%%%%%%%%%%%%%%%%%%%%%%%%%%%
%%%%%%%%%%%%%%%%%%%%%%%%%%%%%%%%%%%%%%%%%%%%%%%%%%%%%%%%%%%%%%%%%%%%%%%%%%
%%%%%%%%%%%%%%%%%%%%%%%%%%%%%%%%%%%%%%%%%%%%%%%%%%%%%%%%%%%%%%%%%%%%%%%%%%

function n = compatibility(rd,ry,ld,ly,m,mm,mindist)
    for i=1 : 1 : (m+mm+1)
        d = sqrt((ry-ly(i))^2);
        if d <= (rd/2+ld(i)/2+mindist)
            n=1;
            break
        else
            n=0;
        end
    end
end

%%%%%%%%%%%%%%%%%%%%%%%%%%%%%%%%%%%%%%%%%%%%%%%%%%%%%%%%%%%%%%%%%%%%%%%%%%

function [nn,rd_new,ry_new,p] = periodicity(rd,ry,ld,ly,m,mm,mindist,RVElength)
    p=0;
    rd_new=rd;
    ry_new=ry;

    if ry > (RVElength-rd/2+mindist)
        ry_new = ry-RVElength;
        p=p+1;
    end
    if ry < (rd/2-mindist)
        ry_new = ry+RVElength;
        p=p+1;
    end

    if p==0 % Not edge & Not cornet
        nn=0;
    end

    if p==1 % Edge
        for i=1 : 1 : (m+mm+1)
            d = sqrt((ry_new-ly(i))^2);
            if d <= (rd/2+ld(i)/2+mindist)
                nn=1;
                break
            else
                nn=0;
            end
        end
    end

end
```

❖ Python script for stiffness prediction

```python
# -*- coding: mbcs -*-
from part import *
from material import *
from section import *
from assembly import *
from step import *
from interaction import *
from load import *
from mesh import *
from optimization import *
from job import *
from sketch import *
from visualization import *
from connectorBehavior import *
from abaqus import *
from abaqusConstants import *

import __main__
import section
import regionToolset
import displayGroupMdbToolset as dgm
import part
import material
import assembly
import step
import interaction
import load
import mesh
import optimization
import job
import sketch
import visualization
import xyPlot
import displayGroupOdbToolset as dgo
import connectorBehavior

from caeModules import *
from odbAccess import *
from numpy import *
import math

averagestrains=zeros([3,3])
averagestresses=zeros([3,3])
stif=zeros([3,3])
RVEstrain=0.0001    # 0.01%
RVEpredisp=[0.0000,0.0000,0.0000]

RVElength=140.0 # micrometer
Fd=7.0          # micrometer
meshsize=(Fd/2)/4

###########Part###########
```

```python
mdb.models['Model-1'].ConstrainedSketch(name='__profile__', sheetSize=400.0)
mdb.models['Model-1'].sketches['__profile__'].rectangle(point1=(-Fd, -Fd),
    point2=(RVElength+Fd, RVElength+Fd))
mdb.models['Model-1'].Part(dimensionality=TWO_D_PLANAR, name='Part-1', type=
    DEFORMABLE_BODY)
mdb.models['Model-1'].parts['Part-1'].BaseShell(sketch=
    mdb.models['Model-1'].sketches['__profile__'])
del mdb.models['Model-1'].sketches['__profile__']

mdb.models['Model-1'].ConstrainedSketch(gridSpacing=10.0, name='__profile__',
    sheetSize=400.0, transform=
    mdb.models['Model-1'].parts['Part-1'].MakeSketchTransform(
    sketchPlane=mdb.models['Model-1'].parts['Part-1'].faces[0],
    sketchPlaneSide=SIDE1, sketchOrientation=RIGHT, origin=(0.0, 0.0, 0.0)))
mdb.models['Model-1'].parts['Part-1'].projectReferencesOntoSketch(filter=
    COPLANAR_EDGES, sketch=mdb.models['Model-1'].sketches['__profile__'])

f=open('Locations.txt','r')
line=f.readlines()
for i in range(1,len(line)):
    a=line[i].split()
    lx=float(a[0])
    ly=float(a[1])
    mdb.models['Model-1'].sketches['__profile__'].CircleByCenterPerimeter(center=(
        lx, ly), point1=(lx+Fd/2, ly))
f.close()

mdb.models['Model-1'].parts['Part-1'].PartitionFaceBySketch(faces=
    mdb.models['Model-1'].parts['Part-1'].faces[0]
    , sketch=mdb.models['Model-1'].sketches['__profile__'])
del mdb.models['Model-1'].sketches['__profile__']

f=open('Voids.txt','r')
line=f.readlines()
b=line[1].split()
if b[0]=='YES':
    mdb.models['Model-1'].ConstrainedSketch(gridSpacing=10.0, name='__profile__',
        sheetSize=400.0)
    for i in range(2,len(line)):
        a=line[i].split()
        lx=float(a[0])
        ly=float(a[1])
        ld=float(a[2])
        mdb.models['Model-1'].sketches['__profile__'].CircleByCenterPerimeter(center=(
            lx, ly), point1=(lx+ld/2, ly))
    mdb.models['Model-1'].parts['Part-1'].Cut(sketch=
        mdb.models['Model-1'].sketches['__profile__'])
    del mdb.models['Model-1'].sketches['__profile__']
f.close()

                #Cutting left and right
mdb.models['Model-1'].ConstrainedSketch(gridSpacing=10.0, name='__profile__',
    sheetSize=400.0)
mdb.models['Model-1'].sketches['__profile__'].rectangle(point1=(RVElength, -Fd),
    point2=(RVElength+Fd, RVElength+Fd))
mdb.models['Model-1'].sketches['__profile__'].rectangle(point1=(0.0, -Fd),
```

```
    point2=(-Fd, RVElength+Fd))
mdb.models['Model-1'].parts['Part-1'].Cut(sketch=
    mdb.models['Model-1'].sketches['__profile__'])
del mdb.models['Model-1'].sketches['__profile__']


              #Cutting top and bottom
mdb.models['Model-1'].ConstrainedSketch(gridSpacing=10.0, name='__profile__',
    sheetSize=400.0)
mdb.models['Model-1'].sketches['__profile__'].rectangle(point1=(-Fd, -Fd),
    point2=(RVElength+Fd, 0.0))
mdb.models['Model-1'].sketches['__profile__'].rectangle(point1=(-Fd, RVElength),
    point2=(RVElength+Fd, RVElength+Fd))
mdb.models['Model-1'].parts['Part-1'].Cut(sketch=
    mdb.models['Model-1'].sketches['__profile__'])
del mdb.models['Model-1'].sketches['__profile__']

###########Property###########

mdb.models['Model-1'].Material(name='fiber')
mdb.models['Model-1'].materials['fiber'].Elastic(table=((22000000000.0, 0.25),
    ))
mdb.models['Model-1'].Material(name='matrix')
mdb.models['Model-1'].materials['matrix'].Elastic(table=((3312000000.0, 0.38),
    ))

mdb.models['Model-1'].HomogeneousSolidSection(material='fiber', name=
    'Section-fiber', thickness=1.0)
mdb.models['Model-1'].HomogeneousSolidSection(material='matrix', name=
    'Section-matrix', thickness=1.0)

face=mdb.models['Model-1'].parts['Part-1'].faces.getByBoundingBox(
    0.0,0.0,0.0,RVElength,RVElength,0.0)
for i in range(len(face)):
    area=face[i].getSize()
    area=area/RVElength**2
    if area>0.3:
        target1=face[i]
        print('Matrix volume fraction is:')
        print(area)
        break
p=target1.pointOn
mdb.models['Model-1'].parts['Part-1'].Set(faces=
    mdb.models['Model-1'].parts['Part-1'].faces.findAt(
    ((p[0][0],p[0][1],p[0][2]),),), name='Set-matrix')
mdb.models['Model-1'].parts['Part-1'].SectionAssignment(offset=0.0,
    offsetField=", offsetType=MIDDLE_SURFACE, region=
    mdb.models['Model-1'].parts['Part-1'].sets['Set-matrix'], sectionName=
    'Section-matrix', thicknessAssignment=FROM_SECTION)

f=open('Locations.txt','r')
line=f.readlines()
for i in range(1,len(line)):
    a=line[i].split()
    lx=float(a[0])
    ly=float(a[1])
    mdb.models['Model-1'].parts['Part-1'].Set(faces=
```

```
        mdb.models['Model-1'].parts['Part-1'].faces.getByBoundingBox
        (lx-Fd/2,ly-Fd/2,0.0,lx+Fd/2,ly+Fd/2,1.0), name='Set-fiber-%d'%i)
    mdb.models['Model-1'].parts['Part-1'].SectionAssignment(offset=0.0,
        offsetField='', offsetType=MIDDLE_SURFACE, region=
        mdb.models['Model-1'].parts['Part-1'].sets['Set-fiber-%d'%i], sectionName=
        'Section-fiber', thicknessAssignment=FROM_SECTION)
f.close()


###########Assembly###########

mdb.models['Model-1'].rootAssembly.DatumCsysByDefault(CARTESIAN)
mdb.models['Model-1'].rootAssembly.Instance(dependent=OFF, name='Part-1-1',
    part=mdb.models['Model-1'].parts['Part-1'])


###########Step###########

mdb.models['Model-1'].StaticStep(name='Step-1', previous='Initial')
mdb.models['Model-1'].fieldOutputRequests['F-Output-1'].setValues(variables=(
    'S', 'E', 'U', 'EVOL'))


###########Reference point###########

mdb.models['Model-1'].rootAssembly.ReferencePoint(point=(RVElength*1.1, RVElength/2, 0.0))
mdb.models['Model-1'].rootAssembly.ReferencePoint(point=(RVElength/2,   RVElength+10,   0.0))          #edges
Ref.point#

mdb.models['Model-1'].rootAssembly.ReferencePoint(point=(RVElength*1.5,   RVElength/2,   0.0))        #verticies
Ref.point#
mdb.models['Model-1'].rootAssembly.ReferencePoint(point=(RVElength*1.6, RVElength/2, 0.0))

mdb.models['Model-1'].rootAssembly.Set(name='dummyedge-RL', referencePoints=(
    mdb.models['Model-1'].rootAssembly.referencePoints.findAt((RVElength*1.1, RVElength/2, 0.0),), ))
mdb.models['Model-1'].rootAssembly.Set(name='dummyedge-TB', referencePoints=(
    mdb.models['Model-1'].rootAssembly.referencePoints.findAt((RVElength/2, RVElength+10, 0.0),), ))

mdb.models['Model-1'].rootAssembly.Set(name='dummyvertex-AC', referencePoints=(
    mdb.models['Model-1'].rootAssembly.referencePoints.findAt((RVElength*1.5, RVElength/2, 0.0),), ))
mdb.models['Model-1'].rootAssembly.Set(name='dummyvertex-BD', referencePoints=(
    mdb.models['Model-1'].rootAssembly.referencePoints.findAt((RVElength*1.6, RVElength/2, 0.0),), ))


###########Mesh###########

mdb.models['Model-1'].rootAssembly.setMeshControls(allowMapped=False,
    elemShape=TRI, regions=
    mdb.models['Model-1'].rootAssembly.instances['Part-1-1'].faces.getByBoundingBox(
    0.0,0.0,0.0,RVElength,RVElength,0.0))
mdb.models['Model-1'].rootAssembly.setElementType(elemTypes=(ElemType(
    elemCode=CPE4R, elemLibrary=STANDARD), ElemType(elemCode=CPE3,
    elemLibrary=STANDARD, secondOrderAccuracy=OFF, distortionControl=DEFAULT)),
    regions=(
    mdb.models['Model-1'].rootAssembly.instances['Part-1-1'].faces.getByBoundingBox(
    0.0,0.0,0.0,RVElength,RVElength,0.0), ))
mdb.models['Model-1'].rootAssembly.seedPartInstance(deviationFactor=0.1,
    minSizeFactor=0.1, regions=(
    mdb.models['Model-1'].rootAssembly.instances['Part-1-1'], ), size=meshsize)
```

```
mdb.models['Model-1'].rootAssembly.generateMesh(regions=(
    mdb.models['Model-1'].rootAssembly.instances['Part-1-1'], ))


############Set###########

edgeR=mdb.models['Model-1'].rootAssembly.instances['Part-1-1'].nodes.getByBoundingBox(
    RVElength,0.01,0.0,RVElength,RVElength-0.01,0.0)
for i in range(1,len(edgeR)+1):
    mdb.models['Model-1'].rootAssembly.Set(name='edgeR-%d'%i, nodes=edgeR[i-1:i])
    coord=edgeR[i-1].coordinates
    edgeL=mdb.models['Model-1'].rootAssembly.instances['Part-1-1'].nodes.getByBoundingBox(
        0.0,coord[1],0.0,0.0,coord[1],0.0)
    mdb.models['Model-1'].rootAssembly.Set(name='edgeL-%d'%i, nodes=edgeL[0:1])

edgeT=mdb.models['Model-1'].rootAssembly.instances['Part-1-1'].nodes.getByBoundingBox(
    0.01,RVElength,0.0,RVElength-0.01,RVElength,0.0)
for i in range(1,len(edgeT)+1):
    mdb.models['Model-1'].rootAssembly.Set(name='edgeT-%d'%i, nodes=edgeT[i-1:i])
    coord=edgeT[i-1].coordinates
    edgeB=mdb.models['Model-1'].rootAssembly.instances['Part-1-1'].nodes.getByBoundingBox(
        coord[0],0.0,0.0,coord[0],0.0,0.0)
    mdb.models['Model-1'].rootAssembly.Set(name='edgeB-%d'%i, nodes=edgeB[0:1])

#/////////////////////////////////////////////////////////////////////////

vertex=mdb.models['Model-1'].rootAssembly.instances['Part-1-1'].nodes.getByBoundingBox(
    0.0,0.0,0.0,0.0,0.0,0.0)
mdb.models['Model-1'].rootAssembly.Set(name='vertexC-1', nodes=vertex[0:1])

vertex=mdb.models['Model-1'].rootAssembly.instances['Part-1-1'].nodes.getByBoundingBox(
    RVElength,0.0,0.0,RVElength,0.0,0.0)
mdb.models['Model-1'].rootAssembly.Set(name='vertexB-1', nodes=vertex[0:1])

vertex=mdb.models['Model-1'].rootAssembly.instances['Part-1-1'].nodes.getByBoundingBox(
    0.0,RVElength,0.0,0.0,RVElength,0.0)
mdb.models['Model-1'].rootAssembly.Set(name='vertexD-1', nodes=vertex[0:1])

vertex=mdb.models['Model-1'].rootAssembly.instances['Part-1-1'].nodes.getByBoundingBox(
    RVElength,RVElength,0.0,RVElength,RVElength,0.0)
mdb.models['Model-1'].rootAssembly.Set(name='vertexA-1', nodes=vertex[0:1])

###########Equations###########

edge=[edgeR,edgeT]
name=['edgeRL','edgeTB']
couple=[['R','L'],['T','B']]
dummy=['RL','TB']
for k in range(1,3):          #number of pairs
    for j in range(1,3):      #number of coordinates (X & Y)
        for i in range(1,len(edge[k-1])+1):
            mdb.models['Model-1'].Equation(name='%s-%d-%d'%(name[k-1],j,i), terms=((1.0, 'edge%s-%d'%(couple[k-
1][0],i), j), (
                -1.0, 'edge%s-%d'%(couple[k-1][1],i), j), (1.0, 'dummyedge-%s'%dummy[k-1], j)))

name=['vertexAC','vertexBD']
couple=[['A','C'],['B','D']]
```

```
dummy=['AC','BD']
for k in range(1,3):          #number of pairs
    for j in range(1,3):      #number of coordinates (X & Y)
        mdb.models['Model-1'].Equation(name='%s-%d'%(name[k-1],j), terms=((1.0, 'vertex%s-1'%couple[k-1][0], j), (
            -1.0, 'vertex%s-1'%couple[k-1][1], j), (1.0, 'dummyvertex-%s'%dummy[k-1], j)))


############Load###########

mdb.models['Model-1'].DisplacementBC(amplitude=UNSET, createStepName='Step-1',
    distributionType=UNIFORM, fieldName='', fixed=OFF, localCsys=None, name=
    'BC-rigid body', region=mdb.models['Model-1'].rootAssembly.sets['vertexC-1'],
    u1=0.0, u2=0.0, ur3=UNSET)

#RVEpredisp=[0.0001,0.0000,0.0000]

for n in range(3):
    RVEpredisp=[0.0000,0.0000,0.0000]
    RVEpredisp[n]=RVEstrain*RVElength

    mdb.models['Model-1'].DisplacementBC(amplitude=UNSET, createStepName='Step-1',
        distributionType=UNIFORM, fieldName='', fixed=OFF, localCsys=None, name=
        'BC-1', region=mdb.models['Model-1'].rootAssembly.sets['dummyedge-RL'],
        u1=-RVEpredisp[0], u2=-RVEpredisp[2], ur3=UNSET)              #edge force
    mdb.models['Model-1'].DisplacementBC(amplitude=UNSET, createStepName='Step-1',
        distributionType=UNIFORM, fieldName='', fixed=OFF, localCsys=None, name=
        'BC-2', region=mdb.models['Model-1'].rootAssembly.sets['dummyedge-TB'],
        u1=-RVEpredisp[2], u2=-RVEpredisp[1], ur3=UNSET)

    mdb.models['Model-1'].DisplacementBC(amplitude=UNSET, createStepName='Step-1',
        distributionType=UNIFORM, fieldName='', fixed=OFF, localCsys=None, name=
        'BC-3', region=mdb.models['Model-1'].rootAssembly.sets['dummyvertex-AC'],
        u1=-RVEpredisp[0]-RVEpredisp[2], u2=-RVEpredisp[2]-RVEpredisp[1], ur3=UNSET)
    mdb.models['Model-1'].DisplacementBC(amplitude=UNSET, createStepName='Step-1',      #vertex force
        distributionType=UNIFORM, fieldName='', fixed=OFF, localCsys=None, name=
        'BC-4', region=mdb.models['Model-1'].rootAssembly.sets['dummyvertex-BD'],
        u1=-RVEpredisp[0]+RVEpredisp[2], u2=-RVEpredisp[2]+RVEpredisp[1], ur3=UNSET)

    ###########Element###########

    elements=0
    element=mdb.models['Model-1'].rootAssembly.instances['Part-1-1'].elements
    elements=len(element)

    ###########Job###########

    job=mdb.Job(name='Job-%d'%(n+1), model='Model-1', description='', type=ANALYSIS,
        atTime=None, waitMinutes=0, waitHours=0, queue=None, memory=90,
        memoryUnits=PERCENTAGE, getMemoryFromAnalysis=True,
        explicitPrecision=SINGLE, nodalOutputPrecision=SINGLE, echoPrint=OFF,
        modelPrint=OFF, contactPrint=OFF, historyPrint=OFF, userSubroutine='',
        scratch='', multiprocessingMode=DEFAULT, numCpus=4, numDomains=4,
        numGPUs=0)

    mdb.jobs['Job-%d'%(n+1)].submit(consistencyChecking=OFF)
    job.waitForCompletion()
```

```
############Odb############

session.mdbData.summary()
o3 = session.openOdb(name='C:/Temp/Job-%d.odb'%(n+1))
session.viewports['Viewport: 1'].setValues(displayedObject=o3)
odb = session.odbs['C:/Temp/Job-%d.odb'%(n+1)]

RVEvolume=0
volume=[]

s11=[]
s22=[]            #stresses
s12=[]

ss11=0
ss22=0             #volume average stresses
ss12=0


e11=[]
e22=[]            #strains
e12=[]

ee11=0
ee22=0             #volume average strains
ee12=0

session.writeFieldReport(fileName='volume.txt', append=OFF,
    sortItem='Element Label', odb=odb, step=0, frame=1,
    outputPosition=WHOLE_ELEMENT, variable=(('EVOL', WHOLE_ELEMENT), ))

f=open('volume.txt','r')
line=f.readlines()
j=19
for i in range(elements):
    if line[j]=='\n':
        a=line[j+8].split()
        RVEvolume=RVEvolume+float(a[1])
        j=j+16
    a=line[j].split()
    b=float(a[1])
    volume.append(b)
    j=j+1
a=line[-3].split()
RVEvolume=RVEvolume+float(a[1])
f.close()

for k in range(1,4):
    if k==3:           #shear stresses
        session.writeFieldReport(fileName='stress12.txt', append=OFF,
            sortItem='Element Label', odb=odb, step=0, frame=1,
            outputPosition=INTEGRATION_POINT, variable=(('S', INTEGRATION_POINT, ((
            COMPONENT, 'S12'), )), ))
        f=open('stress12.txt','r')
        line=f.readlines()
        j=19
```

168

```
        for i in range(elements):
            if line[j]=='\n':
                j=j+18
            a=line[j].split()
            b=float(a[2])
            s12.append(b)
            j=j+1
        f.close()

    if k<3:              #normal stresses
        session.writeFieldReport(fileName='stress%d%d.txt'%(k,k), append=OFF,
            sortItem='Element Label', odb=odb, step=0, frame=1,
            outputPosition=INTEGRATION_POINT, variable=(('S', INTEGRATION_POINT, ((
            COMPONENT, 'S%d%d'%(k,k)), )), ))
        f=open('stress%d%d.txt'%(k,k),'r')
        line=f.readlines()
        j=19
        for i in range(elements):
            if line[j]=='\n':
                j=j+18
            a=line[j].split()
            b=float(a[2])
            if k==1:
                s11.append(b)
            if k==2:
                s22.append(b)
            j=j+1
        f.close()

for i in range(elements):
    ss11=ss11+s11[i]*volume[i]
    ss22=ss22+s22[i]*volume[i]
    ss12=ss12+s12[i]*volume[i]
ss11=ss11/(RVElength**2)
ss22=ss22/(RVElength**2)
ss12=ss12/(RVElength**2)

#//////////////////////////////////////////////////////////////////////////////

for k in range(1,4):
    if k==3:              #shear strains
        session.writeFieldReport(fileName='strain12.txt', append=OFF,
            sortItem='Element Label', odb=odb, step=0, frame=1,
            outputPosition=INTEGRATION_POINT, variable=(('E', INTEGRATION_POINT, ((
            COMPONENT, 'E12'), )), ))
        f=open('strain12.txt','r')
        line=f.readlines()
        j=19
        for i in range(elements):
            if line[j]=='\n':
                j=j+18
            a=line[j].split()
            b=float(a[2])
            e12.append(b)
            j=j+1
        f.close()
```

```python
        if k<3:               #normal strains
            session.writeFieldReport(fileName='strain%d%d.txt'%(k,k), append=OFF,
                sortItem='Element Label', odb=odb, step=0, frame=1,
                outputPosition=INTEGRATION_POINT, variable=(('E', INTEGRATION_POINT, ((
                COMPONENT, 'E%d%d'%(k,k)), )), ))
            f=open('strain%d%d.txt'%(k,k),'r')
            line=f.readlines()
            j=19
            for i in range(elements):
                if line[j]=='\n':
                    j=j+18
                a=line[j].split()
                b=float(a[2])
                if k==1:
                    e11.append(b)
                if k==2:
                    e22.append(b)
                j=j+1
            f.close()

    for i in range(elements):
        ee11=ee11+e11[i]*volume[i]
        ee22=ee22+e22[i]*volume[i]
        ee12=ee12+e12[i]*volume[i]
    ee11=ee11/(RVElength**2)
    ee22=ee22/(RVElength**2)
    ee12=ee12/(RVElength**2)

    if n==0:
        stif[0][n]=ss11/RVEstrain
        stif[1][n]=ss22/RVEstrain
        stif[2][n]=ss12/RVEstrain
    if n==1:
        stif[0][n]=ss11/RVEstrain
        stif[1][n]=ss22/RVEstrain
        stif[2][n]=ss12/RVEstrain
    if n==2:
        stif[0][n]=ss11/(2*RVEstrain)
        stif[1][n]=ss22/(2*RVEstrain)
        stif[2][n]=ss12/(2*RVEstrain)

    averagestresses[n][0]=ss11
    averagestresses[n][1]=ss22
    averagestresses[n][2]=ss12

    averagestrains[n][0]=ee11
    averagestrains[n][1]=ee22
    averagestrains[n][2]=ee12

print('stiffness matrix')
stif1=mat(stif)
print(stif1)
compliance=stif1**(-1)
print('compliance matrix')
print(compliance)
```

CHAPTER 5

Contributions, conclusions and future work

5. Contributions, conclusions and future work

5.1. Contributions

Extensive research has been conducted to optimize the processing parameters of Automated Fiber Placement (AFP), such as temperature, consolidation force and deposition rate, with the aim of achieving composite quality comparable to that produced by conventional methods. In parallel, the mechanical performance of Carbon/PEEK thermoplastic composite laminates has been commonly evaluated through Interlaminar Shear Strength (ILSS), typically measured using the Short-Beam Shear (SBS) test. However, there remains a notable gap in the availability of interface strength data for thermoplastic composite laminates produced via AFP in-situ consolidation, information that is critical for the development of reliable and accurate finite element simulations. Additionally, material properties found in technical datasheets generally correspond to composites fabricated by compression molding or autoclave curing, which do not reflect the unique microstructural characteristics introduced by the AFP method. These include increased void content, non-uniform fiber distribution, and variations in the degree of crystallinity, all of which significantly influence the mechanical performance of composite materials, especially in the transverse direction where matrix behavior is dominant. Furthermore, the occurrence of warpage in AFP-manufactured thermoplastic composite laminates, in the absence of a heated mandrel, poses significant challenges for experimental characterization of the final composite component. To overcome these limitations, this dissertation introduces advanced simulation methodologies at both macro and micro scales aimed at accurately predicting the interlaminar bonding strength and the effective material properties (i.e., stiffness and strength) of in-situ-consolidated Carbon/PEEK thermoplastic composite laminates. This method enables virtual testing, offering a reliable alternative to conventional experimental characterization. The main contributions of the present thesis are summarized below:

- A three-dimensional numerical model was developed to determine the interface strength properties of Carbon/PEEK thermoplastic composite laminates fabricated using the AFP in-situ consolidation process. This model accounted for both intralaminar and interlaminar damage mechanisms. To this end, two sets of composite specimens, one produced through AFP in-situ consolidation and the other through autoclave re-consolidation, were manufactured

and tested using the Short-Beam Shear (SBS) experiment. Subsequently, a 3D finite element analysis incorporating cohesive elements was conducted to computationally derive the interface strength values associated with the AFP-processed thermoplastic composite laminates, based on the ILSS results obtained from the SBS experiments.

- Under transverse loading, failure in composite materials often initiates with matrix microcracking, which plays a key role in the progression of damage. To predict the transverse tensile strength of Carbon/PEEK thermoplastic composite material fabricated through the AFP in-situ consolidation process, a micromechanical analysis was performed. This research incorporated key manufacturing-related factors, such as fiber volume fraction, void content, interlaminar resin-rich areas, and degree of crystallinity, by generating two-dimensional Representative Volume Elements (RVEs) with randomly distributed fibers. These RVEs were created using microstructural data obtained from micrographic examination and Differential Scanning Calorimetry (DSC) analysis. It is also important to note that the plastic behavior of the neat PEEK resin, as well as its damage initiation and propagation, was explicitly modeled in the finite element simulations.

- The presence of voids, interlaminar resin-rich regions, and a reduced degree of crystallinity can also significantly affect the stiffness properties of composite materials, especially in the transverse direction. In this context, the effective stiffness properties of Carbon/PEEK thermoplastic composites produced by AFP in-situ consolidation were predicted. Two-dimensional Representative Volume Elements (RVEs), generated based on both longitudinal and transverse cross-sections, were employed to quantify the impact of AFP-induced microstructural variations. Ultimately, the stiffness properties were predicted through the application of Periodic Boundary Conditions (PBCs) combined with Asymptotic Homogenization Theory (AHT).

5.2. Conclusions

The in-situ consolidation capability of the Automated Fiber Placement (AFP) process offers notable advantages in reducing both manufacturing time and costs when compared to traditional autoclave-based fabrication of thermoplastic composites. Despite these benefits, the AFP technique introduces certain limitations due to its shorter exposure time to heat and pressure and a

comparatively faster cooling rate, conditions that differ significantly from the prolonged curing cycles used in autoclave processing. This limited processing time can negatively influence the final quality of the composite laminates. In response to the identified gaps in the existing literature regarding the Carbon/PEEK thermoplastic composite laminates fabricated by Automated Fiber Placement (AFP) in-situ consolidation, the present thesis addresses three core research objectives focused on understanding the mechanical behavior resulting from the AFP process: (1) to determine the interface strength parameters critical to modeling delamination failure, (2) to predict the transverse tensile strength, and (3) to predict the effective stiffness properties, with particular attention to the transverse direction where the matrix phase plays a dominant role in governing the composite material response. The following conclusions were drawn through the mechanical characterization and finite element simulation of in-situ-consolidated Carbon/PEEK thermoplastic composite laminates manufactured by the AFP technique:

- The first objective of the present thesis, which involved the numerical estimation of interface strength properties using the results from Short-Beam Shear (SBS) testing, was addressed. To accurately simulate the delamination failure mode observed during the SBS experiment, cohesive elements were inserted between the composite layers to capture the interlaminar damage. Additionally, a user-defined VUMAT subroutine was implemented to incorporate the Hashin failure criteria, allowing for the prediction of intralaminar damage initiation and progression, particularly in areas near the loading nose and supports, to improve the accuracy of the simulation. The results indicated that the normal and shear interface strengths of AFP-manufactured Carbon/PEEK thermoplastic composite laminates were 36 MPa and 45 MPa, respectively, values approximately 36% lower than those corresponding to laminates produced by autoclave treatment. These interface properties are crucial for enabling precise finite element simulations of in-situ consolidated thermoplastic composites, especially for the modelling of delamination as a possible failure mode.

- Micrographic examination revealed notable differences between the specimens produced by AFP in-situ consolidation and those subjected to autoclave re-consolidation, particularly in terms of fiber volume fraction, void content, and the presence of interlaminar resin-rich regions. Additionally, Differential Scanning Calorimetry (DSC) analysis was conducted on both types of laminates to determine their degrees of crystallinity. The autoclave-

174

reconsolidated Carbon/PEEK specimens demonstrated a degree of crystallinity of 35%, a fiber volume fraction of 60% with uniform fiber distribution, and minimal void formation. In contrast, the AFP-fabricated specimens showed a reduction in the degree of crystallinity and fiber volume fraction to 25% and 56%, respectively, along with the presence of 12% interlaminar resin pockets and approximately 1.5% void content.

- To determine the mean values of fiber volume fraction, void content, and interlaminar resin pocket percentage, 30 micrographs from various locations were examined. Histogram plots were generated for these microstructural factors, and their standard deviations were calculated. Parametric studies were then carried out to assess how variations in each factor influence the material properties resulting from AFP in-situ consolidation process. The findings indicated that, unlike stiffness, transverse tensile strength is not significantly affected by fiber volume fraction, while resin-rich area and void content affect it substantially. Accordingly, normal distribution diagrams were developed for each factor, and the corresponding minimum and maximum transverse tensile strength values were reported. Additionally, the effect of void distribution was investigated to highlight its significance in addition to the role of total void percentage.

- The response of composite materials in the fiber direction is primarily influenced by the fiber volume fraction. However, in the transverse direction, the material behavior is strongly affected by matrix-related microstructural features induced by the AFP in-situ consolidation, as mentioned above. The second key objective of the present thesis was achieved: predicting the transverse tensile strength of Carbon/PEEK thermoplastic composite materials manufactured by the AFP in-situ consolidation process. The finite element modeling incorporated the Drucker–Prager plasticity model alongside a ductile failure criterion. This combination enabled the RVE simulations to capture both the plastic deformation and failure progression in the neat PEEK resin, including the onset and evolution of matrix cracks. According to the results, the transverse tensile strength of AFP-processed Carbon/PEEK thermoplastic composite material was reduced up to 46.9 MPa, approximately 44% lower than that of the autoclave-reconsolidated counterpart.

- To meet the third objective of the present thesis, the effective stiffness properties of Carbon/PEEK thermoplastic composites produced by AFP in-situ consolidation were

predicted, taking into account the previously discussed microstructural variations. The RVE simulations were conducted using the ABAQUS Scripting Interface (ASI), with MATLAB employed to generate the corresponding RVE geometries. The findings revealed that the AFP in-situ process may lead to a reduction in stiffness properties compared to the autoclave manufacturing method. Specifically, the longitudinal modulus, transverse modulus and out-of-plane shear modulus were decreased by approximately 7%, 10%, and 20%, respectively. However, the out-of-plane Poisson's ratio showed no noticeable change. These considerable reductions in stiffness and strength properties highlight the importance of accounting for AFP-specific microstructural effects during the design and simulation of thermoplastic composite laminates.

5.3. Future work

The methodology established in this dissertation successfully meets its outlined primary objectives. Nevertheless, there remains potential for further development to gain deeper insights into the characterization of Carbon/PEEK thermoplastic laminates manufactured through in-situ Automated Fiber Placement (AFP). Building on the outcomes of the present thesis, the following research directions can be recommended to further enhance and complement the proposed approach:

- Generally, the available literature offers limited insight into the fatigue behavior of composites fabricated by the AFP process, with most existing studies focusing on thermoset laminates and defects such as tow gaps [143,144]. Notably, no studies have been reported on the fatigue performance of in-situ-consolidated thermoplastic composite laminates. Given that one of the primary distinctions between AFP-made thermoplastic composite laminates and those manufactured using autoclave treatment lies in the interlaminar bonding quality, the Short-Beam Shear (SBS) fatigue test is proposed as a suitable method for such investigations. While no standardized procedure currently exists for this specific fatigue test, a few studies [145–150] have adapted the ASTM D2344 standard [12] with certain modifications to accommodate fatigue loading conditions. Considering the microstructural differences, degree of crystallinity variations, and incomplete process associated with the AFP technique, the SBS fatigue test is

expected to offer a more meaningful and relevant assessment than conventional tension–tension fatigue tests [151] in this context.

- The material model adopted for the neat PEEK resin in Chapter 3 was formulated specifically for tensile loading scenarios. Consequently, the micromechanical analysis was limited to predicting the transverse tensile strength of AFP in-situ-consolidated Carbon/PEEK thermoplastic composite. However, if this model were extended to also represent compressive and shear loading conditions, the proposed simulation framework could be used to predict additional strength parameters, such as transverse compressive strength and out-of-plane shear strength, for AFP-fabricated thermoplastic composite materials. Therefore, a promising avenue for future research involves characterization of the neat PEEK resin under compressive and shear loads. This would enable the development of corresponding material models that capture plastic deformation, damage initiation and propagation in the matrix, thereby enhancing the predictive capabilities of the proposed finite element model for Carbon/PEEK thermoplastic composite material manufactured by AFP in-situ consolidation.

- Warpage introduced during the AFP in-situ consolidation of thermoplastic composite materials presents a major challenge in producing flat coupons suitable for standard mechanical experiments, such as tensile testing. To address this limitation, Chapters 3 and 4 proposed a micromechanical simulation approach to characterize in-situ-consolidated Carbon/PEEK thermoplastic composite, based on experimental data obtained from micrographic examination and DSC analysis. Although this finite element framework was validated by generating RVEs representing autoclave-processed samples and comparing simulation results with values reported in the technical datasheet, it cannot be assumed to fully capture the mechanical behavior of the AFP-fabricated thermoplastic composite material with complete accuracy. To increase confidence in the simulation outcomes, one possible research direction is micro-scale tensile testing. This method would utilize a specialized tensile stage capable of applying precise, uniform and low-magnitude displacements to small specimens, approximately 3 cm in length. Such a small sample size minimizes the influence of manufacturing-related defects during testing, as discussed in the Appendix of Chapter 3. Alternatively, tensile characterization could be conducted on rigid tube specimens following the ASTM D638 standard [152]. While this method can circumvent the problem of warpage effect during

manufacturing and testing, it involves substantial specimen machining and requires customized grips to accommodate the tube geometry. Incorporating experimental results from either method would enhance the reliability of the proposed micromechanical model and may guide future refinements to improve the accuracy of the predicted material properties.

References

[1]   Oromiehie E, Prusty BG, Compston P, Rajan G. Automated fibre placement based composite structures: Review on the defects, impacts and inspections techniques. Compos Struct 2019;224:110987. https://doi.org/10.1016/j.compstruct.2019.110987.

[2]   Schiel I, Raps L, Chadwick AR, Schmidt I, Simone M, Nowotny S. An investigation of in-situ AFP process parameters using CF/LM-PAEK. Advanced Manufacturing: Polymer & Composites Science 2020;6:191–7. https://doi.org/10.1080/20550340.2020.1826772.

[3]   Venkatesan C, Zulkifli F, Silva A. Effects of processing parameters of infrared-based automated fiber placement on mechanical performance of carbon fiber-reinforced thermoplastic composite. Compos Struct 2023;309:116725. https://doi.org/10.1016/j.compstruct.2023.116725.

[4]   Liu J, Wang S, Yang H, Zhu D, Guangquan Y. Processing and characterization of high-performance thermoplastic composites manufactured by laser-assisted automated fiber placement in-situ consolidation and hot-press. J Eng Fiber Fabr 2024;19. https://doi.org/10.1177/15589250241254440.

[5]   Shadmehri F, Hoa SV, Fortin-Simpson J, Ghayoor H. Effect of in situ treatment on the quality of flat thermoplastic composite plates made by automated fiber placement (AFP). Advanced Manufacturing: Polymer & Composites Science 2018;4:41–7. https://doi.org/10.1080/20550340.2018.1444535.

[6]   Arquier R, Iliopoulos I, Régnier G, Miquelard-Garnier G. Consolidation of continuous-carbon-fiber-reinforced PAEK composites: a review. Mater Today Commun 2022;32:104036. https://doi.org/10.1016/j.mtcomm.2022.104036.

[7]   Pitchumani R, Ranganathan S, Don RC, Gillespie JW, Lamontia MA. Analysis of transport phenomena governing interfacial bonding and void dynamics during thermoplastic tow-placement. Int J Heat Mass Transf 1996;39:1883–97. https://doi.org/10.1016/0017-9310(95)00271-5.

[8]   Ranganathan S, Advani SG, Lamontia MA. A Non-Isothermal Process Model for Consolidation and Void Reduction during In-Situ Tow Placement of Thermoplastic Composites. J Compos Mater 1995;29:1040–62. https://doi.org/10.1177/002199839502900803.

[9]   Khan MA, Mitschang P, Schledjewski R. Tracing the Void Content Development and Identification of its Effecting Parameters during in Situ Consolidation of Thermoplastic Tape Material. Polymers and Polymer Composites 2010;18:1–15. https://doi.org/10.1177/096739111001800101.

[10]   Khodaei A, Shadmehri F. Intimate contact development for automated fiber placement of thermoplastic composites. Composites Part C: Open Access 2022;8:100290. https://doi.org/10.1016/j.jcomc.2022.100290.

[11]   Avenet J, Levy A, Bailleul J-L, le Corre S, Delmas J. Adhesion of high performance thermoplastic composites: Development of a bench and procedure for kinetics identification. Compos Part A Appl Sci Manuf 2020;138:106054. https://doi.org/10.1016/j.compositesa.2020.106054.

[12]   ASTM D2344 / D2344M. Standard Test Method for Short-Beam Strength of Polymer Matrix Composite Materials and Their Laminates. ASTM International, West Conshohocken, PA 2016. https://doi.org/10.1520/D2344_D2344M-16.

[13]   Cai X, Shadmehri F, Hojjati M, Chen J, Hoa SV. Determination of optimum process conditions for processing AS4/APC-2 thermoplastic composites by automated fiber placement. The Society for the Advancement of Material and Process Engineering (SAMPE) conference, 2012.

[14]   Oromiehie E, Gain AK, Prusty BG. Processing parameter optimisation for automated fibre placement (AFP) manufactured thermoplastic composites. Compos Struct 2021;272:114223. https://doi.org/10.1016/j.compstruct.2021.114223.

[15]   Qureshi Z, Swait T, Scaife R, El-Dessouky HM. In situ consolidation of thermoplastic prepreg tape using automated tape placement technology: Potential and possibilities. Compos B Eng 2014;66:255–67. https://doi.org/10.1016/j.compositesb.2014.05.025.

[16]   Khan MA, Mitschang P, Schledjewski R. Identification of some optimal parameters to achieve higher laminate quality through tape placement process. Advances in Polymer Technology 2010;29:98–111. https://doi.org/10.1002/adv.20177.

[17]   Stokes-Griffin CM, Compston P. The effect of processing temperature and placement rate on the short beam strength of carbon fibre–PEEK manufactured using a laser tape placement process. Compos Part A Appl Sci Manuf 2015;78:274–83. https://doi.org/10.1016/j.compositesa.2015.08.008.

[18]   Camanho PP, Dávila CG. Mixed-mode decohesion finite elements for the simulation of delamination in composite materials. 2002.

[19]   Camanho PP, Davila CG, de Moura MF. Numerical Simulation of Mixed-Mode Progressive Delamination in Composite Materials. J Compos Mater 2003;37:1415–38. https://doi.org/10.1177/0021998303034505.

[20]   Turon A, Camanho PP, Costa J, Renart J. Accurate simulation of delamination growth under mixed-mode loading using cohesive elements: Definition of interlaminar strengths and elastic stiffness. Compos Struct 2010;92:1857–64. https://doi.org/10.1016/j.compstruct.2010.01.012.

[21]   Turon A, Camanho PP, Soto A, González E V. Analysis of Delamination Damage in Composite Structures Using Cohesive Elements. Comprehensive Composite Materials II, Elsevier; 2018, p. 136–56. https://doi.org/10.1016/B978-0-12-803581-8.10059-1.

[22]   Ghayour M, Ganesan R, Hojjati M. Flexural response of composite beams made by Automated Fiber Placement process: Effect of fiber tow gaps. Compos B Eng 2020;201:108368. https://doi.org/10.1016/j.compositesb.2020.108368.

[23]   Yang Y, Liu X, Wang Y-Q, Gao H, Li R, Bao Y. A progressive damage model for predicting damage evolution of laminated composites subjected to three-point bending. Compos Sci Technol 2017;151:85–93. https://doi.org/10.1016/j.compscitech.2017.08.009.

[24]   El-Sisi AE-DA, El-Emam HM, Salim HA, Sallam HE-DM. Efficient 3D modeling of damage in composite materials. J Compos Mater 2015;49:817–28. https://doi.org/10.1177/0021998314525983.

[25]   Pham DC, Cui X, Ren X, Lua J. A discrete crack informed 3D continuum damage model and its application for delamination migration in composite laminates. Compos B Eng 2019;165:554–62. https://doi.org/10.1016/j.compositesb.2019.02.045.

[26]   Hashin Z. Failure Criteria for Unidirectional Fiber Composites. J Appl Mech 1980;47:329–34. https://doi.org/10.1115/1.3153664.

[27]   Liu H, Liu J, Ding Y, Zhou J, Kong X, Harper LT, et al. Modelling damage in fibre-reinforced thermoplastic composite laminates subjected to three-point bend loading. Compos Struct 2020;236:111889. https://doi.org/10.1016/j.compstruct.2020.111889.

[28] Tierney J, Gillespie JW. Modeling of In Situ Strength Development for the Thermoplastic Composite Tow Placement Process. J Compos Mater 2006;40:1487–506. https://doi.org/10.1177/0021998306060162.

[29] Hoa SV, Hoang DM, Simpson J. Manufacturing procedure to make flat thermoplastic composite laminates by automated fibre placement and their mechanical properties. Journal of Thermoplastic Composite Materials 2017;30:1693–712. https://doi.org/10.1177/0892705716662516.

[30] Chapman TJ, Gillespie JW, Pipes RB, Manson J-AE, Seferis JC. Prediction of Process-Induced Residual Stresses in Thermoplastic Composites. J Compos Mater 1990;24:616–43. https://doi.org/10.1177/002199839002400603.

[31] Tsukada T, Minakuchi S, Takeda N. Identification of process-induced residual stress/strain distribution in thick thermoplastic composites based on in situ strain monitoring using optical fiber sensors. J Compos Mater 2019;53:3445–58. https://doi.org/10.1177/0021998319837199.

[32] Parambil NK, Chen BR, Deitzel JM, Gillespie JW. A methodology for predicting processing induced thermal residual stress in thermoplastic composite at the microscale. Compos B Eng 2022;231:109562. https://doi.org/10.1016/j.compositesb.2021.109562.

[33] Zhang C, Wang Y, Lou M, Liang W, Yang D, Qi X. Process-induced residual stress analysis of reinforced layer of reinforced thermoplastic pipes. Polym Compos 2025. https://doi.org/10.1002/pc.29908.

[34] Oromiehie E, Garbe U, Gangadhara Prusty B. Porosity analysis of carbon fibre-reinforced polymer laminates manufactured using automated fibre placement. J Compos Mater 2020;54:1217–31. https://doi.org/10.1177/0021998319875491.

[35] Oromiehie E, Gain AK, Donough MJ, Prusty BG. Fracture toughness assessment of CF-PEEK composites consolidated using hot gas torch assisted automated fibre placement. Compos Struct 2022;279:114762. https://doi.org/10.1016/j.compstruct.2021.114762.

[36] Fereidouni M, Hoa S Van. In-situ consolidation of thermoplastic composites by automated fiber placement: Characterization of defects. Journal of Thermoplastic Composite Materials 2025;38:471–511. https://doi.org/10.1177/08927057241251837.

[37] Pourahmadi E, Ganesan R, Shadmehri F. Micromechanical characterization of Carbon/PEEK thermoplastic composite material in-situ consolidated by automated fiber placement: Stiffness prediction. Compos Sci Technol 2024;246:110390. https://doi.org/10.1016/j.compscitech.2023.110390.

[38] Comer AJ, Ray D, Obande WO, Jones D, Lyons J, Rosca I, et al. Mechanical characterisation of carbon fibre–PEEK manufactured by laser-assisted automated-tape-placement and autoclave. Compos Part A Appl Sci Manuf 2015;69:10–20. https://doi.org/10.1016/j.compositesa.2014.10.003.

[39] Saenz-Castillo D, Martín MI, Calvo S, Rodriguez-Lence F, Güemes A. Effect of processing parameters and void content on mechanical properties and NDI of thermoplastic composites. Compos Part A Appl Sci Manuf 2019;121:308–20. https://doi.org/10.1016/j.compositesa.2019.03.035.

[40] Ray D, Comer AJ, Lyons J, Obande W, Jones D, Higgins RMO, et al. Fracture toughness of carbon fiber/polyether ether ketone composites manufactured by autoclave and laser-assisted automated tape placement. J Appl Polym Sci 2014;132. https://doi.org/10.1002/app.41643.

[41] Chanteli A, Bandaru AK, Peeters D, O'Higgins RM, Weaver PM. Influence of repass treatment on carbon fibre-reinforced PEEK composites manufactured using laser-assisted automatic tape placement. Compos Struct 2020;248:112539. https://doi.org/10.1016/j.compstruct.2020.112539.

[42] Ghayoor H, Marsden CC, Hoa SV, Melro AR. Numerical analysis of resin-rich areas and their effects on failure initiation of composites. Compos Part A Appl Sci Manuf 2019;117:125–33. https://doi.org/10.1016/j.compositesa.2018.11.016.

[43] Preibisch S, Saalfeld S, Tomancak P. Globally optimal stitching of tiled 3D microscopic image acquisitions. Bioinformatics 2009;25:1463–5. https://doi.org/10.1093/bioinformatics/btp184.

[44] Schneider CA, Rasband WS, Eliceiri KW. NIH Image to ImageJ: 25 years of image analysis. Nat Methods 2012;9:671–5. https://doi.org/10.1038/nmeth.2089.

[45] Wang M, Zhang P, Fei Q, Guo F. Computational evaluation of the effects of void on the transverse tensile strengths of unidirectional composites considering thermal residual stress. Compos Struct 2019;227:111287. https://doi.org/10.1016/j.compstruct.2019.111287.

[46] Talbott MF, Springer GS, Berglund LA. The Effects of Crystallinity on the Mechanical Properties of PEEK Polymer and Graphite Fiber Reinforced PEEK. J Compos Mater 1987;21:1056–81. https://doi.org/10.1177/002199838702101104.

[47] Pisani WA, Radue MS, Chinkanjanarot S, Bednarcyk BA, Pineda EJ, Waters K, et al. Multiscale modeling of PEEK using reactive molecular dynamics modeling and micromechanics. Polymer (Guildf) 2019;163:96–105. https://doi.org/10.1016/j.polymer.2018.12.052.

[48] Aboudi J. Mechanics of composite materials: a unified micromechanical approach. Elsevier; 2013.

[49] Gusev AA, Hine PJ, Ward IM. Fiber packing and elastic properties of a transversely random unidirectional glass/epoxy composite. Compos Sci Technol 2000;60:535–41. https://doi.org/10.1016/S0266-3538(99)00152-9.

[50] Ghayoor H, Hoa SV, Marsden CC. A micromechanical study of stress concentrations in composites. Compos B Eng 2018;132:115–24. https://doi.org/10.1016/j.compositesb.2017.09.009.

[51] Bahmani A, Li G, Willett TL, Montesano J. Three-dimensional microscopic assessment of randomly distributed representative volume elements for high fiber volume fraction unidirectional composites. Compos Struct 2018;192:153–64. https://doi.org/10.1016/j.compstruct.2018.02.075.

[52] Ohser J, Mücklich F. Statistical Analysis of Microstructures in Materials Science. Practical Metallography 2001;38:538–9. https://doi.org/10.1515/pm-2001-380907.

[53] Yang L, Yan Y, Ran Z, Liu Y. A new method for generating random fibre distributions for fibre reinforced composites. Compos Sci Technol 2013;76:14–20. https://doi.org/10.1016/j.compscitech.2012.12.001.

[54] Melro A, Camanho P, Pinho S. Generation of random distribution of fibres in long-fibre reinforced composites. Compos Sci Technol 2008;68:2092–102. https://doi.org/10.1016/j.compscitech.2008.03.013.

[55] Trias D, Costa J, Mayugo JA, Hurtado JE. Random models versus periodic models for fibre reinforced composites. Comput Mater Sci 2006;38:316–24. https://doi.org/10.1016/j.commatsci.2006.03.005.

[56] Romanov V, Lomov S V., Swolfs Y, Orlova S, Gorbatikh L, Verpoest I. Statistical analysis of real and simulated fibre arrangements in unidirectional composites. Compos Sci Technol 2013;87:126–34. https://doi.org/10.1016/j.compscitech.2013.07.030.

[57] Mehdikhani M, Straumit I, Gorbatikh L, Lomov S V. Detailed characterization of voids in multidirectional carbon fiber/epoxy composite laminates using X-ray micro-computed tomography. Compos Part A Appl Sci Manuf 2019;125:105532. https://doi.org/10.1016/j.compositesa.2019.105532.

[58] Mehdikhani M, Petrov NA, Straumit I, Melro AR, Lomov S V., Gorbatikh L. The effect of voids on matrix cracking in composite laminates as revealed by combined computations at the micro- and meso-scales. Compos Part A Appl Sci Manuf 2019;117:180–92. https://doi.org/10.1016/j.compositesa.2018.11.009.

[59] González C, LLorca J. Mechanical behavior of unidirectional fiber-reinforced polymers under transverse compression: Microscopic mechanisms and modeling. Compos Sci Technol 2007;67:2795–806. https://doi.org/10.1016/j.compscitech.2007.02.001.

[60] Yang L, Yan Y, Liu Y, Ran Z. Microscopic failure mechanisms of fiber-reinforced polymer composites under transverse tension and compression. Compos Sci Technol 2012;72:1818–25. https://doi.org/10.1016/j.compscitech.2012.08.001.

[61] Totry E, González C, LLorca J. Prediction of the failure locus of C/PEEK composites under transverse compression and longitudinal shear through computational micromechanics. Compos Sci Technol 2008;68:3128–36. https://doi.org/10.1016/j.compscitech.2008.07.011.

[62] Liu PF, Li XK. Explicit finite element analysis of failure behaviors of thermoplastic composites under transverse tension and shear. Compos Struct 2018;192:131–42. https://doi.org/10.1016/j.compstruct.2018.02.037.

[63] Fedulov BN, Safonov AA, Kantor MM, Lomov SV. Modelling of thermoplastic polymer failure in fiber reinforced composites. Compos Struct 2017;163:293–301. https://doi.org/10.1016/j.compstruct.2016.11.091.

[64] Kitagawa Y, Yoshimura A, Arai M, Goto K, Sugiura N. Experimental and numerical evaluation of effects of kidney-shape carbon fiber on transverse cracking of carbon fiber reinforced plastics. Compos Part A Appl Sci Manuf 2022;152:106690. https://doi.org/10.1016/j.compositesa.2021.106690.

[65] Rueda-Ruiz M, Herráez M, Sket F, Gálvez F, González C, Molina-Aldareguia JM. Study of the effect of strain rate on the in-plane shear and transverse compression response of a composite ply using computational micromechanics. Compos Part A Appl Sci Manuf 2023;168:107482. https://doi.org/10.1016/j.compositesa.2023.107482.

[66] Elnekhaily SA, Talreja R. Effects of micro voids on the early stage of transverse crack formation in unidirectional composites. Compos Part A Appl Sci Manuf 2023;167:107457. https://doi.org/10.1016/j.compositesa.2023.107457.

[67] CYTEC. APC-2-PEEK Thermoplastic Polymer. 2012.

[68] Xia Z, Zhang Y, Ellyin F. A unified periodical boundary conditions for representative volume elements of composites and applications. Int J Solids Struct 2003;40:1907–21. https://doi.org/10.1016/S0020-7683(03)00024-6.

[69]   Taheri-Behrooz F, Pourahmadi E. A 3D RVE model with periodic boundary conditions to estimate mechanical properties of composites. Structural Engineering and Mechanics 2019;72:713–22. https://doi.org/10.12989/sem.2019.72.6.713.

[70]   Ashouri Vajari D, González C, Llorca J, Legarth BN. A numerical study of the influence of microvoids in the transverse mechanical response of unidirectional composites. Compos Sci Technol 2014;97:46–54. https://doi.org/10.1016/j.compscitech.2014.04.004.

[71]   Qi L, Chao X, Tian W, Ma W, Li H. Numerical study of the effects of irregular pores on transverse mechanical properties of unidirectional composites. Compos Sci Technol 2018;159:142–51. https://doi.org/10.1016/j.compscitech.2018.02.020.

[72]   Chao X, Qi L, Cheng J, Tian W, Zhang S, Li H. Numerical evaluation of the effect of pores on effective elastic properties of carbon/carbon composites. Compos Struct 2018;196:108–16. https://doi.org/10.1016/j.compstruct.2018.05.014.

[73]   Tai J-H, Kaw A. Transverse shear modulus of unidirectional composites with voids estimated by the multiple-cells model. Compos Part A Appl Sci Manuf 2018;105:310–20. https://doi.org/10.1016/j.compositesa.2017.11.026.

[74]   Dong C. Effects of Process-Induced Voids on the Properties of Fibre Reinforced Composites. J Mater Sci Technol 2016;32:597–604. https://doi.org/10.1016/j.jmst.2016.04.011.

[75]   Jiang H, Ren Y, Liu Z, Zhang S. Microscale finite element analysis for predicting effects of air voids on mechanical properties of single fiber bundle in composites. J Mater Sci 2019;54:1363–81. https://doi.org/10.1007/s10853-018-2928-6.

[76]   Niu X, Sun Z, Song Y. Transverse Tensile Properties of 3 Dimension-4 Directional Braided Cf/SiC Composite Based on Double-Scale Model. Applied Composite Materials 2018;25:1001–19. https://doi.org/10.1007/s10443-017-9648-y.

[77]   Dong J, Huo N. A two-scale method for predicting the mechanical properties of 3D braided composites with internal defects. Compos Struct 2016;152:1–10. https://doi.org/10.1016/j.compstruct.2016.05.025.

[78]   Dong J, Gong Y. Influence of void defects on progressive tensile damage of three-dimensional braided composites. J Compos Mater 2018;52:2033–45. https://doi.org/10.1177/0021998317737829.

[79]   Huang T, Gong Y. A multiscale analysis for predicting the elastic properties of 3D woven composites containing void defects. Compos Struct 2018;185:401–10. https://doi.org/10.1016/j.compstruct.2017.11.046.

[80]   Chen J, Fu K, Li Y. Understanding processing parameter effects for carbon fibre reinforced thermoplastic composites manufactured by laser-assisted automated fibre placement (AFP). Compos Part A Appl Sci Manuf 2021;140:106160. https://doi.org/10.1016/j.compositesa.2020.106160.

[81]   August Z, Ostrander G, Michasiow J, Hauber D. Recent developments in automated fiber placement of thermoplastic composites. SAMPE J 2014;50:30–7.

[82]   Tafreshi OA, Hoa S Van, Shadmehri F, Hoang DM, Rosca D. Heat transfer analysis of automated fiber placement of thermoplastic composites using a hot gas torch. Advanced Manufacturing: Polymer & Composites Science 2019;5:206–23. https://doi.org/10.1080/20550340.2019.1686820.

[83]   Brasington A, Francis B, Godbold M, Harik R. A review and framework for modeling methodologies to advance automated fiber placement. Composites Part C: Open Access 2023;10:100347. https://doi.org/10.1016/j.jcomc.2023.100347.

[84]   Brasington A, Sacco C, Halbritter J, Wehbe R, Harik R. Automated fiber placement: A review of history, current technologies, and future paths forward. Composites Part C: Open Access 2021;6:100182. https://doi.org/10.1016/j.jcomc.2021.100182.

[85]   Abaqus V. 6.14 Documentation. Dassault Systemes Simulia Corporation 2014;651.

[86]   Lopes CS, Camanho PP, Gürdal Z, Maimí P, González EV. Low-velocity impact damage on dispersed stacking sequence laminates. Part II: Numerical simulations. Compos Sci Technol 2009;69:937–47. https://doi.org/10.1016/j.compscitech.2009.02.015.

[87]   Ebina M, Yoshimura A, Sakaue K, Waas AM. High fidelity simulation of low velocity impact behavior of CFRP laminate. Compos Part A Appl Sci Manuf 2018;113:166–79. https://doi.org/10.1016/j.compositesa.2018.07.022.

[88]   Bondyra A, Klasztorny M, Szurgott P, Gotowicki P. Numerical Modelling and Experimental Verification of Glass-Polyester Mixed Laminate Beam Bending Test. Acta Mechanica et Automatica 2012;6:1–18.

[89]   Sun CX, Yoon KJ. Characterization of Elastic-Plastic Behavior of AS4/PEEK Thermoplastic Composite for Temperature Variation. J Compos Mater 1991;25:1297–313. https://doi.org/10.1177/002199839102501003.

[90]   Sun CT, Chen JL. A Simple Flow Rule for Characterizing Nonlinear Behavior of Fiber Composites. J Compos Mater 1989;23:1009–20. https://doi.org/10.1177/002199838902301004.

[91]   ASTM D3518 / D3518M. Standard Test Method for In-Plane Shear Response of Polymer Matrix Composite Materials by Tensile Test of a ±45° Laminate. ASTM International, West Conshohocken, PA 2013. https://doi.org/10.1520/D3518_D3518M-13.

[92]   ASTM D3039 / D3039M. Standard Test Method for Tensile Properties of Polymer Matrix Composite Materials. ASTM International, West Conshohocken, PA 2017. https://doi.org/10.1520/D3039_D3039M-17.

[93]   Rice JR. A Path Independent Integral and the Approximate Analysis of Strain Concentration by Notches and Cracks. J Appl Mech 1968;35:379–86. https://doi.org/10.1115/1.3601206.

[94]   Sun CT, Jin Z-H. Energy Release Rate. Fracture Mechanics, Elsevier; 2012, p. 77–103. https://doi.org/10.1016/B978-0-12-385001-0.00004-3.

[95]   Lu X, Ridha M, Chen BY, Tan VBC, Tay TE. On cohesive element parameters and delamination modelling. Eng Fract Mech 2019;206:278–96. https://doi.org/10.1016/j.engfracmech.2018.12.009.

[96]   Ye Q, Chen P. Prediction of the cohesive strength for numerically simulating composite delamination via CZM-based FEM. Compos B Eng 2011;42:1076–83. https://doi.org/10.1016/j.compositesb.2011.03.021.

[97]   van der Meer FP, Sluys LJ, Hallett SR, Wisnom MR. Computational modeling of complex failure mechanisms in laminates. J Compos Mater 2012;46:603–23. https://doi.org/10.1177/0021998311410473.

[98] Chen BY, Tay TE, Baiz PM, Pinho ST. Numerical analysis of size effects on open-hole tensile composite laminates. Compos Part A Appl Sci Manuf 2013;47:52–62. https://doi.org/10.1016/j.compositesa.2012.12.001.

[99] Chen BY, Tay TE, Pinho ST, Tan VBC. Modelling the tensile failure of composites with the floating node method. Comput Methods Appl Mech Eng 2016;308:414–42. https://doi.org/10.1016/j.cma.2016.05.027.

[100] Zhi J, Chen B-Y, Tay T-E. Geometrically nonlinear analysis of matrix cracking and delamination in composites with floating node method. Comput Mech 2019;63:201–17. https://doi.org/10.1007/s00466-018-1591-8.

[101] Turon A, Dávila CG, Camanho PP, Costa J. An engineering solution for mesh size effects in the simulation of delamination using cohesive zone models. Eng Fract Mech 2007;74:1665–82. https://doi.org/10.1016/j.engfracmech.2006.08.025.

[102] Soto A, González EV, Maimí P, Turon A, Sainz de Aja JR, de la Escalera FM. Cohesive zone length of orthotropic materials undergoing delamination. Eng Fract Mech 2016;159:174–88. https://doi.org/10.1016/j.engfracmech.2016.03.033.

[103] Yoon KJ, Sun CT. Characterization of Elastic-Viscoplastic Properties of an AS4/PEEK Thermoplastic Composite. J Compos Mater 1991;25:1277–96. https://doi.org/10.1177/002199839102501002.

[104] Turon A, Camanho PP, Costa J, Dávila CG. A damage model for the simulation of delamination in advanced composites under variable-mode loading. Mechanics of Materials 2006;38:1072–89. https://doi.org/10.1016/j.mechmat.2005.10.003.

[105] Naderi M, Khonsari MM. Stochastic analysis of inter- and intra-laminar damage in notched PEEK laminates. Express Polym Lett 2013;7:383–95. https://doi.org/10.3144/expresspolymlett.2013.35.

[106] Liu H, Liu J, Kaboglu C, Chai H, Kong X, Blackman BRK, et al. Experimental and numerical studies on the behaviour of fibre-reinforced composites subjected to soft impact loading. Procedia Structural Integrity 2019;17:992–1001. https://doi.org/10.1016/j.prostr.2019.08.132.

[107] Yokozeki T, Ogihara S, Yoshida S, Ogasawara T. Simple constitutive model for nonlinear response of fiber-reinforced composites with loading-directional dependence. Compos Sci Technol 2007;67:111–8. https://doi.org/10.1016/j.compscitech.2006.03.024.

[108] Benzeggagh ML, Kenane M. Measurement of mixed-mode delamination fracture toughness of unidirectional glass/epoxy composites with mixed-mode bending apparatus. Compos Sci Technol 1996;56:439–49. https://doi.org/10.1016/0266-3538(96)00005-X.

[109] Pourahmadi E, Shadmehri F, Ganesan R. Interlaminar shear strength of Carbon/PEEK thermoplastic composite laminate: Effects of in-situ consolidation by automated fiber placement and autoclave re-consolidation. Compos B Eng 2024;269:111104. https://doi.org/10.1016/j.compositesb.2023.111104.

[110] Elnekhaily SA, Talreja R. Damage initiation in unidirectional fiber composites with different degrees of nonuniform fiber distribution. Compos Sci Technol 2018;155:22–32. https://doi.org/10.1016/j.compscitech.2017.11.017.

[111] Elnekhaily SA, Zhuang L, Talreja R. Formation of transverse cracks in cross ply laminates in an environment of nonuniformly distributed fibers. Compos Sci Technol 2024;253:110651. https://doi.org/10.1016/j.compscitech.2024.110651.

[112] Gao S-L, Kim J-K. Cooling rate influences in carbon fibre/PEEK composites. Part 1. Crystallinity and interface adhesion. Compos Part A Appl Sci Manuf 2000;31:517–30. https://doi.org/10.1016/S1359-835X(00)00009-9.

[113] Blundell DJ, Osborn BN. The morphology of poly(aryl-ether-ether-ketone). Polymer (Guildf) 1983;24:953–8. https://doi.org/10.1016/0032-3861(83)90144-1.

[114] Trias D, Costa J, Turon A, Hurtado J. Determination of the critical size of a statistical representative volume element (SRVE) for carbon reinforced polymers. Acta Mater 2006;54:3471–84. https://doi.org/10.1016/j.actamat.2006.03.042.

[115] Mokhov S, Roper G, Meza CA, et al. Speed: Gina Cody School HPC Facility: Scripts, Tools, and Refs. Zenodo 2024. https://doi.org/10.5281/zenodo.13363464.

[116] Chevalier J, Morelle XP, Bailly C, Camanho PP, Pardoen T, Lani F. Micro-mechanics based pressure dependent failure model for highly cross-linked epoxy resins. Eng Fract Mech 2016;158:1–12. https://doi.org/10.1016/j.engfracmech.2016.02.039.

[117] D'Mello RJ, Maiarù M, Waas AM. Effect of the curing process on the transverse tensile strength of fiber-reinforced polymer matrix lamina using micromechanics computations. Integr Mater Manuf Innov 2015;4:119–36. https://doi.org/10.1186/s40192-015-0035-y.

[118] Naderi M, Apetre N, Iyyer N. Effect of interface properties on transverse tensile response of fiber-reinforced composites: Three-dimensional micromechanical modeling. J Compos Mater 2017;51:2963–77. https://doi.org/10.1177/0021998316681189.

[119] D'Mello RJ, Waas AM. Influence of Unit Cell Size and Fiber Packing on the Transverse Tensile Response of Fiber Reinforced Composites. Materials 2019;12:2565. https://doi.org/10.3390/ma12162565.

[120] Hetrick DR, Sanei SHR, Bakis CE, Ashour O. Evaluating the effect of variable fiber content on mechanical properties of additively manufactured continuous carbon fiber composites. Journal of Reinforced Plastics and Composites 2021;40:365–77. https://doi.org/10.1177/0731684420963217.

[121] Kaw AK. Mechanics of composite materials. CRC press; 2005.

[122] Datoo MH. Mechanics of fibrous composites. Springer Science & Business Media; 2012.

[123] Mahishi JM, Adams DF. Fracture behaviour of a single-fibre graphite/epoxy model composite containing a broken fibre or cracked matrix. J Mater Sci 1983;18:447–56. https://doi.org/10.1007/BF00560634.

[124] Shioya M, Takaku A. Estimation of fibre and interfacial shear strength by using a single-fibre composite. Compos Sci Technol 1995;55:33–9. https://doi.org/10.1016/0266-3538(95)00078-X.

[125] DiBenedetto AT, Gurvich MR. Statistical simulation of fiber fragmentation in a single-fiber composite. Compos Sci Technol 1997;57:543–55. https://doi.org/10.1016/S0266-3538(97)00008-0.

[126] Okabe T, Takeda N. Estimation of strength distribution for a fiber embedded in a single-fiber composite: experiments and statistical simulation based on the elasto-plastic shear-lag approach. Compos Sci Technol 2001;61:1789–800. https://doi.org/10.1016/S0266-3538(01)00080-X.

[127] Zhong W, Pan N. A Computer Simulation of Single Fiber Pull Out Process in a Composite. J Compos Mater 2003;37:1951–69. https://doi.org/10.1177/002199803036267.

[128] Nishikawa M, Okabe T, Takeda N. Determination of interface properties from experiments on the fragmentation process in single-fiber composites. Materials Science and Engineering: A 2008;480:549–57. https://doi.org/10.1016/j.msea.2007.07.067.

[129] Koohbor B, Montgomery CB, Sottos NR. Identification of RVE length scale in fiber composites via combined optical and SEM digital image correlation. Compos Sci Technol 2022;227:109613. https://doi.org/10.1016/j.compscitech.2022.109613.

[130] Tian W, Chao X, Fu MW, Qi L. An algorithm for generation of RVEs of composites with high particle volume fractions. Compos Sci Technol 2021;207:108714. https://doi.org/10.1016/j.compscitech.2021.108714.

[131] Tian W, Chao X, Fu MW, Qi L. An advanced method for efficiently generating composite RVEs with specified particle orientation. Compos Sci Technol 2021;205:108647. https://doi.org/10.1016/j.compscitech.2021.108647.

[132] Bai W, Gong Z, Li Y, Liu J. Determination of the representative volume element model critical size for carbon fiber reinforced polymer composites. Compos Sci Technol 2023;234:109946. https://doi.org/10.1016/j.compscitech.2023.109946.

[133] Kari S, Berger H, Rodriguez-Ramos R, Gabbert U. Computational evaluation of effective material properties of composites reinforced by randomly distributed spherical particles. Compos Struct 2007;77:223–31. https://doi.org/10.1016/j.compstruct.2005.07.003.

[134] Gusev AA. Numerical Identification of the Potential of Whisker- and Platelet-Filled Polymers. Macromolecules 2001;34:3081–93. https://doi.org/10.1021/ma001979b.

[135] Wang Z, Wang X, Zhang J, Liang W, Zhou L. Automatic generation of random distribution of fibers in long-fiber-reinforced composites and mesomechanical simulation. Mater Des 2011;32:885–91. https://doi.org/10.1016/j.matdes.2010.07.002.

[136] Vaughan TJ, McCarthy CT. A combined experimental–numerical approach for generating statistically equivalent fibre distributions for high strength laminated composite materials. Compos Sci Technol 2010;70:291–7. https://doi.org/10.1016/j.compscitech.2009.10.020.

[137] Pathan MV, Tagarielli VL, Patsias S, Baiz-Villafranca PM. A new algorithm to generate representative volume elements of composites with cylindrical or spherical fillers. Compos B Eng 2017;110:267–78. https://doi.org/10.1016/j.compositesb.2016.10.078.

[138] Fiedler B, Hojo M, Ochiai S, Schulte K, Ochi M. Finite-element modeling of initial matrix failure in CFRP under static transverse tensile load. Compos Sci Technol 2001;61:95–105. https://doi.org/10.1016/S0266-3538(00)00198-6.

[139] Ismail Y, Yang D, Ye J. A DEM model for visualising damage evolution and predicting failure envelope of composite laminae under biaxial loads. Compos B Eng 2016;102:9–28. https://doi.org/10.1016/j.compositesb.2016.07.004.

[140] Zacherl L, Shadmehri F, Rother K. Determination of convective heat transfer coefficient for hot gas torch (HGT)-assisted automated fiber placement (AFP) for thermoplastic composites. Journal of Thermoplastic Composite Materials 2023;36:73–95. https://doi.org/10.1177/0892705720982363.

[141] Yang L, Li Z, Sun T, Wu Z. Effects of Gear-Shape Fibre on the Transverse Mechanical Properties of Unidirectional Composites: Virtual Material Design by Computational Micromechanics. Applied Composite Materials 2017;24:1165–78. https://doi.org/10.1007/s10443-016-9580-6.

[142] Gao X, Yuan L, Fu Y, Yao X, Yang H. Prediction of mechanical properties on 3D braided composites with void defects. Compos B Eng 2020;197:108164. https://doi.org/10.1016/j.compositesb.2020.108164.

[143] Elsherbini YM, Hoa SV. Experimental and numerical investigation of the effect of gaps on fatigue behavior of unidirectional carbon/epoxy automated fiber placement laminates. J Compos Mater 2017;51:759–72. https://doi.org/10.1177/0021998316655393.

[144] Elsherbini YM, Hoa SV. Fatigue threshold-stress determination in AFP laminates containing gaps using IR thermography. Compos Sci Technol 2017;146:49–58. https://doi.org/10.1016/j.compscitech.2017.04.006.

[145] Pipes R. Interlaminar Shear Fatigue Characteristics of Fiber-Reinforced Composite Materials. Composite Materials: Testing and Design (Third Conference), 1974, p. 419–31. https://doi.org/10.1520/STP35502S.

[146] Bevan LG. Axial and short beam shear fatigue properties of cfrp laminates. Composites 1977. https://doi.org/10.1016/0010-4361(77)90107-0.

[147] May M, Hallett SR. An assessment of through-thickness shear tests for initiation of fatigue failure. Compos Part A Appl Sci Manuf 2010. https://doi.org/10.1016/j.compositesa.2010.07.005.

[148] Makeev A. Interlaminar shear fatigue behavior of glass/epoxy and carbon/epoxy composites. Compos Sci Technol 2013;80:93–100. https://doi.org/10.1016/j.compscitech.2013.03.013.

[149] Kotik H, Perez Ipiña J. Frequency effect in short-beam shear fatigue of a glass fiber reinforced polyester composite. Int J Fatigue 2016;90:116–24. https://doi.org/10.1016/j.ijfatigue.2016.04.025.

[150] Kotik HG, Perez Ipiña JE. Short-beam shear fatigue behavior of fiber metal laminate (Glare). Int J Fatigue 2017;95:236–42. https://doi.org/10.1016/j.ijfatigue.2016.11.001.

[151] ASTM D3479 / D3479M. Standard Test Method for Tension-Tension Fatigue of Polymer Matrix Composite Materials. ASTM International, West Conshohocken, PA 2012. https://doi.org/10.1520/D3479_D3479M-12.

[152] ASTM D638. Test Method for Tensile Properties of Plastics. ASTM International, West Conshohocken, PA 2014. https://doi.org/10.1520/D0638-14.